The Deployment and Performance of Indoor/Outdoor DS-CDMA Systems with Multiuser Detection

Adrian Victor Pais

A thesis submitted in partial fulfilment of the requirements for the degree of
Doctor of Philosophy in Electrical and Electronic Engineering,
The University of Auckland, 2007.

Abstract

This thesis investigates the deployment and performance of indoor/outdoor DS-CDMA systems assuming both conventional receivers and multiuser detection receivers at the base stations.

In the first part of this thesis, measured propagation data and a DS-CDMA system performance testbed (based on a Monte Carlo analysis) are used to quantify both the downlink and uplink outage probabilities for a variety of deployment scenarios: (a) indoor-only systems; (b) interfering indoor/outdoor systems; and (c) interfering indoor systems located adjacent to each other. The results reveal that optimal indoor deployment strategies are heavily dependent on both the location and strength of interference emanating from outdoors. Indoor base station deployment strategies that are optimal in the absence of outdoor interference are often suboptimal if outdoor interference is present.

In the second part of this thesis, two simple multiuser detection techniques are chosen for implementation in the DS-CDMA system performance testbed: successive interference cancellation (SIC) and parallel interference cancellation (PIC). The performance estimation results show that orders-of-magnitude improvements in uplink outage probability are possible with both SIC and PIC. The extent of these improvements is dependent on the deployment strategy used, the fractional residual interference cancellation error, and the uplink power control algorithm (for the case of SIC). If perfect interference cancellation is assumed, it is evident from the results of this thesis that the cancellation of signals in parallel (PIC) provides no additional benefit to system performance than ranking and cancelling the signals sequentially (SIC).

Dedication

To my Lord Jesus Christ, thank you for coming into my life and filling me with so much hope, purpose and ambition.

To my mum, dad and sister, thank you for your unfailing love and support.

Acknowledgements

Towards the end of writing this thesis I found my Lord and Saviour Jesus Christ. There is nothing greater than this. I am so grateful to Him for being with me all the time. He has bestowed on me unique talents and gifts and surrounded me with many wonderful people. Without Him, I never would have had the courage and resilience to do this thesis. Words cannot express my thanks to my spiritual advisor, Andy Pigg, who helped me transform my faith and grow closer to God. Andy, you are truly a remarkable servant of God. I pray that He will bless you and your ministry abundantly.

To my supervisors Kevin Sowerby and Michael Neve, thank you for your valuable advice and direction. Thank you also for allowing me the freedom to do many things outside this thesis, such as the paper competitions I have entered and the organisations I have been involved in.

To the examiners of this thesis, thank you for your comments, which were most useful and helped increase the quality and clarity of this thesis significantly.

To my friends in the Radio Systems Group: Derek Lee, Jochem Roelvink, Brad Sowden, Grace Sung, Alex Wong and Joseph Wong – I will always remember and cherish the times we spent. At times doing a PhD can be so demanding, but the good nature and humour within our group helped me to keep my sanity.

To the technicians of the Radio Systems Group, Phil Lacey and Mark Twiname, thank you for your help during the measurement campaigns I conducted for this thesis.

To Jeffrey Andrews of the University of Texas (Austin), thank you for the most useful discussions we had regarding multiuser detection.

To Vodafone New Zealand and the Foundation for Research, Science and Technology, thank you for the support you gave me in the form of a doctoral scholarship. I am grateful to many people from Vodafone New Zealand for their advice and support during this thesis, in particular Arasaratnam Sathyendran (Sathy), Alan Murch and Darren Chew. I would also like to thank the Radio Network Design team at Vodafone New Zealand, led by Amy Oding, for the opportunity to gain practical experience while writing this thesis.

I have made many friends and been involved in several organisations (IEEE, EPS and World Vision) during the course of my PhD. Many thanks to all of you for making this such a fruitful experience for me.

I would especially like to thank my friends Boaz Habib and Matthew and Ruth Fidow for their support throughout this thesis and for always being there for me.

Last but not least to mum, dad and my sister Maria, no words can express how grateful I am for your love and support throughout my life. Thank you for always encouraging me and helping me realise that I am talented and gifted especially during the times when I had doubts about my abilities. I love you. This thesis is dedicated to you.

Contents

List of Abbreviations and Acronyms

16QAM	16 Quadrature Amplitude Modulation
AWGN	Additive White Gaussian Noise
BER	Bit Error Rate
BPSK	Binary Phase Shift Keying
CW	Continuous Wave
DECT	Digital Enhanced Cordless Telecommunications
DS-CDMA	Direct Sequence Code Division Multiple Access
FDMA	Frequency Division Multiple Access
FH-CDMA	Frequency Hopping Code Division Multiple Access
HSDPA	High Speed Downlink Packet Access
HSUPA	High Speed Uplink Packet Access
MAI	Multiple Access Interference
MIMO	Multiple-Input-Multiple-Output
MLSE	Maximum Likelihood Sequence Estimator
MMSE	Minimum Mean Square Error
PC	Power Control
PIC	Parallel Interference Cancellation
PPM-CDMA	Pulse Position Modulation Code Division Multiple Access
QPSK	Quadrature Phase Shift Keying
RMS	Root Mean Square
SIC	Successive Interference Cancellation
SIR	Signal to Interference Ratio
TDMA	Time Division Multiple Access
UMTS	Universal Mobile Telecommunications System
VCO	Voltage Controlled Oscillator
Wi-Fi	Wireless Fidelity
WiMAX	Worldwide Interoperability for Microwave Access

Chapter 1

Introduction

1.1 The evolution of wireless communication systems

Wireless communication systems have evolved so rapidly in recent times that they have become embedded in the very fabric of modern society. As of the end of 2005, there were approximately 2 billion wireless subscribers worldwide, and this number is projected to increase to approximately 4 billion by the end of 2011 [1]. While the first mobile phone services were available to the general public in twenty-five major American cities in the 1940s [2], the mobile phone has only become a commodity during the last decade. This has been fuelled by a variety of technical developments including the miniaturisation of radio equipment, better RF circuit fabrication processes and improved multiple access techniques that utilise limited spectrum with greater efficiency. The associated reduction in cost and improvement in service quality has increased consumer demand to the extent that the number of mobile phones has already exceeded the number of fixed-line phones in several countries, including the continent of Africa if considered as a whole [3].

It is widely believed that wireless communication systems have the potential to bridge the *digital divide* [4–6]. A major reason for this is the lower cost for deploying and operating wireless communication systems in comparison to traditional fixed-line communication systems. Some of the most promising technologies for bridging the digital divide are Wi-Fi, WiMAX, and a variety of cellular systems [6]. Clearly, the technical developments in the field of wireless communication systems have huge implications on social, economic and political development [4–6]. For this reason engineers have a major role to play in designing and optimising wireless communication systems for the benefit of humankind and for equality of access to information.

At present, wireless communication systems utilising several different wireless standards are in operation or are being deployed [2]. The Wi-Fi standard has emerged as a popular technology for high performing, high capacity wireless access within localised areas such as buildings, while a number of different cellular systems (e.g. 3rd genera-

tion systems) are being used to provide seamless wireless access over large geographic areas. New standards for wireless access (using innovative spread spectrum techniques and modulation schemes) are also being developed, e.g. WiMAX.

In 2005, a study by Japan's NTT DoCoMo found that 70 percent of calls in a 3rd generation system originate from buildings [7]. With the requirement for high speed data services, cellular operators have recognised that their networks often have insufficient coverage and capacity within buildings. Additionally, both Wi-Fi and cellular operators have noticed an increasing demand not only for indoor wireless services but also for seamless coverage between indoors and outdoors to provide 'true mobility'.

In the future, one or more wireless technologies may be used to provide seamless access between indoors and outdoors. In a 3rd generation cellular system, dedicated picocells could be integrated within the wider macro-/microcellular network to provide service to indoor mobile subscribers. Alternatively, given the popularity of Wi-Fi systems for indoor coverage, mobile devices could use Wi-Fi when indoors and automatically switch to 3rd generation cellular systems in areas where there is no Wi-Fi coverage (e.g. outdoors). The wireless technologies that are 'successful' in the future will largely be driven by financial and business factors such as the market conditions and the cost to wireless operators.

Regardless of the exact wireless technologies used to provide seamless indoor/outdoor coverage, the interference between indoors and outdoors will have a major influence on system performance. For example, if separate and uncoordinated Wi-Fi systems are operating in two adjacent buildings, they will present interference to each other thereby causing performance degradation. In a 3rd generation cellular system there might be a macrocellular base station located outdoors coexisting with nearby picocellular base stations located in a building. In this case, wireless operators will need to evaluate the influence of interference 'spilling over' between the macro- and picocells and develop strategies for optimal system deployment.

Wireless operators will need to deploy their systems so that levels of interference are minimised and system performance is optimised. Additionally, with the availability of new technologies (e.g. multiuser detection), wireless operators should have the foresight to design existing systems so that they can be evolved cost effectively to yield optimal performance.

1.2 Code Division Multiple Access (CDMA)

One of the major challenges in designing wireless communication systems is that there is limited bandwidth available for mobile subscribers. Due to their excellent utilisation of spectrum, spread spectrum techniques are specified in several wireless standards (including both Wi-Fi and 3rd generation cellular systems). One such example is Code Division

Multiple Access (CDMA), which is used in 3rd generation implementations (including both UMTS/WCDMA and CDMA2000 1x) due to its excellent multiuser properties, flexibility and security.

CDMA differs from other multiple access techniques (e.g. FDMA and TDMA) in that all mobiles share the same bandwidth, whereas FDMA and TDMA divide the bandwidth into frequency slots and time slots respectively (shown in Figure 1.1) [2]. In CDMA, each mobile is allocated a unique spreading code (a pseudorandom binary sequence) that uniquely distinguishes it from other mobiles. When a message sequence (i.e. packet-switched data or circuit-switched voice) is sent from a base station to a mobile, it is digitised and spread over the entire bandwidth of the channel using the mobile's unique spreading code. When the mobile receives the signal, it uses its spreading code to decode the message sequence. Although the codes are designed to be completely orthogonal to each other, in practice there are non-orthogonalities that cause mutual interference presented to other mobiles [2]. For this reason CDMA is often termed a 'user-limited' or 'interference-limited' system, because a higher number of mobiles in the system implies that there will be more mutual interference presented to each individual mobile (i.e. a noise rise).

While CDMA may be implemented as either frequency hopping CDMA (FH-CDMA) or direct sequence CDMA (DS-CDMA), the focus of this thesis is on the latter technique due to its popularity in commercial implementations [2].

1.3 Multiuser detection

Multiuser detection is a technology that is likely to be available for implementation in DS-CDMA systems in the future [9–13]. As stated in Section 1.2, DS-CDMA is essentially an interference-limited system. This implies that as the system is loaded with more mobiles, the level of mutual interference increases and therefore system performance is degraded. Although several techniques have been developed to compensate for this performance degradation – e.g. directional antennas, macrodiversity, multiple-input-multiple-output (MIMO) systems, modulation and error control coding [2] – none of these techniques directly combat the problem of interference itself; rather they attempt to *avoid* interference.

Multiuser detection is a class of digital signal processing techniques that uses information inherent in DS-CDMA systems to *minimise* or *cancel* interference by jointly detecting the mobiles sharing the channel. Due to the computational complexity of multiuser detection, it is envisaged that it will only be implemented at the base station for uplink system performance enhancement [9–13]. Performing multiuser detection at the base station requires a description of *the received signal from each mobile* as well as *knowledge of what the channel did to that signal when it was transmitted* [10]. In practice channel

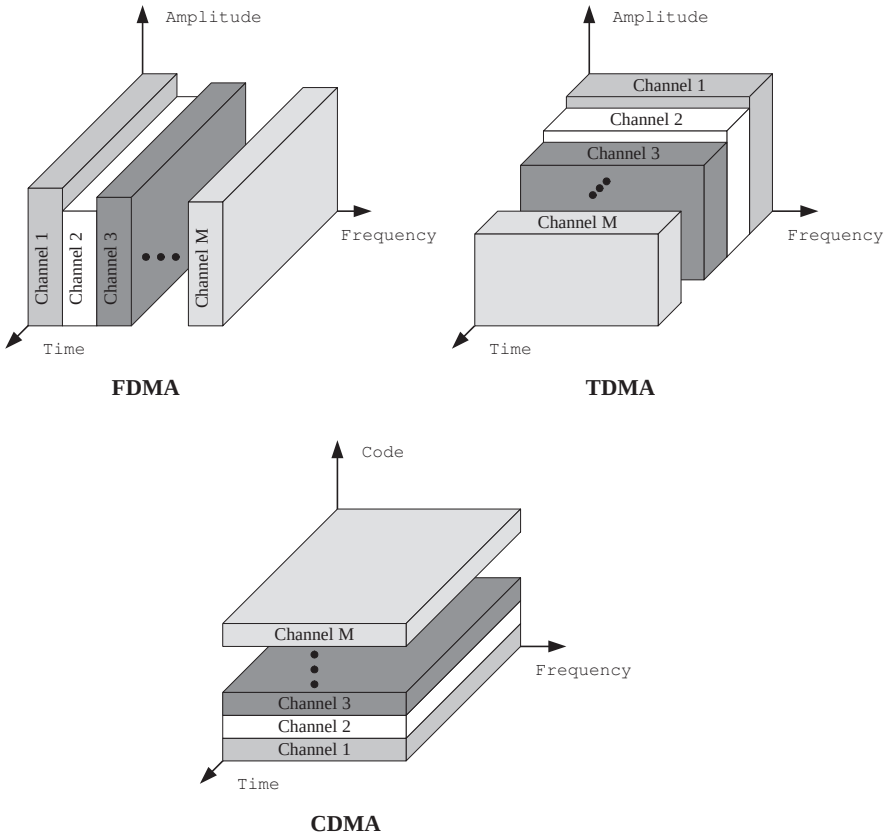

Figure 1.1: A comparison between FDMA, TDMA and CDMA [8].

estimation is used to obtain amplitude and/or phase information of the incoming mobiles' signals. Based on this information the signals of the various mobiles are regenerated using their known spreading codes, after which mutual interference is removed either by direct interference cancellations or linear transformation techniques at the base station receiver outputs.

At the time of writing this thesis multiuser detection has been researched for two decades since its conception. While there have been some prototypes of the technology developed in academia and industry [14–18], there has been little or no take-up of the technology in commercial wireless systems for a number of reasons. Firstly, the complexity and cost of even the least complex multiuser detection techniques is high. Secondly, throughput requirements for communication systems are primarily downlink biased and therefore other less complex techniques to improve downlink performance have often had higher priority in industry implementations (e.g. packet scheduling techniques and HSDPA [19]). Last but not least, there is still limited knowledge of the practical performance gains achievable with multiuser detection in realistic propagation environments [10], as well as the influence of multiuser detection on system-related issues such as base station placement and power control. In particular, there is very little known about the per-

formance of multiuser detection in indoor/outdoor DS-CDMA systems, which this thesis aims to address.

1.4 Purpose, objectives and significance of this thesis

The purpose of this thesis is to investigate the performance of indoor/outdoor DS-CDMA systems for a variety of deployment scenarios that wireless operators are likely to use. Of particular importance in this thesis is determining the 'key' factors influencing system performance and developing strategies for optimally deploying indoor/outdoor DS-CDMA systems. With the pending availability of multiuser detection commercially, this thesis investigates not only the implementation of conventional receivers at the base stations but also two different multiuser detection receivers. The outcome of this thesis is a set of deployment guidelines that are likely to be useful for wireless operators.

The objectives of this thesis are as follows:

- to determine the propagation phenomena and environmental features influencing the performance of indoor/outdoor DS-CDMA systems and their impact on system design.
- to develop guidelines for optimally deploying indoor/outdoor DS-CDMA systems based on evaluating a variety of realistic deployment scenarios.
- to determine the influence of one or more multiuser detection techniques on the performance of indoor/outdoor DS-CDMA systems and provide relevant guidelines for optimal system deployment.
- to compare and contrast the performance of indoor/outdoor DS-CDMA systems operating with and without multiuser detection techniques.

Several previous studies have investigated wireless system performance in *either* indoor [20–27] *or* outdoor environments [2, 28–30]. However, there are very few published papers investigating indoor/outdoor DS-CDMA system performance. To the author's knowledge, no previous study specifically investigates impact of base station deployment (i.e. placement) on the performance of indoor/outdoor DS-CDMA systems. Previous research has also not considered the influence of multiuser detection on the deployment of indoor/outdoor DS-CDMA systems. This issue is also likely to be important for wireless operators in the future and is a major contribution of the research documented in this thesis.

The findings of this thesis are applicable to any system that uses spread spectrum as the multiple access technique. As stated earlier, several radio network implementation standards exist for wireless systems. Two major examples of these standards are

WCDMA/UMTS and CDMA2000 1x. While several implementation differences exist between these standards (e.g. the bandwidth, system architecture and power control algorithms used), the underlying factors influencing system performance are similar. Therefore, in this thesis a generic interference-limited DS-CDMA system is investigated using simple, fundamental parameters common to any practical implementation.

1.5 Contributions and structure of this thesis

This thesis is comprised of ten chapters. The unique contributions of this thesis are detailed in Chapters 4, 5, 7, 8 and 9 and publications relating to this thesis are in [31–35].

The thesis begins by investigating the deployment and performance of conventional indoor/outdoor DS-CDMA systems *without* multiuser detection. Following this, the impact of multiuser detection on the deployment and performance of indoor/outdoor DS-CDMA systems is investigated. A detailed overview the chapters in this thesis is given below.

Chapter 2 gives a background to propagation in mixed indoor/outdoor environments including important propagation phenomena observed in practice. Additionally, a literature survey of propagation models that can be used to estimate signal strength is presented. Due to the limited accuracy and applicability of the propagation models developed to date, it is proposed that propagation measurements be conducted to obtain exact measured propagation data which can be used for the estimates of system performance outlined in subsequent chapters.

Chapter 3 introduces the basic concepts of DS-CDMA systems and presents a method for estimating the performance of DS-CDMA systems using simple parameters. An overview of studies evaluating DS-CDMA system performance in mixed indoor/outdoor environments is also presented. In this chapter, signal correlation is shown to have a significant influence on DS-CDMA system performance. The outcome of this chapter is a DS-CDMA performance evaluation model that is used throughout this thesis and an understanding of the likely influence of the propagation environment on indoor/outdoor DS-CDMA systems.

Chapter 4 presents a propagation study of three mixed indoor/outdoor environments. The study was conducted to obtain propagation data which could be used in subsequent performance analyses. This chapter presents details of the environments in which the propagation measurements were conducted as well as the equipment used and the measurement procedure. The results presented include typical mean received signal strengths observed and signal correlation levels.

Chapter 5 evaluates the performance of indoor/outdoor DS-CDMA systems using the propagation data and models discussed in Chapter 4. To the author's knowledge this is the first study on DS-CDMA performance and base station deployment in indoor/outdoor

environments that uses measured propagation data. A Monte Carlo analysis to quantify both downlink and uplink performance is presented. Following this, a scenario-based approach is used to compare the performance of several deployment scenarios. The outcome of this chapter is a set of guidelines for deploying indoor/outdoor DS-CDMA systems *without* the use of multiuser detection.

Chapter 6 introduces multiuser detection and presents a survey of multiuser detection techniques in the literature. Two techniques, namely successive interference cancellation (SIC) and parallel interference cancellation (PIC) are chosen for further investigation. Models for quantifying the performance of both SIC and PIC are presented. These models are integrated into the system performance testbed (outlined in subsequent Chapters 7 and 8). This chapter also overviews previous studies in which multiuser detection performance has been estimated and shows that no previous research has been published relating multiuser detection to indoor/outdoor DS-CDMA system deployment.

Chapter 7 investigates the uplink performance gains attainable in indoor/outdoor DS-CDMA systems with the implementation of SIC. The integration of the SIC model into the Monte Carlo system performance analysis is described. SIC performance is likely to be related to uplink power control. For this reason, the performance of SIC with various uplink power control algorithms is also investigated and related to the deployment strategy. The outcome of this chapter is a set of guidelines on how to deploy indoor/outdoor DS-CDMA systems if SIC is implemented at the base station. To the author's knowledge this is the first ever study that investigates the system level performance of SIC in indoor/outdoor DS-CDMA systems.

Chapter 8 evaluates the uplink performance gains attainable in indoor/outdoor DS-CDMA systems with the implementation of PIC. The integration of the PIC model into the Monte Carlo system performance analysis is discussed. The PIC performance gains are related to the system deployment strategy and compared with the performance gains attainable with SIC. To the author's knowledge, this is the first investigation into the performance of PIC in indoor/outdoor DS-CDMA systems.

Chapter 9 presents a set of guidelines for deploying indoor/outdoor DS-CDMA systems (for both conventional and multiuser detection receivers) based on the findings from Chapters 5, 7 and 8. Recommendations for future work are also presented.

Chapter 10 presents the key conclusions from this thesis.

Appendix A details the propagation measurement equipment used to conduct the propagation measurement campaigns discussed in Chapter 4.

Appendix B presents a full set of signal correlation results for the transmitters deployed in the propagation measurement campaigns. In Chapter 4 it is shown that signal correlation is an important propagation phenomenon that influences system performance.

In this thesis, system performance is measured in terms of an outage probability (as introduced in Chapter 3). **Appendix C** presents a simple method to determine the system performance gain in terms of the capacity of serviceable mobiles using the graphs in this thesis.

Chapter 2

The mixed indoor/outdoor propagation environment

2.1 Introduction

This thesis investigates the deployment and performance of indoor/outdoor DS-CDMA systems assuming both conventional receivers and multiuser detection receivers at the base stations. Of particular importance to this investigation is the acquisition of information that accurately represents the behaviour of signals that propagate into and within buildings. This information can then be input into a model that estimates the performance of DS-CDMA systems, which is introduced in Chapter 3.

In mixed indoor/outdoor propagation environments, signals propagate indoors, outdoors and between indoors and outdoors. Consider a hypothetical cellular system operating in the mixed indoor/outdoor propagation environment shown in Figure 2.1. This system consists of base stations and mobiles located on several floors of two buildings coexisting with a base station and mobiles located outdoors. To analyse the performance of this system it is necessary to estimate the signal strengths received by each and every mobile from each and every base station (and vice versa).

Clearly, different obstacles are encountered by the signals depending on the relative locations of the base stations and mobiles. For example, the path between an outdoor mobile and outdoor base station in Figure 2.1 is line-of-sight with no intervening obstacles, whereas the path between an outdoor mobile and indoor base station in either Building A or Building B encounters a side of the building and in-building features (e.g. partitions and the central concrete core).

This chapter begins in Section 2.2 by giving an overview of the phenomena influencing the propagation of radio signals. Typical received signal strength profiles are presented and commonly observed characteristics such as distance-dependence, shadowing and fad-

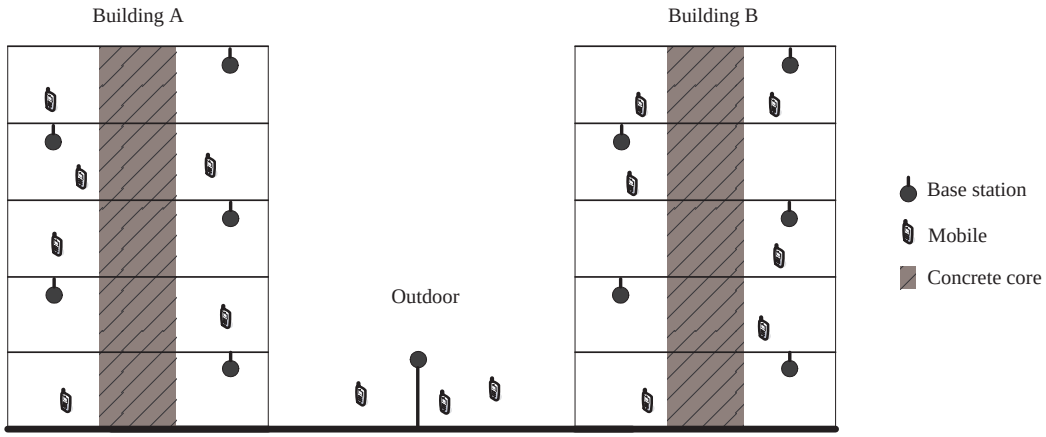

Figure 2.1: The mixed indoor/outdoor propagation environment.

ing are explained. Wideband channel characteristics are overviewed and their behaviour in mixed indoor/outdoor propagation environments is discussed.

Several propagation models have been developed to predict propagation behaviour into and within buildings. Section 2.3 evaluates the propagation modelling approaches presented in the literature. These models are divided into two categories based on the propagation paths for which the path loss is predicted, namely (i) indoor-to-indoor; and (ii) outdoor-to-indoor. The relevance of these models for use in this thesis is discussed. Finally, Section 2.4 summarises this chapter.

The material presented in this chapter is especially relevant to the propagation measurement campaigns outlined in Chapter 4, as well as the system performance estimations discussed in Chapters 5, 7,and 8.

2.2 An overview of radio propagation

The performance of a cellular system is ultimately dependent on the effect that the channel has on the signals propagating through it [36]. The path between a base station and a mobile may vary from having complete line-of-sight with no intervening obstacles to non-line-of-sight with one or more different obstacles between and around them. If the behaviour of the propagation channel is predicted accurately, radio frequency engineers can confidently predict the coverage area, estimate system performance and design cellular systems so that interference is minimised and system capacity is maximised [2, 36].

This section begins by discussing the key phenomena influencing the propagation of radio signals (Section 2.2.1). Typical received signal strength profiles and relevant statistical models for representing received signal strength are presented in Section 2.2.2. Finally the implications of wideband channel characteristics in mixed indoor/outdoor environments are discussed in Section 2.2.3.

2.2.1 Factors influencing the propagation of radio signals

The radio propagation channel is generally time-varying. A signal received by a mobile is usually a combination of several components of the original, transmitted signal from the base station [2,36]. Each component may have traversed a different propagation path and therefore encountered different obstacles during its transmission. This is demonstrated in Figure 2.2, which shows a diagram of the signal components for a transmission between a base station (located outdoors) and a mobile (located indoors) in an urban area. The signal received by the mobile is made up of the following components:

- **Direct path** – propagation path directly between the transmitter and receiver.
- **Diffracted path** – the signal propagates around the edge of a building or obstacle.
- **Reflected path** – nearby buildings or obstacles reflect the signal.
- **Scattered path** – corners of buildings or obstacles cause scattering of the signal in several different directions.

Due to the multitude of paths traversed by the signal components, this phenomenon is known as *multipath* propagation. The received signal at a mobile is fundamentally the summation of the individual component signals that arrive with different amplitudes and phases, and therefore can be represented mathematically, as outlined in Section 2.2.2.

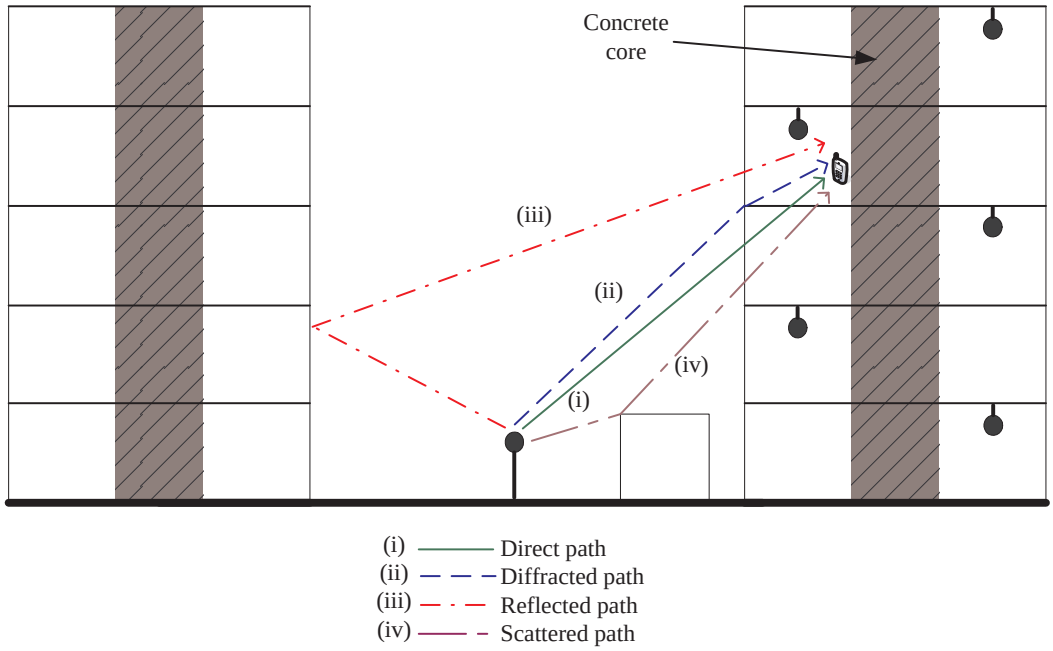

Figure 2.2: Propagation paths between a base station (located outdoors) and a mobile (located indoors).

2.2.2 Received signal strength

2.2.2.1 Received signal strength variation

The accurate modelling of received signal strength in mixed indoor/outdoor propagation environments is of particular importance to this thesis. Regardless of the specific propagation environment, there exist long-, medium- and short-term variations in received signal strength due to the many different phenomena influencing the propagation of signals [2, 36].

Long-term variations describe the general reduction in received signal strength over long distances (usually hundreds of wavelengths of the radio frequency carrier). In general, a distance-dependent decay in received signal strength is apparent with increasing distance from the transmitter [2, 36].

Medium-term variations occur due to shadowing obstacles (e.g. hills and buildings in outdoor environments or concrete cores in indoor environments) that attenuate the signal. While medium-term variations do not usually occur over very short distances (around ten wavelengths of the radio frequency carrier), they are observed to occur over longer distances (typically sixty wavelengths of the radio frequency carrier) [2,36]. Medium-term variations are usually termed *shadowing*.

Short-term variations in received signal strength occur due to the many different signal components arriving at the receiver which may combine constructively or destructively, causing significant variations over distances as low as half a wavelength (this is only 7.5 cm for a 2 GHz radio frequency carrier). In practice it has been observed that the received signal strength can vary by as much as three to four orders of magnitude (30 to 40 dB) because of short-term variations [2, 36]. Short-term variations are often termed *fading* of the received signal.

In [37], a propagation experiment was conducted within a building to obtain a typical received signal strength profile. In this experiment, a 1.8 GHz transmitter was deployed at a fixed location and measurements of the received signal strength were made using a mobile test receiver. Figure 2.3 is a plan showing the location of the transmitter (TA) and the measurement path over which measurements of the received signal strength were made using the test receiver (RA). The transmitter (TA) was deployed in a corridor that was at right angles to the corridor in which the measurements were taken. This meant that at certain locations along the measurement path there was a line-of-sight between the transmitter and receiver (between 1 and 2.8 metres from Point A, shown in Figure 2.3), while at other locations there was no line-of-sight.

Figure 2.4 is a graph of the received signal strength taken on the measurement path [37]. This graph shows both the measured received signal strength (in red) as well as the lo-

cal area[1] mean received signal strength (in blue). The local area mean received signal strength was calculated by averaging the measured received signal strength values over a 1 metre radius. It should be noted that in calculating the local area mean received signal strength, the short-term effects (i.e. fading) were averaged. Therefore, the local area mean received signal strength accounts for long- and medium-term variations but not short-term variations in the measured, instantaneous received signal strength.

It is evident from Figure 2.4 that the highest local area mean received signal strength is observed when the receiver has a line-of-sight path with the transmitter (i.e. between 1 and 2.8 metres from Point A). For distances greater than 2.8 metres from Point A, a gradual reduction in the local area mean received signal strength is observed for two reasons: firstly, due to the increasing distance between the transmitter and receiver (long-term variation), and secondly, due to the shadowing caused by the walls obstructing the line-of-sight path between the transmitter and receiver (medium-term variation).

The measured received signal strength profile shows the short-term fading around the local area mean signal strength. As discussed previously, the fading is observed to cause a reduction in signal strength by as much as 30 to 40 dB relative to the local area received mean signal strength.

2.2.2.2 Statistical distributions to model signal strength variation

Short-term variations (fading)

Short-term variations in signal strength occur due to the arrival of several different signal components at the receiver. Assuming that there is not a significant line-of-sight signal component, it has been shown that short-term variations (fading) around the local area mean received signal may be modelled using a Rayleigh distribution, the probability density function (pdf) of which is [2, 26, 36]

$$p(r) = \frac{r}{\sigma^2} \exp\left(-\frac{r^2}{2\sigma^2}\right), \tag{2.1}$$

where r is the received signal strength (in units of voltage) and $2\sigma^2$ is the time averaged power of the received signal. The Rayleigh distribution can be justified theoretically by Clarke's model, which assumes that the received signal is a continuum of a number of equal magnitude components. These components have random phases that are statistically independent and uniformly distributed between 0 and 2π.

[1]The *local area mean* received signal strength is the mean received signal strength averaged over a sufficient distance such that variations due to fading are eliminated, but variations due to distance-dependence and shadowing are represented. In this thesis the local area mean received signal strength is often simply termed as the mean received signal strength.

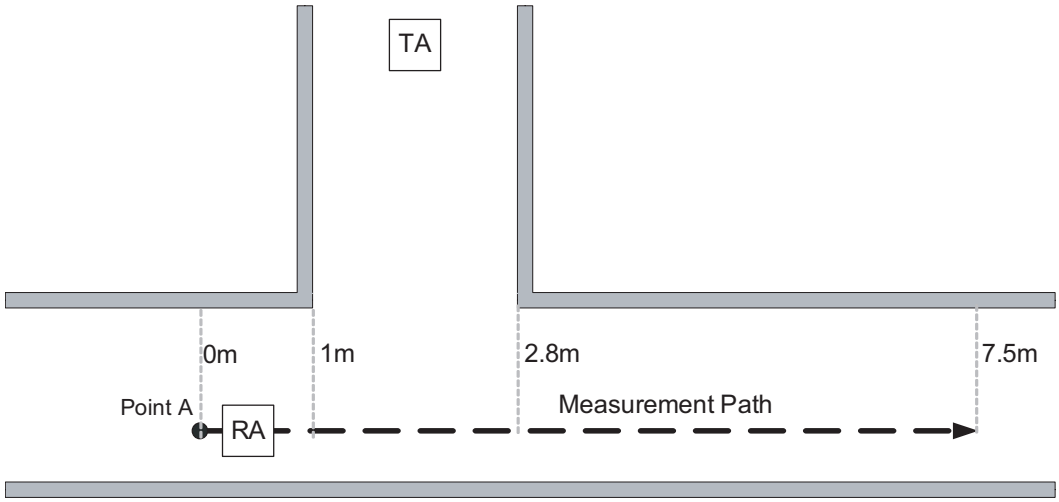

Figure 2.3: Plan of a simple propagation experiment to obtain a received signal strength profile. TA is the location of the 1.8 GHz transmitter, while measurements are taken using the receiver RA along the measurement path [37].

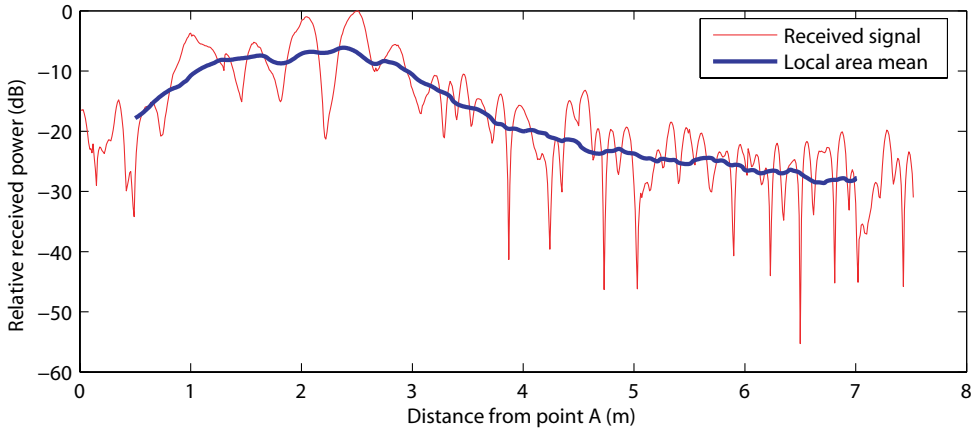

Figure 2.4: Received signal strength along the measurement path for the experiment [37] shown in Figure 2.3. The frequency of operation is 1.8 GHz.

If the received signal strength is expressed in terms of power (i.e. units of mW), it can be shown that the received signal power is modelled using an exponential distribution as follows [2, 26, 36]

$$p(r_w) = \frac{1}{\overline{r}} \exp\left(\frac{-r_w}{\overline{r}}\right), \tag{2.2}$$

where r_w is the received signal strength (mW), and $\overline{r}$ is the local area mean received signal strength (mW).

The Rayleigh and exponential distributions for modelling short-term variations in signal strength assume that there is no dominant (line-of-sight) component between the transmitter and receiver. It has been shown that if there is a dominant component, the Rician distribution is more representative [2, 26, 36]. In this thesis, however, it is assumed that the Rayleigh and exponential distributions are sufficiently accurate for modelling short-term variations as the majority of mobiles in the wireless communication systems considered herein do not have line-of-sight with the base station.

Medium-term variations (shadowing)

Medium-term variations in signal strength occur due to the shadowing caused by obstacles blocking the line-of-sight path between a transmitter and receiver. Assuming that the signal strength is measured in logarithmic units (i.e. dBm), a normal distribution has been found to be representative of the medium-term variations around the wide area mean received signal strength. The pdf of the normal distribution is [2, 26, 36]

$$p\left(\overline{R}\right) = \frac{1}{\sqrt{2\pi\sigma^2}} \exp\left[\frac{-\left(\overline{R} - m\right)^2}{2\sigma^2}\right], \tag{2.3}$$

where $\overline{R}$ is the local area[2] mean received signal strength (dBm), m is the wide area[3] mean received signal strength (dBm) and σ is the standard deviation about the wide area mean received signal strength (dB).

If the received signal strength is expressed in units of mW, the lognormal distribution is commonly used to model medium-term variations around the wide area mean received signal strength. The pdf of the lognormal distribution is [2, 26, 36]

[2]The *local area mean* received signal strength is the mean received signal strength averaged over a sufficient distance such that variations due to fading are eliminated, but variations due to distance-dependence and shadowing are represented. In this thesis the local area mean received signal strength is often simply termed as the mean received signal strength.

[3]The *wide area mean* received signal strength is the mean signal strength averaged over a sufficient distance such that variations due to both fading and shadowing are eliminated, but variations due to distance-dependence are represented.

$$p(\overline{r}) = \frac{10}{\ln(10)\sqrt{2\pi}\sigma\overline{r}} \exp\left[\frac{-(20\log_{10}(\overline{r}) - m)^2}{2\sigma^2}\right], \tag{2.4}$$

where $\overline{r}$ is the *local area* mean received signal strength (mW), m is the *wide area* mean received signal strength (dBm) and σ is the standard deviation about the wide area mean received signal strength (dB).

Modelling both short- and medium-term variations

It has been shown by Suzuki [38] that both the Rayleigh distribution (that models short-term signal strength variation) and the lognormal distribution (that models medium-term signal strength variation) may be combined into a single distribution that accounts for both the short- and medium-term signal variation. This combined distribution (known as the Suzuki distribution) is essentially a Rayleigh distribution with a lognormally varying mean. The pdf of the received signal, r_w, assuming a Suzuki distribution is [38]

$$p(r_w) = \int_0^\infty \frac{1}{\overline{r}} \exp\left[\frac{-r_w}{\overline{r}}\right] \cdot \frac{10}{\ln(10)} \cdot \frac{1}{\sqrt{2\pi\sigma^2}} \cdot \frac{1}{\overline{r}} \cdot \exp\left[\left(\frac{-10\log(\overline{r}) - m}{2\sigma^2}\right)\right] d\overline{r}, \tag{2.5}$$

where $\overline{r}$ (mW) is the local area mean received signal strength (which is modelled using the lognormal distribution described by (2.4)). The parameters m (dBm) and σ (dB) are the wide area mean received signal strength and the standard deviation about the wide area mean received signal strength respectively.

2.2.3 Wideband channel characteristics

In Section 2.2.2, it was shown that short-term variations in received signal strength can be modelled using a Rayleigh distribution. This distribution assumes that the received signal is a summation of several components that have similar amplitudes and random phases (due to multipath propagation). In practice, this is accurate for narrowband channels (i.e. for signals transmitted within a 'narrow' frequency range). However, in wideband channels (over which signals are transmitted over a wide range of frequencies), it is likely that the phasor sum of the various multipath signal components will be frequency dependent [2, 26, 36].

In the time domain, this phenomenon manifests itself as a variation in the time delay encountered by the symbols transmitted. Due to multipath propagation, a symbol replica may arrive 'late' and if it has a significant magnitude, it will interfere with a subsequent symbol received 'earlier'. This is commonly known as intersymbol interference (ISI) which

results in the distortion of symbols and therefore incorrect bit detections. Equalisers are commonly used to mitigate the effects of ISI [2, 36].

In the frequency domain, the *coherence bandwidth* is used to represent the range of frequencies over which multipath components will undergo similar distortions thereby causing *flat fading* (and therefore no intersymbol interference). If the bandwidth of the signal is greater than that of the coherence bandwidth, then *frequency selective* fading will occur. By definition, narrowband channels have a bandwidth that is much lower than the coherence bandwidth of the channel and therefore do not suffer from frequency selective fading. On the other hand, wideband channels have a bandwidth greater than the coherence bandwidth of the channel and therefore suffer from frequency selective fading [2, 36].

In practice, the wideband channel response may be obtained by using pulse techniques to obtain channel power delay profiles [26]. A typical sequence of power delay profiles obtained in an office building environment at 1.8 GHz [26] is shown in Figure 2.5. Each successive profile starts approximately 0.5 microseconds after the previous profile. For each of these profiles, there is a dominant signal component followed by weaker (delayed) components. If delayed components of significant magnitude arrive at the receiver, this is likely to cause ISI.

Various useful statistical parameters may be obtained from power delay profiles. The root mean square (RMS) delay spread and coherence bandwidth are important examples of such parameters. By obtaining these parameters, it is possible to determine the maximum channel bandwidth for which frequency selective fading will not occur.

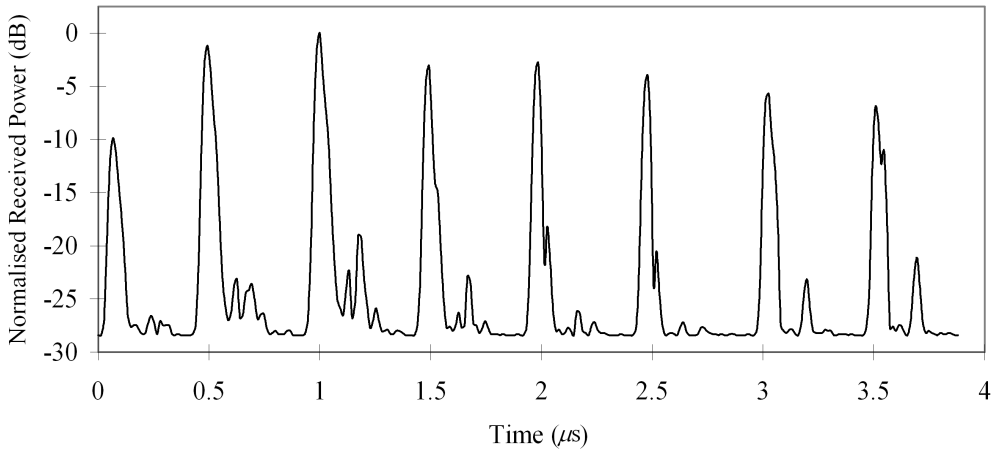

Figure 2.5: Power delay profiles obtained in an office building environment at 1.8 GHz [26].

The RMS delay spread is a parameter that represents the standard deviation of the time delays for the various multipath signal components received. Previous wideband measurement studies have shown that the RMS delay spread is dependent on the envi-

ronment in which the signals propagate. In outdoor environments, there are likely to be relatively large distances between and around the mobiles and base stations. As a result, there are often significant signal components with large time delays. However, in buildings where the propagation paths are much shorter, the signal components usually have shorter time delays [2, 26, 36].

In indoor environments, RMS delay spreads have been observed to range from 25 ns to 100 ns when both transmitter and receiver are located indoors [39–44]. If the transmitter is located outdoors, RMS delay spreads of up to 320 ns have been observed indoors [39–44].

In DS-CDMA systems the specified chip rate is very high (e.g. the maximum chip rate specified in WCDMA/UMTS and cdma2000 is 3.84 Mcps) [45], meaning that it is possible that the coherence time of a chip will be much less than the relative time delays encountered by the various multipath components (equating to several chips' difference in arrival time). Whereas other digital systems often require an equaliser to mitigate ISI, in DS-CDMA systems the multipath components (if delayed in time by more than one chip) merely represent multiple versions of the signal at the receiver. This is because there is very little correlation between chip sequences [2].

The multipath components in a wideband channel contain useful information about the individual mobiles. This phenomenon can be exploited by using a RAKE receiver to detect and decode each individual multipath component. In essence, the time delayed versions of the original signal are detected using separate correlators. These time delayed versions are then combined in order to improve the signal to noise ratio at the receiver. It is often useful to implement RAKE receivers outdoors where the delay between mutipath components is usually large [2].

2.2.3.1 Approach in this thesis

In this thesis a channel bandwidth of 5 MHz is assumed, as this is commonly used in practical DS-CDMA systems (e.g. WCDMA/UMTS) [45]. The maximum chip rate of 3.84 Mcps specified in WCDMA/UMTS and cdma2000 [45] corresponds to a chip time of approximately 260 ns per chip. For a RAKE receiver to distinguish between multipath components, there must be a relative time delay of at least one chip time (i.e. 260 ns) between them. This corresponds to a multipath difference of 78 metres. Given the relatively short distances between the transmitters and mobiles in the indoor/outdoor environments considered in this thesis, it is unlikely that there will be any multipath components of significant magnitude that would have traversed this distance. The relatively low RMS delay spreads reported in the literature (i.e. up to 100 ns indoors and 320 ns from outdoor to indoor [39–44]) confirm this reasoning. Therefore, the wideband channel characteristics are unlikely to have an impact on the indoor/outdoor DS-CDMA systems considered in this thesis and for this reason a RAKE receiver is unlikely to provide significant additional

benefit. Consequently, in this thesis it is assumed that the multipath components cannot be distinguished from each other because the channel behaviour in the indoor/outdoor environments considered is essentially narrowband.

2.3 Propagation modelling approaches

Section 2.2 presented an overview of the radio propagation phenomena in wireless communication systems and discussed the commonly observed variations in received signal strength due to short, medium, and long-term effects. Additionally, it was shown that the levels of RMS delay spread observed in mixed indoor/outdoor environments are unlikely to influence the performance of indoor/outdoor DS-CDMA systems for the channel bandwidth considered in this thesis.

In this thesis, the accurate representation of received signal strength is of paramount importance. A plethora of measurement campaigns have been conducted in a wide variety of buildings to better understand the behaviour of radio propagation [46–54]. Furthermore, to enable the efficient planning of wireless communication systems, numerous propagation models have been developed to predict radio propagation behaviour [2,36,44,55–57]. A variety of methods have been used to develop these propagation models. Predictions from these models have been compared with measured propagation data to assess their accuracy. The purpose of this section is to evaluate relevant propagation models reported in the literature and to assess their appropriateness and accuracy for use in this thesis.

The propagation models presented in this section are used to estimate the mean path loss between a transmitter and a receiver. The mean path loss accounts for the the losses due to both distance dependency and shadowing (i.e. long- and medium-term variations) but not due to fading (i.e. short-term variations). The mean path loss, PL (dB), between a transmitter and receiver is defined as

$$PL = P_t - \overline{P_r}, \tag{2.6}$$

where $\overline{P_r}$ is the mean received signal strength (dBm) and P_t is the transmit power (dBm). In this thesis, accurate mean path losses for both indoor-to-indoor propagation paths and outdoor-to-indoor propagation paths are required. The models for both these categories are now described in turn.

2.3.1 Indoor-to-indoor propagation models

Indoor-to-indoor propagation models are relevant for predicting the mean path loss for cases in which the transmitter and receiver are both located indoors. Due to the variety of

building types and indoor environmental features, the accurate prediction of mean path loss has proven to be particularly challenging.

Most indoor-to-indoor propagation models have been developed using empirical or semi-empirical techniques that attempt to minimise the mean square error between measured propagation data and the predicted mean path losses from the model [2, 36]. To improve prediction accuracy, more input information is required (e.g. the types and locations of partitions in the buildings). This in turn makes the model highly specific to particular building types and therefore less applicable to a wide variety of other indoor propagation environments.

This section summarises a number of indoor-to-indoor propagation models reported in the literature. For a system with base stations and mobiles located indoors, it is important to model the path loss *within* a floor of interest as well as *between* floors. Propagation modelling approaches for both of these cases are now discussed.

Propagation modelling within floors

Modelling propagation within a floor of interest is required for cases where the transmitter and receiver are on the *same* floor. Previous research shows that the mean path loss is related to the distance between a transmitter and receiver. The mean received signal strength is generally found to decay with the distance between the transmitter and receiver. A simple model [58, 59] to represent this is the log-distance propagation model, which predicts the mean path loss, $PL\,(d)$(dB), between a transmitter and receiver separated by a distance d

$$PL\,(d) = PL\,(d_o) + 10n \log\left(\frac{d}{d_o}\right). \tag{2.7}$$

In (2.7), $PL\,(d_o)$ is the mean path loss (dB) measured at a specified distance, d_o, and n is commonly known as the path loss exponent. The parameter, n, determines the rate of increase in the path loss with distance and is dependent on the level of clutter in the propagation environment. For example, if there is line-of-sight propagation between a transmitter and receiver in an open space (e.g. a large room or corridor), values for n are reported in the literature [27, 44] to vary from $1 \leq n \leq 3$. For non line-of-sight cases (e.g. between rooms separated by several partitions), values for n are reported in the literature to vary from $2.45 \leq n \leq 6.5$ [27, 44].

In (2.7) only the increase in path loss due to distance is considered and the path loss variations that occur due to shadowing are not included. The model described in (2.7) can be modified to include the effect of shadowing [55]

$$PL\,(d) = PL\,(d_o) + 10n \log\left(\frac{d}{d_o}\right) + X_\sigma, \tag{2.8}$$

where X_σ (dB) is a shadowing parameter that may be modelled using a zero-mean Gaussian random variable. The parameter X_σ is essentially a variability in the distance-dependent path loss that occurs due to the shadowing caused by obstacles such as partitions and building structural features (e.g. concrete cores).

In the literature, it is shown that the models represented by (2.7) and (2.8) do not provide a good fit to measured propagation data collected in indoor environments [26]. However, the simplicity of the models means that they can be applied easily to a wide variety of indoor propagation environments because the only input information required is the transmitter-receiver separation distance and the shadowing parameter. The lack of accuracy in the above models occurs because they are only a function of distance and the impact of specific propagation environment features (e.g. the intervening walls and partitions) are not accounted for.

Researchers have attempted to consider the impact of intervening walls and obstacles by adding relevant attenuation factors to the distance-dependent path loss models described by (2.7) and (2.8). Such a model was first proposed by Seidel [55]

$$PL\,(d) = PL\,(d_o) + 10n \log\left(\frac{d}{d_o}\right) + k \cdot WAF + X_\sigma, \tag{2.9}$$

where WAF is a wall attenuation factor, which is defined as the additional attenuation due to the intervening wall. The parameter k in (2.9) is the number of intervening walls. The wall attenuation factor, WAF, is heavily dependent on the type of intervening wall, e.g. from previous measurements reported in the literature, the WAF for concrete walls is as high as 20 dB, while the WAF for partitions is as low as 1.5 dB [2, 51, 55, 60].

The inclusion of the wall attenuation factor in (2.9) has been shown to yield more accurate mean path loss predictions than the distance-dependent models represented by (2.7) and (2.8). However, additional input information is required regarding the types of intervening walls.

Propagation modelling between floors

Modelling propagation between floors is required when the transmitter and receiver are on different floors of a building. The intervening floors between the transmitter and receiver are likely to have a significant influence on the mean path loss.

Motley and Keenan [47] proposed the seminal model for propagation between floors. This model includes a discrete attenuation factor representing the influence of intervening floors. Similar to Seidel's model for intervening walls within a single floor (described by (2.9)), Motley and Keenan's model is based on the distance-dependent model of (2.8) but adds an additional attenuation factor accounting for each intervening floor between the transmitter and receiver [47]

$$PL(d) = PL(d_o) + 10n \log\left(\frac{d}{d_o}\right) + k \cdot FAF + X_\sigma. \tag{2.10}$$

In (2.10), FAF (dB) is the attenuation of a single floor and k is the number of intervening floors between the transmitter and receiver. The floor attenuation factor, FAF, is the additional attenuation due to the intervening floor. The parameter d is the three-dimensional separation distance between the transmitter and receiver.

Motley and Keenan's model assumes that the same incremental attenuation is presented by each floor separating the transmitter and receiver. However, propagation measurements conducted by several researchers have shown that for a large number of floors, the incremental attenuation of each additional floor decreases with an increasing number of floors between a transmitter and receiver [2]. For a better fit with measured data and to account for the asymptotic behaviour in floor attenuation, researchers have attempted to modify Motley and Keenan's model. One such model was developed by Lafortune and Lecours [26, 61], who proposed an increase in the total attenuation by the logarithm of the number of intervening floors

$$PL(d) = PL(d_o) + 10n \log\left(\frac{d}{d_o}\right) + \log(k+1) \cdot FAF + X_\sigma, \tag{2.11}$$

Mean path loss predictions from Lafortune and Lecours' model give a significantly better fit to measured propagation data than Motley and Keenan's model [26, 61].

Several more propagation models have also been developed by using the distance-dependent model as a base and adding additional factors depending on the layout and features of the indoor environment [47, 50, 55, 62, 63]. However, the indoor propagation models developed to-date are either too generalised (so that their predictions lack the accuracy required in this thesis) or are too specific to particular building types (so that their applicability is limited).

2.3.2 Outdoor-to-indoor propagation models

Radio propagation within buildings has been investigated to a greater extent than radio propagation into buildings. A limited number of outdoor-to-indoor propagation measurement campaigns [57, 64–68] have been conducted previously by researchers and usually only general observations have been reported from the collected propagation data.

Previous research on outdoor-to-indoor propagation has often been concerned with determining the penetration loss for propagation into buildings [56]. The penetration loss is the additional attenuation due to the signal propagation through the side of a building. Also of interest is the received signal variability for signals propagating from outdoors to

indoors as well as the effect of building height, construction materials and frequency of operation.

The penetration loss has been found to be related to both the signal frequency and the height of the building. Researchers have shown that the outdoor-to-indoor penetration loss generally decreases with increasing frequency. For example, measurements taken in a variety of buildings by researchers in Liverpool [64] obtained average penetration losses of 16.4 dB, 11.6 dB and 7.6 dB on the ground floor of the buildings for frequencies of 441 MHz, 896.5 MHz and 1400 MHz, respectively. As stated in Section 2.2.3, a channel bandwidth of 5 MHz is assumed in this thesis. The measurements in [64] demonstrate that over this relatively small bandwidth the penetration loss is likely to remain the same.

With increasing height of the building, the penetration loss has been shown to initially decrease for the first few levels of the building and then increase. For example, Turkmani [64,65] reported that the penetration loss decreased by 2 dB per level from the ground level up to the ninth level of a building and then increased above the ninth level.

The majority of outdoor-to-indoor propagation models have been developed by using semi-empirical or empirical methods. Several researchers have developed outdoor-to-indoor propagation models using a three-step process [57, 64–68]:

1. from outdoors to the edge of the building, a distance-dependent path loss with a given path loss attenuation factor is assumed;

2. from the edge of the building to within the building, the signal undergoes a penetration loss as it propagates into the building; and

3. within the building, indoor-to-indoor propagation models are used ranging from simple distance-dependent models to more accurate propagation models that require site-specific input information.

It is apparent from existing research that further outdoor-to-indoor measurements and propagation modelling is required to improve the accuracy of outdoor-to-indoor propagation models [57, 64–68].

2.3.3 Other propagation modelling approaches

The indoor-to-indoor and outdoor-to-indoor propagation models reviewed in this chapter have primarily used empirical or semi-empirical techniques in their development. These techniques have the benefit that all propagation factors (both known and unknown) are accounted for implicitly. However, a drawback of these techniques is that for greater accuracy to be achieved, more input information is required and the propagation model becomes increasingly specific to the propagation environment under consideration.

Ray-tracing is a deterministic technique that is applicable to modelling *any* indoor propagation environment [69–71]. One such example of ray-tracing is based on geometrical optics [2]. In this model, a building is modelled as a set of polygonal walls, with each wall having an electromagnetic classification depending on its construction material. Based on this information, multipath propagation phenomena such as reflection, scattering and diffraction are modelled and the mean path loss is calculated. There are possibly thousands of propagation paths between a transmitter and receiver. If too many propagation paths are considered, the ray-tracing problem becomes prohibitively computationally intensive. Therefore researchers have developed a number of algorithms to determine the most significant propagation paths between a transmitter and receiver. Inaccuracies in geometrical optics are caused by both the limited computational power available as well as various assumptions that are made to make the solution tractable (e.g. diffraction is modelled assuming perfect conductivity).

2.3.4 Propagation modelling approach in this thesis

Sections 2.3.1 and 2.3.2 outlined the approaches for modelling mean path loss variations for two cases of propagation paths: indoor-to-indoor and outdoor-to-indoor. Although there is a large body of research on indoor-to-indoor propagation, only a few studies have been performed for outdoor-to-indoor propagation. The indoor-to-indoor propagation models previously developed generally have a distance-dependent path loss and factors to represent the additional attenuation caused by environment features, e.g. wall and floor attenuation factors. The outdoor-to-indoor propagation models developed to date are based on only a limited number of propagation measurement campaigns and therefore cannot be used confidently for a wide range of propagation environments.

Due to the uncertainty and inaccuracies inherent in propagation models developed in the literature, this thesis is based entirely on using measured propagation data collected in mixed indoor/outdoor environments. The benefit of this approach is that no assumptions are made on how signals propagate into and within buildings as the propagation data is based on actual measurements. Therefore, any subsequent performance analyses that use the propagation data can be conducted with great confidence. Any conclusions drawn from the performance analyses, while strictly applicable to the buildings in which the measurements are made, also give insight into the deployment of systems in other buildings of similar construction.

2.4 Summary

This chapter introduced the propagation phenomena commonly observed in practice and various propagation models that can be used to predict propagation behaviour in mixed indoor/outdoor environments. It was shown that variations in received signal strength include short-, medium- and long-term variations. These variations occur due to fading, shadowing and distance-dependence respectively. It was also shown that the wideband channel characteristics observed from previous studies are unlikely to influence the performance of the indoor/outdoor DS-CDMA systems considered in this thesis because of the relatively small time delays between multipath components.

The propagation models reviewed in this chapter include both indoor-to-indoor propagation models and outdoor-to-indoor propagation models. The first class of models predict the mean path loss for cases where the transmitter and receiver are both located indoors. The latter class of propagation models predict the mean path loss for cases where the transmitter is located outdoors and the receiver is located indoors. It was shown that both the indoor-to-indoor and outdoor-to-indoor propagation models developed to-date have limited accuracy and applicability to a wide range of environments. For this reason it was decided to conduct propagation measurements in a variety of mixed indoor/outdoor environments (described in Chapter 4) and use the collected propagation data to assess system performance.

Chapter 3 introduces methods to evaluate the performance of DS-CDMA systems as well as previous studies investigating their performance.

Chapter 3

Evaluating the performance of DS-CDMA systems

3.1 Introduction

The purpose of this thesis is to investigate the deployment and performance of indoor/outdoor DS-CDMA systems that operate with either conventional receivers or multiuser detection receivers at the base stations. Chapter 2 highlighted the radio propagation phenomena observed in practice and the statistical methods to represent received signal strength. The propagation modelling approaches presented in the literature were shown to be insufficient for accurate prediction of propagation in mixed indoor/outdoor environments. Therefore, it was decided that propagation measurements be conducted to obtain exact measured data that could be used in the performance analyses conducted for this thesis.

The purpose of this chapter is to give an overview of conventional DS-CDMA systems (i.e. without the implementation of multiuser detection). Of particular importance are the key factors that influence system performance and the methods to assess system performance. This chapter begins by presenting techniques to estimate downlink and uplink DS-CDMA system performance in Section 3.2. In subsequent chapters, these techniques are used in conjunction with measured propagation data to quantify DS-CDMA system performance for various hypothetical deployment scenarios. The factors influencing DS-CDMA system performance in various propagation environments (indoor, outdoor and mixed indoor/outdoor) are discussed in Section 3.3. A survey of previous studies evaluating DS-CDMA system performance is presented in Section 3.4. Signal correlation is a key propagation phenomenon that influences DS-CDMA system performance; this phenomenon is reviewed in Section 3.5. Finally, a summary of this chapter is presented in Section 3.6.

3.2 Estimation of DS-CDMA system performance

It is well known that in DS-CDMA systems all mobiles share the same bandwidth and are distinguished by their unique spreading codes [2, 45, 72]. Non-orthogonalities between mobiles' spreading codes manifest themselves as mutual interference to other mobiles. For this reason, DS-CDMA systems are often termed to be *interference-limited*.

A key engineering parameter used to quantify system performance is the outage probability. This represents the likelihood that a mobile within a DS-CDMA system will have an outage, which occurs if the bit error rate (BER) of its message sequence is above a pre-defined threshold. In practical cellular systems, the outage probability is likely to influence almost all commonly used key performance indicators (KPIs) such as the data rate, dropped call rate, and admission rate [45, 73].

In DS-CDMA systems, communication is required both from the base station to the mobile (downlink[1]) and the mobile to the base station (uplink[2]). Separate frequency bands are used for the downlink and the uplink. On the downlink, the purpose of the mobile receiver is to determine its message sequence from its own base station's signal in the presence of interfering signals emanating from other base stations. On the uplink, the base station receiver must determine a message sequence from each mobile in its own cell in the presence of interfering signals emanating from several mobiles located both within and outside its own cell. In comparison to the downlink, the uplink is likely to have several more interfering signals as there are generally more mobiles than base stations in the system.

Techniques for estimating downlink and uplink system performance (in terms of outage probabilities) are presented in Sections 3.2.1 and 3.2.2 respectively. These techniques use basic, fundamental DS-CDMA parameters that allow for an evaluation of the key propagation factors influencing system performance regardless of the specific implementation standard used. This allows for generalised deployment guidelines to be developed and comparisons to be made between various deployment scenarios investigated in this thesis.

3.2.1 Downlink DS-CDMA system performance

This section presents a basic model for estimating downlink DS-CDMA system performance based on the derivations in [30] and [74]. Two fundamental assumptions are made in this model: firstly, pseudonoise (PN) spreading codes are used and; secondly, the transmitted sequences of the mobiles are asynchronous to each other (with random time delays within a chip period). In essence, this means that both *intra-cell* and *inter-cell* interfer-

[1]The downlink is also commonly known as the forward link.
[2]The uplink is also commonly known as the reverse link.

ence will exist on the downlink. This model has been chosen in this thesis as it represents the worst-case scenario for the downlink and gives a basis for comparison to other studies upon which the research in this thesis relates to [25, 26, 29, 30].

It should be noted, however, that commercially deployed DS-CDMA systems (e.g. WCDMA/UMTS) use Walsh codes to provide perfect orthogonality for mobiles (sharing the same cell) on the downlink [45]. This equates to no *intra-cell* interference on the downlink (assuming that there is little time dispersion in the channel, which is the case in indoor/outdoor environments where base stations and mobiles are located relatively close together). In this case, it has been found that the downlink system performance estimates are *not significantly different* from those obtained with the model used in this thesis (which assumes that intra-cell interference exists on the downlink due to non-orthogonalities between the mobiles' spreading codes).[3]

Single cell downlink DS-CDMA system performance

On the downlink, the purpose of a mobile is to detect its own signal in the presence of interference from signals transmitted by base stations to other mobiles. A seminal evaluation of DS-CDMA performance was presented in [74] and analyses a system that has K mobiles within a single cell. The result of this derivation is widely used in wireless communications research today.

The signal transmitted by the single base station to each mobile, $s_k(t)$, is given by

$$s_k(t) = \sqrt{2P} a_k(t) b_k(t) \cos(\omega_c t + \theta_k), \tag{3.1}$$

where k is an identifier for the mobile of interest, P is the signal power, ω_c is the frequency of the carrier, and θ_k represents the phase of the kth mobile's signal. In (3.1), $b_k(t)$ represents the data signal (binary information sequence) for the kth mobile (made up of unit amplitude rectangular pulses of duration T), while $a_k(t)$ represents the spreading code of the kth mobile (made up of unit amplitude rectangular pulses of duration T_c).

The signal received at each individual mobile, k, is actually a summation of the signals for all K mobiles served by the base station. Assuming an asynchronous DS-CDMA system, the received signal, $r(t)$, is given by

$$r(t) = n(t) + \sum_{k=1}^{K} \sqrt{2P} a_k(t - \tau_k) b_k(t - \tau_k) \cos(\omega_c t + \phi_k). \tag{3.2}$$

[3] Inter-cell interference has an extremely dominant influence on downlink system performance because its fading is completely uncorrelated with the desired signal. If intra-cell interference exists on the downlink (as is assumed in the model used in this thesis), it will have a very minor impact on system performance because it fades in unison with the desired signal.

In (3.2), $\phi_k = \theta_k - \omega_c \tau_k$ and $n(t)$ is the background channel noise which is assumed to be an additive white Gaussian noise (AWGN) process with two-sided power spectral density $N_o/2$.

The received signal $r(t)$ is passed through a correlation receiver matched to the spreading code of the mobile of interest. The output from the correlation receiver of the kth mobile is given by

$$Z_k = \int_0^T r(t)\, a_k(t) \cos \omega_c t \, dt. \tag{3.3}$$

Further analysis of the correlation receiver output, Z_k, can be found in [74] where it is shown that Z_k may be decomposed into several terms as

$$Z_k = D_k + N_k + I_k. \tag{3.4}$$

In (3.4), D_k is the desired component, N_k is interference from the AWGN process (this includes thermal noise), and I_k is the interference presented to the kth mobile from the other mobiles.

It is shown in [74] that the signal-to-interference ratio (SIR) for the kth mobile is defined as

$$SIR_k = \frac{\mathrm{E}(D_k)}{[\mathrm{Var}(I_k) + \mathrm{Var}(N_k)]^{1/2}}, \tag{3.5}$$

where $\mathrm{E}(D_k)$ is the expected value of D_k and $\mathrm{Var}(I_k)$ and $\mathrm{Var}(N_k)$ are the variances of I_k and N_k respectively.

The expected value of the desired component D_k is given by

$$\mathbf{E}(D_k) = \sqrt{\frac{P}{2}} T. \tag{3.6}$$

The variance of the AWGN process is given by

$$\mathbf{Var}(N_k) = \frac{1}{4} N_o T, \tag{3.7}$$

while for single path channels it can be shown that the variance of the interference from other mobiles is approximately equal to [74, 75]

$$\mathbf{Var}(I_k) = \frac{PT^2(K-1)}{3N}. \tag{3.8}$$

Therefore for single path channels, the SIR for the kth mobile, SIR_k, is given by [4]

[4] Randomly offset PN codes have a cross-correlation of $\frac{2}{3N}$ and therefore attenuate the interference correspondingly, as evident in the first term of (3.9) [75].

$$SIR_k = \frac{\sqrt{\frac{P}{2}}T}{\left(\frac{PT^2(K-1)}{6N} + \frac{N_oT}{4}\right)^{1/2}} = \left[\frac{2\,(K-1)}{3N} + \frac{N_o}{2E_b}\right]^{-1/2}, \tag{3.9}$$

where E_b is the energy per bit. In (3.8) and (3.9), N is the processing gain, which is the ratio of the time period of the data sequence to that of the spreading code sequence.

Multiple cell downlink DS-CDMA performance

A performance evaluation technique to extend (3.9) to account for interference presented from multiple cells is outlined in [30]. Assuming that the signal from each base station arrives at the mobile asynchronously and the system is interference limited (i.e. background noise due to receiver imperfections is minimal), the SIR for the kth mobile is given by [30]

$$SIR_k = \frac{1}{\sqrt{\frac{2}{3N}\,(K-1+\beta_k)}}, \tag{3.10}$$

where β_k is the ratio of the total downlink inter-cell interference power to the power of the desired signal. For example, assuming that there are J base stations with unique identifiers $j = 1, 2, 3...J$, the value of β_k for a mobile served by the base station $j = 1$ is given by

$$\beta_k = \frac{P_2 + P_3 + ... + P_J}{P_1}, \tag{3.11}$$

where P_j is the received power of the signal from the jth base station and P_1 is the power of the desired signal from the base station identified by $j = 1$. It should be noted that the received powers of the signals from each of the base stations undergoes independent fading, and that the total power transmitted by each base station increases in proportion to the number of mobiles it serves.

A given transmission from an individual base station is comprised of the waveforms of several mobiles that have been combined together. Therefore, in a given base-to-mobile link, the waveforms will fade in unison with each other because they traverse the same path [30]. It is assumed that non-orthogonalities exist between the spreading codes for these waveforms, which causes *intra-cell* interference. The intra-cell interference is represented by the term $K - 1$ in (3.10).

Assuming that the multiple access interference is approximately Gaussian-distributed, the SIR of the signal received by a mobile k may be mapped to a bit error rate (BER) using the complementary Gauss probability integral, i.e. [26]

$$BER_k = \frac{1}{\sqrt{2\pi}} \int_{SIR_k}^{\infty} \exp\left(\frac{-y^2}{2}\right) dy. \tag{3.12}$$

If BER_k in (3.12) is above a pre-defined threshold[5] for adequate reception (assumed to be 0.02 in this thesis), then an outage will occur. The assumption that the multiple access interference is Gaussian distributed is valid for a large number of interferers, for large spreading sequences and when the interference emanates from a sufficiently large number of independent components.

If there are only a small number of mobiles in the system, (3.12) has been shown to underestimate the BER. An improved Gaussian approximation has been developed by Morrow and Lehnert [76] to yield more accurate BER predictions. However, this technique requires significantly more computational effort than the standard Gaussian approximation used to derive (3.12). In this thesis sufficiently long spreading codes and a large number of independent interfering components are assumed and for this reason the standard Gaussian approximation is considered to be sufficiently accurate.

3.2.2 Uplink DS-CDMA system performance

On the uplink of a DS-CDMA system, the base station has to decode the signals of mobiles within its cell in the presence of interference presented from other mobiles (located both within and outside its cell). The mobiles' signals are received at the base station asynchronously and with different time delays. Using a similar derivation to that in Section 3.2.1, it may be shown that the instantaneous uplink SIR for a mobile k is given by [30]

$$SIR_k = \frac{1}{\sqrt{\frac{2}{3N}\left(\frac{\psi_k+\beta_k}{\phi_k}\right)}}, \tag{3.13}$$

where ψ_k is the ratio of the summation of the interference from mobiles connected to the base station of interest (i.e. intra-cell interference), β_k is the ratio of the summation of the interference from mobiles connected to other base stations (i.e. inter-cell interference) and ϕ_k is the instantaneous signal power of the desired mobile k. Similar to the downlink case, the complementary Gauss probability integral (described by (3.12)) can be used to determine the BER based on the instantaneous uplink SIR.

The uplinks of DS-CDMA systems potentially suffer from the *near-far effect* which is the phenomenon whereby mobiles close to the base station have stronger received signals than those further away. As a result, mobiles close to the base station have better performance than those further away. This is undesirable because there is a lack of fairness in performance for mobiles across the system. In conventional systems, uplink power control attempts to ameliorate the near-far effect by allocating transmit powers to the mobiles so

[5]The chosen BER of 0.02 would be the upper limit of tolerable error rates in wireless communications networks.

that their signals are received at the base station with the same power; i.e. the intra-cell interference term ψ_k in (3.13) will then be approximately the same for all k. In reality, however, perfect power control is not possible due to inevitable signalling delays between the base station and mobiles. In this thesis it is assumed that power control is sufficiently accurate so that the mobiles adjust their transmit power to ensure that their mean received signal strengths at the base station are the same. However, short-term variations due to fading cannot be eliminated and are assumed to cause differences in the mobiles' instantaneous received signal strengths at the base station.

3.3 Applicability to propagation environments

In Chapter 2, it was shown that the propagation environment can have a significant influence on signals transmitted between base stations and mobiles. For this reason, it is important for radio frequency engineers to understand the influence of the propagation environment on DS-CDMA system performance and thereby develop strategies for optimal system deployment.

In DS-CDMA systems, all mobiles share the same bandwidth. Therefore, adjacent cells present interference to each other. Due to the phenomenon of cell breathing, the coverage area of a cell might vary depending on the number of mobiles in the system and for this reason radio frequency engineers must tradeoff capacity with coverage [2,45]. To increase system capacity, new cells must be introduced to the network and the configurations of surrounding cells (e.g. antenna downtilt angles and transmitter power levels) must be optimised. The integration of a new cell is particularly challenging, as it should be ensured that there is minimal spillage to adjacent cells while also ensuring that there is seamless coverage for mobile users.

The key challenge for engineers in designing DS-CDMA systems is to identify the dominant sources of interference and minimise their impact on system performance. Levels of interference are strongly influenced by the surrounding propagation environment and the system deployment strategy. Based on the material presented in Chapter 2, this section highlights the major propagation-related factors influencing DS-CDMA performance and deployment in outdoor, indoor and mixed indoor/outdoor environments. Additionally, the differences in system design philosophies for the various environments are discussed.

3.3.1 Outdoor environments

Outdoor environments can vary from being sparse rural to densely populated urban. The type of terrain and clutter associated with the outdoor environment influences the deployment strategy used. For example, in sparse rural areas without significant propagation

obstacles, a single antenna can provide coverage to a radius of a few kilometres assuming line-of-sight. To the contrary in dense urban areas, closely spaced obstacles such as buildings present a challenging propagation environment with significantly more propagation loss and therefore a single antenna might only provide a coverage radius of as low as 100 metres.

In outdoor environments the placement of base stations to provide coverage is essentially a *two-dimensional* problem as base stations and mobiles are usually located at 'ground' level and are displaced from each other horizontally. Figure 3.1 shows the likely desired and interfering signals on the downlink and uplink of an idealised uniform macrocellular DS-CDMA system. On the downlink, the purpose of the mobile is to detect its own desired signal in the presence of interference emanating from its own base station (*intra-cell* interference) and other base stations (*inter-cell* interference). Inter-cell interference may be minimised by carefully choosing base station locations and optimising various system parameters (e.g. antenna downtilt angles). On the uplink, the base station must decode the signal of the desired mobile in the presence of interference emanating from several other mobiles within the same cell (*intra-cell* interference) and other cells (*inter-cell* interference).

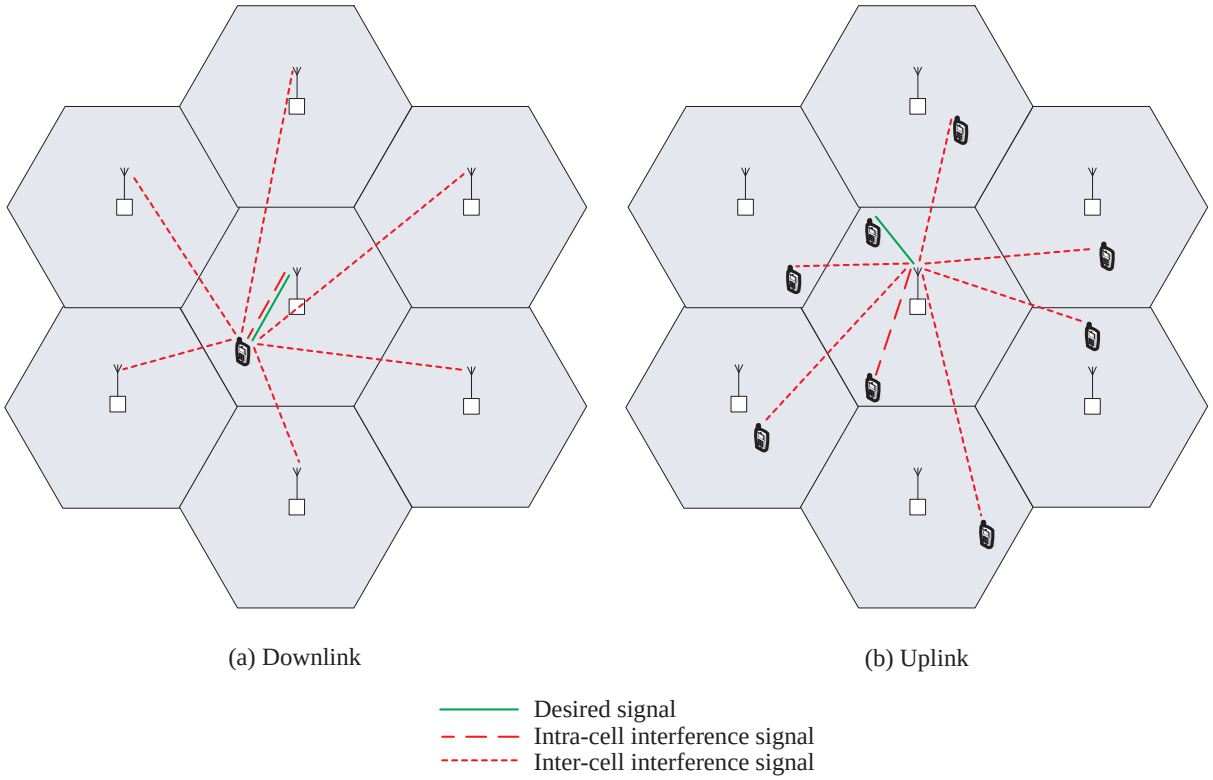

Figure 3.1: Desired and interfering signals on the downlink and uplink for an idealised uniform macrocellular DS-CDMA system.

3.3.2 Indoor environments

Examples of indoor environments include office blocks, apartment buildings and shopping malls. There are both similarities and differences in the construction and architectural features of indoor environments. For example, 'traditional' buildings generally have a steel-reinforced concrete framework and transparent windows on the outside with partitions indoors, whereas contemporary buildings often have tinted windows on the outside with open plan offices indoors. These features are likely to significantly influence the propagation of radio signals and therefore the deployment strategies that yield optimal performance.

To demonstrate the implications of radio propagation on indoor system performance, Figure 3.2 shows typical signal paths on the downlink and uplink of a hypothetical three-level indoor DS-CDMA system. With respect to the middle level of the building, it is clear that interference emanates from not only the same level but also from the levels above and below. The indoor DS-CDMA system shown in Figure 3.2 differs from outdoor DS-CDMA systems in that the base stations and mobiles are in a *three-dimensional* configuration. Additionally, obstacles such as internal concrete cores, walls and partitions are likely to cause significant variations in received signal strength within much shorter distances than those observed in outdoor environments [26].

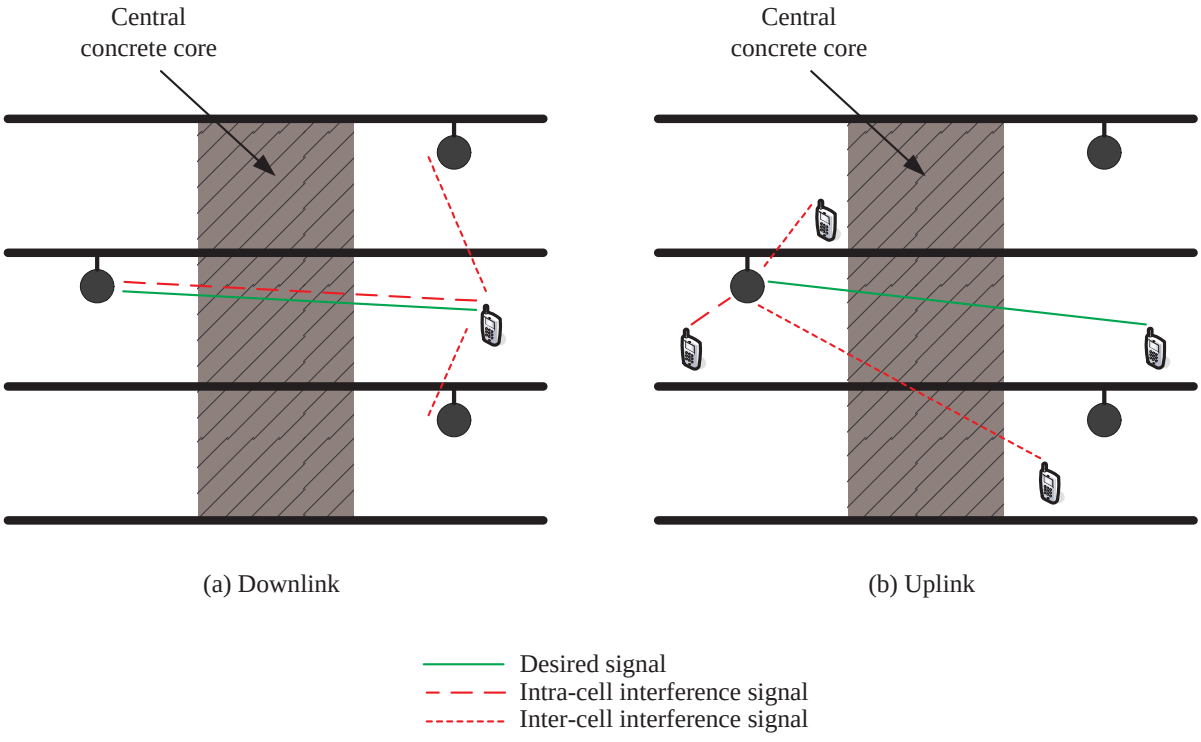

Figure 3.2: Desired and interfering signals on the downlink and uplink for a three-dimensional indoor DS-CDMA system.

In Figure 3.2, the central concrete core is likely to significantly attenuate the transmitted signals. The floors separating the levels and internal partitions are also likely to significantly attenuate the transmitted signals. The floor attenuations are of benefit to system performance as they reduce *inter-cell* interference from other floors both on the downlink and the uplink [14, 25].

On the downlink of the system shown in Figure 3.2, the desired signal and intra-cell interference signal are likely to undergo significant attenuation due to the central concrete core. However, the inter-cell interference is likely to be high due to the close proximity of the mobile to the base stations on the levels above and below it. Clearly, if the base station positions are modified, this serves to change the levels of downlink intra- and inter-cell interference. This in turn influences the SIR performance for mobiles across the system.

On the uplink of the system shown in Figure 3.2, power control ensures that the desired mobile's signal (shown in green) is received at the base station with approximately the same power as the intra-cell interference signal. The total inter-cell interference presented to the base station on the middle level is dependent on the locations of both the base stations and mobiles on other levels. For example, the mobile on the top level is likely to have a high transmit power due to the long separation distance to its base station and the presence of the central concrete core. Therefore, it presents high levels of inter-cell interference to the base station on the middle level. However, the mobile on the lowest level is likely to present very little interference as it will be allocated a low transmit power due to its close proximity to the base station serving it.

It is clear from the above descriptions of the downlink and uplink of the hypothetical DS-CDMA system that system performance is heavily dependent on the three-dimensional positions of the base stations and the relative locations of the mobiles.

3.3.3 Mixed indoor/outdoor environments

In mixed indoor/outdoor environments base stations are likely to be deployed indoors on one or more levels of a building as well as in other buildings nearby or outdoors in the near vicinity of the building. A comparison of the downlink and the uplink of a hypothetical indoor/outdoor DS-CDMA system is shown in Figure 3.3. In this system three base stations are located in a building and two base stations are located outdoors.

For the downlink, the mobile on the middle floor must decode its own signal in the presence of inter-cell interference emanating from floors above and below it, as well as inter-cell interference emanating from the outdoor base stations. For the uplink, the base station must decode the signal from the desired mobile on the middle floor in the presence of intra- and inter-cell interference emanating from both mobiles within the building as well as inter-cell interference emanating from mobiles located outdoors.

The locations of the outdoor base stations and mobiles are likely to influence the performance experienced by mobiles located indoors. This in turn, influences the indoor deployment strategy that yields optimal performance.

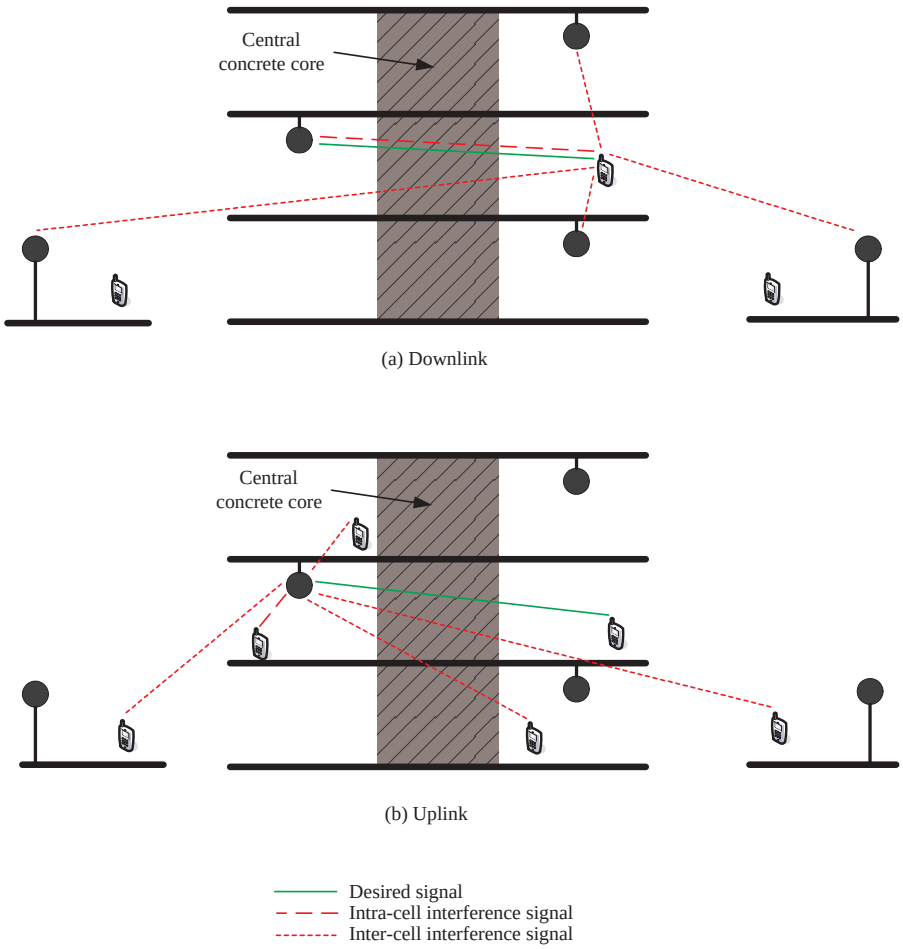

Figure 3.3: Desired and interfering signals on the downlink and uplink for a hypothetical indoor/outdoor DS-CDMA system.

3.4 An overview of studies investigating DS-CDMA system performance

Several previous studies have investigated DS-CDMA performance in a variety of propagation environments. The techniques to assess system performance include analytical [30,74] and statistical (simulation) [25,26,77,78] approaches. Section 3.2 presented an analytical model to estimate DS-CDMA system performance developed by Pursley [74]. This model can be used to estimate the downlink and uplink outage probabilities for a single cell DS-CDMA system assuming that the interference is Gaussian distributed. Milstein and Rappaport [30] have extended this model to estimate outage probabilities for multiple-

cell DS-CDMA systems. These techniques have since been the basis of the many studies investigating DS-CDMA performance.

The purpose of this thesis is to investigate the deployment and performance of indoor/outdoor DS-CDMA systems. Of particular importance in this investigation is the impact of outdoor interference on indoor system deployment. The majority of previous studies have focused on systems that are deployed in *either* indoor [20–27] *or* outdoor environments [2, 28–30]. Due to the growing need to integrate indoor and outdoor DS-CDMA systems, there are also a number of investigations that have considered DS-CDMA system performance in mixed indoor/outdoor environments, outlined below.

In [77], an interference analysis is conducted for dedicated indoor DS-CDMA systems assuming that interference emanates from outdoors. This investigation largely focuses on the impact of soft handovers and levels of outdoor interference (for both line-of-sight and non line-of-sight cases) on indoor system capacity. It is based on path loss propagation models such as the Walfisch-Ikegami model (for propagation outdoors) and a multiple wall model (for propagation indoors) [79, 80].

The effect of indoor traffic hotspots on overall wireless network performance is studied in [78]. In this study, an idealised uniform macrocellular network is assumed with hotspots at various locations (e.g. within a macrocell or at the border between two macrocells). This study is also based on using propagation models and focuses on the impact of issues such as the hotspot load and the hotspot location on network performance. In [81], an evaluation of the impact of soft handover and co-channel interference (e.g. leakage from indoors to outdoors) on the design of indoor DS-CDMA systems is evaluated. This study is based on both a theoretical analysis and measurements conducted in an operating DS-CDMA network.

The limited number of studies discussed above largely focus on the impact of issues such as soft handover, antenna downtilt angles, sectorisation and pilot power on DS-CDMA system performance. Additionally, for the vast majority of studies the propagation channel is generally modelled using basic indoor and outdoor-to-indoor propagation models that use an attenuation factor to account for outdoor-to-indoor penetration loss. To the author's knowledge, prior to the research conducted for this thesis, there have been no studies investigating the influence of outdoor interference on the optimal base station deployment strategies for indoor DS-CDMA systems.

3.5 Signal correlation

Previous research has shown that the level of correlation between desired and interfering signals can have significant implications on system performance [25, 26, 82–84]. As a result, if this phenomenon is accounted for during system design, significant improvements

in performance can be realised. The downlink performance of a DS-CDMA system is ultimately dependent on the SIR of the received signal at the mobile. Variations in the mean received strengths of the desired and interfering signals (i.e. ignoring short-term variations due to fading) occur across the system and are directly related to the relative locations of the mobiles and base stations. If a desired signal is strongly correlated with one or more interfering signals, this is likely to yield appreciable performance gains assuming that there is a sufficient margin between the mean received strengths of the two signals [25, 26]. To the contrary, a negative or small correlation between desired and interfering signals is likely to result in reduced performance than if positive correlation was present. This is demonstrated in Figure 3.4, which compares the mean received desired and interfering signal strengths assuming (a) completely positively correlated and (b) completely negatively correlated cases. It is clearly evident from this figure that positive correlation ensures that the SIR margin is maintained across the coverage area, whereas negative correlation results in variations in the SIR margin, which is likely to cause poorer performance.

In operational cellular systems, a high correlation occurs due to commonality in propagation paths encountered by the desired and interfering signals. Assuming that measured mean path loss data is available across a geographic area, the degree of correlation between two signals, i and j, can be quantified using a correlation coefficient, ρ, which is defined as [25]

$$\rho = \frac{\sum_{k=1}^{K} \left(PL_{ik} - \overline{PL_{iK}}\right)\left(PL_{jk} - \overline{PL_{jK}}\right)}{\sqrt{\sum_{k=1}^{K} \left(PL_{ik} - \overline{PL_{iK}}\right)^2}\sqrt{\sum_{k=1}^{K} \left(PL_{jk} - \overline{PL_{jK}}\right)^2}}. \tag{3.14}$$

In (3.14), the measurement locations across the geographic area are numbered $k = 1$ to K, PL_{ik} is the mean path loss from transmitter i to measurement location k and $\overline{PL_{iK}}$ is the mean of the mean path losses from transmitter i to the K measurement locations across the geographic area. Similarly, PL_{jk} is the mean path loss from transmitter j to measurement location k and $\overline{PL_{jK}}$ is the mean of the mean path losses from transmitter j to the K measurement locations across the geographic area.

The correlation coefficient, ρ, can vary from $\rho = -1$ to $\rho = 1$. A very high correlation coefficient (i.e. if ρ is close to 1) is observed between desired and interfering signals when they are strongly correlated with each other. If $\rho = 0$, then the desired and interfering signals are completely uncorrelated with each other. If a strongly negative correlation exists between a desired and interfering signal (i.e. if ρ is close to -1), this indicates that if the desired signal is strong then it is highly likely that the interfering signal will be weak (and vice versa).

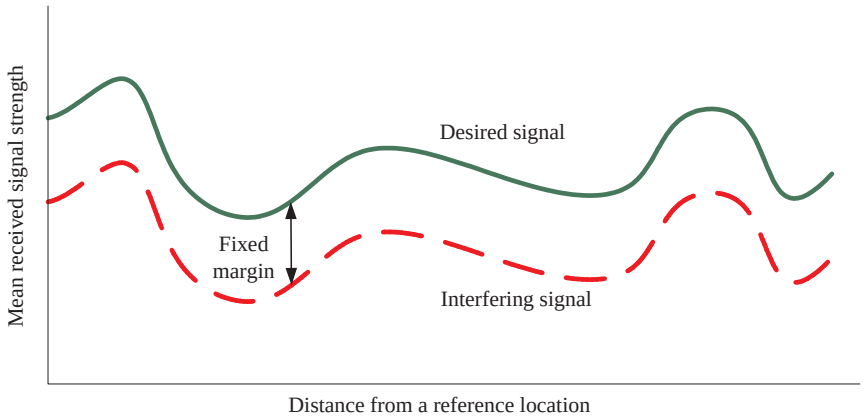

(a) Positive correlation

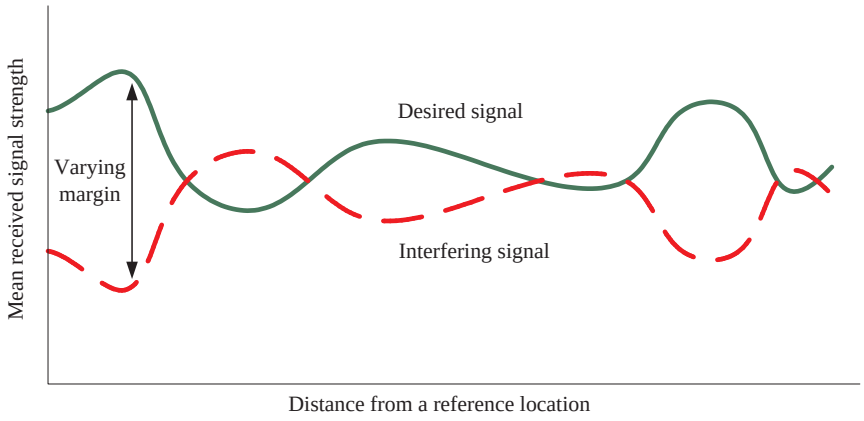

(b) Negative correlation

Figure 3.4: Positive and negative correlation between desired and interfering signals.

The level of signal correlation has been observed to vary depending on the propagation environment. The signal correlations observed in outdoor, indoor and mixed indoor/outdoor environments are now discussed.

Outdoor environments

Due to the two-dimensional layout of outdoor DS-CDMA systems, there is very little likelihood of obtaining strongly positive or strongly negative correlation coefficients between desired and interfering signals. Previous research based on outdoor propagation measurements have shown that the correlation coefficients in outdoor environments typically vary from -0.3 to 0.4 [82–84]. These relatively low levels of correlation are unlikely to influence the performance of a typical 'uniform' two-dimensional macrocellular system with respect to completely uncorrelated cases.

Indoor environments

An experimental study conducted in [25,26] yielded correlation coefficients as high as 0.96 and as low as -0.54 in multi-floor indoor environments. In [25, 26], it is also shown that placing indoor base stations to yield high correlation coefficients (specifically deploying vertically aligned base stations) improves system performance, while negative correlation coefficients (specifically deploying vertically offset base stations) are detrimental.

To explain the correlation behaviour in indoor environments, compare the downlink of the vertically aligned configuration and that of the vertically offset configuration shown in Figure 3.5. In the vertically aligned configuration the desired signal received by the mobile has a similar propagation path as the interfering signals from the base stations on the floors above and below the mobile. Due to distance-dependent propagation loss and the shadowing caused by the central concrete core, the desired and interfering signals encounter similar mean path losses. This results in high levels of correlation (as much as 0.96) between the desired and interfering signals.

By contrast, in the vertically offset configuration, the desired signal received by the mobile is negatively correlated (as low as -0.54) with the interfering signals from the base stations on floors above and below the mobile. This causes increased variations in the SIR across the coverage area, and as a result the average downlink outage probability is higher.

On the uplink, the vertically aligned configuration has also been observed to outperform the vertically offset configuration. However, assuming the presence of power control on the uplink, the differences in performance observed between the configurations are not as pronounced as those on the downlink [25, 26].

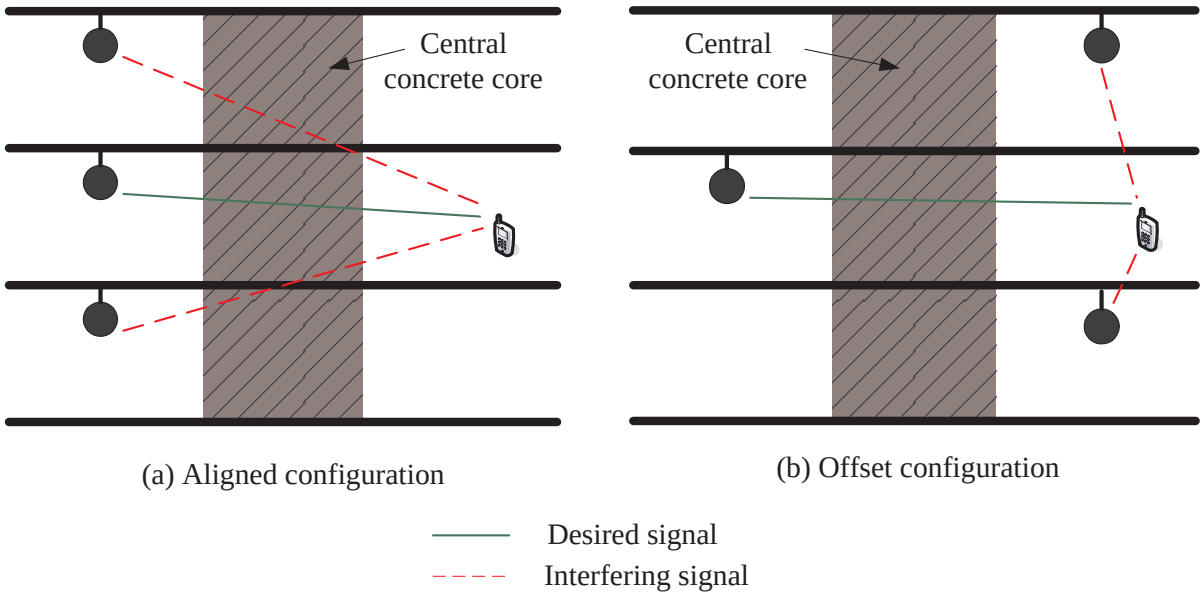

Figure 3.5: Comparison of aligned and offset configurations of indoor DS-CDMA systems.

Mixed indoor/outdoor environments

In the case of systems with both outdoor and indoor base stations (i.e. mixed indoor/outdoor systems), there has been no previous research to quantify signal correlation. This information could be useful in deploying future wireless systems in which macro/microcellular systems must coexist with picocellular networks and is a contribution of this thesis, as is described in Chapters 4 and 5.

3.6 Summary

This chapter has presented a simple technique for evaluating the performance of both the downlink and uplink of a DS-CDMA system using parameters such as the processing gain, voice activity factor, and the received powers for the mobiles sharing the channel. The key differences between the downlink and uplink of a DS-CDMA system have been discussed. It has been shown that DS-CDMA system performance is strongly related to the propagation environment and therefore base stations can be deployed to optimise performance.

An in-depth overview of previous studies evaluating DS-CDMA system performance has been provided to demonstrate the contributions of this thesis. Most of the previous studies in the literature use simple propagation models and mainly focus on the performance of *either* outdoor DS-CDMA systems *or* indoor DS-CDMA systems. This thesis is unique in that it considers the performance of mixed *indoor/outdoor* DS-CDMA systems and extends this in subsequent chapters to include the implementation of multiuser detection.

Chapter 4 discusses a study to acquire measured propagation data in mixed indoor/outdoor environments, while Chapter 5 uses this data to assess conventional DS-CDMA system performance for various deployment strategies based on a simulation model developed using the material presented in this chapter.

Chapter 4

Propagation measurement study of mixed indoor/outdoor environments

4.1 Introduction

Chapters 2 and 3 discussed the propagation phenomena that exist in mixed indoor/outdoor environments and reviewed previous research showing that these phenomena can significantly influence the performance of DS-CDMA systems. In Chapter 2, it was shown that several propagation models have been developed to predict signal strength in various environments (e.g. indoor and mixed indoor/outdoor environments). The predictions of these models have been compared with measured propagation data obtained from a plethora of propagation measurement campaigns. However, despite this extensive research the propagation models developed to date have both limited accuracy and limited applicability to a wide range of environments. Additionally propagation data collected in previous campaigns are not widely available. For these reasons, it was decided to conduct three propagation measurement campaigns to obtain measured propagation data which could be used in the DS-CDMA system performance estimation test bed discussed in Chapter 5. This chapter details these propagation measurement campaigns (conducted in two different mixed indoor/outdoor environments) in Section 4.2. Key propagation results are presented in Section 4.3. A summary of this chapter is presented in Section 4.4.

4.2 Propagation measurements

The purpose of conducting the propagation measurements was to acquire mean path loss data for several propagation paths between combinations of transmitters and receivers located both indoors and outdoors. This involved deploying transmitters at strategic indoor and outdoor locations and measuring the mean received signal strength at various

indoor locations using a mobile test receiver and data acquisition system. The outcome of each measurement campaign was a database of mean path losses calculated using the measured mean received signal strength data.

Section 4.2.1 describes the two propagation environments in which the three measurement campaigns were conducted, while Section 4.2.2 presents the transmitter and receiver locations chosen for each measurement campaign. Finally, Section 4.2.3 gives an overview of the measurement equipment used and the strategy with which the receiver locations were selected.

4.2.1 Propagation environments

The propagation measurements were conducted in two mixed indoor/outdoor environments located at The University of Auckland:

- **Environment E1** – School of Engineering buildings and
- **Environment E2** – Functions and Science buildings.

These environments were chosen because they consist of buildings that are typical of many office buildings of contemporary architecture. All the buildings in both Environments E1 and E2 are constructed from steel-reinforced concrete and have transparent windows on the outside. Additionally, all but one of the buildings have layouts with internal partitions separating offices. However, there are also some important architectural differences between the buildings in each environment that are likely to cause differences in radio propagation behaviour. For example, Environment E1 consists of a building with a centrally located steel-reinforced concrete core while in Environment E2 none of the buildings have this feature. Environments E1 and E2 are described in Sections 4.2.1.1 and 4.2.1.2 respectively, while a summary of the two environments is in Section 4.2.1.3.

4.2.1.1 Environment E1 – School of Engineering buildings

The School of Engineering buildings are comprised of three buildings: the Tower Block, Library Block and Lecture Theatre Block. Figure 4.1 is a three-dimensional drawing of these buildings and Figure 4.2 is a photograph of the buildings viewed from a similar angle to that in Figure 4.1.

The Tower Block is typical of many office buildings of conventional architecture and is constructed from steel-reinforced concrete. Its horizontal dimensions are 18.5m by 18.5m. It has twelve levels (two of which are below street level) and a central steel-reinforced concrete core which houses two lifts, a stairwell and services, surrounded by a square-shaped corridor and offices. Floors separating each level are made from steel-reinforced

concrete. Windows on the outside of the building are transparent and internal partitions separating the offices are made from drywall (also called plasterboard). Fascia beams can be seen on the outside of the building separating each level. The separation distance between the levels in the Tower Block is 3 metres. A layout of Level 8 of the Tower Block is shown in Figure 4.3. This layout is typical of the majority of the levels in the Tower Block.

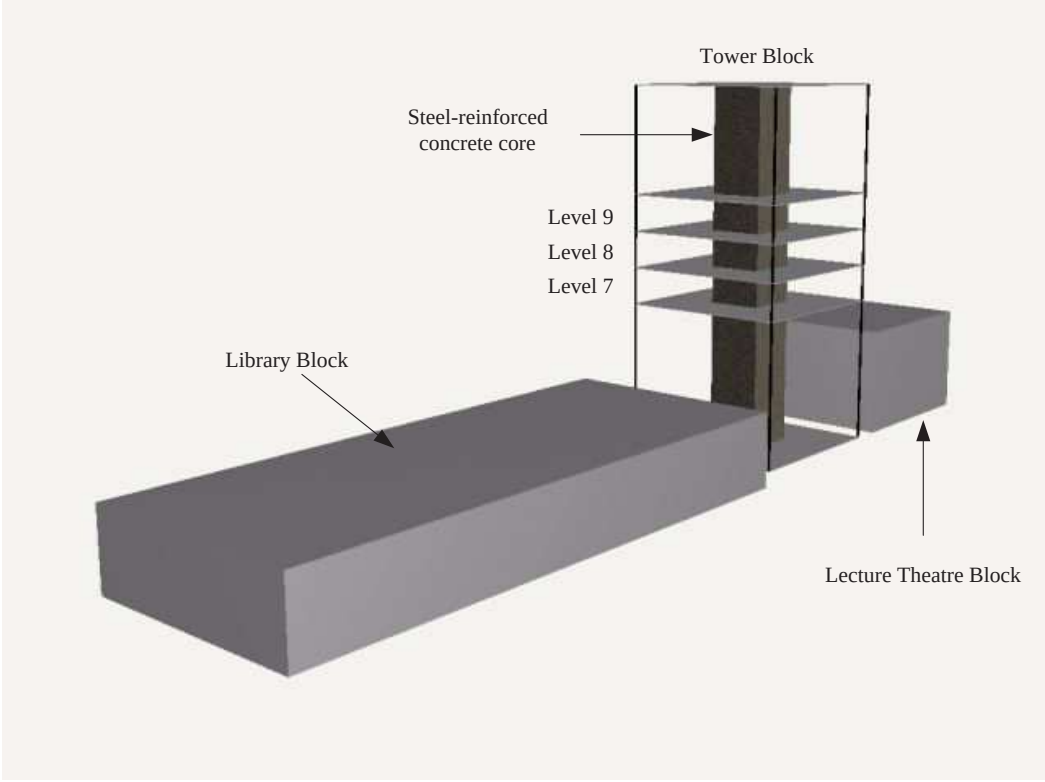

Figure 4.1: Three-dimensional view of Environment E1 (School of Engineering buildings).

The Library and Lecture Theatre Blocks are located on either side of the Tower Block, and are each separated from the Tower Block by approximately 10 metres. The Library Block is of horizontal dimensions 60 metres by 25 metres and its roof is aligned to Level 5 of the Tower Block. The Lecture Theatre Block has horizontal dimensions 18.5 metres by 18.5 metres and its roof is aligned to Level 6 of the Tower Block. Both the Library and Lecture Theatre Blocks are constructed from steel-reinforced concrete. The internal features of the Library and Lecture Theatre Blocks are not of interest in this thesis as measurements were not made inside these buildings nor transmitters deployed inside them.

4.2.1.2 Environment E2 – Functions and Science buildings

The Functions and Science buildings are located adjacent to each other as shown in the plan in Figure 4.4. An open area courtyard separates the buildings by 20 metres. The

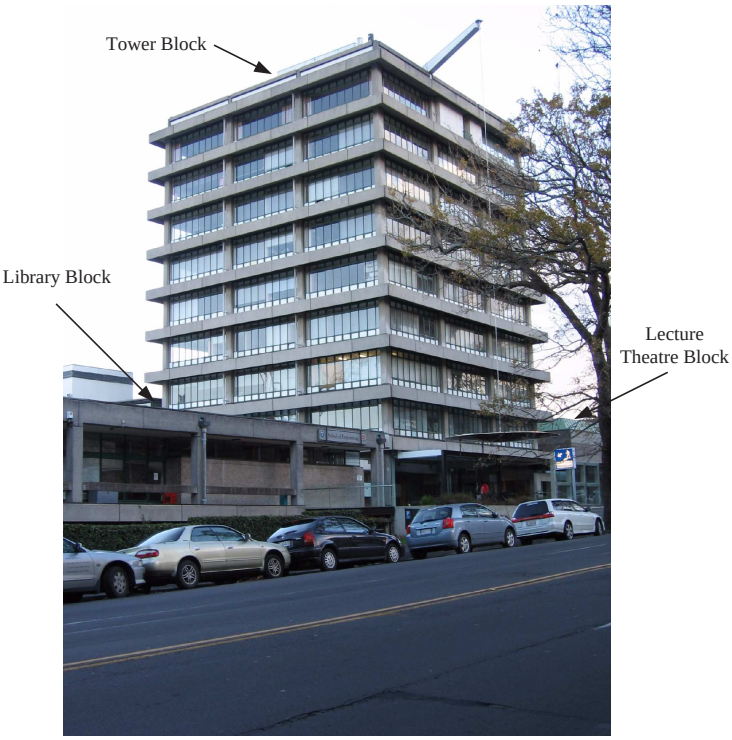

Figure 4.2: Photograph of Environment E1 (School of Engineering buildings).

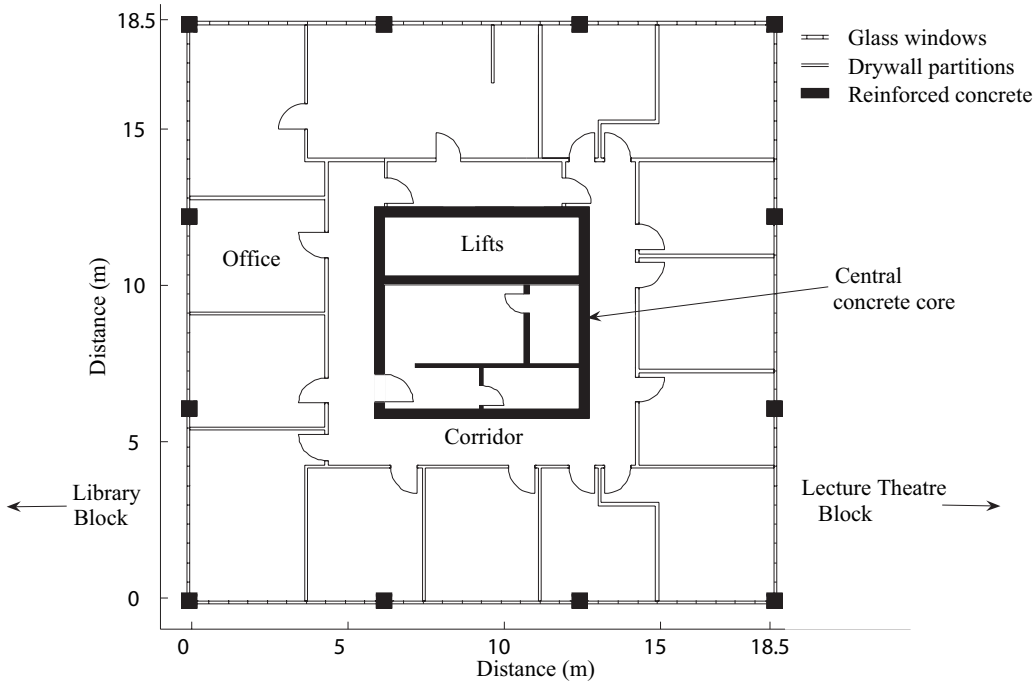

Figure 4.3: Layout of Level 8 of the Tower Block in Environment E1.

outer walls of both buildings are constructed from steel-reinforced concrete, with transparent windows on the outside of each level. In both buildings, the floors separating the levels are constructed from steel-reinforced concrete. Figures 4.5 and 4.6 are photographs of the Functions and Science buildings respectively.

The Functions building has three levels and is of horizontal dimensions 15 metres by 30 metres. The layout of Level 2 of the Functions building is shown in Figure 4.7. It is noticeable that this level is mainly an open space with the exception of a few concrete pillars and a timber serving counter.

The Science building also has three levels and is of horizontal dimensions 25 metres by 38 metres. The layout of Level 2 of the Science building is shown in Figure 4.8. This level mainly consists of offices separated by drywall partitions. The exception to this is the centrally located glass-enclosed open-plan office space which has three glass partitions (see Figure 4.8).

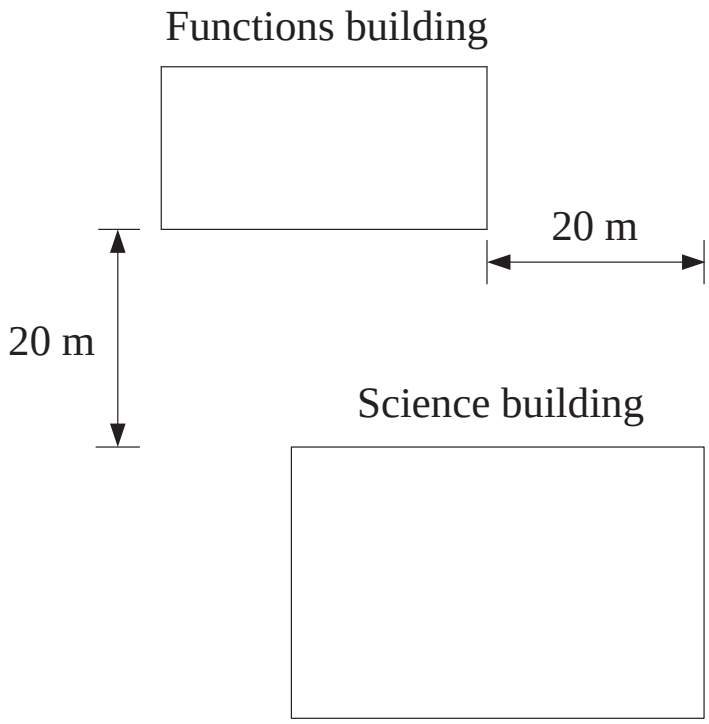

Figure 4.4: Plan of the Functions and Science buildings.

4.2.1.3 Summary of propagation environments

Figure 4.9 is a scale drawing of the horizontal dimensions of Environments E1 and E2. All the buildings shown are constructed from steel-reinforced concrete and have transparent external windows. The major difference between the two environments is that the Tower Block in Environment E1 has a central steel-reinforced concrete core while the buildings in Environment E2 do not have this feature.

Figure 4.5: Photograph of the Functions building in Environment E2.

Figure 4.6: Photograph of the Science building in Environment E2.

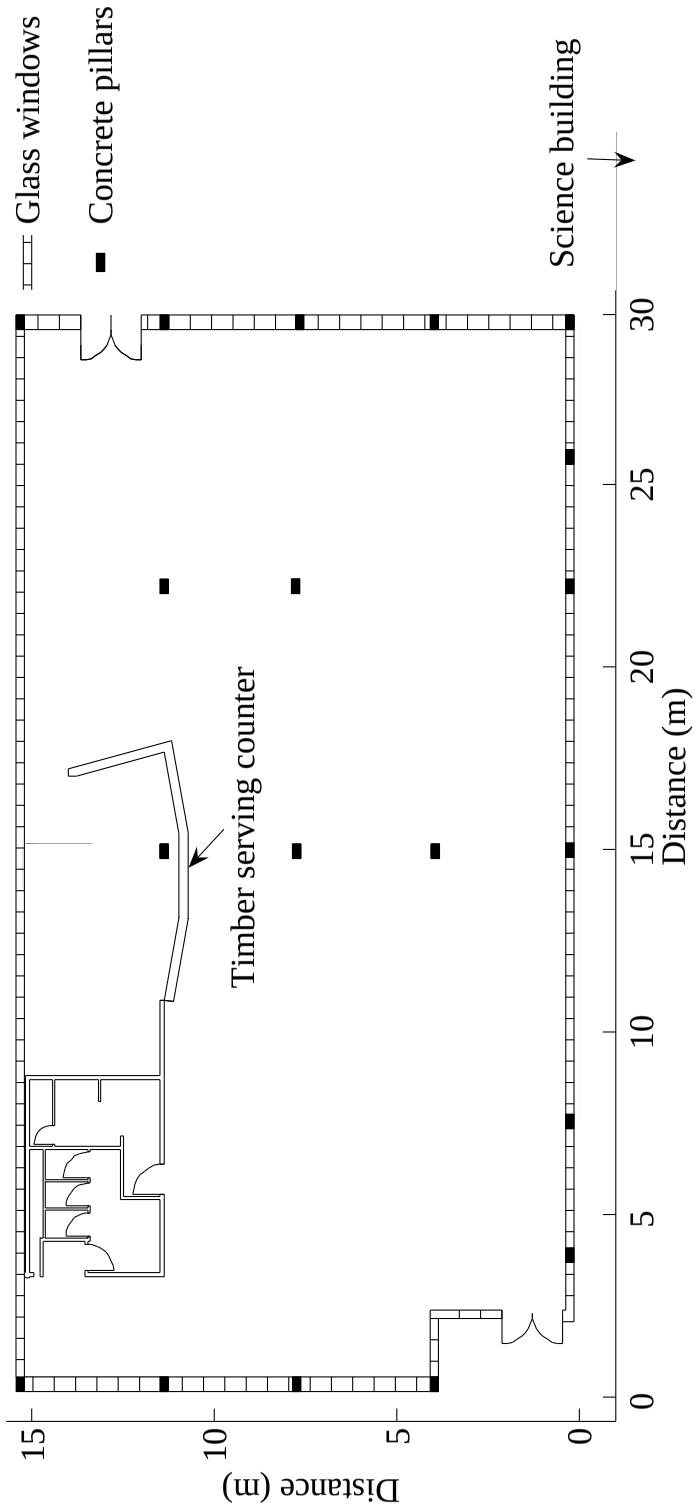

Figure 4.7: Layout of Level 2 of the Functions building.

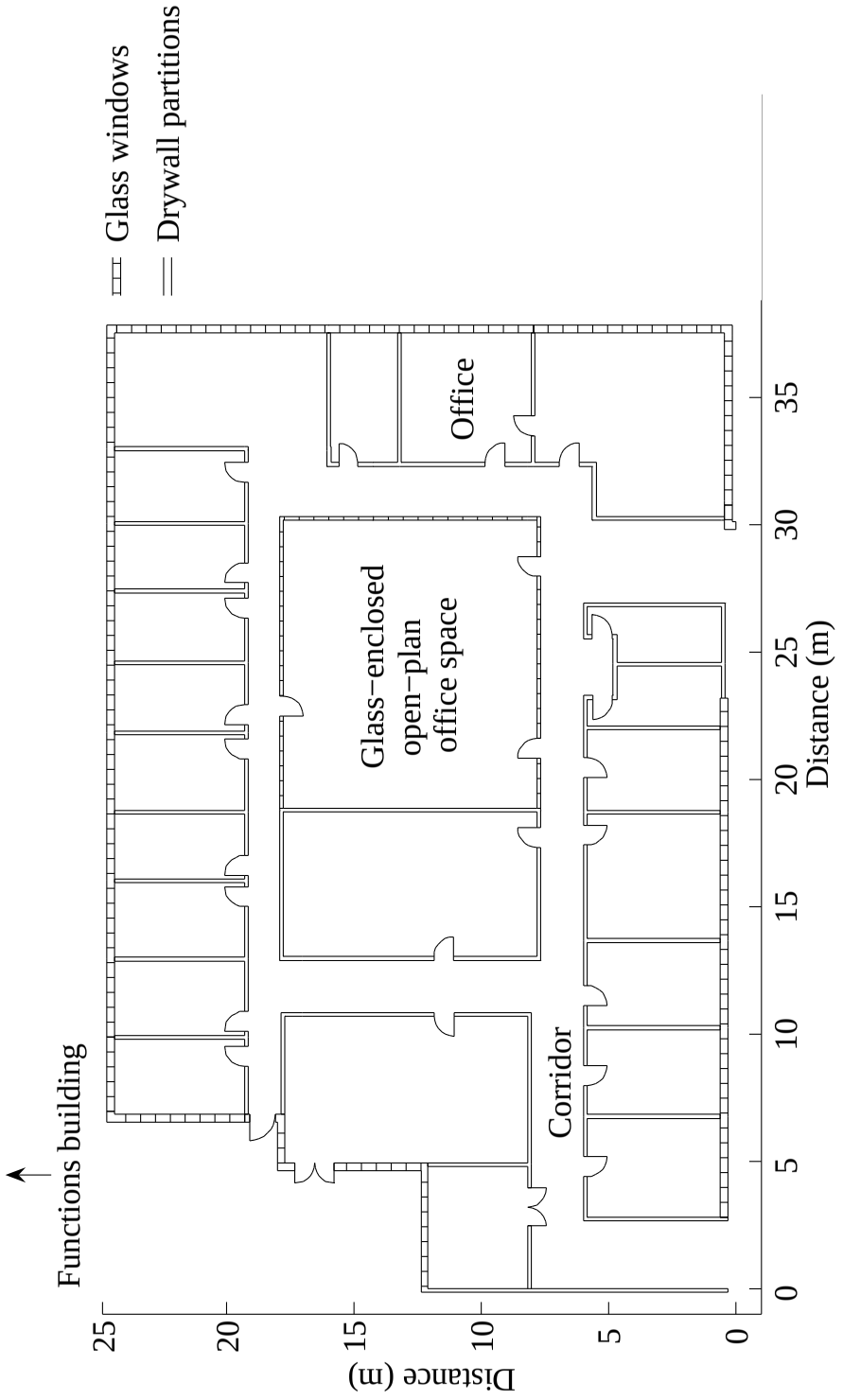

Figure 4.8: Layout of Level 2 of the Science building.

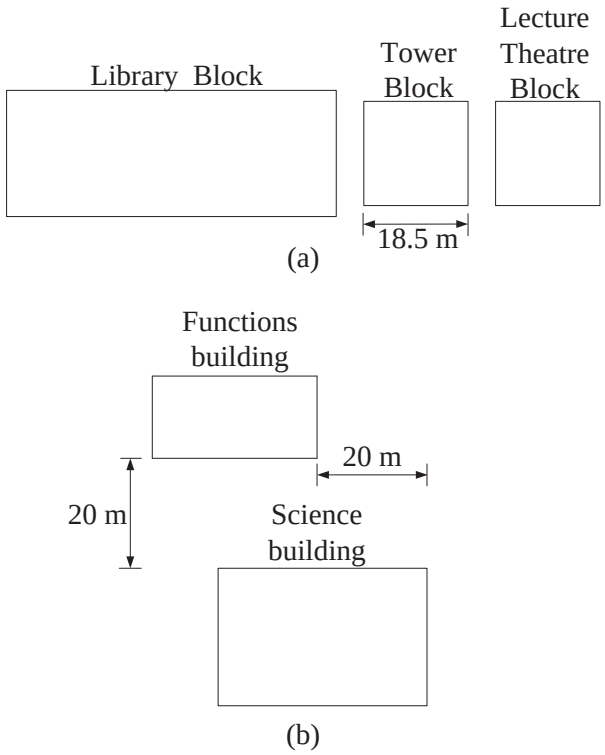

Figure 4.9: Scale drawing of (a) Environment E1 and (b) Environment E2.

4.2.2 Propagation measurement campaigns

Three propagation measurement campaigns were conducted in the two propagation environments described in Section 4.2.1. The locations of the transmitters and receivers in each campaign were chosen to investigate a variety of deployment scenarios.

- **Propagation Measurement Campaign A (PM A) – Single floor indoor system coexisting with outdoor system.**
  This study was conducted in Environment E1. Transmitters were deployed on a *single level* of the Tower Block as well as outdoors on the roofs of *both* the Library Block and Lecture Theatre Block. Measurements were made at various locations on the level on which the indoor transmitters were deployed.

- **Propagation Measurement Campaign B (PM B) – Multi-floor indoor system coexisting with outdoor system.**
  This study was also conducted in Environment E1. Transmitters were deployed on *multiple levels* of the Tower Block and outdoors on the roof of the Library Block. Measurements of the mean received signal strength were made at various locations on a single level inside the Tower Block.

- **Propagation Measurement Campaign C (PM C) – Adjacent indoor systems.**
  This study was conducted in Environment E2. Transmitters were deployed on a *single* level of each of the Functions and Science buildings. Measurements were conducted in *both* the Functions and Science buildings.

While transmitters were deployed both indoors and outdoors in PM A and PM B, measurements of the mean received signal strength were only conducted indoors.

4.2.2.1 Propagation Measurement Campaign A (PM A)

In PM A, six transmitters were deployed on Level 8 of the Tower Block, four transmitters were deployed on the roof of the Library Block and two transmitters were deployed on the roof of the Lecture Theatre Block. A three-dimensional view of the buildings with the transmitter locations is shown in Figure 4.10, while a plan view is shown in Figure 4.11. Transmitters located indoors on Level 8 of the Tower Block are labeled I_1 to I_6, transmitters located on the Library Block are labeled O_1 to O_4, and transmitters on the Lecture Theatre Block are labeled O_5 and O_6. Transmitter O_3, located on the roof of the Library Block, was positioned 3 metres above O_2 using a mast. This allowed a comparison between O_3 and the transmitters on the Lecture Theatre Block (which were positioned at the same height as O_3). Measurements of the mean received signal strength were made at 42 locations on Level 8 of the Tower Block, as shown in Figure 4.12. Also shown in Figure 4.12 are the locations of the transmitters positioned on Level 8.

4.2.2.2 Propagation Measurement Campaign B (PM B)

In PM B, which was conducted in Environment E1, six transmitters were deployed on Levels 7, 8 and 9 of the Tower Block and six transmitters were deployed outdoors on the roof of the Library Block. The locations at which the transmitters were deployed are shown in Figure 4.13. The transmitters located indoors are labeled I_1 to I_6 and the transmitters located outdoors on the roof of the Library Block are labeled O_1 to O_6. Measurements of the mean received signal strength (from which the mean path losses were calculated) were made at 52 locations on Level 8 of the Tower Block, as shown in Figure 4.14. Also shown in Figure 4.14 are the locations of the transmitters positioned on Level 8. Note that the other indoor transmitters were deployed at locations directly above or below those on Level 8.

4.2.2.3 Propagation Measurement Campaign C (PM C)

Propagation measurements for PM C were conducted in Environment E2. As shown in Figure 4.15, five transmitters were placed on Level 2 of the Functions building and five

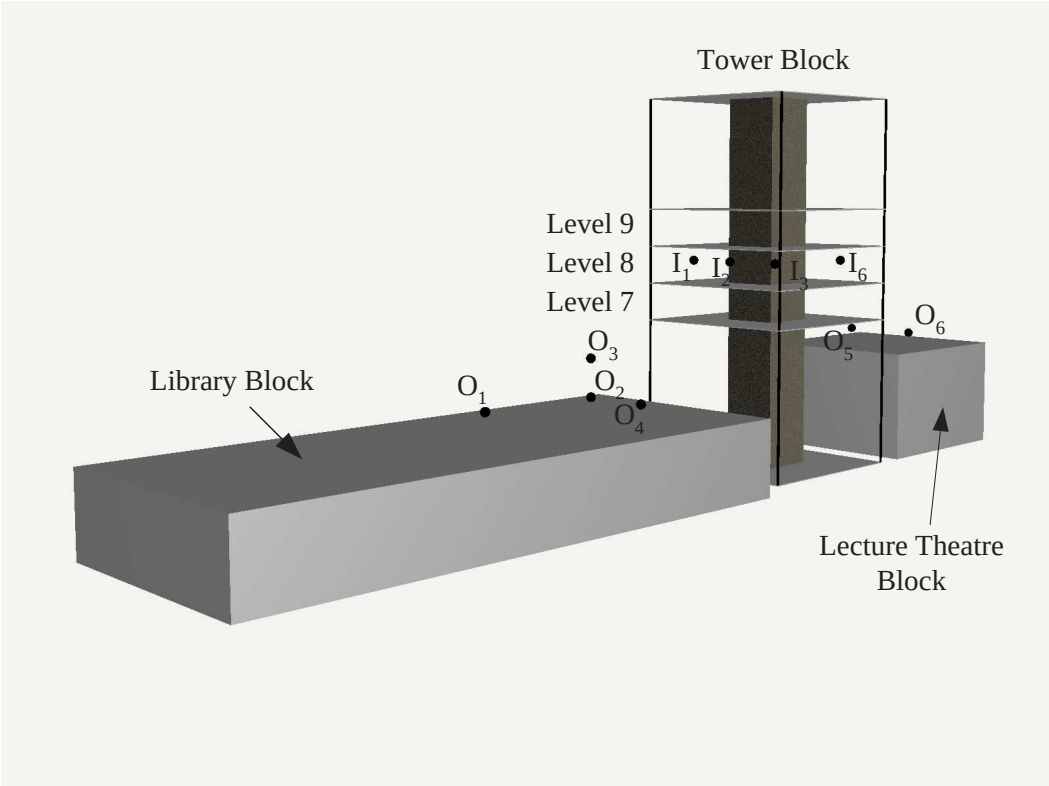

Figure 4.10: Transmitter locations in PM A (Three-dimensional view). N.B. I_4 and I_5 are obscured from this view.

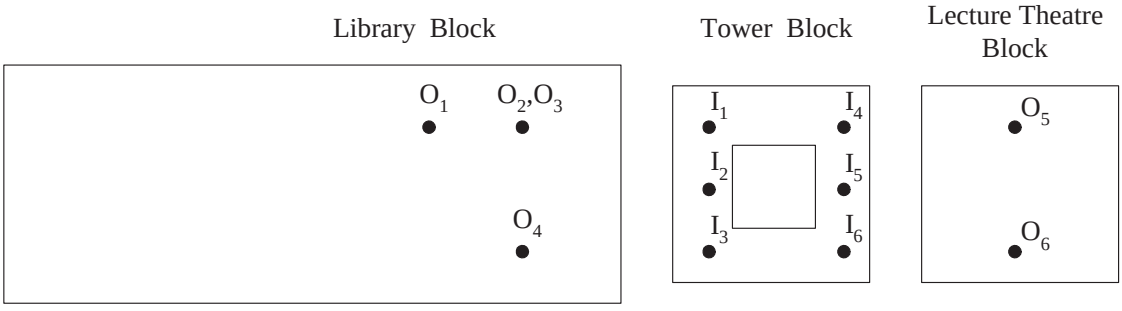

Figure 4.11: Transmitter locations in PM A (Plan view).

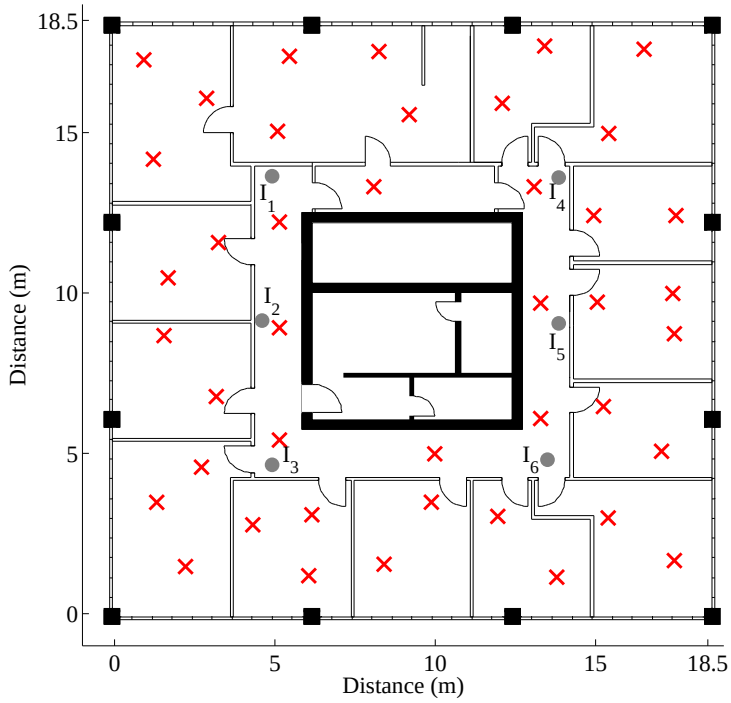

Figure 4.12: Measurement locations on Level 8 of the Tower Block in PM A (Shown by ×s). Transmitter locations I_1 to I_6 (also located on Level 8) are shown by •s.

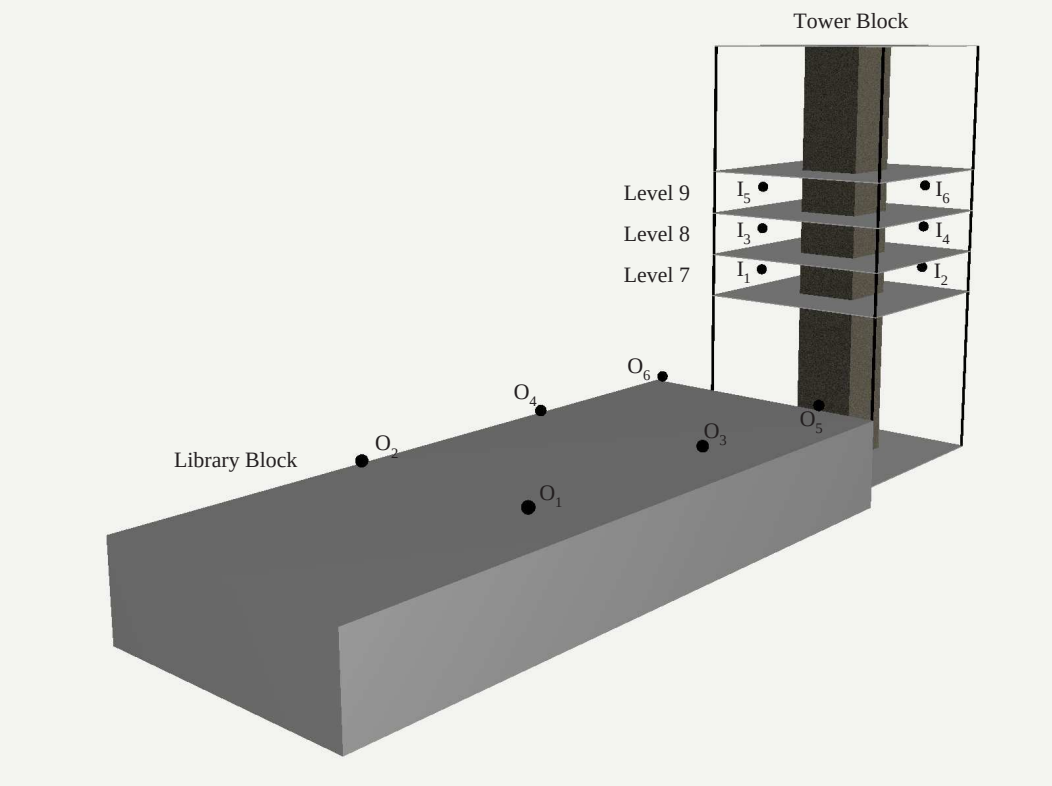

Figure 4.13: Transmitter locations in PM B.

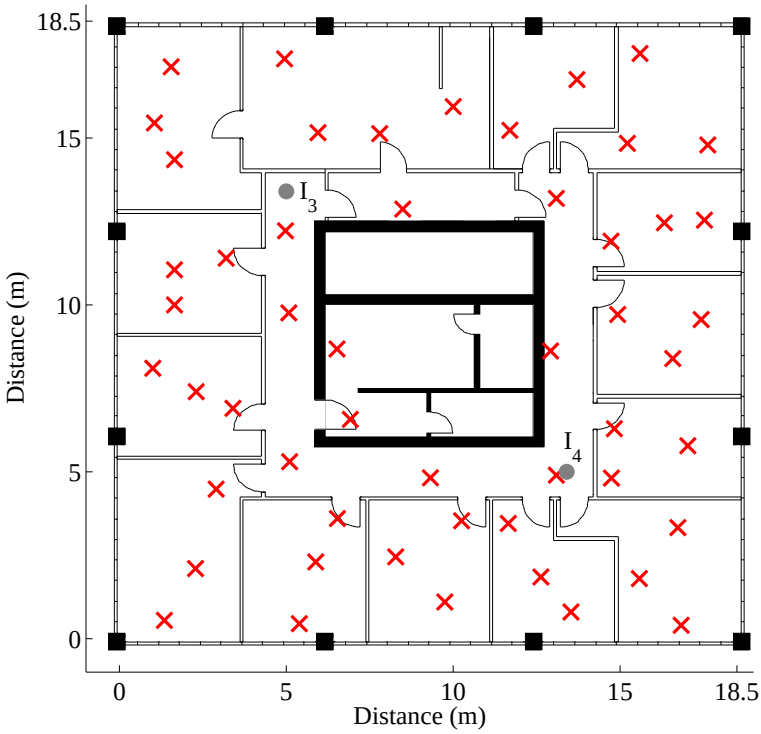

Figure 4.14: Measurement locations on Level 8 of the Tower Block in PM B (Shown by ×s). Transmitter locations I_3 and I_4 are shown by the •s.

transmitters were placed on Level 2 of the Science building. Measurements were conducted on Level 2 of both buildings. Figures 4.16 and 4.17 show the transmitter and receiver measurement locations for Level 2 of the Functions building and Level 2 of the Science building respectively.

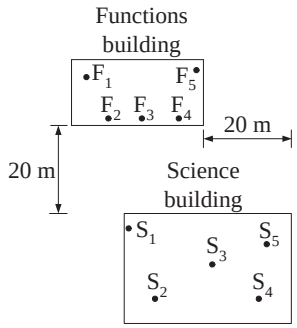

Figure 4.15: Transmitter locations in PM C.

4.2.2.4 Summary of propagation measurement campaigns

Table 4.1 summarises the three propagation measurement campaigns that were conducted in two mixed indoor/outdoor environments in The University of Auckland. In all measurement campaigns, transmitters were deployed at locations both inside the building of

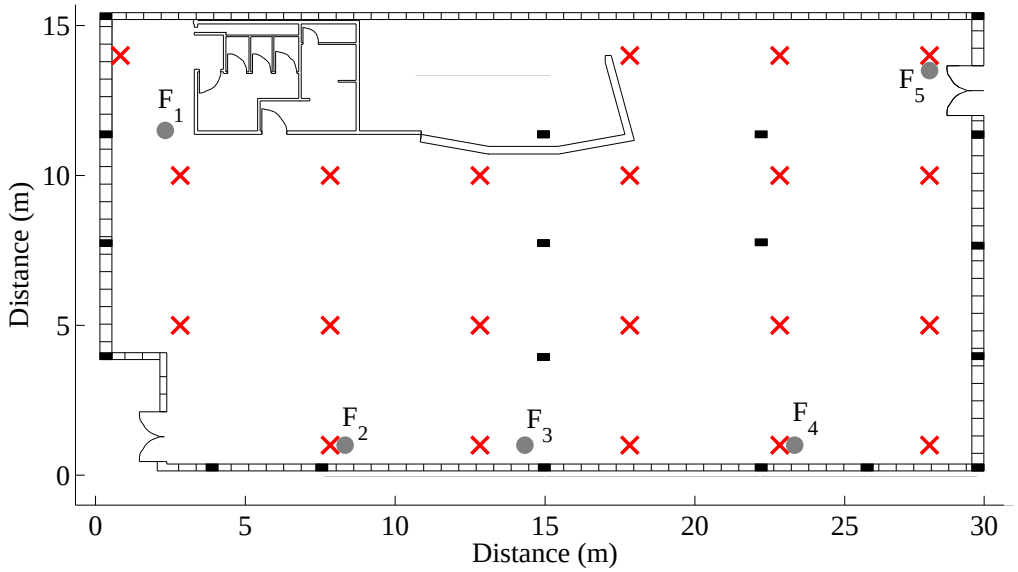

Figure 4.16: Measurement locations (×) and transmitter locations (•) on Level 2 of the Functions building in PM C.

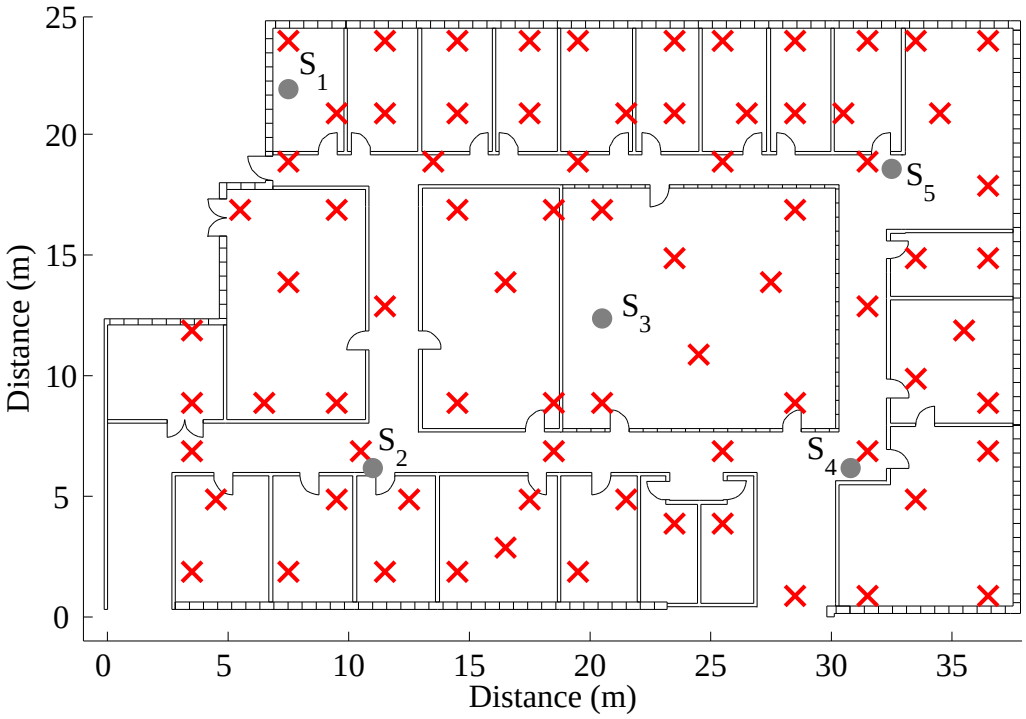

Figure 4.17: Measurement locations (×) and transmitter locations (•) on Level 2 of the Science building in PM C.

interest as well as externally on the roofs of nearby buildings (PM A and PM B) or inside other buildings (PM C). While PM B used a multi-floor indoor transmitter configuration, both PM A and PM C used single floor configurations. Measurements of the mean received signal strength were conducted at indoor locations only.

PM Campaign	Environment	Transmitter locations	Indoor transmitter configuration	Measurement locations
A	E1	Tower Block Library Block† Lecture Theatre Block†	Single level	Tower Block
B	E1	Tower Block Library Block†	Multiple level	Tower Block
C	E2	Science Building Functions Building	Single level	Science Building Functions Building

Table 4.1: Summary of the propagation measurement campaigns.
†Transmitters located on roof.

4.2.3 Measurement setup and strategy

In Section 4.2.2, three propagation measurement campaigns were discussed. In each of these campaigns, transmitters were positioned at fixed locations within and outside buildings and measurements of received signal strength were made at several locations indoors. The purpose of this section is to outline the equipment used for the measurements as well as the strategy for conducting the measurements.

4.2.3.1 Measurement setup

The measurement equipment included *transmitting equipment* and *receiving equipment*. The transmitting equipment included several custom-built narrowband transmitters connected to discone antennas. The receiving equipment was comprised of a half-wave dipole antenna connected to an ESVN40 test receiver and laptop. A block diagram of the overall measurement setup is shown in Figure 4.18.

To explain how the measurement equipment was set up in a given propagation measurement campaign, a diagram of the transmitter locations in PM B[1] (discussed in Section 4.2.2.2) is reproduced in Figure 4.19, while a diagram of the measurement locations is reproduced in Figure 4.20. In PM B, transmitting equipment (i.e. a single narrowband

[1]PM B was conducted in The University of Auckland School of Engineering buildings. Transmitters were deployed inside the Tower Block and on the roof of the adjacent Library Block. Measurements of received signal strength were made on Level 8 of the Tower Block.

transmitter connected to a discone antenna) was placed at each of the strategically chosen transmitter locations shown in Figure 4.19. Once the transmitting equipment was set up at *all* the transmitter locations, the receiver equipment was used to take measurements at each of the measurement locations shown in Figure 4.20. A similar procedure was used in the other propagation measurement campaigns.

Transmitting equipment – The narrowband transmitters are capable of being programmed to transmit continuous wave (sinusoidal) *narrowband* signals at frequencies up to 2 GHz with a transmitting power of 16 dBm. The DECT band of frequencies ranging from 1880 to 1885.5 MHz were used for transmissions, with the individual transmitters programmed to transmit at centre frequencies 0.5 MHz apart, as specified in Table 4.2. The mean path loss response (for a fixed path) across this range of frequencies has been found to be flat [26]. Each transmitter was connected to an omnidirectional discone antenna.

Receiving equipment – The narrowband transmissions were received using a half-wave dipole antenna connected to an ESVN40 test receiver. The ESVN40 test receiver was controlled by measurement software on a laptop to step through the range of individual transmitter frequencies (shown in Table 4.2) and take measurements of instantaneous received signal strength from each of the transmitters. The dipole antenna was rotated in a 1 metre diameter circular locus and approximately 2000 *instantaneous* signal strength samples were taken for each narrowband transmission. These instantaneous signal strength samples were then averaged to obtain the *mean* strength of the received signal from each transmitter. It should be noted that the ESVN40 test receiver is noncoherent and therefore only amplitude (i.e. received power) information was obtained. This information was sufficient for the subsequent system performance analysis in which phase information was not required.

Further information about the measurement equipment can be found in Appendix A.

4.2.3.2 Measurement strategy

In each of the three propagation measurement campaigns, the receiver measurement locations were chosen to be as randomly spread across the measurement area as possible with the constraint that some regions of the measurement area were inaccessible. The number of receiver measurement locations in each measurement campaign were chosen to be sufficient for the accuracy of the subsequent DS-CDMA performance analysis based on the guidelines in [26]. In all the propagation measurement campaigns, both the transmitting discone antenna and receiving half wave dipole antenna were positioned 1.8 metres above the ground, as it was assumed that this would ensure optimal received signal strength (based on the guidelines in [26]).

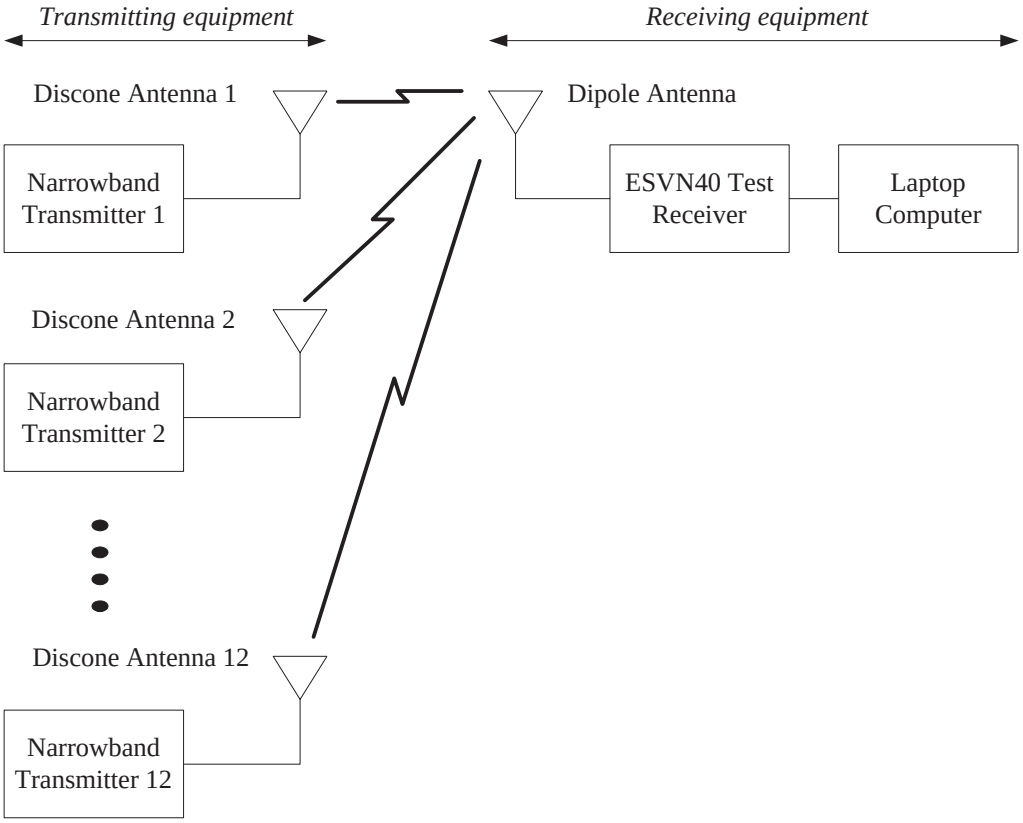

Figure 4.18: Propagation measurement equipment setup.

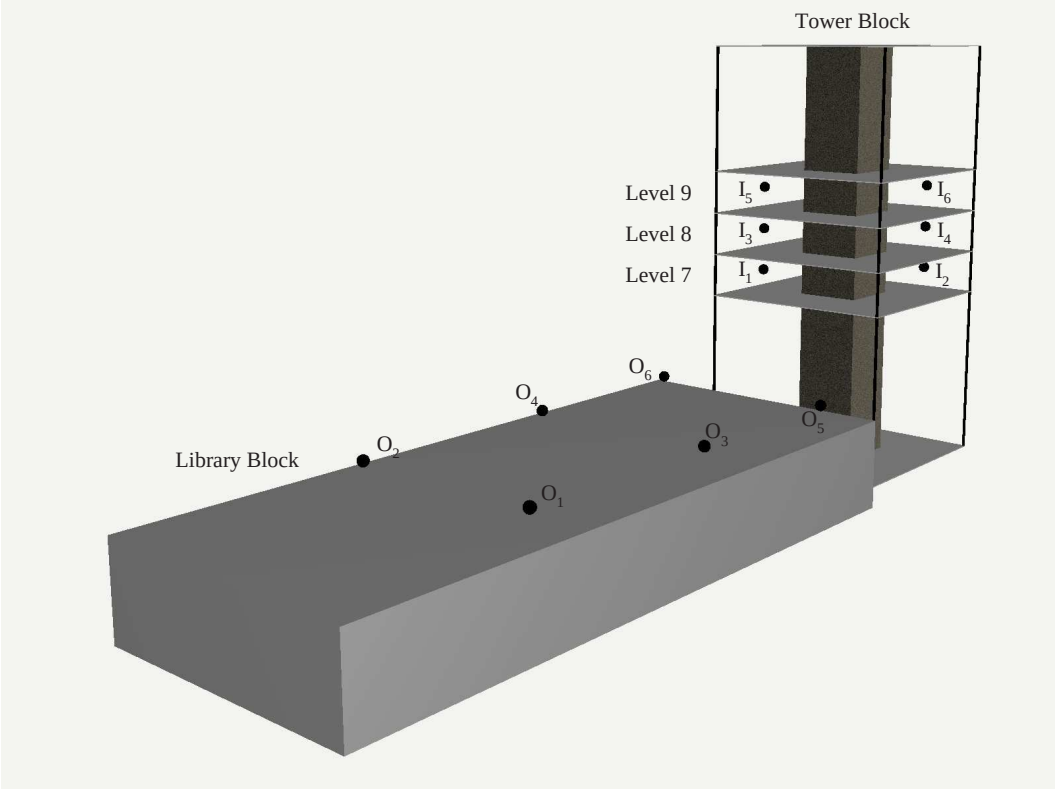

Figure 4.19: Transmitter locations in PM B.

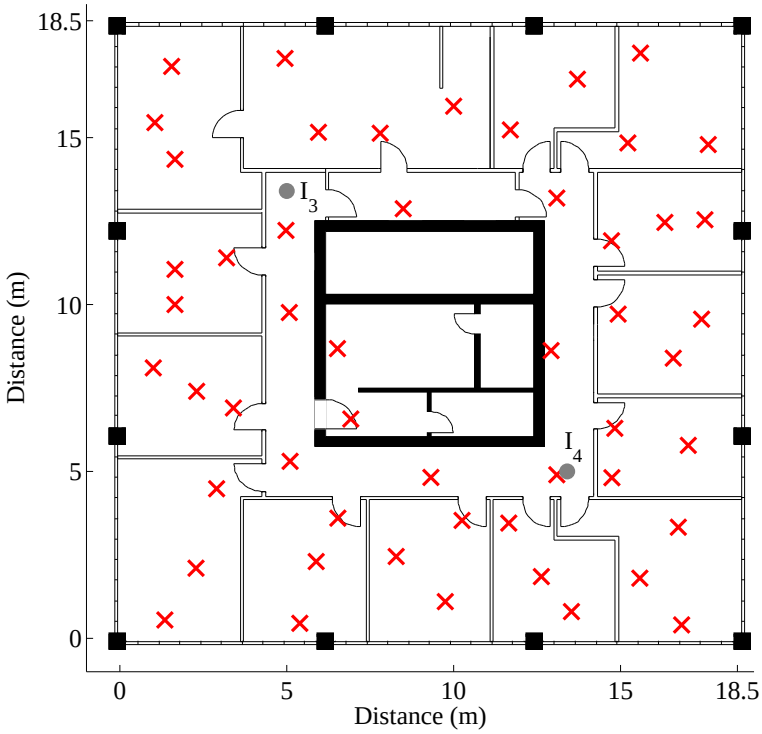

Figure 4.20: Measurement locations on Level 8 of the Tower Block in PM B (Shown by ×s). Transmitter locations I_3 and I_4 are shown by the •s.

Transmitter number	**Centre frequency (MHz)**
1	1880.0
2	1880.5
3	1881.0
4	1881.5
5	1882.0
6	1882.5
7	1883.0
8	1883.5
9	1884.0
10	1884.5
11	1885.0
12	1885.5

Table 4.2: Centre frequencies for the transmitters used in the propagation measurement campaigns. Note that narrowband sinusoidal signals are transmitted.

4.3 Propagation results

The purpose of this section is to present the key findings from the three propagation measurement campaigns discussed in Section 4.2. To depict typical propagation behaviour, Section 4.3.1 presents coverage maps produced using the mean path loss data collected in the propagation measurement campaigns. The correlation coefficients for the transmitters deployed in the propagation measurement campaigns are presented in Section 4.3.2.

4.3.1 Mean path loss coverage maps

The mean path loss variations for the transmitters deployed in the three propagation measurement campaigns are best represented using coverage maps. The coverage maps of the mean path loss across the measurement area in each of the propagation measurement campaigns have been generated by interpolating between the mean path loss data collected at the discrete locations at which measurements were made. The purpose of this section is to present examples of the coverage maps for each measurement campaign.

4.3.1.1 Propagation Measurement Campaign A (PM A)

Coverage maps showing the mean path across Level 8 from indoor transmitter I_2 (also positioned on Level 8) and outdoor transmitter O_6 (positioned on the roof of the Lecture Theatre Block) are shown in Figures 4.21 and 4.22 respectively.

It is evident from Figure 4.21 that the signal from indoor transmitter I_2 channels to both ends of the corridor facing it. The mean path loss is observed to vary from 30 dB to in excess of 90 dB. The central steel-reinforced concrete core is observed to cause significant attenuation of the signal – the difference in path loss from one side of the concrete core (where I_2 is located) to the other side is 50 dB.

Figure 4.22 shows that outdoor transmitter O_6 uniformly illuminates the right hand side of Level 8. There is also a signalling 'channelling' effect that is noticed in the two corridors facing the outdoor transmitter O_6. As expected the mean path losses across the floor are generally higher than those observed in Figure 4.21 for the indoor transmitter I_2.

4.3.1.2 Propagation Measurement Campaign B (PM B)

A coverage map showing the mean path loss across Level 8 from I_3 (also located on Level 8) is shown in Figure 4.23. This coverage map shows that the mean path loss across Level 8 from I_3 varies from approximately 43 dB to 98 dB. The region diagonally opposite to I_3 (on the other side of the central steel-reinforced concrete core) exhibits relatively high mean path losses exceeding 75 dB. This is likely to be because the central reinforced-steel

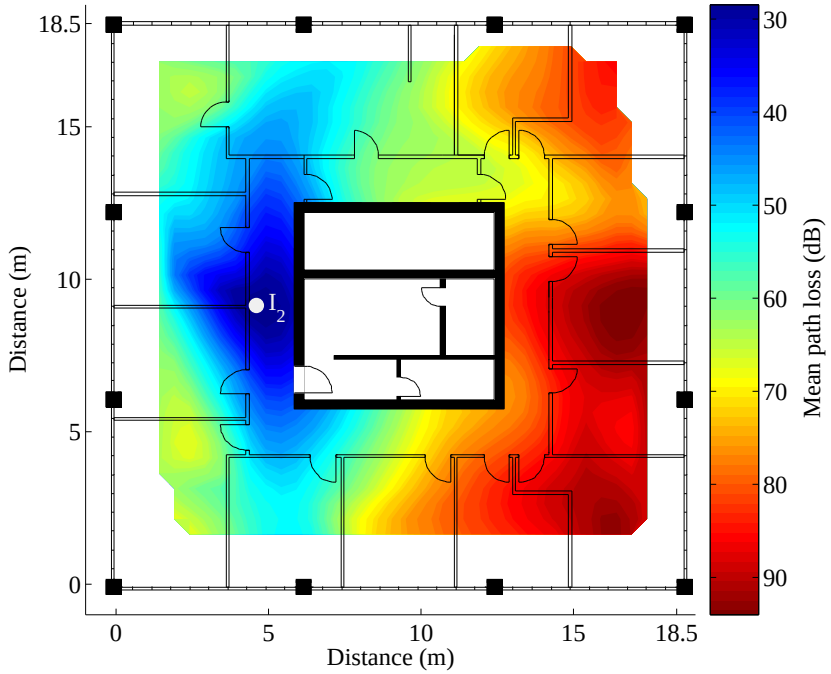

Figure 4.21: Mean path loss across Level 8 from indoor transmitter I_2 in PM A.

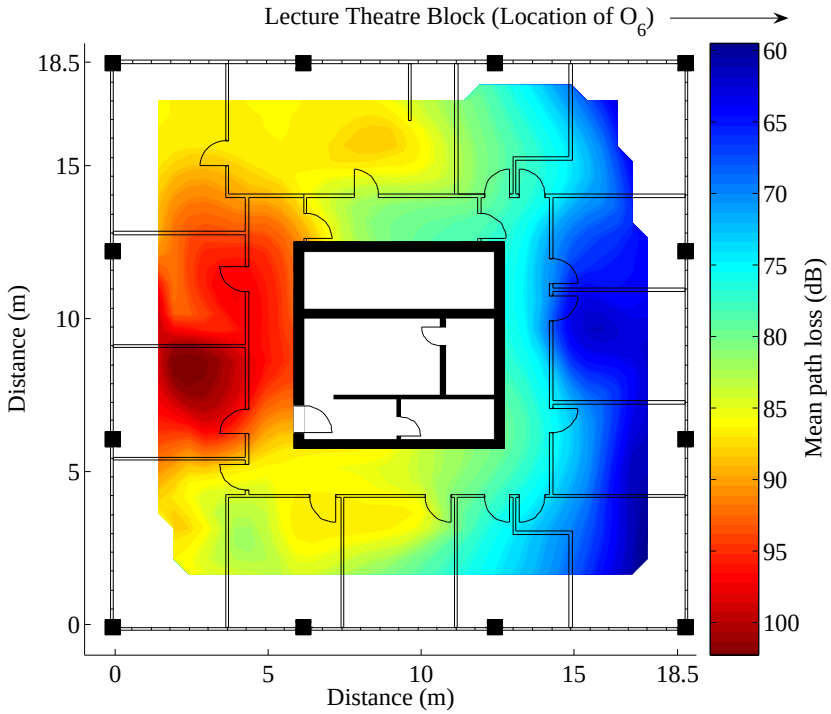

Figure 4.22: Mean path loss across Level 8 from outdoor transmitter O_6 in PM A. (N.B. O_6 is positioned on the roof of the Lecture Theatre Block, which is to the right of the above map.)

concrete core significantly attenuates the transmitted signal. Additionally, it is apparent that the signal from I_3 is 'channelled' through the two corridors facing it.

A coverage map of the mean path loss across Level 8 from outdoor transmitter O_1 is shown in Figure 4.24. The mean path loss across Level 8 varies from approximately 75 dB to 108 dB. As expected, these mean path losses are higher than those observed for I_3 (shown in Figure 4.23) due to the greater distance dependent propagation loss and outdoor-to-indoor penetration loss experienced by the signal emanating from O_1. The coverage map shows that the side of the building closest to the transmitter is uniformly illuminated by O_1 and a 'channelling' effect is visible in the lower horizontal corridor. Additionally, the central reinforced-steel concrete core attenuates the signal strongly as demonstrated by the high mean path loss in the area at the right hand side of Level 8. Similar propagation behaviour has been observed from coverage maps of the mean path losses from the other transmitters deployed in PM B.

The propagation behaviour observed in PM B is generally similar to that observed in PM A.

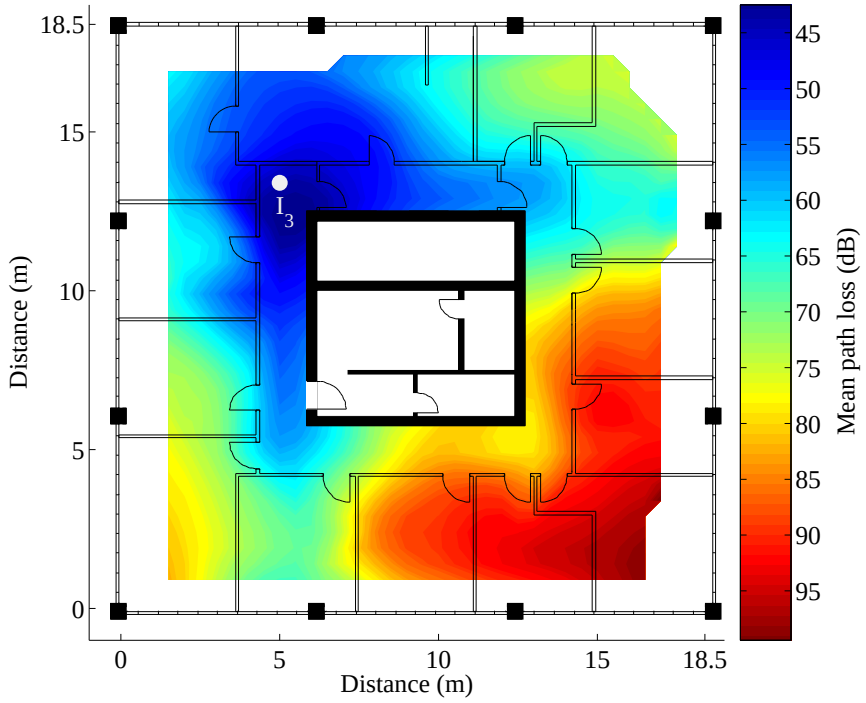

Figure 4.23: Mean path loss across Level 8 from indoor transmitter I_3 in PM B.

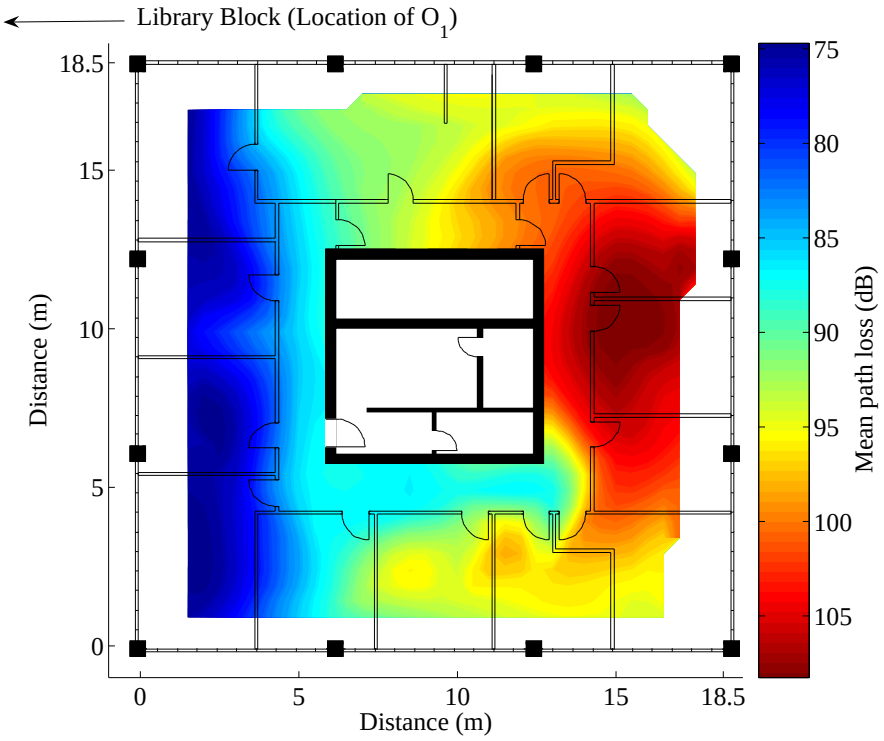

Figure 4.24: Mean path loss across Level 8 from outdoor transmitter O_1 in PM B. (N.B. O_1 is positioned on the roof of the Library Block, which is to the left of the above map.)

4.3.1.3 Propagation Measurement Campaign C (PM C)

In PM C, propagation measurements were conducted on Level 2 of both the Functions and Science buildings. For this reason, examples of the mean path loss coverage maps are presented for each of the buildings.

Mean path loss coverage maps for measurements taken in Functions building

Figure 4.25 shows the mean path loss variation across Level 2 of the Functions building from F_3 (also located on Level 2 of the Functions building). The mean path losses observed vary from approximately 43 dB to 66 dB. The maximum mean path loss of 66 dB is much less than that observed for the indoor transmitters in both PM A and PM B (which had mean path losses as high as 98 dB), despite the propagation distances being similar. This is likely to be because the Functions building does not have a central steel-reinforced concrete core or internal partitions that cause shadowing of the transmitted signal.

A coverage map showing the mean path loss across Level 2 of the Functions building from S_3 (located on Level 2 of the Science building) is shown in Figure 4.26. The mean path losses vary from 95 dB to 113 dB. Similar to the findings in PM A and PM B, these relatively high path losses are due to the signal attenuation caused by both the

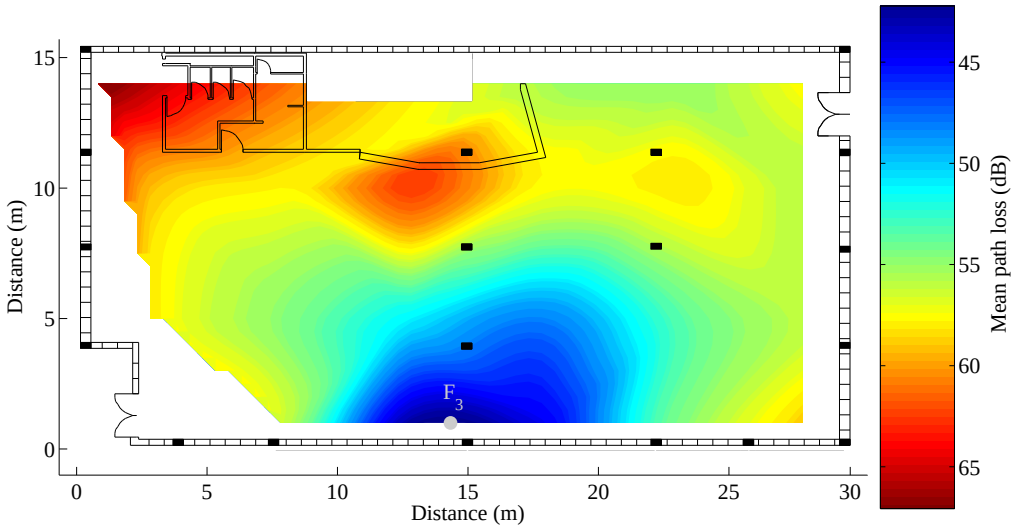

Figure 4.25: Mean path loss across Level 2 of the Functions building from F_3 in PM C.

separation distance between the Functions building and the Science building and the outdoor-to-indoor penetration loss as the signal propagates into the Functions building.

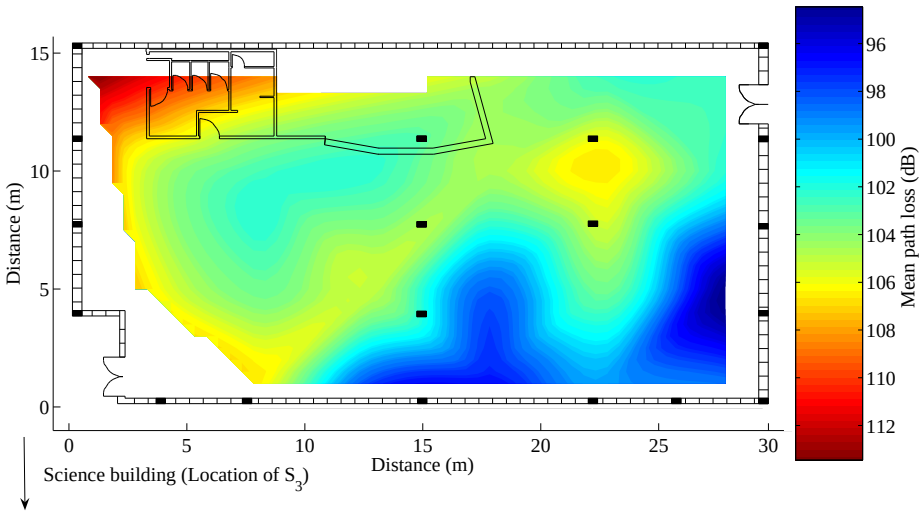

Figure 4.26: Mean path loss across Level 2 of the Functions building from S_3 in PM C. (N.B. S_3 is positioned in the Functions building which is located below this map.)

Mean path loss coverage maps for measurements taken in Science building

A coverage map showing the mean path loss across Level 2 of the Science building from S_3 is shown in Figure 4.27. The mean path loss varies from 47 dB to 81 dB. In the Science building, the maximum mean path loss (81 dB) observed for S_3 is greater than that

observed (66 dB) in the Functions building for F_3. This is likely to be due to both the greater propagation distance and the presence of partitions in the Science building.

The mean path loss variation across Level 2 of the Science building from F_3 (located in the Functions building) is shown in Figure 4.28. Similar to the observations in PM A and PM B for the outdoor transmitters, it is apparent that Level 2 of the Science building is illuminated well in the area closest to the Functions building, but the signal level gradually reduces with distance.

4.3.2 Correlation coefficients

In Chapter 3, it was shown that the level of correlation between desired and interfering signals can have a significant impact on system performance. If a desired signal is strongly correlated with an interfering signal, this is likely to yield appreciable performance gains if there is a sufficient margin between the mean received strengths of the two signals [25,26]. The degree of correlation between two signals, i and j, can be quantified using a correlation coefficient, ρ, which is defined as

$$\rho = \frac{\sum_{k=1}^{K} \left(PL_{ik} - \overline{PL_{iK}}\right)\left(PL_{jk} - \overline{PL_{jK}}\right)}{\sqrt{\sum_{k=1}^{K} \left(PL_{ik} - \overline{PL_{iK}}\right)^2}\sqrt{\sum_{k=1}^{K} \left(PL_{jk} - \overline{PL_{jK}}\right)^2}}, \tag{4.1}$$

where the measurement locations on the floor of interest are numbered 1 to K, PL_{ik} is the mean path loss from transmitter i to measurement location k and $\overline{PL_{iK}}$ is the mean of the mean path losses from transmitter i to the K measurement locations on the floor of interest. Similarly, PL_{jk} is the mean path loss from transmitter j to measurement location k and $\overline{PL_{jK}}$ is the mean of the mean path losses from transmitter j to the K measurement locations on the floor of interest.

4.3.2.1 Propagation Measurement Campaign A (PM A)

A sample of the correlation coefficients between the received signals from transmitters deployed in PM A are shown in Table 4.3. For convenience, the relative locations of the transmitters deployed in PM A are shown in Figure 4.29. Table 4.3 classifies the correlation coefficients into three categories based on the locations of the associated transmitters. The various scenarios are denoted by the syntax AB, where A and B represent the transmitters whose signals are correlated.

If both transmitters are located *indoors* on Level 8 of the Tower Block, it is evident that the correlation coefficient is positive if the transmissions emanate from the same side of the building. If the transmitters are immediately adjacent to each other (e.g. I_1I_2 and I_2I_3), a very strong positive correlation is observed. However, for a greater separation distance (e.g. I_1I_3 and I_4I_6), a weak positive correlation is observed. This is likely to be

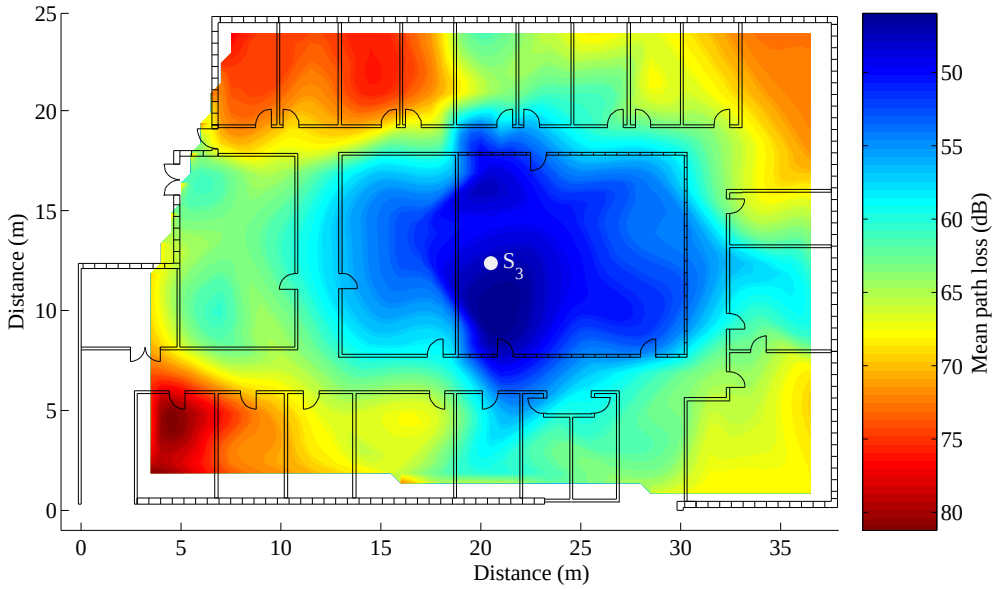

Figure 4.27: Mean path loss across Level 2 of the Science building from S_3 in PM C.

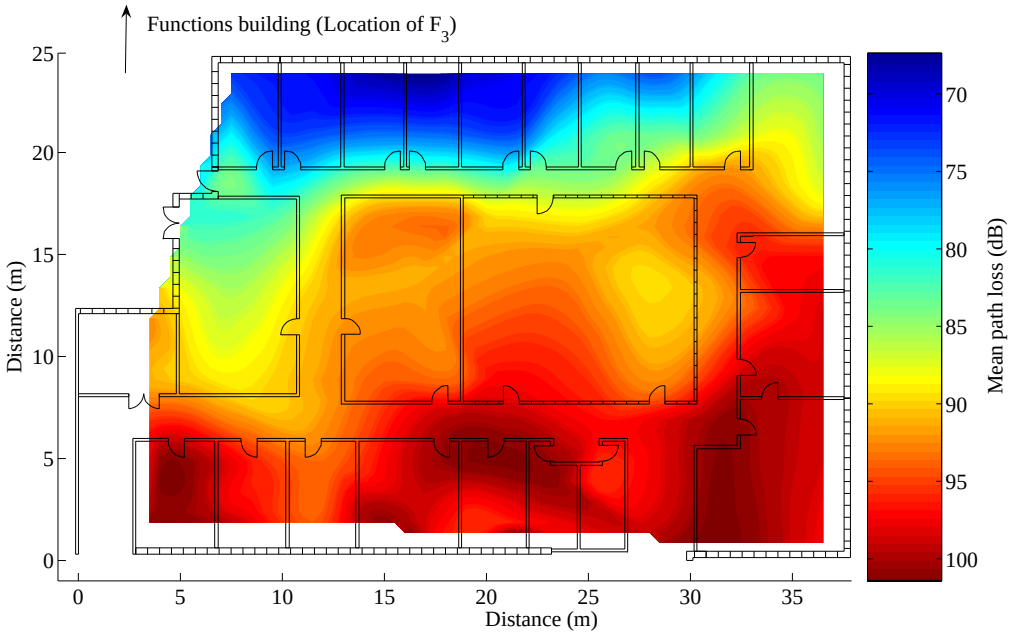

Figure 4.28: Mean path loss across Level 2 of the Science building from F_3 in PM C. (N.B. F_3 is positioned in the Functions building which is located above this map.)

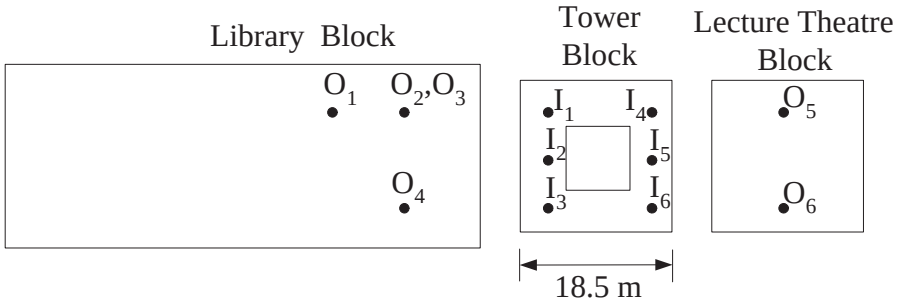

Figure 4.29: Locations of transmitters deployed in PM A.

Locations of transmitters					
Indoor		Outdoor		Indoor and Outdoor	
Scenario	ρ	Scenario	ρ	Scenario	ρ
I_1I_2	0.80	O_1O_2	0.91	I_1O_1	0.41
I_2I_3	0.71	O_3O_4	0.80	I_2O_3	0.67
I_1I_3	0.35	O_5O_6	0.90	I_3O_4	0.28
I_4I_6	0.18	O_3O_6	-0.75	I_3O_6	-0.66
I_1I_6	-0.66	O_4O_5	-0.44	I_2O_5	-0.77
I_2I_5	-0.75	O_1O_5	-0.60	I_5O_2	-0.88

Table 4.3: Correlation coefficients for transmitters deployed in PM A.

because there is less similarity in propagation paths for the signals if the transmitters are located further away from each other. Finally, if the transmitters are located on opposite sides of the building, a negative correlation is observed between the signals emanating from them.

Now consider the correlations for the signals from transmitters located *outdoors* on the roofs of the Library and Lecture Theatre Blocks. If the outdoor transmissions emanate from the same side of the Tower Block (i.e. both transmitters are located on the roof of either the Library Block or Lecture Theatre Block), a very strong positive correlation is observed. However, if the outdoor transmissions emanate from opposite sides of the Tower Block, a negative correlation is observed.

If one of the transmitters is located *indoors* in the Tower Block and the other is located *outdoors* on the roof of either the Library Block or the Lecture Theatre Block, a moderately positive correlation is observed if the indoor transmitter is located on the side of the building that is closest to the outdoor transmitter (e.g. I_2O_3 and I_3O_4). However, the transmissions are negatively correlated if the indoor transmitter is located on the side of the building that is furthest from the outdoor transmitter (e.g. I_3O_6, I_2O_5 and I_5O_2).

The observations discussed above can be confirmed by the correlations for signals emanating from other pairs of transmitters. The full set of correlation results for all pairs of transmitters can be found in Appendix B.

4.3.2.2 Propagation Measurement Campaign B (PM B)

A sample of the correlation coefficients between the signals from transmitters deployed in PM B are shown in Figure 4.4. The relative locations of the transmitters are shown in Figure 4.30. Similar to Section 4.3.2.1, the correlation coefficients are classified into three categories depending on the locations of the associated transmitters.

First consider the correlation coefficients between the signals emanating from the *indoor* transmitters, assuming that at least one of the transmitters is located on the measurement floor (i.e. Transmitter I_3 or I_4 located on Level 8 of the Tower Block). It is

Locations of transmitters					
Indoor		Outdoor		Indoor and Outdoor	
Scenario	ρ	Scenario	ρ	Scenario	ρ
I_3I_1	0.95	O_1O_2	0.96	I_3O_1	0.34
I_3I_5	0.96	O_3O_4	0.97	I_3O_6	0.49
I_1I_5	0.97	O_5O_6	0.78	I_4O_1	-0.33
I_3I_2	-0.46	O_3O_6	0.86	I_4O_6	-0.51
I_3I_6	-0.55	O_2O_5	0.90	I_4O_2	-0.34

Table 4.4: Correlation coefficients for the transmitters deployed in PM B for measurements taken on Level 8.

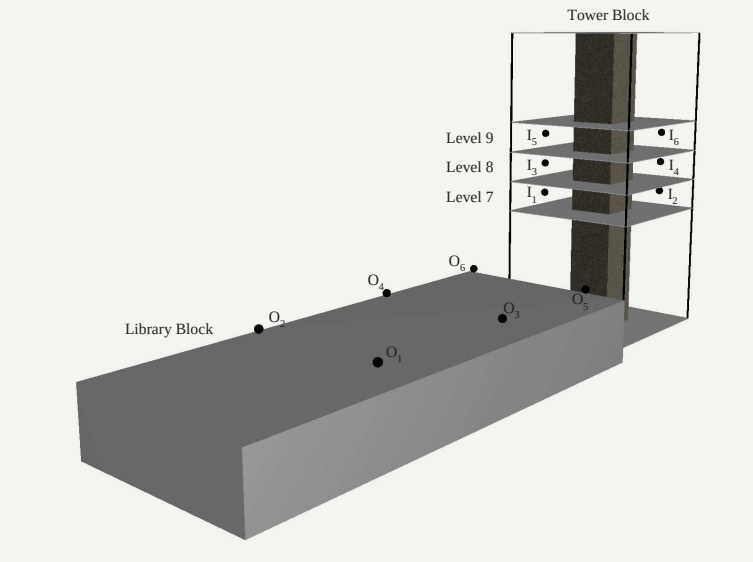

Figure 4.30: Transmitter locations in PM B.

evident that if the transmitters are vertically aligned with each other (e.g. I_3I_1), the correlation coefficient is very high. This indicates that the mean path losses for the signals emanating from vertically aligned transmitters are very strongly correlated with each other. In a realistic system this would mean that the desired signal would be strongly correlated with the interfering signal. However, if the transmitters are vertically offset from each other (e.g. I_3I_2), then the signals emanating from them are negatively correlated with each other. This implies that at any given measurement location if the desired signal is strong, the interfering signal is likely to be weak and vice versa.

Now consider the correlation coefficients between signals emanating from transmitters located *outdoors*. These signals are all very strongly correlated with each other. This is expected as the signals emanating from all the outdoor transmitters are likely to traverse similar propagation paths to the measurement locations on Level 8 of the Tower Block.

Finally, consider the correlation coefficients between a signal emanating from an *indoor* transmitter and another signal emanating from an *outdoor* transmitter. A strong correlation exists if the indoor transmitter is located on the side of the Tower Block that is nearest to the outdoor transmitter. However, a moderately negative correlation exists if the indoor transmitter is located on the opposite side of the Tower Block in relation to the outdoor transmitter.

The trends observed in PM B match well with those observed in PM A. The full set of correlation results for PM B can be found in Appendix B.

4.3.2.3 Propagation Measurement Campaign C (PM C)

In PM C transmitters were deployed and measurements taken on Level 2 of both the Functions and Science buildings. For this reason, separate data sets were obtained for each of the Functions building and Science building. Therefore, the correlation coefficients are presented for each data set individually so that meaningful observations can be made.

A sample of the correlation coefficients between the transmitter signals for measurements taken in the Functions building and Science building are shown in Tables 4.5 and 4.6 respectively. For convenience, the relative locations of the transmitters deployed in this campaign are shown in Figure 4.31.

First consider the correlation coefficients for the measurements taken in the *Functions building* (Table 4.5). The observations made are similar to those for PM A and PM B (discussed in Sections 4.3.2.1 and 4.3.2.2). The received signals from the transmitters located in the *Functions building* are positively correlated if there is likely to be significant commonality in their propagation paths (e.g. F_2F_3 and F_3F_4). However, for transmitters located on opposite ends of the *Functions building* (e.g. F_1F_4 and F_2F_5) a negative correlation is observed. If both transmitters are located in the adjacent *Science building*, a moderate or strongly positive correlation is observed. Finally, if one of the transmitters

Locations of transmitters					
Functions building		Science building		Functions and Science Buildings	
Scenario	ρ	Scenario	ρ	Scenario	ρ
F_2F_3	0.20	S_4S_2	0.43	F_3S_1	0.66
F_3F_4	0.52	S_5S_1	0.47	F_4S_5	0.74
F_1F_4	-0.57	S_1S_3	0.52	F_4S_3	0.72
F_2F_5	-0.14	S_4S_1	0.53	F_1S_4	-0.31
F_2F_4	-0.26	S_5S_2	0.45	F_5S_2	0.14
F_1F_5	-0.69	S_4S_5	0.87	F_5S_1	0.07

Table 4.5: Correlation coefficients for transmitters deployed in PM C for measurements taken in the Functions building.

Locations of transmitters					
Functions building		Science building		Functions and Science buildings	
Scenario	ρ	Scenario	ρ	Scenario	ρ
F_2F_3	0.95	S_4S_2	-0.23	F_3S_1	0.69
F_3F_4	0.95	S_5S_1	-0.29	F_4S_5	0.31
F_1F_4	0.89	S_1S_3	-0.26	F_4S_3	-0.15
F_2F_5	0.91	S_4S_1	-0.79	F_1S_4	-0.42
F_2F_4	0.92	S_1S_2	0.37	F_5S_2	-0.55
F_1F_5	0.92	S_4S_5	0.43	F_5S_1	0.40

Table 4.6: Correlation coefficients for transmitters deployed in PM C for measurements taken in the Science building.

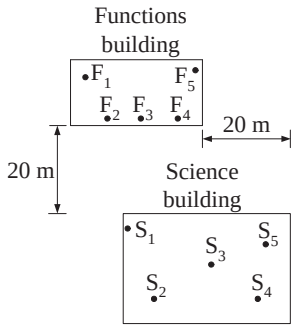

Figure 4.31: Locations of transmitters deployed in PM C.

is located in the *Functions building* and the other is located in the *Science building*, a strongly positive, very weak or moderately negative correlation is observed depending on the relative locations of the transmitters.

Similar trends are apparent from the correlation coefficients for the measurements taken in the *Science building* (shown in Table 4.6). The signals emanating from transmitters located in the *Science building* are positively correlated if they are likely to share similar propagation paths (e.g. S_1S_2 and S_4S_5), and are negatively correlated if they emanate from opposite ends of the Science building (e.g. S_5S_1 and S_1S_3). A very strong positive correlation is observed for transmitters located in the *Functions building*. If one of the transmitters is located in the *Functions building* and the other is located in the *Science building*, the correlation coefficients are strongly positive, very weak or moderately negative depending on the relative locations of the transmitters.

Similar observations have been made for other pairs of transmitters and the comprehensive correlation results for PM C can be found in Appendix B.

4.4 Summary

This chapter has outlined three propagation measurement campaigns that were conducted in two separate mixed indoor/outdoor environments. While both these environments consist of buildings with conventional architecture, some important differences between them were highlighted. Each of the propagation measurement campaigns involved deploying transmitters at strategic locations (both indoors and outdoors) and measuring the mean received signal strength at various indoor locations. The resulting propagation database is the basis for the subsequent system performance analyses discussed in Chapters 5, 6 and 7.

In this chapter, several mean path loss coverage maps have been presented for the transmitters deployed in the propagation measurement campaigns. These coverage maps show that the mean path loss variation is likely to be significantly influenced by both the building architecture as well as internal partitions.

As signal correlation can potentially have a significant impact on system performance, correlation coefficients have been presented for the transmitters deployed in the campaigns. These correlation coefficients varied from strongly positive to moderately negative depending on the relative locations of the transmitters. In general, a positive correlation was apparent when signals are likely to traverse similar propagation paths, while a negative correlation was apparent when signals are likely to traverse 'opposing' propagation paths.

Chapter 5

Deployment and performance of indoor/outdoor DS-CDMA systems

5.1 Introduction

Chapter 4 presented three propagation measurement campaigns that were conducted to measure the mean path losses for several propagation paths between transmitters and receivers deployed in two different mixed indoor/outdoor environments. While the database obtained from the measurement campaigns gives an excellent indication of the underlying signal propagation behaviour, it does not quantify the performance of realistic systems that might operate in the environments under consideration.

In this chapter, the performance of hypothetical indoor/outdoor DS-CDMA base station configurations are estimated using the propagation database discussed in Chapter 4. The estimates of system performance are related to both the deployment strategy and the underlying propagation phenomena observed in Chapter 4. The outcome of this chapter is a set of guidelines to deploy indoor/outdoor DS-CDMA systems for a variety of deployment scenarios, based on a performance evaluation of both the downlink and uplink.

Section 5.2 presents the method for estimating the performance of the downlink and uplink of a conventional voice-based DS-CDMA system. The three propagation measurement campaigns represent three generalised cases in which wireless operators might deploy their systems. For each of these cases, a scenario-based approach is used to compare the performances of several possible base station configurations. The deployment scenarios are presented in Section 5.3 and form the basis for the performance comparisons throughout this thesis. Section 5.4 presents the performance estimation results for the deployment scenarios investigated in each of the three propagation measurement campaigns, while Section 5.5 outlines the important guidelines for deploying conventional indoor/outdoor DS-CDMA systems based on the performance estimates. Finally Section 5.6 summarises the main findings of this chapter.

It should be noted that the results presented in this chapter are relevant to *conventional* DS-CDMA systems that operate *without* multiuser detection. The implications of multiuser detection on indoor/outdoor DS-CDMA system deployment and performance are investigated in Chapters 6 to 8. Due its high signal processing complexity, multiuser detection is likely to be implemented at the base station only (i.e. for the enhancement of uplink performance). Therefore, the uplink performance results presented in this chapter are particularly relevant for comparison in the subsequent chapters that investigate multiuser detection.

5.2 System performance estimation

5.2.1 Overview

A system performance estimation was conducted to quantify the downlink and uplink performance of a conventional voice-based DS-CDMA system. This system performance estimation is based on the DS-CDMA system model derived in Chapter 3 and uses the mean path loss propagation data discussed in Chapter 4. System performance is quantified in terms of a 'mean outage probability' that represents the likelihood that a mobile in an area will have an outage. Mean outage probabilities are estimated for both the downlink and uplink of the various deployment scenarios considered. Key assumptions about the DS-CDMA system are outlined in Section 5.2.2, while the algorithm for estimating the downlink and uplink performance is presented in Section 5.2.3.

5.2.2 DS-CDMA system assumptions

It is assumed that a voice-based DS-CDMA system operates in the environments in which the propagation measurements were taken. The system uses a chosen combination of the base stations deployed in the propagation measurement campaigns. Mobiles may be located at any of the discrete locations at which measurements were made in the propagation measurement campaigns. A fixed processing gain of 511 and a voice activity factor of 0.5 are assumed. Separate frequency bands are used for the downlink and uplink. Further assumptions are that BPSK modulation is used, random spreading codes are allocated to mobiles and the received baseband signal pulse is perfectly rectangular. Base stations are assumed to transmit signals with a power of 20 dBm per mobile[1] unless otherwise stated.

[1]In commercially deployed DS-CDMA systems, base stations usually have a specified total transmit power threshold. If the system is sufficiently loaded, this threshold may be reached and further mobiles are not permitted to connect. For the purpose of analysis, it is assumed in this thesis that the system is not loaded to this extent and therefore this threshold is never reached.

For the uplink, perfect power control ensures that mobiles adjust their transmit powers so that their signals are received by the base station with the same mean power, i.e. the mobiles do not adjust their transmit powers to account for variations due to short-term fading. Therefore, there are short-term variations in the powers of the signals received by the base station.

It is assumed that short-term fading follows a Rayleigh distribution. The performance of the system is quantified in terms of downlink and uplink outage probabilities. An outage is defined to occur at a potential mobile location if the bit-error rate (BER) exceeds 0.02. At a given mobile location the BER will exceed 0.02 if the instantaneous SIR is below 4.32 dB, as determined by the complementary Gauss probability integral discussed in Section 3.2.1 [2, 25, 26, 74].

5.2.3 Algorithm for estimating DS-CDMA system performance

A flow diagram of the algorithm for estimating the DS-CDMA system performance is shown in Figure 5.1. The method for estimating the downlink and uplink system performance uses a 'semi-static' Monte Carlo analysis. In each iteration of this Monte Carlo analysis, mobiles are randomly placed across the floors of interest and the number of outages on both the downlink and uplink are then determined for mobiles across the floors of interest. This process is repeated for several thousand iterations and at the end of all iterations the *mean* outage probabilities for the downlink and uplink are obtained by dividing the total number of outages in all iterations by the total number of connections to the base station of interest. The DS-CDMA system performance estimation testbed was developed using MATLAB.

For simplicity the methods for estimating the downlink and uplink performance, shown in Figure 5.1, are explained individually in Sections 5.2.3.1 and 5.2.3.2 respectively.

5.2.3.1 Downlink system performance estimation

As stated earlier, the downlink and uplink system outage probabilities are estimated using a 'semi-static' Monte Carlo analysis, a flow diagram of which is shown in Figure 5.1.

The downlink system performance estimation begins in Step (i) where K mobiles are randomly chosen from the discrete measurement locations in a measurement campaign and placed on each floor. A floor is defined as being inside a building of interest or external to the building of interest (e.g. outdoors or in another building). A mobile is identified by a unique identifier m, which corresponds to its physical location at the three-dimensional coordinates (x, y, z). There may be one or more base stations in the system, identified by b, where $b \in 1, 2, ...B$.

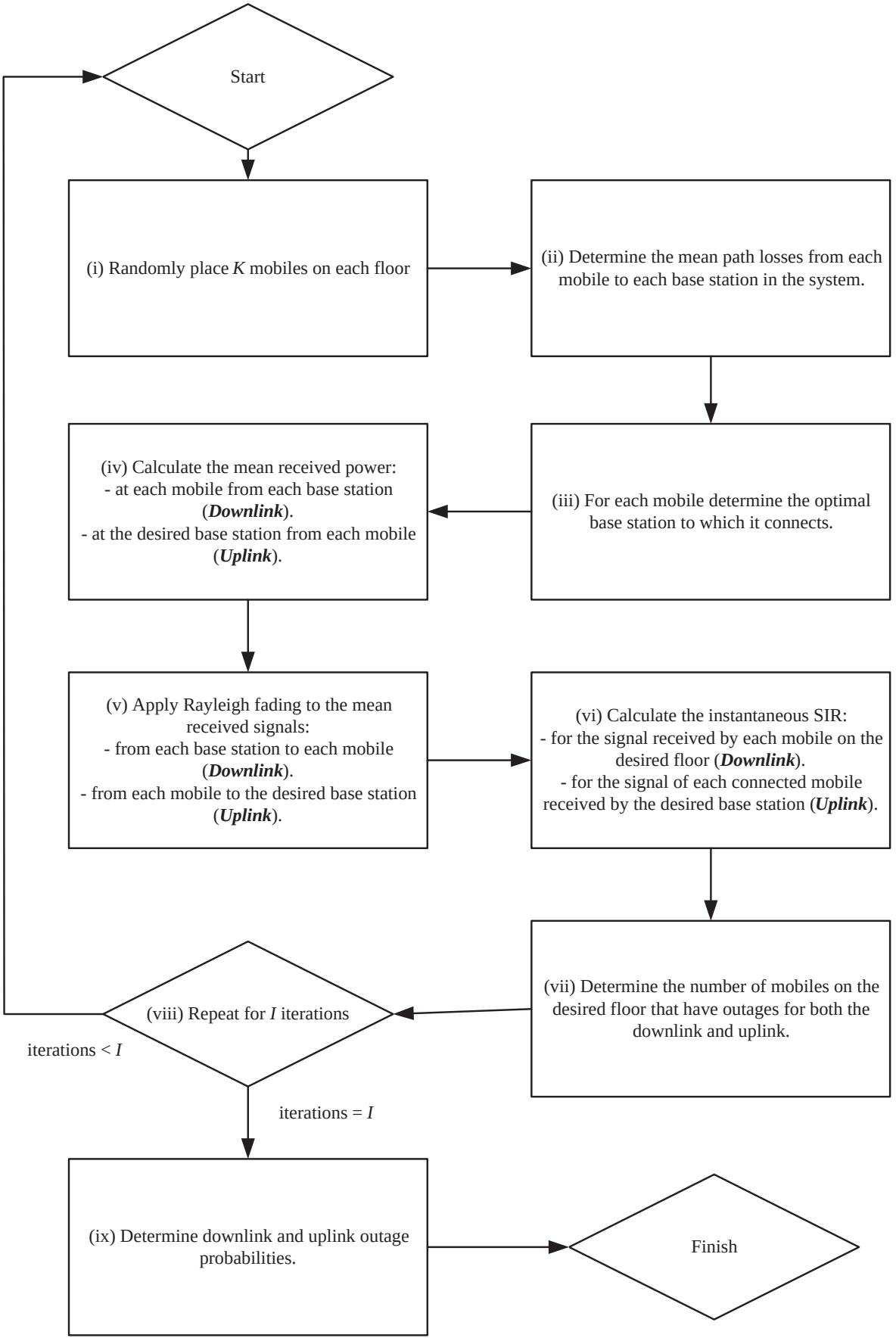

Figure 5.1: System performance estimation algorithm using a Monte Carlo analysis.

In Step (ii), the mean path loss between each of the mobiles and each of the base stations in the system is obtained directly from the mean path loss propagation data collected in the measurement campaigns. The mean path losses are denoted as $PL_b(m)$ (units of dB), where b is the unique identifier for the base station of interest and m is the unique identifier of the mobile of interest.

In Step (iii), the optimal base station, b_{con}, to which each mobile connects is determined by choosing the base station with the maximum received downlink signal power

$$b_{con} = Max_b \left\{ P_{t_b} - PL_b(m) \right\}, \tag{5.1}$$

where P_{t_b} is the transmit power of the base station b. Note that the signal from base station b_{con} is the desired signal for the mobile m while the signals from the other base stations (i.e. if $b \neq b_{con}$) appear as inter-cell interference to that mobile.

In Step (iv), the mean power of the signal received by each mobile from each base station is calculated using

$$\overline{P_{r_b}}(m) = P_{t_b} - PL_b(m), \tag{5.2}$$

where $\overline{P_{r_b}}(m)$ is the mean received power of the signal from base station b at the mobile m (in units of dBm) and P_{t_b} is the transmit power of the signal from base station b (also in units of dBm).

Step (v) simulates short-term fading in each of the desired and interfering signals received by the mobiles. As stated in Section 5.2.2, due to short-term fading the signal envelope (units of voltage) is assumed to follow a Rayleigh distribution. Statistical theory shows that the short-term fading of the signals in terms of power (units of watts) may be modelled using an exponential distribution. In particular, the *instantaneous* received signal strengths, $P_{r_b}(m)$ (in units of dBm), can be modelled as

$$P_{r_b}(m) = 10 \log_{10} (X), \tag{5.3}$$

where the exponential random variable X has the probability density function

$$p_X(x) = \frac{1}{\mu} \exp\left(\frac{-x}{\mu}\right). \tag{5.4}$$

In (5.4), μ is the mean received signal power at the relevant mobile m from the relevant base station b in linear units, i.e. $\mu = 10^{\frac{\overline{P_{r_b}}(m)}{10}}$.

It is assumed that i_b mobiles are connected to each base station b. In Step (vi), the instantaneous SIR for each mobile located on the desired floor is determined using

$$SIR_{Mobile} = \frac{1}{\sqrt{\frac{2\alpha}{3N}(i_{b_{con}} - 1 + \beta)}}, \tag{5.5}$$

where α is the voice activity factor (assumed to be 0.5), N is the processing gain (assumed to be 511), $i_{b_{con}}$ represents the total number of mobiles connected to the base station serving the mobile of interest (*Mobile*), and β is the ratio of the total instantaneous *inter-cell* interference power to the instantaneous desired signal power.

Mobiles connected to a base station different from that of the mobile of interest (*Mobile*) present inter-cell interference, such that β is

$$\beta = \frac{\text{Inter-cell interference power}}{\text{Desired power}} = \frac{\sum_{b=1, b \neq b_{con}}^{B} i_b \cdot 10^{\frac{P_{r_b}(Mobile)}{10}}}{10^{\frac{P_{r_{b_{con}}}(Mobile)}{10}}}, \tag{5.6}$$

where B is the total number of base stations in the system.

In Step (vii), the number of mobiles on the desired floor that have outages is calculated by determining whether the instantaneous SIR at the relevant location, SIR_{Mobile} is below a threshold at which the BER is 0.02. As stated earlier, this threshold is equivalent to an SIR of 4.32 dB according to the complementary Gauss probability integral.

In Step (viii), all the previous steps are repeated for I iterations, such that the resulting mean downlink outage probability (calculated in the subsequent step) is accurate to four decimal places.

In Step (ix), the mean downlink outage probability is calculated by dividing the number of outages by the number of mobiles on the desired floor in all iterations.

5.2.3.2 Uplink system performance estimation

The uplink system performance estimation (summarised in Figure 5.1) is similar to the downlink system performance estimation described in Section 5.2.3.1, except that the outage probability is estimated for signals received at the base station.

Steps (i) to (iii) for the uplink system performance estimation are identical to those described in Section 5.2.3.1 for the downlink system performance estimation.

The base station for which the performance is determined is known as the desired base station. Assuming perfect uplink power control, Step (iv) calculates the mean received power, $\overline{P_{r_{b_{des}}}}(m)$, from each mobile at the desired base station, b_{des}, using

$$\overline{P_{r_{b_{des}}}}(m) = P_{des} + PL_{b_{con}}(m) - PL_{b_{des}}(m), \tag{5.7}$$

where P_{des} is the mean received power (dB) at the desired base station, $PL_{b_{con}}(m)$ is the mean path loss between the unique mobile m (located at the three-dimensional coordinates (x, y, z)) and the base station to which the mobile is connected (b_{con}). In (5.7), $PL_{b_{des}}(m)$

is the mean path loss between the unique mobile location m and the desired base station, b_{des}, for which the performance is being quantified.

In Step (v), Rayleigh fading is applied to the signal from each mobile, m, to the desired base station, b_{des}, using an exponential distribution. In particular, the *instantaneous* received signal strengths, $P_{r_{b_{des}}}(m)$ (in units of dBm), are modelled as

$$P_{r_{b_{des}}}(m) = 10\log_{10}(X), \tag{5.8}$$

where the exponential random variable X has the probability density function

$$p_X(x) = \frac{1}{\mu}\exp\left(\frac{-x}{\mu}\right). \tag{5.9}$$

In (5.9), μ is the mean received signal power at the desired base station b_{des} from the mobile m in linear units, i.e. $\mu = 10^{\frac{\overline{P_{r_{b_{des}}}}(m)}{10}}$.

In Step (vi) the instantaneous SIR is determined for each mobile, *Mobile,* which is connected to the desired base station. It is assumed that *other* mobiles connected to the desired base station have the unique identifiers $m = 1, 2, 3 \ldots i$. The mobiles connected to *other* base stations have the unique identifiers $m = i{+}1, i{+}2, i{+}3, \ldots j$. The instantaneous SIR for the mobile, *Mobile*, connected to the desired base station is

$$SIR_{Mobile} = \frac{1}{\sqrt{\frac{2\alpha}{3N}(\gamma+\beta)}}, \tag{5.10}$$

where the ratio of the intra-cell interference power to the desired power for the mobile on the uplink is

$$\gamma = \frac{\text{Intra-cell interference power}}{\text{Desired power}} = \frac{\sum_{m=1}^{i} 10^{\frac{P_{r_{b_{des}}}(m)}{10}}}{10^{\frac{P_{r_{b_{des}}}(Mobile)}{10}}} \tag{5.11}$$

and the ratio of the inter-cell interference power to the desired power for the mobile on the uplink is

$$\beta = \frac{\text{Inter-cell interference power}}{\text{Desired power}} = \frac{\sum_{m=i+1}^{j} 10^{\frac{P_{r_{b_{des}}}(m)}{10}}}{10^{\frac{P_{r_{b_{des}}}(Mobile)}{10}}}. \tag{5.12}$$

In Step (vii), the number of mobiles that have outages on the uplink is calculated by determining whether the instantaneous SIR for each mobile is below a certain threshold at which the BER is greater than 0.02.

In Step (viii) the above process (from Steps (i) to (vii)) is repeated for a given number of iterations (I) such that the resulting mean uplink outage probability is accurate to four decimal places.

Finally in Step (ix) the mean uplink outage probability is calculated by dividing the total number of mobiles having outages in all iterations by the total number of connections made to the desired base station in all iterations.

5.3 Scenarios

In this thesis, a scenario-based approach is used to compare the performance estimates for various hypothetical deployment configurations. The scenarios have been chosen based on the deployment configurations that wireless operators are likely to deploy.

Table 5.1 summarises these scenarios, together with the deployment configurations and the propagation measurement campaigns that investigate them. The scenarios shown are the basis for meaningful comparisons of the performance results throughout this chapter and subsequent Chapters 7 and 8, in which the implementation of multiuser detection is investigated. For simplicity, only the signal between each mobile and the base station to which it is connected (i.e. the desired base station) is shown. Any interfering signals presented to either the mobiles (on the downlink) or the base stations (on the uplink) are not shown but may be inferred from the deployment configuration diagrams.

As shown in Table 5.1, the three scenarios investigated are as follows:

- ***Indoor-only*** – Base stations and mobiles are located indoors and there is no interference emanating from outdoors. This scenario is investigated using all three propagation measurement campaigns. In PM A and PM C, this scenario is investigated assuming base stations and mobiles on a single floor of a building. In PM B, this scenario is investigated using base stations and mobiles located on *three separate* floors of a building. The results of this scenario are useful for wireless operators designing dedicated indoor DS-CDMA systems which have no external interference presented to them.

- ***Interfering indoor/outdoor*** – An indoor DS-CDMA system (having base stations and mobiles indoors) coexists with an outdoor DS-CDMA system (having base stations and mobiles located outdoors). The two systems share the same bandwidth and therefore mutually interfere with each other. This scenario is investigated using mean path loss propagation data from PM A and PM B. Of particular importance to the investigation is the influence of outdoor interference on the optimal deployment strategy used for the indoor DS-CDMA system. The results of this scenario are useful for wireless operators wishing to integrate indoor picocellular systems and outdoor macro-/microcellular systems.

- ***Interfering adjacent*** – Two separate indoor DS-CDMA systems located in adjacent buildings mutually interfere with each other. This scenario is investigated using mean path loss propagation data from PM C.

Scenario	Layout of base stations and mobiles	PM A	PM B	PM C
Indoor-only	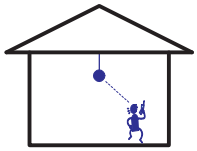	√	√	√
Interfering indoor/outdoor	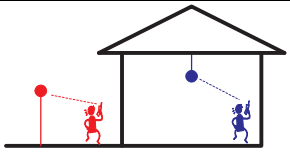	√	√	
Interfering adjacent	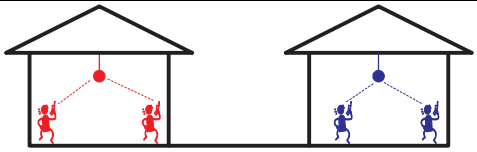			√

Table 5.1: Deployment scenarios considered in this thesis. N.B. In the *interfering indoor/outdoor* and *interfering adjacent* scenarios, the system shown in red shares the same bandwidth as the system shown in blue. However, the systems operate separately and are uncoordinated. For this reason, the systems mutually interfere with each other.

5.4 System performance estimation results

This section presents the system performance estimation results for the generalised scenarios shown in Table 5.1 using the results from the three propagation measurement campaigns described in Chapter 4. The estimates have been made using the Monte Carlo analysis described in Section 5.2.3.

The propagation measurement campaigns form three general cases of indoor/outdoor systems that are investigated in this thesis:

- Single floor indoor system coexisting with outdoor system (PM A), presented in Section 5.4.1.
- Multi-floor indoor system coexisting with outdoor system (PM B), presented in Section 5.4.2.
- Two adjacent indoor systems coexisting with each other (PM C), presented in Section 5.4.3.

5.4.1 Single floor indoor system coexisting with outdoor system (PM A)

This section investigates the deployment and performance of a single floor indoor system that coexists with an outdoor system, using measured mean path loss data from PM A. In PM A, transmitters were deployed on a single floor of the Tower Block of the School of Engineering at The University of Auckland as well as outdoors on the roofs of the adjacent Library Block and Lecture Theatre Block (shown in Figure 5.2). The following sections present the downlink and uplink performance estimates for the *indoor-only* scenario (Section 5.4.1.1) and the *interfering indoor/outdoor* scenario (Section 5.4.1.2).

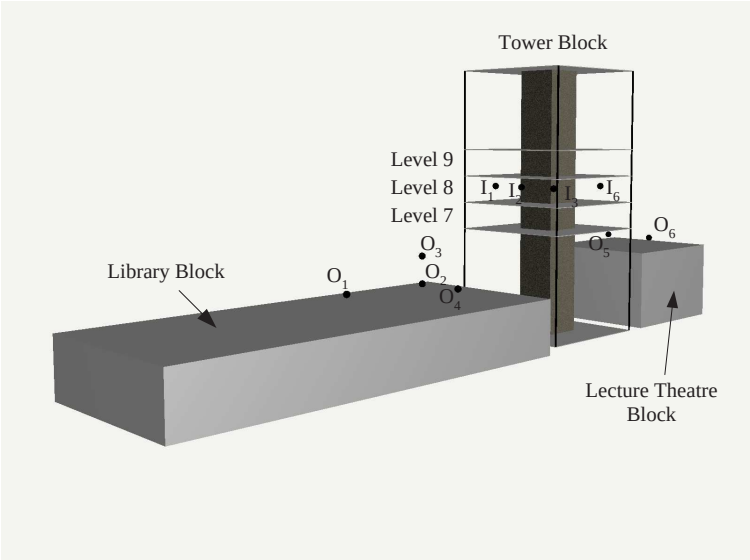

Figure 5.2: Transmitter locations in PM A. N.B. Transmitters I_4 and I_5 are obscured from view by the central steel-reinforced concrete core in the Tower Block.

5.4.1.1 Indoor-only scenario

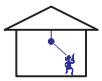

Simple configurations deploying two base stations on a single floor in the Tower Block of the School of Engineering are shown in Table 5.2. Configurations Ad.x have the base stations **ad**jacently located within 5 metres of each other. In Configurations Di.x, the base stations are **di**agonally opposite each other, while in Configurations Op.x the base stations are located on **op**posite sides of the building. Finally Configurations Si.x have the base stations on the same **si**de of the building but with a longer separation distance than those in Configurations Ad.x. For simplicity, the central steel-reinforced concrete core is not shown in the diagrams in Table 5.2, but is a key factor that influences system performance.

Configuration	Ad.1	Ad.2	Ad.3	Di.1	Di.2
Layout					
Configuration	Op.1	Op.2	Op.3	Si.1	Si.2
Layout					

Table 5.2: Indoor base station deployment configurations in PM A.

Downlink system performance

Figure 5.3 is a graph comparing the downlink outage probabilities[2] for the base station configurations shown in Table 5.2.

It is clear that the configurations in which the base stations are located close to each other (Ad.x) have significantly worse downlink system performance than any of the other configurations. This is due to the lack of dominance of any one base station throughout the floor, thus causing relatively equal levels of received signal strength from each of the base stations. As a result, the SIR across the floor is poor, resulting in a higher number of outages. The correlation coefficients between the signals of the base stations in Ad.1, Ad.2 and Ad.3 are 0.80, 0.71 and 0.77 respectively. Although all these coefficients are positive, the insufficient margin between the desired and interfering signals results in poor performance.

Two of the configurations with the base stations on opposite sides of the building (Op.2 and Op.3) have the best performance. For the majority of the coverage area, one of the base stations is likely to have a dominant signal due to the relative locations of the base stations. The correlation coefficients between the signals of the base stations in Op.2 and Op.3 are -0.51 and -0.75 respectively. This shows that at any given location on the floor, it is likely that the signal from one base station is strong while the signal from the other base station is weak.

The configurations Di.x, Si.x, and Op.1 have mid-range performance levels in comparison to the configurations discussed previously.

[2]In this thesis, the various deployment configurations are compared on the basis of their relative mean outage probabilities for the downlink/uplink. It is also useful to compare the capacity increase (in terms of the maximum number of serviceable mobiles) at a given mean outage probability. This information can be inferred easily from the graphs in this thesis, as discussed in Appendix C.

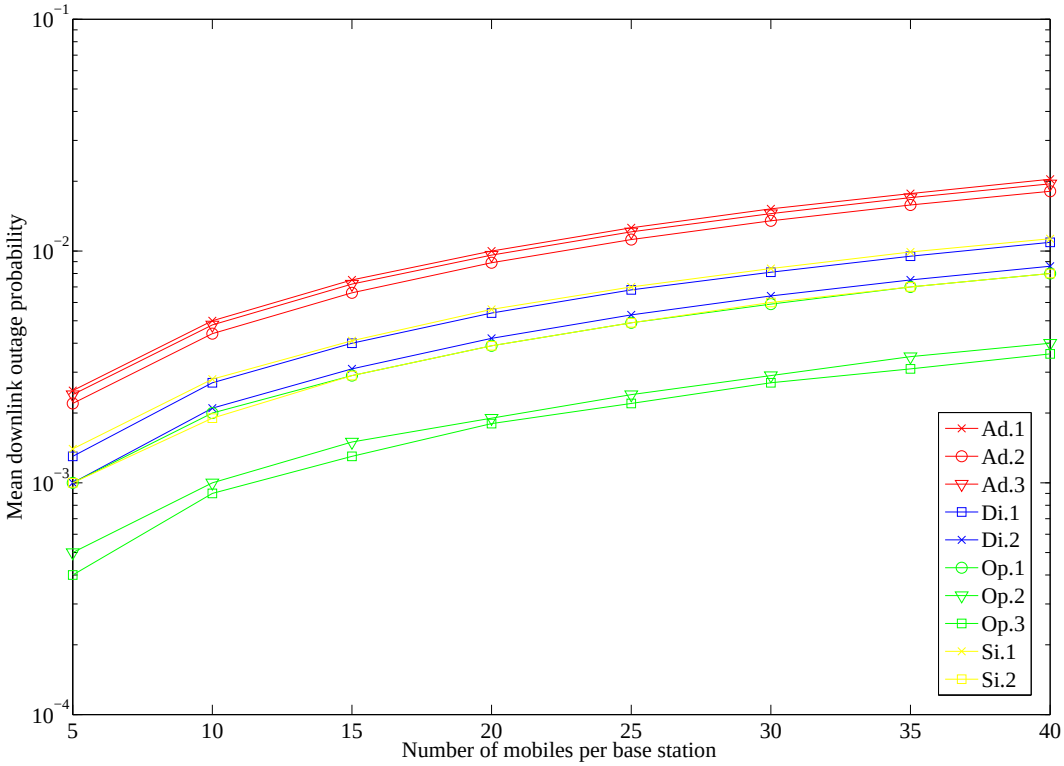

Figure 5.3: Mean downlink outage probability for mobiles on Level 8 of the Tower Block for the configurations shown in Table 5.2 (PM A).

Uplink system performance

Figure 5.4 is a graph comparing the uplink outage probabilities for the base station configurations shown in Table 5.2.

The differences between the outage probabilities of the various deployment configurations on the uplink are much smaller than those observed on the downlink. However, the trends observed on the uplink are similar to those on the downlink. For example, deployment configurations Ad.x have the poorest uplink system performance of any of the deployment configurations, while deployment configurations Op.2 and Op.3 have the best uplink performance of any of the deployment configurations. The smaller differences in outage probabilities on the uplink than the downlink are due to the use of the uplink power control algorithm.

In deployment configurations Ad.x, the relatively short distance between the base stations means that the signals from *all* the mobiles are received at a particular desired base station with similar mean signal strengths (regardless of whether the mobile is connected to the desired base station or the interfering base station). Therefore, the inter-cell interference presented by a mobile connected to the interfering base station is similar to the signal power of a mobile connected to the desired base station. By contrast, in deployment configurations Op.2 and Op.3 the base stations are located on opposite sides of the central steel-reinforced concrete core. From the perspective of the desired base station,

both distance and the central steel-reinforced concrete core 'isolate' the inter-cell interfering mobiles that are connected to the other base station. Therefore, inter-cell interference levels are lower than in deployment configurations Ad.x and as a result improved uplink system performance is attained.

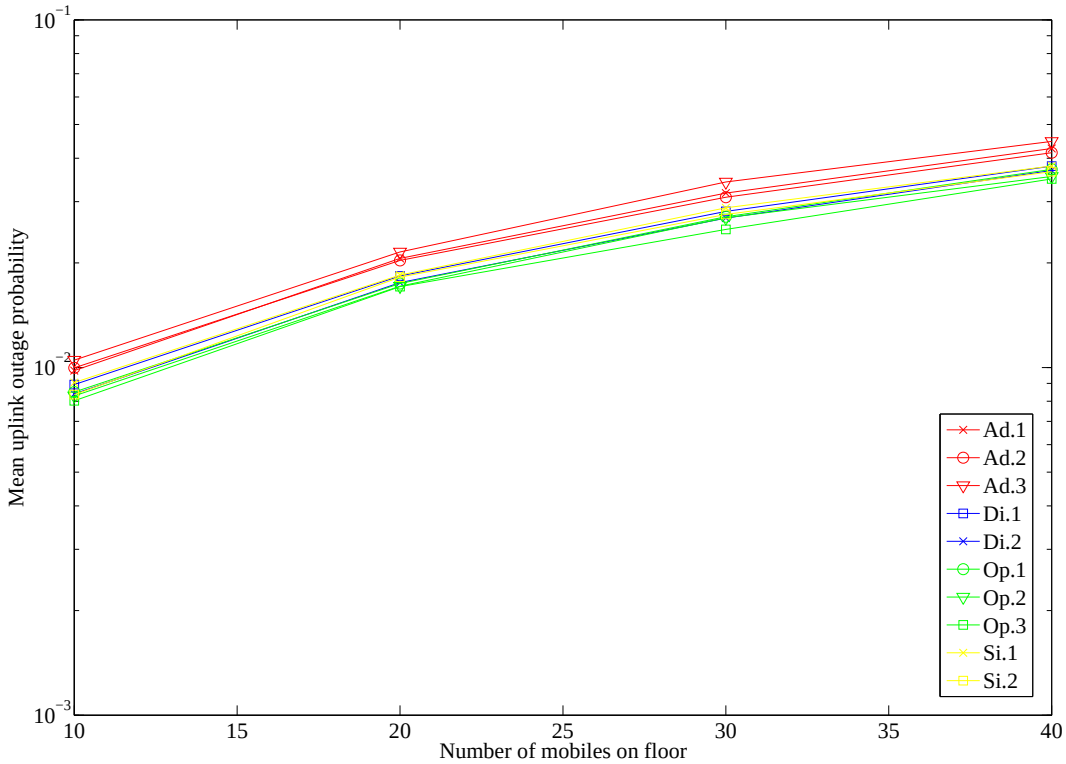

Figure 5.4: Mean uplink outage probability for mobiles on Level 8 of the Tower Block for the configurations shown in Table 5.2 (PM A).

5.4.1.2 Interfering indoor/outdoor scenario

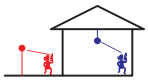

This scenario investigates the influence of an interfering outdoor system on the deployment and performance of a single-floor indoor system operating on Level 8 of the Tower Block at the School of Engineering. Due to the unavailability of measured received mean signal strength data at outdoor locations, it is necessary to investigate the downlink and uplink using separate (but related) deployment configurations. The investigations for the downlink and uplink are now discussed in turn and then related to each other.

Downlink system performance

Several configurations deploying a single base station outdoor DS-CDMA system interfering with a single base station indoor DS-CDMA system are shown in Table 5.3. In Configurations SSI.x, the indoor base station is on the same side of the building as the

interference emanating from the outdoor base station. In Configurations OSI.x, the indoor base station is on the **o**pposite **s**ide of the building in relation to the **i**nterference emanating from the outdoor base station.

Configuration	SSI.1	SSI.2	SSI.3	SSI.4
Layout	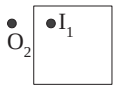	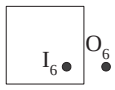	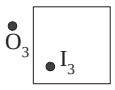	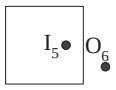
Configuration	**OSI.1**	**OSI.2**	**OSI.3**	**OSI.4**
Layout	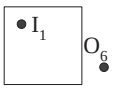	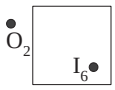	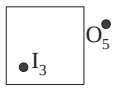	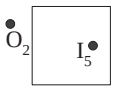

Table 5.3: Interfering indoor/outdoor deployment configurations for which the downlink system performance is investigated in PM A.

Assuming that the outdoor and indoor base stations have the same transmit power, Figure 5.5 is a graph of the downlink performance for indoor mobiles in the various configurations shown in Table 5.3.

It is evident that Configurations SSI.x have significantly better downlink performance than Configurations OSI.x. This behaviour may be explained by a 'shielding effect' caused by the indoor base station in Configurations SSI.x. In these configurations, mobiles located near the side of the building from which the outdoor interference emanates receive a strong desired signal from the indoor base station. While the interference level is also likely to be strong on this side of the building, the high desired signal strength ensures that the SIR levels are also high, resulting in good performance.

For Configurations OSI.x, there are greater variations in the SIR levels inside the building. For example, mobiles located at the side of the building closest to the outdoor interference will receive a weak desired signal from the indoor base station and a strong interfering signal from outdoors, resulting in a poor SIR. However, mobiles close to the indoor base station will receive a strong desired signal and a weak interfering signal from outdoors, resulting in an excellent SIR. The high variations in SIR across the indoor coverage area cause higher outage probabilities than those observed in Configurations SSI.x.

Clearly the behaviour observed may be explained by the levels of correlation between the desired and interfering signals. The correlation coefficients for Configurations SSI.x vary from 0.40 to 0.76 while those for Configurations OSI.x vary from -0.88 to -0.55. The

positive correlation coefficients are beneficial to downlink system performance and the negative correlation coefficients are detrimental.

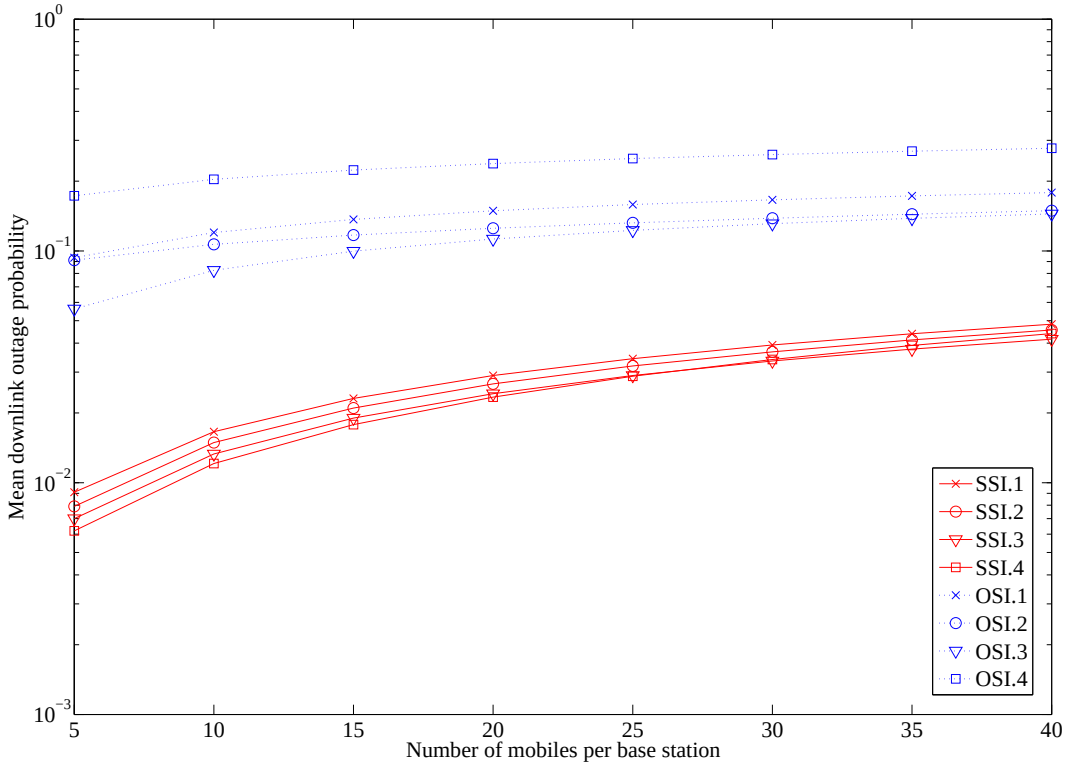

Figure 5.5: Mean downlink outage probability for mobiles on Level 8 of the Tower Block for the configurations shown in Table 5.3 (PM A).

Figure 5.5 compares the mean downlink outage probabilities of the interfering indoor/outdoor configurations based on the assumption that the indoor and outdoor base stations have the same transmit powers. In reality, however, the indoor and outdoor base stations are likely to have different transmit powers or the outdoor base station may be located at any arbitrary distance from the building. Therefore, various levels of outdoor interference may be presented to the indoor system.

To demonstrate the influence of the level of outdoor interference on indoor downlink system performance, Figure 5.6 is a graph of the mean downlink outage probabilities for various outdoor interference power levels relative to the transmit power of the indoor base station. The outdoor interference power is measured indoors at the side of the building nearest to the outdoor base station. It is assumed that there are 20 mobiles served by each of the indoor and outdoor base stations.

It is evident from Figure 5.6 that an increase in outdoor interference power by 10 dB degrades the mean downlink outage probability by as much as an order-of-magnitude. Additionally, there are reduced differences between the mean downlink outage probabilities of the SSI.x and OSI.x deployment configurations with an increase in the outdoor interference power.

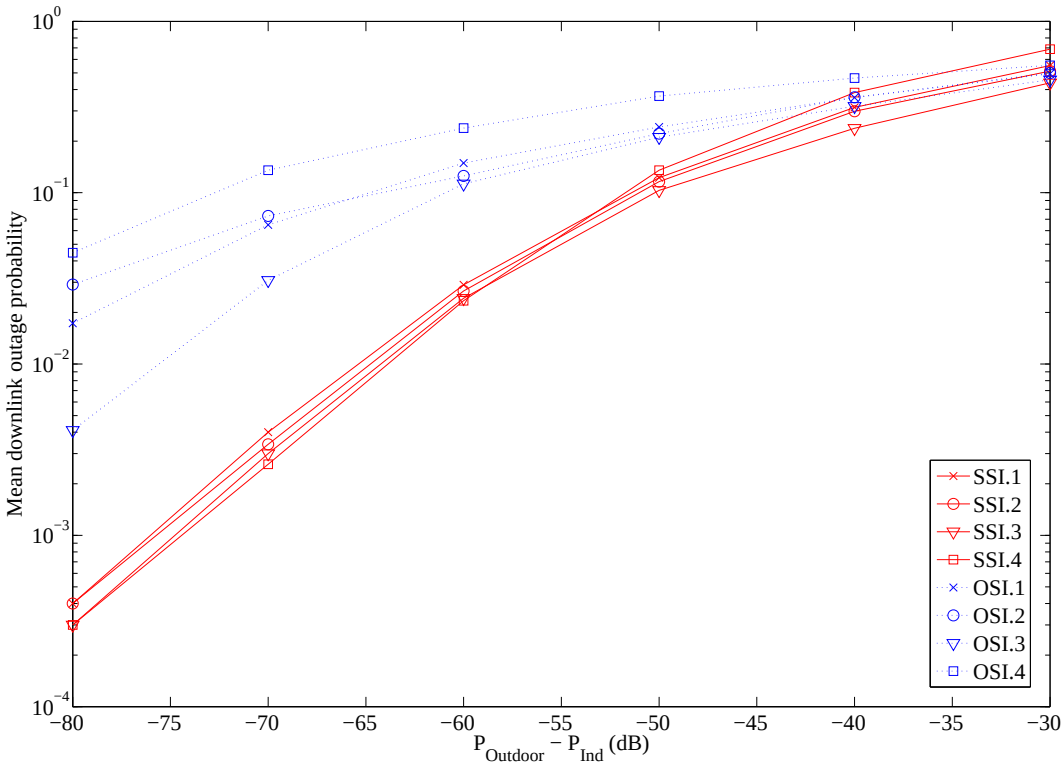

Figure 5.6: Mean downlink outage probability for mobiles on Level 8 of the Tower Block for the configurations shown in Table 5.3 assuming various levels of outdoor interference from one side of the Tower Block (PM A). N.B. In the above graph, $P_{Outdoor}$ is the power of the outdoor interference measured indoors at the side of the building nearest to the outdoor base station, while P_{Ind} is the transmit power of the indoor base station.

Uplink system performance

The uplink system performance is investigated assuming that outdoor interference emanates from outdoor mobiles situated to the left hand side of the building. The deployment configurations considered are shown in Table 5.4. Figure 5.7 is a graph of the mean uplink outage probabilities for the various deployment configurations. It is assumed that there are 20 mobiles indoors and outdoor interference emanates from 20 mobiles. For simplicity, it is further assumed that the signals from the outdoor mobiles are received with the same mean signal strength at the left hand side of the building. The graph shows the mean uplink outage probabilities of the deployment configurations for various outdoor interference power levels (measured indoors at the left hand side of the building) relative to the power controlled mean received power of the indoor mobiles at the indoor base station.

From the graph it is evident that if the indoor base station is nearer to the side of the building from which outdoor interference emanates (i.e. in Configurations SSI.x), there is more significant degradation in the uplink system performance for indoor mobiles. This is to be expected, as the outdoor interference level presented to the indoor base station is higher in this case (i.e. in Configurations SSI.x) than if the indoor base station is further away (Configurations OSI.x) due to both distance dependent loss and the shadowing caused by the central steel-reinforced concrete core.

Configuration	SSI.1	SSI.2	SSI.3
Layout	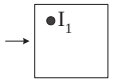	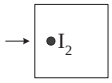	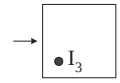
Configuration	**OSI.1**	**OSI.2**	**OSI.3**
Layout	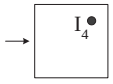	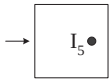	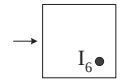

Table 5.4: Interfering indoor/outdoor deployment configurations for which the uplink system performance is investigated in PM A. N.B. Arrows indicate the origin of uplink interference from outdoors.

Summary

This section has investigated the influence of outdoor interference on the performance of simple single base station indoor configurations. On the downlink, it is evident that

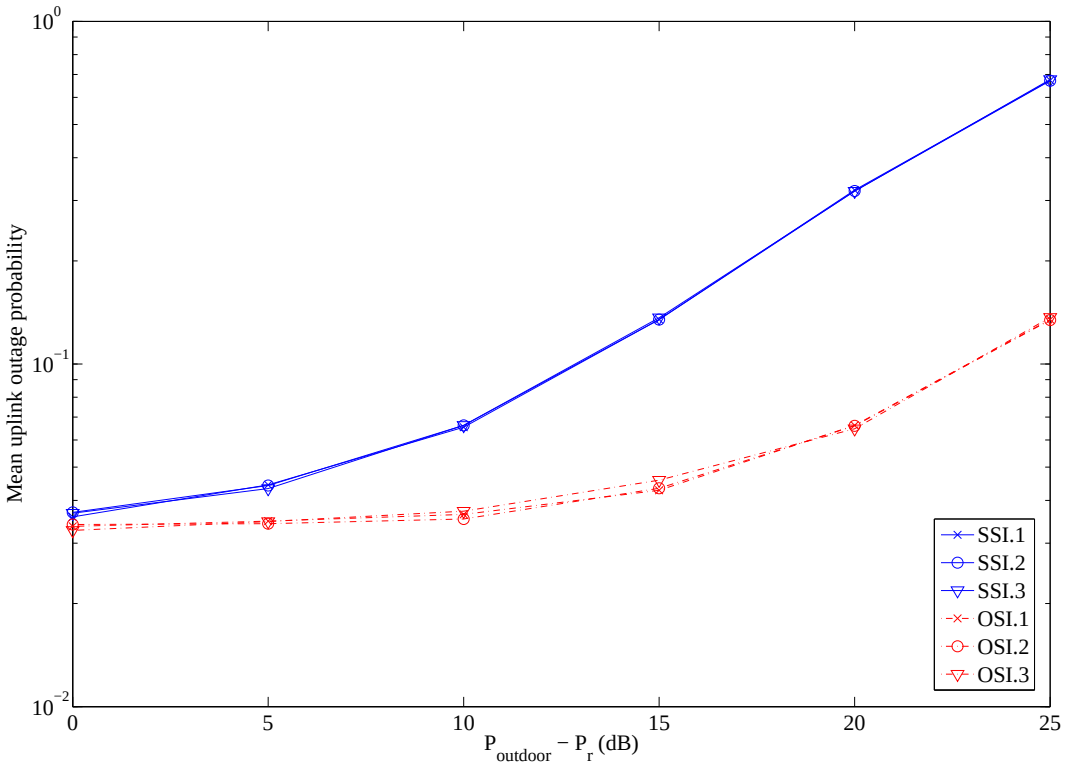

Figure 5.7: Mean uplink outage probability for mobiles on Level 8 for various interfering indoor/outdoor configurations (shown in Table 5.4) assuming 20 mobiles per floor and the outdoor interference level shown (PM A).
N. B. $P_{outdoor}$ is the mean power of each of the outdoor interfering mobile signals measured indoors at one side of the building while P_r is the power controlled mean received power of the indoor mobiles (at the indoor base station).

optimal performance is attained if the indoor base station is located *nearer* to the side of the building from where the outdoor interference emanates. However, on the uplink, optimal performance is attained if the indoor base station is located *further* from the side of the building from where the outdoor interference emanates. Clearly the optimal deployment requirements for the downlink and uplink directly conflict with each other.

5.4.2 Multi-floor indoor system coexisting with outdoor system (PM B)

Using measured mean path loss propagation data from PM B, this section investigates the deployment and performance of base stations in a three-dimensional configuration inside a building (the Tower Block) in the presence of interfering base stations located outdoors on the roof of a nearby building (the Library Block). A three-dimensional drawing of the buildings including the base station locations in PM B is shown in Figure 5.8.

This section begins by presenting the downlink and uplink system performance estimation results for three-dimensional configurations of indoor base stations *without* the influence of outdoor interference (*Indoor-only* scenario). Following this, the influence of outdoor interference on indoor system performance is investigated (*Interfering indoor/outdoor* scenario).

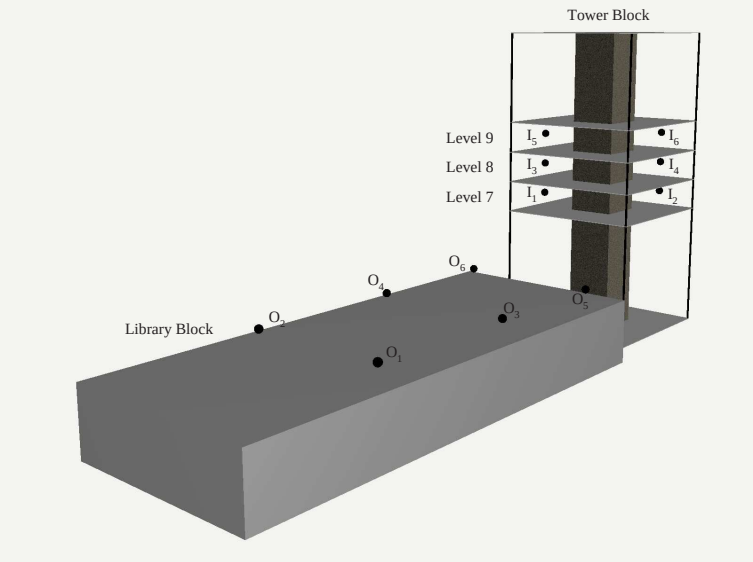

Figure 5.8: Transmitter locations in PM B.

5.4.2.1 Indoor-only scenario

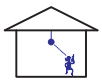

Assuming that a three-dimensional indoor system is operating on Levels 7 to 9 of the Tower Block shown in Figure 5.8, a number of possible base station deployment configurations are shown in Table 5.5. Each of these configurations uses a single base station on each of Levels 7 to 9 of the Tower Block to provide coverage to mobiles also located on Levels 7 to 9.

In Configurations *Aligned 1* and *Aligned 2*, all the base stations are vertically aligned with each other while in Configurations *Offset 1* and *Offset 2* the base stations are vertically offset from each other. In Configurations *Aligned/Offset 1* to *Aligned/Offset 4*, one base station is aligned with the base station on Level 8 while the other is vertically offset from the base station on Level 8.

Config.	Aligned 1	Aligned 2	Offset 1	Offset 2
Base Station Layout	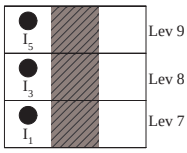	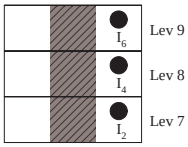	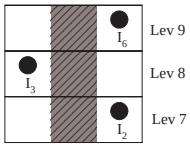	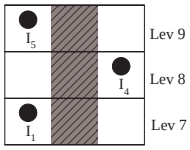
Config.	**Aligned/Offset 1**	**Aligned/Offset 2**	**Aligned/Offset 3**	**Aligned/Offset 4**
Base Station Layout	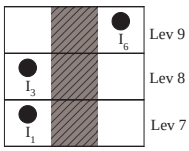	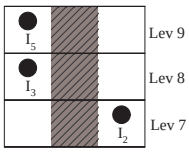	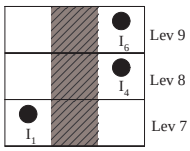	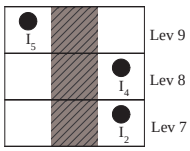

Table 5.5: Front view of indoor base station deployment configurations in PM B (Indoor-only scenario).

Downlink system performance

Figure 5.9 is a graph comparing the mean downlink outage probabilities for mobiles on Level 8 in each of the eight configurations shown in Table 5.5.

The following trends are observed:

1. The aligned configurations *Aligned x* have the lowest mean downlink outage probabilities and therefore exhibit the best performance of all the configurations.

2. The offset configurations *Offset x* have the highest mean downlink outage probabilities and therefore exhibit the worst performance of all the configurations.

3. The configurations containing a single aligned interfering base station and a single offset interfering base station (*Aligned/Offset x*) have performance levels which are in between the performance levels observed for the aligned and the offset configurations listed in 1 and 2 above.

The above trends confirm those observed in [25, 26] and may be explained by the signal correlation levels between the desired and interfering transmissions (presented in Chapter 4). The aligned configurations have a desired transmission that is *positively* correlated with both interfering transmissions while the offset configurations have a desired transmission that is *negatively* correlated with both interfering transmissions. The correlation behaviour in each of the configurations has a direct influence on the SIR across the coverage area (and therefore also the resulting outage probabilities observed). To demonstrate this, contour maps showing the mean SIR[3] across Level 8 for the *Aligned 1* and *Offset 1* configurations are shown in Figures 5.10 and 5.11 respectively. It is evident that in Configuration *Aligned 1*, the mean SIR is very similar throughout Level 8 (varying from 20.7 dB to 22.1 dB). By contrast, in Configuration *Offset 1* there are greater variations in the mean SIR (varying from 17.4 dB to 22.1 dB), together with 'low' mean SIR levels towards the lower right hand side of the floor (shown in red, i.e. a mean SIR of approximately 17.5 dB to 18.5 dB) and transition regions between areas of 'high' and 'low' mean SIR levels (shown in light blue, i.e. a mean SIR of approximately 20.0 to 20.5 dB). This is a direct result of the negative correlation between the desired and interfering signals in Configuration *Offset 1*, ultimately causing higher outage probabilities than those observed in the aligned configurations.

Uplink system performance

Figure 5.12 compares the mean uplink outage probabilities on Level 8 in each of the eight configurations.

The graph of the uplink outage probabilities shown in Figure 5.12 confirms the findings in [25, 26]. The following trends are observed:

1. The differences in performance observed for the various configurations are noticeably smaller on the uplink than the downlink.

[3]The mean SIR has been calculated assuming only long- and medium-term variations in the desired and interfering signals (i.e. effects due to distance-dependent path loss and shadowing) but does not account for short-term variations (i.e. fading). The contour map has been produced by calculating the mean SIR at *each* of the measurement (i.e. mobile) locations on Level 8 and interpolating between them.

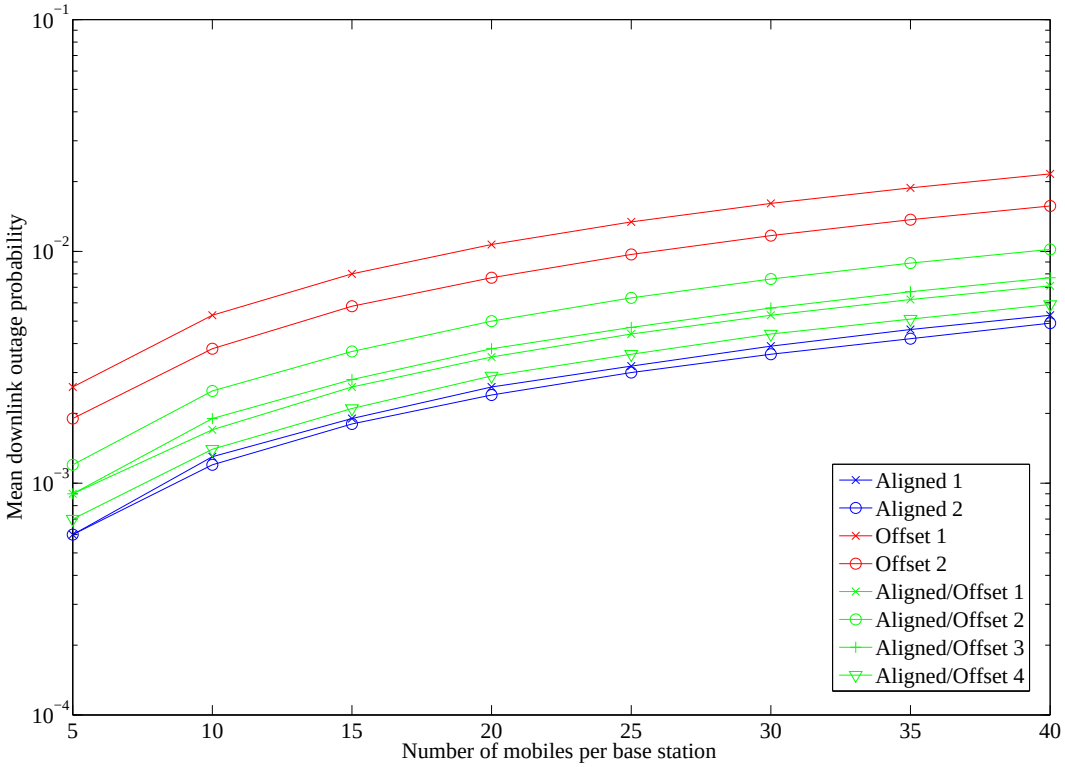

Figure 5.9: Mean downlink outage probability for mobiles on Level 8 of the Tower Block for various indoor base station deployment configurations (Indoor-only scenario) in PM B.

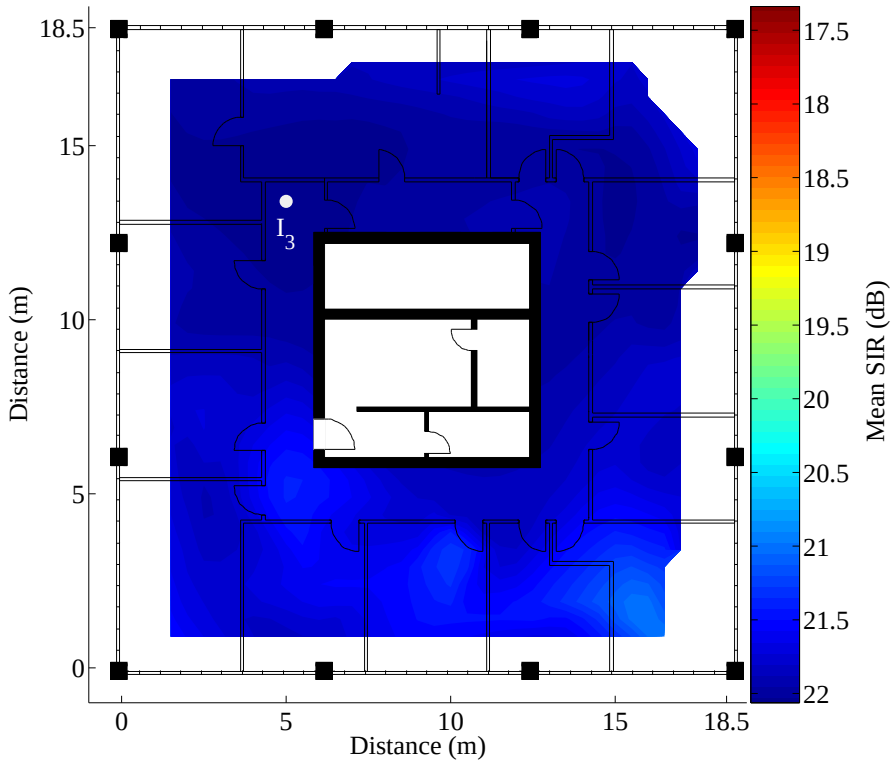

Figure 5.10: Mean SIR across Level 8 for Configuration *Aligned 1* in PM B with 20 mobiles per floor. The base station on Level 8 (I_3) is also shown. The other two base stations (I_1 and I_5) are located on adjacent floors at positions directly below and above I_3.

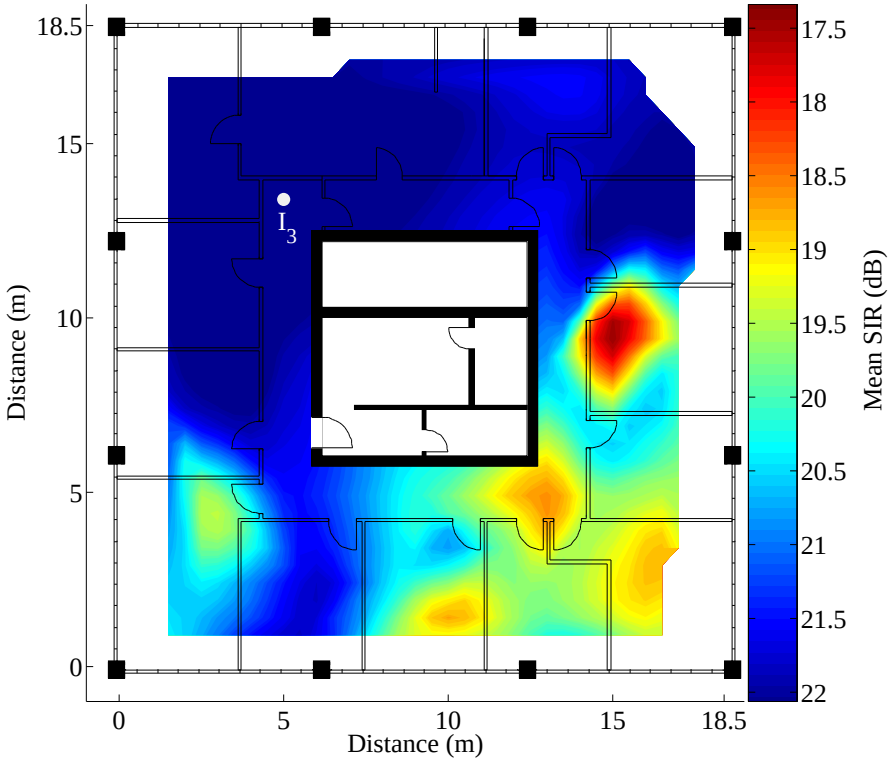

Figure 5.11: Mean SIR across Level 8 for Configuration *Offset 1* in PM B with 20 mobiles per floor. The base station on Level 8 (I_3) is also shown. The other two base stations (I_2 and I_6) are located on adjacent floors at positions offset from I_3.

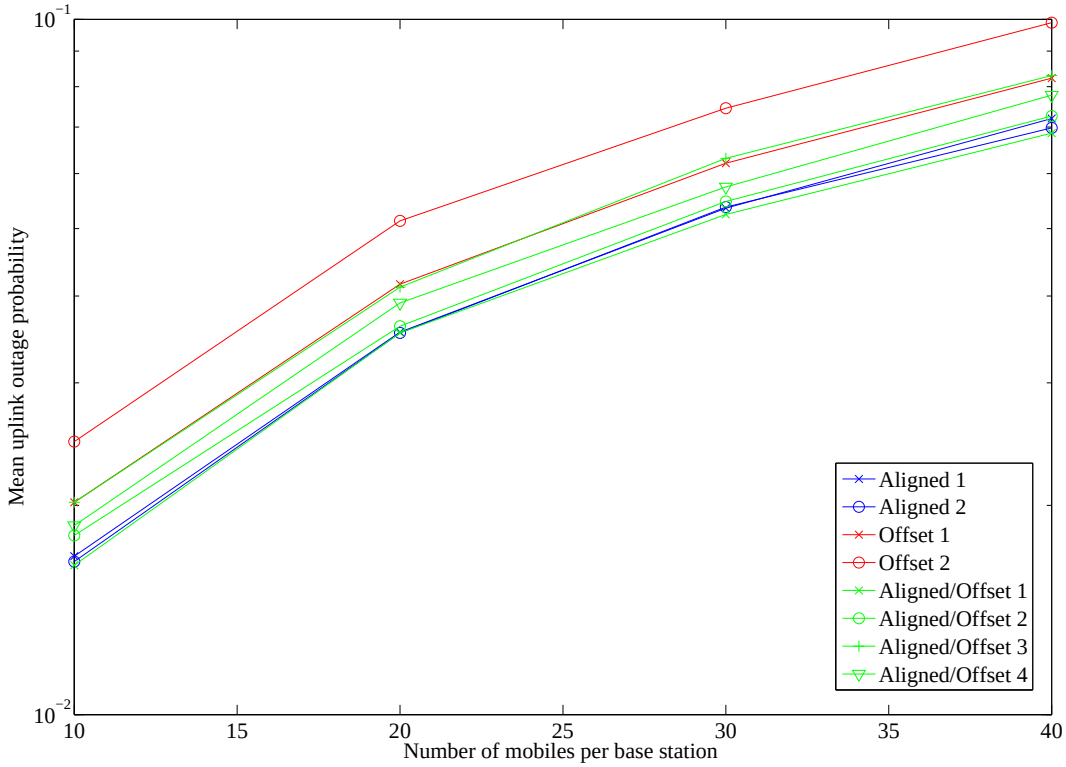

Figure 5.12: Mean uplink outage probability for mobiles on Level 8 of the Tower Block for various indoor base station deployment configurations (Indoor-only scenario) in PM B.

2. The two offset configurations have higher uplink outage probabilities than the two aligned configurations. The configurations with one aligned and one interfering base station have varying levels of performance that are slightly worse than, or similar to, those observed for the aligned configurations.

The smaller differences in outage probability on the uplink than on the downlink, also observed in [25, 26], are primarily due to the presence of power control on the uplink. In essence, power control ensures that the mobiles adjust their transmit powers so that they are received at a similar power level at the base station to which they are connected. In all of the configurations, intra-cell interference is more dominant than inter-cell interference. The levels of intra-cell interference are similar in all the configurations due to power control. Therefore, the disparities in uplink performance between the various configurations are primarily caused by inter-cell interference (i.e. from mobiles on other floors). Because the inter-cell interference is not as dominant as the intra-cell interference, the differences in uplink outage probabilities for the various configurations are small.

5.4.2.2 Interfering indoor/outdoor scenario

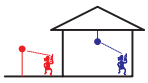

This scenario investigates the influence of outdoor interference on the deployment and performance of a three-dimensional indoor DS-CDMA system operating in the Tower Block at the School of Engineering. Due to the unavailability of measured propagation data outdoors, separate (but related) deployment configurations are investigated for the downlink and the uplink. Evaluation of the system performance for the downlink and uplink are now described in turn.

Downlink system performance

The deployment configurations considered are the same as those in Section 5.4.2.1, except that an interfering outdoor base station (O_9) is introduced, shown in Table 5.6.

Figure 5.13 is a graph of the downlink performance for indoor mobiles located on Level 8 of the Tower Block for the various deployment configurations in Table 5.6. The downlink outage probabilities have been estimated assuming that the outdoor base station, O_9, has the same transmit power as the indoor base stations.

The following observations are made:

1. The worst downlink performance is observed in the configuration *Aligned 2* + O_9. In this configuration, all the indoor base stations are on the side of the building opposite from where the outdoor interference emanates.

Config.	Aligned 1 + O_9	Aligned 2 + O_9	Offset 1 + O_9	Offset 2 + O_9
Base Station Layout	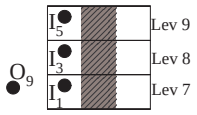	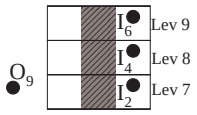	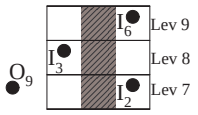	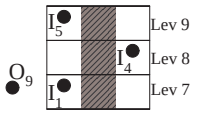
Config.	Aligned/Offset 1 + O_9	Aligned/Offset 2 + O_9	Aligned/Offset 3 + O_9	Aligned/Offset 4 + O_9
Base Station Layout	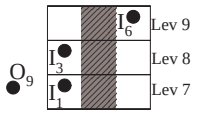	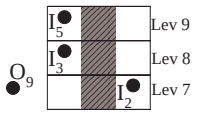	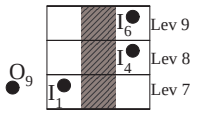	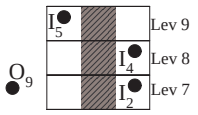

Table 5.6: Front view of interfering indoor/outdoor base station configurations considered in the investigation of downlink system performance in PM B. N.B. The diagrams shown are for indicative purposes only and are not drawn to scale.

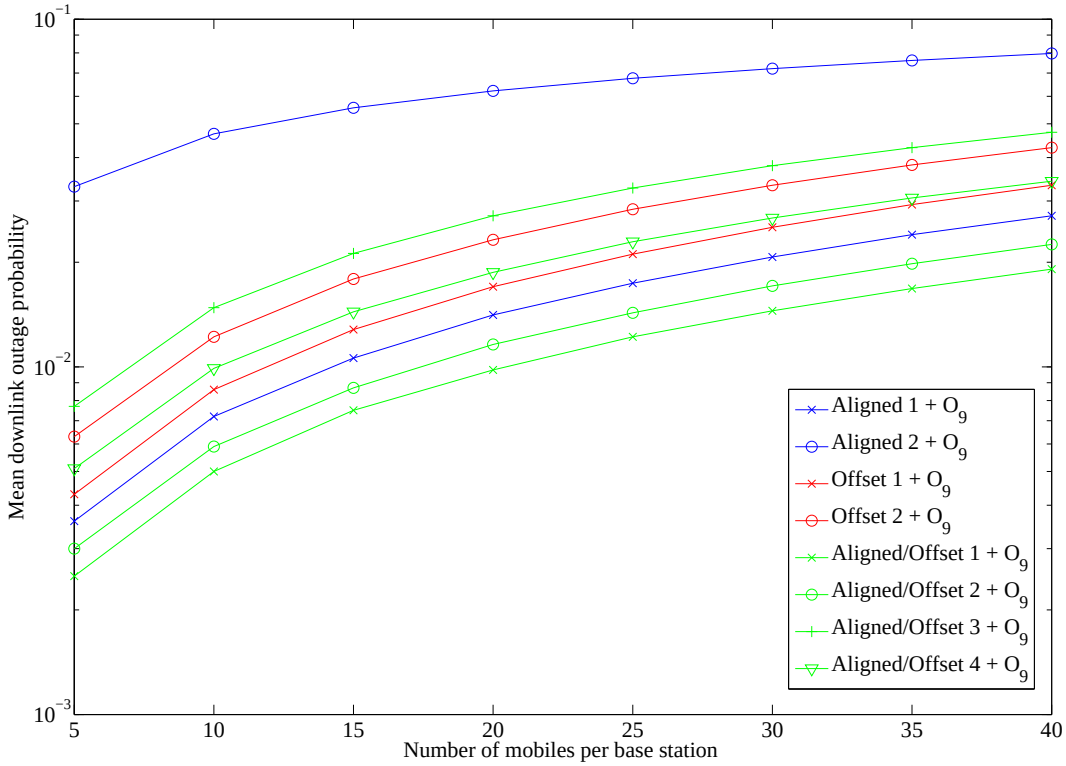

Figure 5.13: Mean downlink probability for mobiles located on Level 8 of the Tower Block for various indoor base station deployment configurations in the interfering indoor/outdoor scenario in PM B.

2. The best downlink performance is observed in configurations *Aligned/Offset 1 + O_9* and *Aligned/Offset 2 + O_9*. In these configurations the desired base station on Level 8 is near the side of the building from where the outdoor interference emanates.

3. The offset configurations have mid-range performance levels.

4. In general, improved performance is achieved if the desired base station on Level 8 is near the side of the building from where the outdoor interference emanates.

Comparing the above observations to the *indoor-only* scenario, it is evident that deployment strategies that are optimal in the absence of outdoor interference are no longer optimal if there is outdoor interference emanating from one side of the building. In the absence of outdoor interference, it was shown in Section 5.4.2.1 that the aligned configurations are optimal while the offset configurations yield the worst performance. However, it is evident from the above results that in the presence of outdoor interference from one side of the building, the performance of one of the aligned deployment configurations (*Aligned 2 + O_9*) is degraded to the extent that it has the worst performance of any of the configurations. Additionally, the performance degradations for both offset configurations in the presence of outdoor interference are less than those experienced by the aligned configurations.

The level of outdoor interference presented to the indoor system is likely to vary depending on the relative proximity and transmit power of the outdoor base station. Figure 5.14 is a graph showing the impact of the power of the outdoor interference (relative to the transmit power of the indoor base station) on the performance of the indoor base station configurations, assuming that there are 20 mobiles outdoors and on each floor indoors. The power of the outdoor interference is measured indoors at the side of the building nearest to the outdoor base station.

The graph shows that the indoor configurations have performance degradations if the outdoor interference power (measured indoors at the side of the building nearest to the outdoor base station) is as low as -100 dB relative to the transmit power of the indoor base stations. It is apparent that the aligned configuration with the indoor base stations furthest from the interfering source (*Aligned 2 + O_9*), suffers from the most performance degradation as the outdoor interference power level increases. For a higher outdoor interference power, the differences in performance between the various configurations are much less than for a lower outdoor interference power.

Uplink system performance

Similar to the downlink, the system performance on the uplink is estimated assuming that outdoor interference emanates from one side of the Tower Block. Table 5.7 shows the

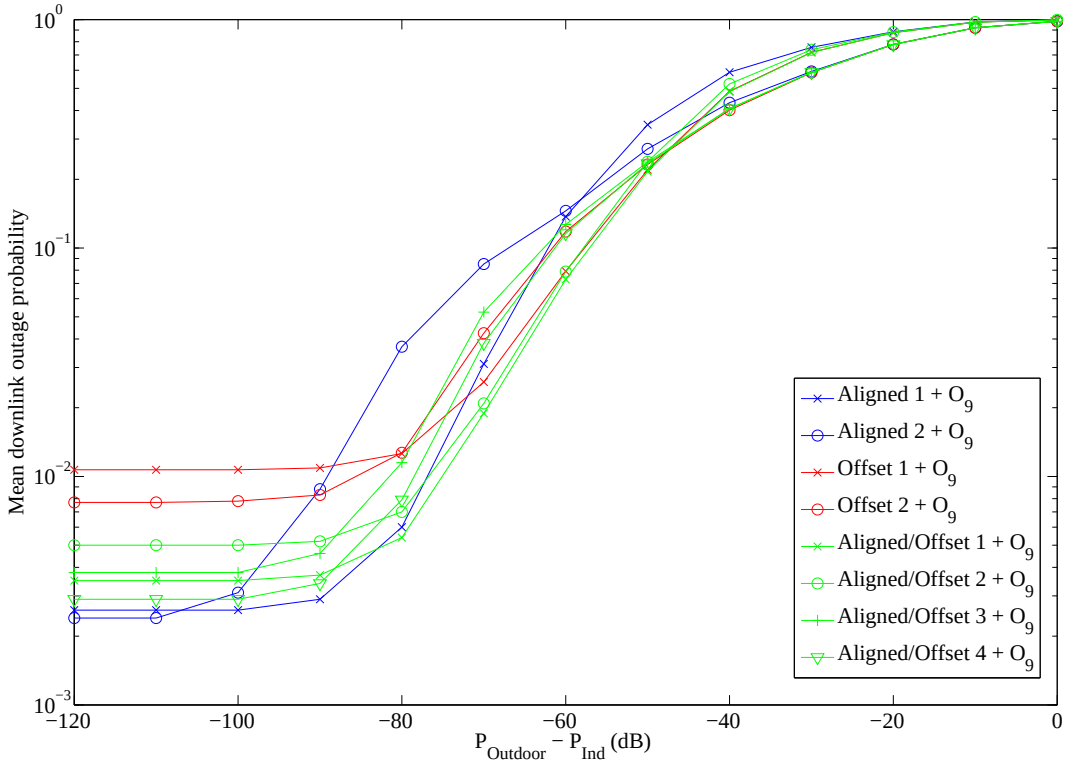

Figure 5.14: Mean downlink outage probability for mobiles on Level 8 assuming 20 mobiles per floor and the outdoor interference level shown (PM B). N.B. $P_{outdoor}$ is the mean power of the outdoor interference measured indoors at the side of the building nearest to the outdoor base station while P_{ind} is the transmit power of the indoor base station.

deployment configurations considered. Figure 5.15 is a graph showing the uplink outage probabilities for mobiles on Level 8 of the Tower Block for various outdoor interference power levels. This graph has been obtained assuming 20 mobiles on each floor indoors. The outdoor interference emanates from 20 mobiles outdoors whose signals arrive at the left side of the building with the same mean power.

Config.	Aligned 1 + OutdoorInt	Aligned 2 + OutdoorInt	Offset 1 + OutdoorInt	Offset 2 + OutdoorInt
Base Station Layout	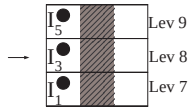	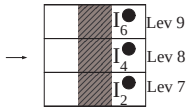	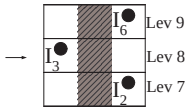	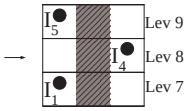
Config.	Aligned/Offset 1 + OutdoorInt	Aligned/Offset 2 + OutdoorInt	Aligned/Offset 3 + OutdoorInt	Aligned/Offset 4 + OutdoorInt
Base Station Layout	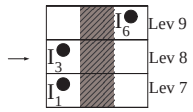	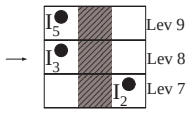	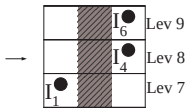	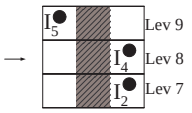

Table 5.7: Front view of interfering indoor/outdoor base station configurations considered in the investigation of uplink system performance in PM B. N.B. Arrows indicate the origin of uplink interference from outdoors.

It is evident from Figure 5.15 that the highest degradation in performance is experienced by the deployment configurations in which the base stations are *closest to* the side of the building from where the outdoor interference emanates. This is similar to the findings for PM A in Section 5.4.1. If the outdoor interference power (measured indoors) at the side of the building is the same as, or less than, the power controlled desired mean received power of the indoor mobiles at the indoor base station (i.e. $P_{outdoor}$ - $P_r \leq 0$ dB), the uplink outage probabilities for the various configurations are the same as those if there was no interference emanating from outdoors.

Summary

This section has investigated the downlink and uplink performance of a three dimensional indoor system in the presence of outdoor interference emanating from one side of the building. It has been shown that the worst performance degradation occurs on the downlink if the base stations are vertically aligned and further away from the side of the

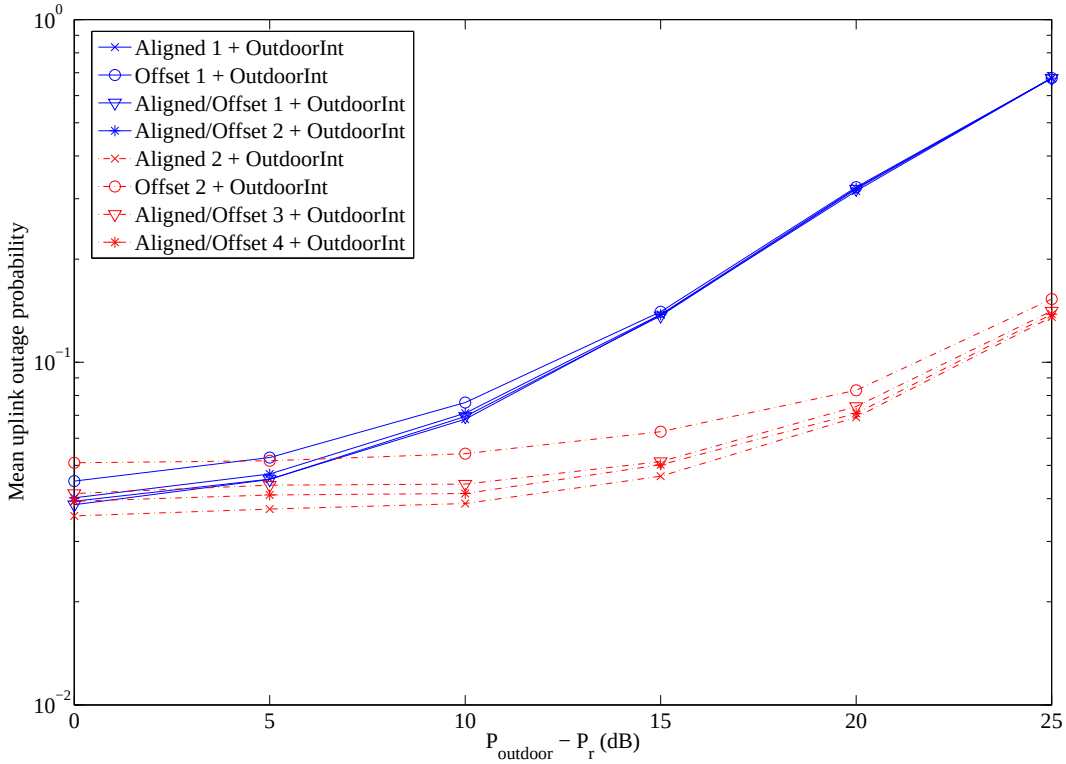

Figure 5.15: Mean uplink outage probability for mobiles on Level 8 assuming 20 mobiles per floor and outdoor interference level shown (PM B). N.B. $P_{outdoor}$ is the mean power of each of the outdoor interfering mobile signals measured indoors at one side of the building while P_r is the power controlled mean received power of the indoor mobiles.

building from which outdoor interference emanates. In general, the downlink performance degradation is minimised if the desired base station is close to the side of the building from which outdoor interference emanates. On the uplink, optimal performance is attained if the desired base station is far from the side of the building from where outdoor interference emanates.

5.4.3 Coexisting single floor indoor systems in adjacent buildings (PM C)

This section investigates the deployment and performance of two indoor DS-CDMA systems operating in two buildings located adjacent to each other. The investigation uses measured propagation data collected from PM C, described in Section 4.2.2.3. Figure 5.16 is a plan of the locations of the transmitters deployed in PM C. Transmitters were deployed and measurements collected on a single floor of the Science building and Functions building at The University of Auckland. These buildings are separated from each other by 60 metres (shown in Figure 5.16).

This section begins by presenting the performance results for simple *indoor* DS-CDMA systems deploying two base stations in each of the Science and Functions buildings (Section 5.4.3.1). These configurations assume that there is no external interference presented to the system. Following this, the deployment and performance of interfering indoor DS-CDMA systems in adjacent buildings is investigated by considering the coexistence of base stations operating in the Science and Functions buildings (Section 5.4.3.2).

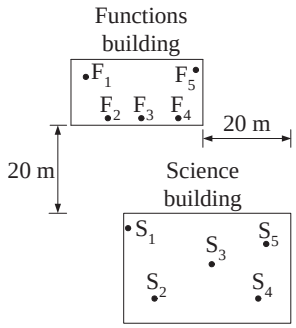

Figure 5.16: Relative locations of transmitters deployed in the Science and Functions buildings in PM C.

5.4.3.1 Indoor-only scenario

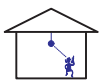

In this scenario, the deployment and performance of simple configurations deploying two base stations are considered for each of the Science and Functions buildings in PM C, assuming that there is no external interference presented.

Science building

Table 5.8 shows a selection of base station configurations for a system deployed on a single floor of the Science building. Configurations S_1S_4 and S_2S_5 have base stations that are diagonally opposite to each other. Configurations S_2S_3 and S_3S_4 have a single base station on the centre of the floor and a base station at one corner of the floor. In Configurations S_1S_2 and S_4S_5, the base stations are located on the left and right hand side of the building respectively. In the system performance analysis, the mobiles are randomly located at positions at which measurements were made on the same floor as the base stations.

Configuration	S_1S_4	S_2S_5	S_2S_3
Layout	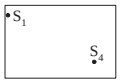	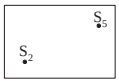	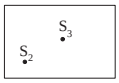
Configuration	S_3S_4	S_1S_2	S_4S_5
Layout	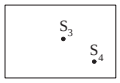	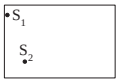	

Table 5.8: Simple indoor configurations deploying two base stations in the Science building (PM C).

A graph of the downlink outage probabilities for the various configurations is shown in Figure 5.17. It is clear from this graph that there are differences in the downlink outage probabilities for the various configurations. Intuition suggests that the configurations with widely separated base stations (e.g. Configurations S_1S_4 and S_2S_5) would have better performance than configurations in which the base stations have a closer separation distance. However, it is evident from Figure 5.17 that there is no apparent relationship between the deployment strategy and the downlink outage probabilities. The placement of base stations influences the *mean* SIR levels across the floor. The behaviour observed is likely to be because signal variations due to short-term fading are more significant than those due to shadowing and distance-dependence (which both influence the *mean* SIR).

A graph of the uplink outage probabilities for the various configurations is shown in Figure 5.18. Similar to the uplink results for the previous propagation measurement campaigns, the observed differences in outage probabilities on the uplink for the various configurations are much less than those observed on the downlink (due to the operation of

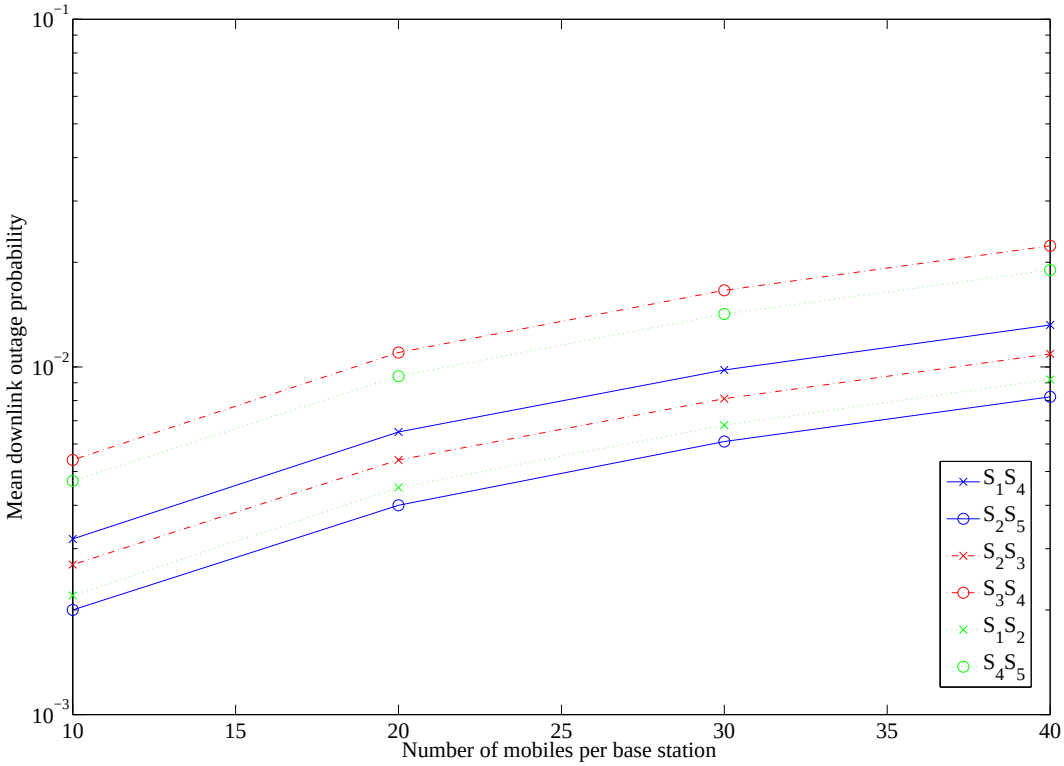

Figure 5.17: Mean downlink outage probabilities for simple indoor base station configurations in the Science building (shown in Table 5.8) in PM C.

uplink power control). However, there is no apparent relationship between the deployment strategy and the differences in uplink outage probabilities.

Functions building

A sample of base station configurations deploying two base stations in the Functions Building is shown in Table 5.9. These configurations are similar to those investigated for the Science building. Configurations F_1F_4 and F_2F_5 have base stations that are diagonally opposite to each other. Configurations F_2F_3 and F_3F_4 have base stations located on the bottom side of the building. In Configurations F_1F_2 and F_4F_5, the base stations are located on the left and right hand side of the building respectively. In the system performance analysis, the mobiles are randomly located at positions at which measurements were made on the same floor as the base stations.

Figures 5.19 and 5.20 are graphs showing the downlink and uplink outage probabilities for the deployment configurations in Table 5.9. The findings for both the downlink and uplink are almost identical to those observed for the Science building; there is no distinct relationship observed between the deployment strategy and the outage probabilities for both the downlink and uplink.

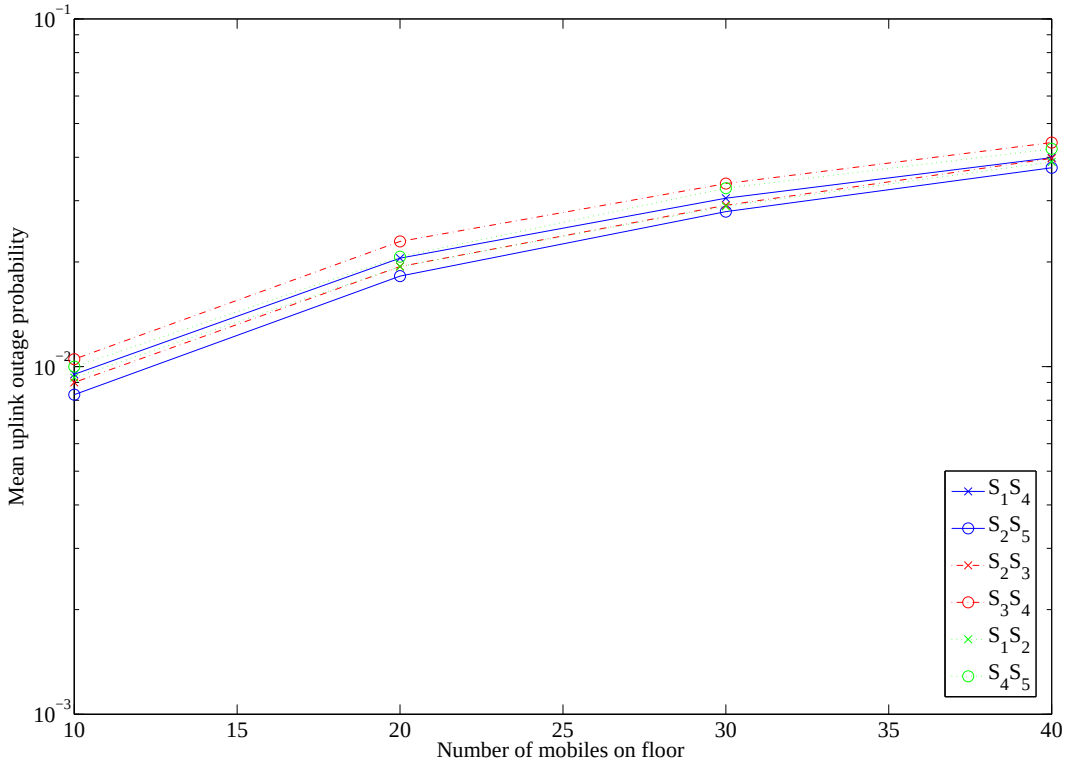

Figure 5.18: Mean uplink outage probabilities for simple indoor base station configurations in the Science building (shown in Table 5.8) in PM C.

Configuration	F_1F_4	F_2F_5	F_2F_3
Layout	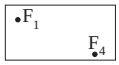	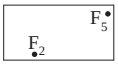	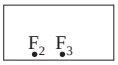
Configuration	F_3F_4	F_1F_2	F_4F_5
Layout	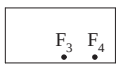	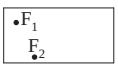	

Table 5.9: Simple indoor configurations deploying two base stations in the Functions building (PM C).

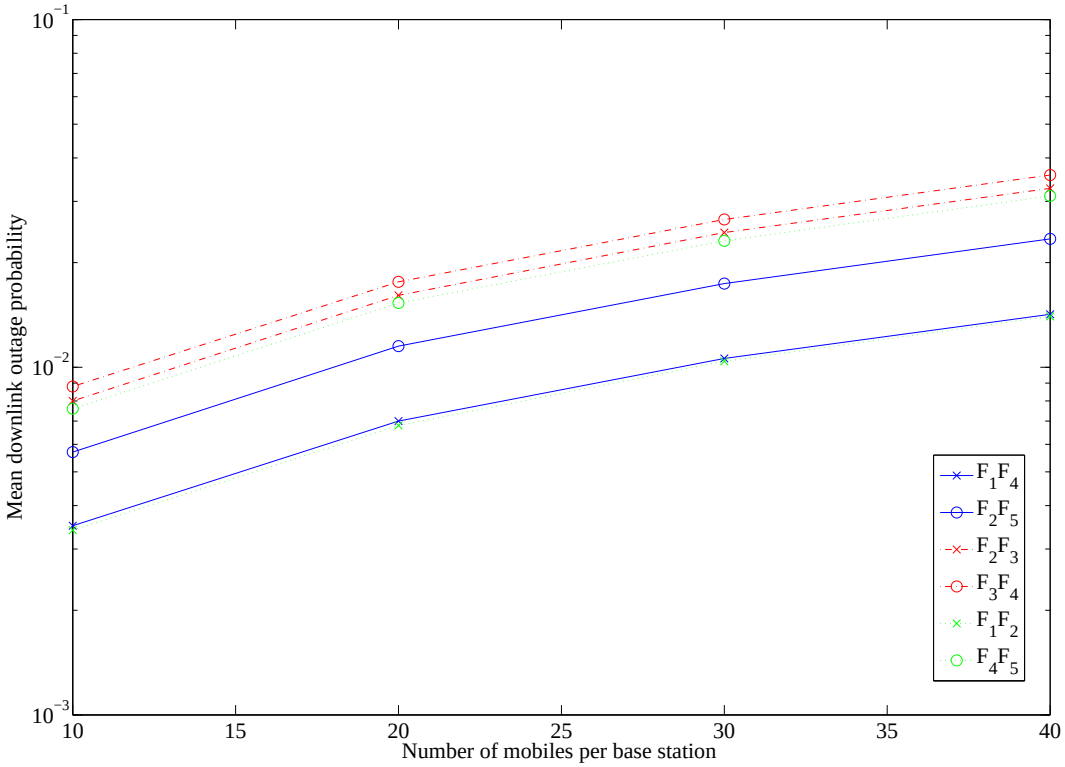

Figure 5.19: Mean downlink outage probabilities for simple indoor base station configurations in the Functions building (shown in Table 5.9) in PM C.

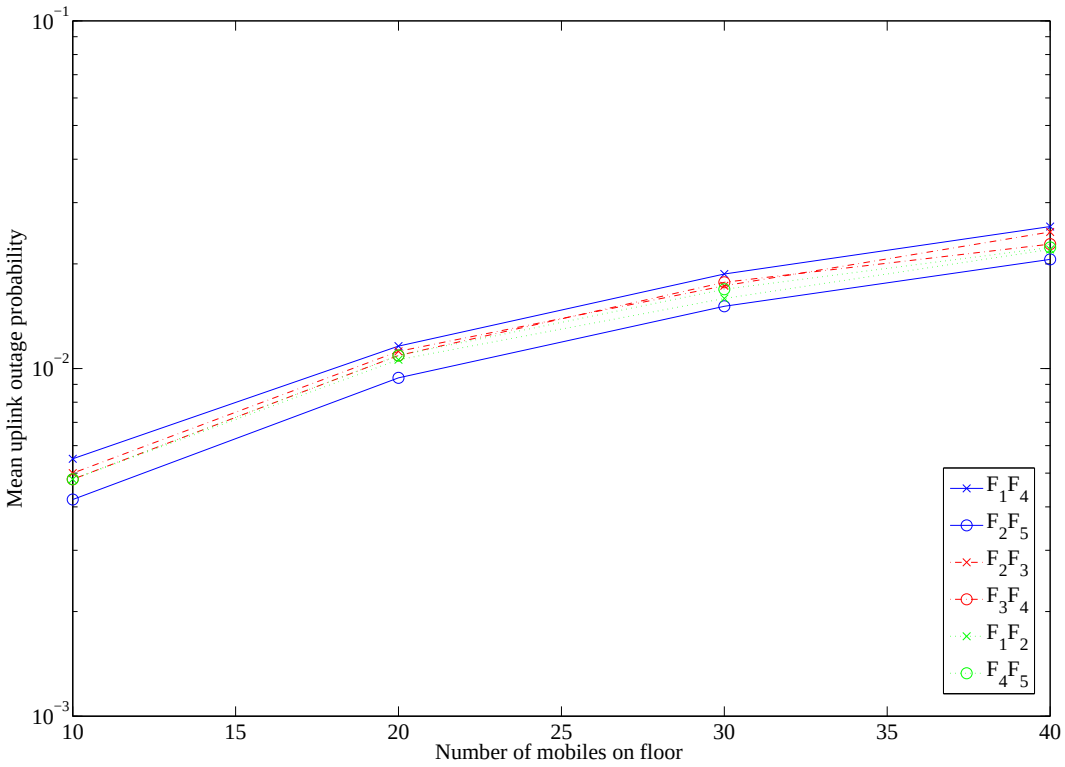

Figure 5.20: Mean uplink outage probabilities for simple indoor base station configurations in the Science building (shown in Table 5.9) in PM C.

5.4.3.2 Interfering adjacent scenario

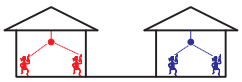

In this scenario, it is assumed that an indoor DS-CDMA system operating in the Functions building mutually interferes with another indoor DS-CDMA system operating in the Science building. In such a scenario it is desirable for wireless operators to 'balance' the performance of the two indoor DS-CDMA systems so that neither system has a significantly worse performance than the other.

Six simple configurations that deploy one base station in the Functions building and one base station in the Science building are shown in Table 5.10. This section begins with an in-depth discussion of the downlink and uplink outage probability estimates for the indoor DS-CDMA system operating in the Science building. It is shown that the performance of the system operating in the Science building is heavily dependent on the interference emanating from the Functions building. The issue of performance 'balancing' between the systems operating in the Science building and Functions building is then investigated by comparing the downlink and uplink outage probability estimates for both systems. Throughout this section it is assumed that there are 20 mobiles randomly located in each of the Science and Functions building.

Configuration	F_1S_1	F_3S_1	F_5S_5
Layout	Functions building F_1 Science building S_1	Functions building F_3 Science building S_1	Functions building F_5 Science building S_5
Configuration	F_1S_4	F_3S_2	F_3S_3
Layout	Functions building F_1 Science building S_4	Functions building F_3 Science building S_2	Functions building F_3 Science building S_3

Table 5.10: Base station deployment configurations investigating interfering adjacent systems in PM C.

System performance in Science building

Figure 5.21 is a graph of the downlink outage probabilities for mobiles in the Science building for the configurations shown in Table 5.10. The graph shows the mean downlink outage probabilities for various relative transmit powers between the base station in the Functions building and that in the Science building. The transmit power for the base station in the Functions building is denoted as P_t(Functions building) while the transmit power for the base station in the Science building is denoted as P_t(Science building). In essence, the signal from the base station in the Functions building appears as interference to mobiles in the Science building.

The following general observations are made for the downlink:

- There are greater differences in the downlink outage probabilities between the various configurations for lower levels of interference emanating from the base station in the Functions building.

- The configurations that yield the best downlink performance for mobiles in the Science building are F_1S_1 and F_5S_5. In these configurations the interfering base stations in the Functions building (F_1 and F_5) are located at the side of the Functions building that is *furthest* from the Science building, while the base stations in the Science building (S_1 and S_5) are located at the side of the Science building that is *nearest* to the Functions building. The correlation coefficient for F_1S_1 is $\rho = 0.54$ and that for F_5S_5 is $\rho = 0.43$. Clearly these moderately high correlation coefficients, coupled with the relatively long distance to the interfering base stations (F_1 and F_5) are beneficial for system performance.

- The configurations that yield the worst downlink performance for mobiles in the Science building are F_3S_2 and F_3S_3. In these configurations the interfering base station in the Functions building, F_3, is at the side of the Functions building *nearest* to the Science building. Base station S_2 in the Science building is located at the side of the Science building that is *furthest* from the Function building, while base station S_3 is located in the *centre* of the Science building. The correlation coefficient for F_3S_2 is $\rho = -0.37$ and that for F_3S_3 is $\rho = -0.26$. These negative correlation coefficients, coupled with the close proximity of the interfering base station (F_3), are detrimental to system performance.

- Mid-range downlink performance levels are observed in configurations F_3S_1 and F_1S_4. In configuration F_3S_1, the base stations are located on the sides of the Science and Functions buildings that are nearest to each other. In configuration F_1S_4, the base stations are located on the sides of the Science and Functions buildings that

are furthest from each other. The correlation coefficient for F_3S_1 is $\rho = 0.69$ and that for F_1S_4 is $\rho = -0.42$.

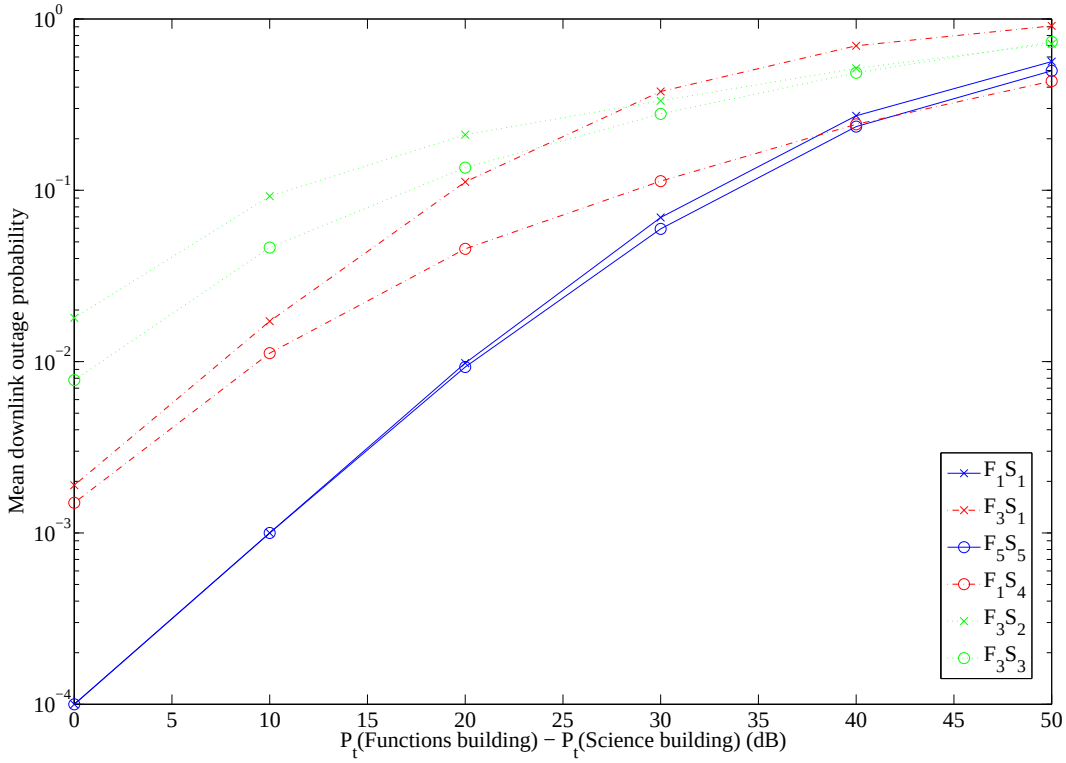

Figure 5.21: Mean downlink outage probabilities for mobiles in the Science building for the interfering indoor/outdoor base station configurations shown in Table 5.10. N.B. P_t(Functions building) is the transmit power of the base station in the Functions building (i.e. interference to mobiles in the Science building) while P_t(Science building) is the transmit power of the base station in the Science building.

Figure 5.22 is a graph comparing the uplink outage probabilities for mobiles in the Science building for the configurations shown in Table 5.10. On the uplink it is assumed that the mobiles adjust their transmit powers so that their signals are received at the base station with a fixed mean signal strength. This graph shows the uplink outage probabilities for various relative mean received power levels between the base station in the Functions building and that in the Science building.

The following general observations are made for the uplink:

- The configurations that yield the *best* uplink performance for mobiles in the Science building are F_3S_2 and F_3S_3. However, for the case of the downlink these configurations were shown to yield the *worst* performance. In these configurations, the base station in the Functions building (F_3) is located near the side of the Functions building that is closest to the Science building. Therefore, the mobiles in the Functions building with the highest transmit powers are likely to be located further away from the Science building than in any of the other configurations.

- The configuration that yields the *worst* uplink performance for mobiles in the Science building is F_1S_1. However, for the case of the downlink this configuration was shown to yield the *best* performance. In F_1S_1, the base station in the Science building (S_1) is located on the side of the Science building that is closest to the Functions building. The base station in the Functions building (F_1) is on the side furthest from the Science building, meaning that the mobiles in the Functions building that have the highest transmit powers are likely to be closer to the Science building than in any of the other configurations.

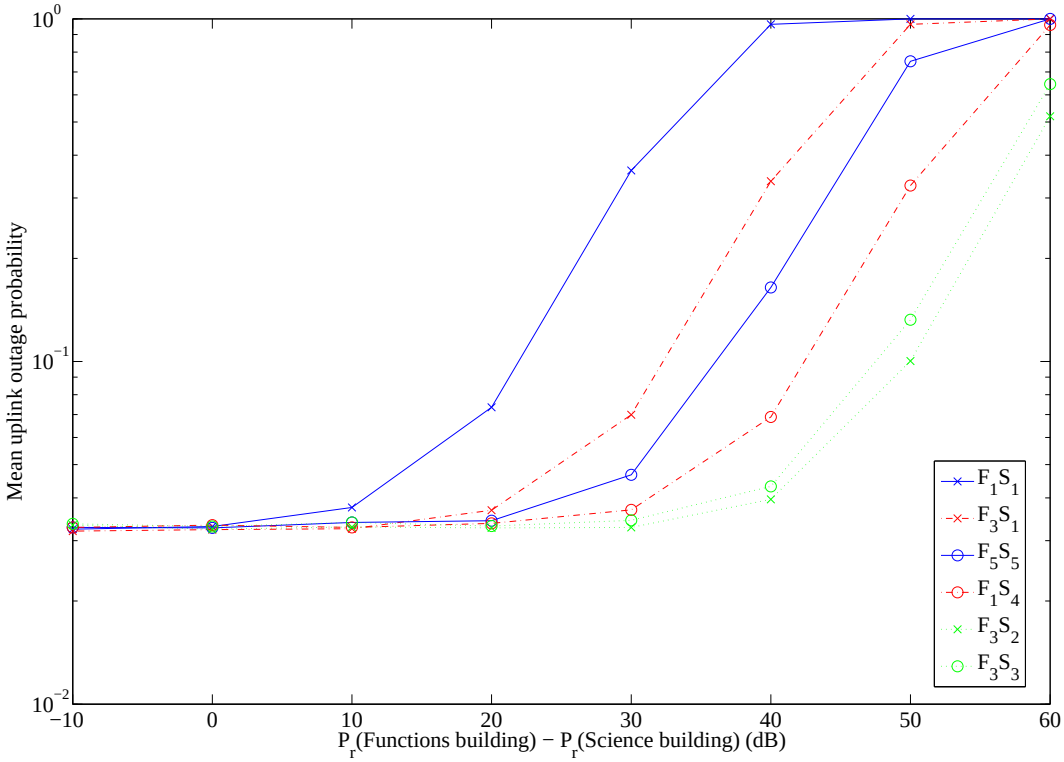

Figure 5.22: Mean uplink outage probabilities for mobiles in the Science building for the interfering indoor/outdoor base station configurations shown in Table 5.10.
N. B. P_r(Functions building) is the power controlled mean received power for mobiles in the Functions building while P_r(Science building) is the power controlled mean received power for mobiles in the Science building.

System performance balancing between the Science and Functions building

This section has considered the design of mutually interfering adjacent indoor DS-CDMA systems using a case study involving base stations deployed in the Science and Functions buildings at The University of Auckland. It has been shown that system performance for the DS-CDMA system operating in the Science building is dependent on both the relative distance between the base stations and the levels of correlation between their signals. Additionally, although some deployment configurations yield the best downlink

performance of any of the deployment configurations investigated, they also yield the worst uplink performance of any of the deployment configurations (or vice versa).

In practice, wireless operators will need to 'balance' the performance for systems operating in the two adjacent buildings so that there is not a significant advantage for one system over the other. The in-depth performance results for the Science building suggest that this is a task that will require trade-offs to be made because the optimal deployment strategies for the downlink and uplink in each system are likely to be different.

To investigate this issue, Table 5.11 compares the mean downlink and uplink outage probabilities for the systems in the Science and Functions buildings. It is assumed that there are 20 mobiles in each building. In obtaining the outage probabilities for the system in the Science building, it is assumed that the transmit power of the interfering base stations and mobiles in the Functions building is 30 dB greater than that in the Science building. Similarly, to allow for a fair comparison, the outage probabilities for the system in the Functions building are obtained assuming that the transmit power of the interfering base stations and mobiles in the Science building is 30 dB greater than that in the Functions building.

Config.	F_1S_1	F_3S_1	F_5S_5	F_1S_4	F_3S_2	F_3S_3
Layout	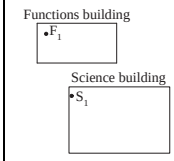	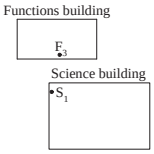	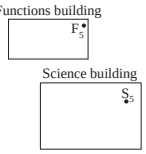	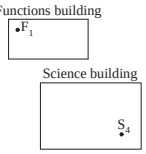	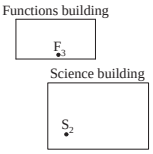	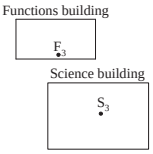
Functions building						
Downlink outage prob.	0.215	0.037	0.015	0.004	0.001	0.001
Uplink outage prob.	0.126	0.762	0.122	0.508	0.985	0.905
Science building						
Downlink outage prob.	0.069	0.377	0.060	0.113	0.333	0.279
Uplink outage prob.	0.361	0.070	0.047	0.037	0.0328	0.034

Table 5.11: Comparison of mean downlink and uplink outage probabilities for interfering adjacent indoor DS-CDMA systems.

The following observations are made:

- It was shown previously that the differences in outage probabilities for the various deployment configurations are related to the levels of interference presented by each indoor system to the other. Table 5.11 shows outage probabilities assuming a fixed level of interference between the buildings, and therefore the outage probabilities shown are simply a 'snapshot' of the two indoor systems at this level of interference.

- Several of the deployment configurations (e.g. F_1S_1, F_3S_1, F_3S_2 and F_3S_3) have significantly different downlink and uplink outage probabilities in both the Science building and Functions building. For example, in the Science building, Configuration F_3S_2 yields a mean downlink outage probability of 0.333, which is among the worst yielded by any of the configurations. However, this configuration also yields a mean uplink outage probability of 0.033 in the Science building, which is the best of any of the configurations. On the other hand, in the Functions building, Configuration F_3S_2 yields excellent performance on the downlink (a mean outage probability of 0.001) and very poor performance on the uplink (a mean outage probability of 0.985). Clearly such large differences in outage probabilities between the downlink and the uplink are undesirable.

- Configurations F_5S_5 and F_1S_4 yield the optimal performance for mobiles in both the Science and Functions buildings. The outage probabilities for these configurations are observed to be 'moderate' on both the downlink and uplink in both systems. This is due to the locations of the base stations and the relative distance between them. For example, in F_1S_4 although a negative correlation is obtained between the signals of the base stations (for mobiles in both the Science building and Functions building), the long distance between the two base stations is beneficial for overall system performance.

Clearly, the design of mutually interfering adjacent indoor DS-CDMA systems is complicated by the 'conflicting' deployment requirements of the systems for optimal performance on the downlink and the uplink. This might require wireless operators to prioritise either the downlink or uplink when deploying the systems. An alternative solution may be to deploy a modified system in which different base stations are used for the downlink and uplink. This would mean that optimal system performance is achievable on both the downlink and uplink. However, the system would require not only more base stations to be deployed (i.e. a greater cost and complexity) but also coordination between the downlink and uplink base stations.

5.5 Implications for system planning and deployment

This chapter has used measured propagation data to evaluate the deployment and performance of three cases of indoor/outdoor DS-CDMA systems. In general, the location and strength of interference emanating on both the downlink and uplink has been shown to have a significant influence on the performance of the system configurations considered. The signal correlation between desired and interfering signals, caused by underlying propagation phenomena such as shadowing and distance-dependent path loss, also has an influence on system performance in both indoor-only systems as well as interfering indoor/outdoor systems. Guidelines for system planning and deployment are now derived from the system performance estimates in this chapter.

Indoor-only DS-CDMA systems

This chapter considered both simple single floor deployment configurations (using two base stations) as well as multi-floor configurations that deploy one base station per floor.

Consider the two deployment configurations shown in Figure 5.23. It has been shown in this chapter that both the downlink and uplink performance of Configuration A are better than that of Configuration B. This is because at any potential mobile location in Configuration A, the signal from one base station is likely to be stronger than the other. Conversely, in Configuration B the close proximity of the base stations means that the signals from both base stations are likely to have similar strength, thereby causing a higher number of outages.

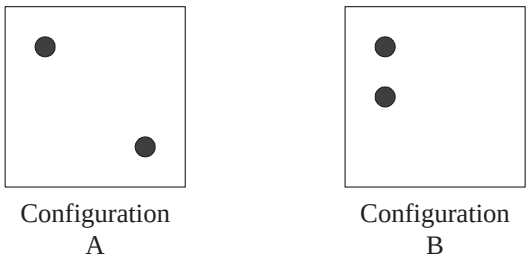

Figure 5.23: Comparison of simple indoor configurations that use two base stations.

For the case of multi-floor indoor DS-CDMA systems, the findings of [25, 26] have been confirmed. The deployment of base stations in a vertically *aligned* configuration has been shown to have better downlink and uplink performance than in a vertically *offset* configuration. This can be explained by the phenomenon of signal correlation, which is largely influenced by in-building features such as concrete cores and floors.

Interfering indoor/outdoor DS-CDMA systems

This chapter has investigated the influence of outdoor interference on two indoor DS-CDMA systems:

- a simple single base station indoor DS-CDMA system with outdoor interference emanating from one side of the building.
- a multi-floor indoor DS-CDMA system with outdoor interference emanating from one side of the building.

Consider the simple single indoor/outdoor base station configurations shown in Figure 5.24. In Configuration A, the indoor base station is on the side of the building nearer to the outdoor base station. In Configuration B, the indoor base station is further away from the side of the building from where the outdoor interference emanates. On the downlink, Configuration A outperforms Configuration B due to the positive correlation between the desired and interfering signals. However, on the uplink Configuration B has better performance than Configuration A as the base station is further from the interference sources (i.e. mobiles) outdoors. Clearly the downlink and uplink have 'conflicting' deployment requirements for optimal performance. In such a situation, wireless operators would have to prioritise either downlink or uplink performance over the other. As the downlink generally requires a higher throughput than the uplink, it is likely that the downlink will have priority over the uplink.

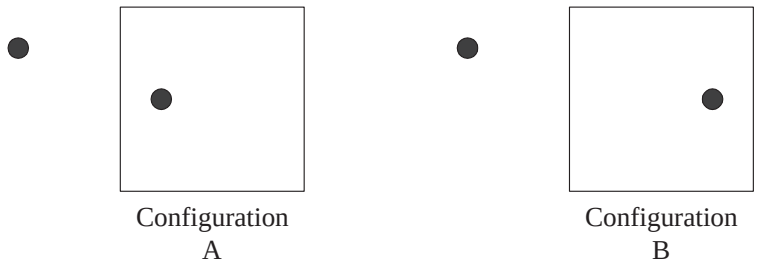

Figure 5.24: Comparison of two interfering indoor/outdoor system configurations.

Now consider the multi-floor indoor base station configurations with outdoor interference emanating from one side of the building, shown in Figure 5.25. The performance results have shown that like the simple single indoor/outdoor base station configurations discussed above, it is difficult to determine the optimal deployment strategy. For this reason, the chosen deployment strategy would largely depend on the wireless operator's objectives and the priority of the downlink with respect to the uplink.

For example, consider the aligned configurations shown in Figure 5.25. While Configuration *Aligned 1* has excellent downlink performance, it has poor uplink performance. Contrary to this, Configuration *Aligned 2* has poor downlink performance and excellent

uplink performance. For Configuration *Offset*, the performance experienced by mobiles would largely depend on which floor the mobile is located. As the offset configurations were shown to be more robust to outdoor interference than the aligned configurations, the downlink performance experienced by mobiles on all floors are moderate (i.e. in between the downlink performance levels of the two aligned configurations). However, the uplink performance is poor for mobiles on the middle floor (as the base station is close to the side of the building from which outdoor interference emanates), while the uplink performance is excellent for mobiles on other floors (as the base station is far from the side of the building from which outdoor interference emanates).

The performance variations on both the downlink and uplink as well as on the various floors of the building make it difficult to choose an optimal deployment strategy.

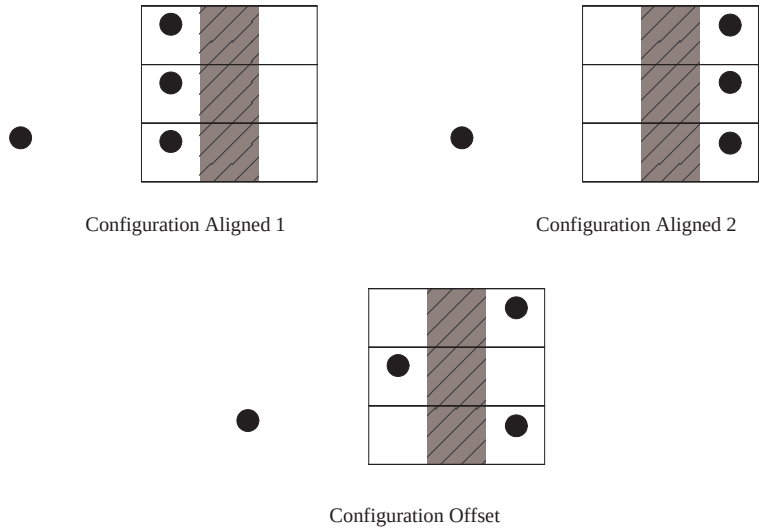

Figure 5.25: Comparison of multi-floor indoor DS-CDMA systems in the presence of outdoor interference.

Interfering adjacent single floor indoor DS-CDMA systems

This chapter has investigated the deployment of two interfering indoor DS-CDMA systems located in buildings that are adjacent to each other. In this situation it would be desirable for wireless operators to ensure that the downlink and uplink performance of *both* systems are optimised. As for the other scenarios discussed above, the relative locations of the base stations and mobiles in the systems have an influence on downlink and uplink performance.

Consider the deployment configurations for two interfering indoor DS-CDMA systems shown in Figure 5.26. The performance estimates have shown that Configuration A will yield excellent downlink performance in System 1 but poor downlink performance in System 2. On the other hand Configuration A will yield poor uplink performance in System 1 and excellent uplink performance in System 2. The disparities in downlink/uplink performance in both systems are undesirable.

However, in Configuration B the downlink and uplink system performance in both systems are moderate in comparison to other deployment configurations investigated. For this reason, optimal performance for both systems is achieved by positioning base stations as far away from each other as possible (as in Configuration B).

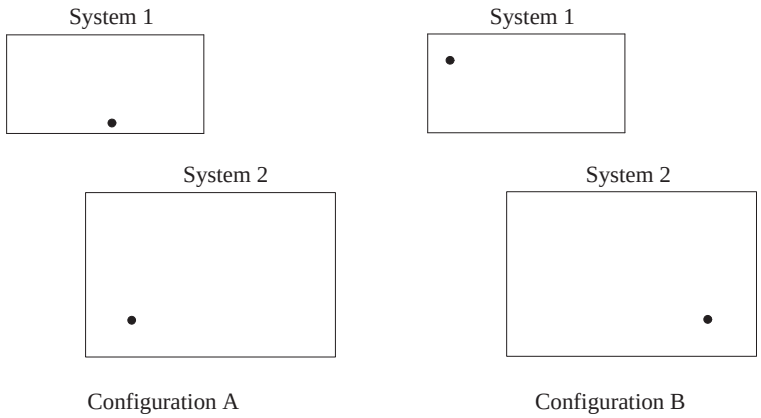

Figure 5.26: Comparison of interfering adjacent single-floor indoor DS-CDMA systems.

5.6 Summary

This chapter has investigated the deployment and performance of indoor/outdoor DS-CDMA systems using results from three propagation measurement campaigns (presented in Chapter 4). A Monte Carlo analysis that estimates the performance for both the uplink and downlink of a DS-CDMA system was presented. This analysis uses simple, fundamental parameters that are generic to any DS-CDMA system regardless of the underlying implementation standard. As a result, generalised deployment guidelines are derived from the performance estimates.

For the case of *indoor-only* DS-CDMA systems (without outdoor interference), this chapter has investigated simple configurations deploying two base stations on a single floor as well as multi-floor deployment configurations with one base station on each floor. For simple base station configurations deploying two base stations to provide coverage on a single floor, the positioning of base stations at opposite corners of the floor yielded significantly better downlink and uplink performance than positioning base stations close together. For deployment on multiple floors, a vertically aligned base station configuration was shown to yield optimal performance on *both* the downlink and the uplink.

For the case of *interfering indoor/outdoor* DS-CDMA systems, both the location and strength of outdoor interference influences the performance experienced by mobiles indoors. Additionally, the downlink and uplink are often observed to have 'conflicting' deployment requirements to yield optimal performance. For example, positioning an indoor base station as close as possible to the side of a building where outdoor interference

emanates is shown to yield *optimal* performance for the downlink but the *worst* performance for the uplink. Therefore, the deployment strategy chosen by a wireless operator would largely depend on the priority of the downlink or uplink over the other. In most information access systems the downlink requires greater throughput than the uplink, and therefore optimising downlink performance would be a priority.

For the case of *interfering indoor* DS-CDMA systems located *adjacent* to each other (with one base station in each system), optimal *overall* performance is achieved by positioning the base stations so that they are as far away from each other as possible. This enables a 'balance' in the performance of both the downlink and uplink in both systems. Several of the other deployment configurations are optimal for the downlink or uplink and suboptimal for the other.

This chapter has considered *conventional* DS-CDMA systems in which interference cannot be cancelled. Chapter 6 introduces multiuser detection as a class of digital signal processing techniques that can be used to minimise or cancel interference on the uplink. Chapters 7 and 8 evaluate the influence of two multiuser detection techniques on the uplink performance of the deployment configurations discussed in this chapter.

Chapter 6

Multiuser detection

6.1 Introduction

A propagation measurement study of the mixed indoor/outdoor environment was described in Chapter 4, while Chapter 5 investigated the deployment and performance of hypothetical indoor/outdoor DS-CDMA system configurations using measured propagation data. The investigation in Chapter 5 was limited to a *conventional* DS-CDMA system in which the receivers at the base stations and mobiles employed matched filters or correlators. These receivers treat the background interference as Gaussian distributed, and an increased number of mobiles in the system implies that more mutual interference will be generated thereby degrading system performance and limiting system capacity.

Multiuser detection is a class of digital signal processing techniques that works on the uplink by *jointly* detecting mobiles for their mutual benefit using channel estimation (to acquire amplitude and phase information) and knowledge of the mobiles' spreading codes. The purpose of this chapter is to give an overview of multiuser detection and identify two multiuser detection techniques for further investigation in indoor/outdoor DS-CDMA systems. A literature review of multiuser detection is presented in Section 6.2. Two non-linear multiuser detection techniques, namely successive interference cancellation (SIC) and parallel interference cancellation (PIC) are identified for further investigation. Simple methods to evaluate the performance of these techniques and the key factors that influence their performance are outlined in Sections 6.3 and 6.4 respectively. An evaluation of previous studies investigating SIC and PIC performance is given in Section 6.5. Finally, Section 6.6 summarises this chapter.

Both SIC and PIC have been integrated in the DS-CDMA system performance testbed described in Chapter 5 and the implications that they have on indoor/outdoor DS-CDMA system deployment and performance are investigated in Chapters 7 and 8.

6.2 A survey of multiuser detection techniques

Multiuser detection was theorised over two decades ago, but despite numerous studies developing and analysing multiuser detection techniques, the technology is still not in widespread use today [9–13, 85]. The reasons for this are manifold, varying from technical to political to financial [10]. The purpose of this section is to outline the benefits and limitations of multiuser detection (Section 6.2.1) and to give an overview of a variety of multiuser detection techniques (Section 6.2.2). At the end of this section, two multiuser detection techniques are chosen for future investigation in this thesis.

6.2.1 Multiuser detection – potential benefits and limitations

To understand the application of multiuser detection, it is necessary to describe the two major factors that limit conventional DS-CDMA system performance on the *uplink*:

- **Interference** – non-orthogonalities in the spreading codes of the mobiles cause multiple access interference (MAI) that limits system performance, as outlined in Chapter 3 [9–13, 85].
- **Near-far effect** – mobiles with *strong* received signals (likely to be *near* the base station) cause a degradation in performance for mobiles with *weak* received signals (likely to be *far* away from the base station). This is likely to cause severe performance variations for mobiles across the system and is therefore undesirable. While uplink power control attempts to ameliorate this problem, errors caused by discrete power adjustments and inevitable signalling delays result in performance and capacity degradations [9–13, 85].

Multiuser detection has the potential to significantly reduce MAI and alleviate the near-far effect on the uplink of DS-CDMA systems. While conventional receivers simply treat MAI as Gaussian distributed noise, multiuser detection uses information inherent in DS-CDMA systems in an attempt to remove MAI and enhance system capacity and performance. In cancelling MAI, the problem of the near-far effect is alleviated because less mutual interference is presented when detecting each individual mobile.

There are several factors that limit the performance gains attainable with multiuser detection, hindering its widespread acceptance in industry to date [9–13]

- Multiuser detection techniques generally require significant processing power and are therefore complex (and costly) to implement and integrate into existing systems;
- Due to the complexity of implementing multiuser detection, it is envisaged that it will only be possible for multiuser detection to be implemented at the base station

for uplink performance enhancement. It is generally agreed that multiuser detection cannot be implemented in mobile devices for downlink enhancement due to its high complexity [9–13]. As future cellular systems require much greater downlink throughput than uplink throughput, technological enhancements implemented in industry have generally focused on other techniques to enhance the downlink throughput (e.g. HSDPA) [86, 87];

- With multiuser detection it is only possible to cancel intra-cell interference using knowledge of the base station's spreading codes within its own cell. Cancelling inter-cell interference, while theoretically possible, presents significant practical challenges due to the requirement of decoding synchronisation between base stations [10, 11];
- The optimal implementation of some multiuser detection techniques requires modifications to conventional radio resource control algorithms (e.g. power control) causing additional complexity [10]; and
- The majority of multiuser detection studies to date have focused on its practical implementation and its performance at the link level (i.e. between a single mobile and base station) [10, 11]. Therefore, there is still a lack of knowledge about the performance gains attainable with multiuser detection in realistic propagation environments as well as its implications on overall system deployment.

Despite the many factors hindering the take-up of multiuser detection in industry, the potential benefits of implementing the technology are not trivial. This thesis attempts to evaluate the potential performance gains in mixed indoor/outdoor propagation environments in which measured propagation data has been obtained.

6.2.2 Multiuser detection techniques

Optimal multiuser detector

Figure 6.1 is a diagram classifying multiuser detectors commonly reported in the literature. The seminal multiuser detection technique was the *optimal multiuser detector* proposed by Verdu in 1986 [88]. This detector uses a maximum likelihood sequence estimator (MLSE) to find the input sequence that maximises the likelihood of the given output sequence at the matched filter receiver or correlator. The resulting problem is essentially a combinatorial optimisation problem which can be solved with an exhaustive search by computing a cost function for every possible argument and selecting the one that maximises the cost function. While the performance gains achieved by the optimal multiuser detector are very high, the computational complexity of the optimal multiuser detector grows exponentially with the number of mobiles. This renders it impractical for

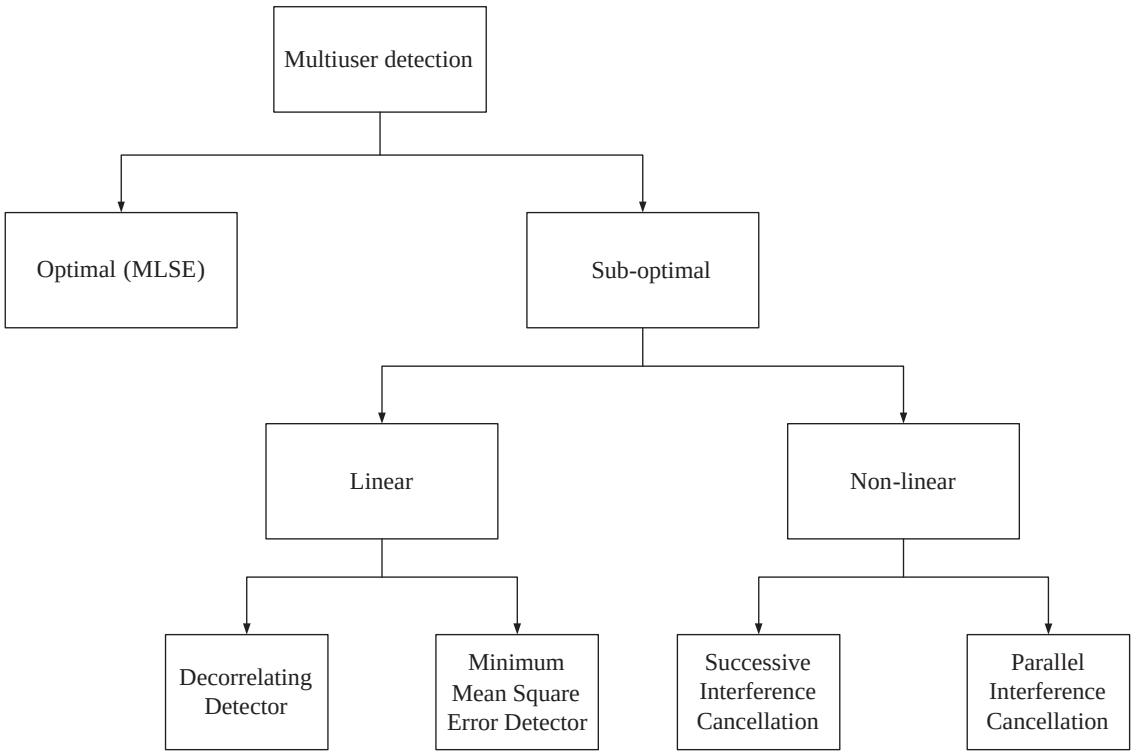

Figure 6.1: A classification of multiuser detection techniques reported in the literature.

implementation in realistic systems. For this reason, multiuser detection research during the last two decades has largely focused on developing *sub-optimal* multiuser detection techniques that seek to trade off performance with complexity.

Sub-optimal multiuser detectors

As shown in Figure 6.1, sub-optimal multiuser detectors may be broadly classified into *linear* and *non-linear* multiuser detectors. Linear multiuser detection techniques apply a fixed transformation to the correlator outputs that attempts to reduce the MAI presented to each mobile on the uplink. While several linear multiuser detectors have been developed, two examples popular in the literature are the decorrelating detector and minimum mean square error (MMSE) detector.

The decorrelating detector applies the inverse cross-correlation matrix of the spreading codes of the mobiles to the outputs of the correlator (with which the decisions regarding the message bits are made) [89, 90]. The correlator outputs may be represented by

$$\mathbf{z} = \mathbf{RWb}+\mathbf{n}, \tag{6.1}$$

where $\mathbf{R}$ is a matrix representing the cross correlations between the mobiles' spreading codes (which causes intra-cell interference), $\mathbf{W}$ is a matrix representing the received amplitudes for the various mobile signals, $\mathbf{b}$ is a vector representing the transmitted message symbols for the mobiles and $\mathbf{n}$ is a vector representing background noise (i.e. thermal noise

and inter-cell interference). If the inverse cross-correlation matrix is applied to (6.1), then the correlator outputs become

$$\mathbf{R}^{-1}\mathbf{z} = \mathbf{R}^{-1}\left(\mathbf{RWb}+\mathbf{n}\right)=\mathbf{Wb}+\mathbf{R}^{-1}\mathbf{n}. \tag{6.2}$$

Clearly (6.2) shows that while intra-cell MAI is removed from the desired signal (i.e. the first term), the background noise is actually amplified by the inverse cross-correlation matrix – this is because the noise term $\mathbf{R}^{-1}\mathbf{n}$ is always equal to or greater than $\mathbf{n}$. The major advantages of the decorrelating detector are that the received amplitudes of the mobile signals do not need to be estimated and its computational complexity is significantly lower than the optimal (MLSE) detector.

The MMSE detector [91, 92] is a linear detector that improves the performance of the decorrelating detector by taking into account the background noise using estimates of the received signal powers. Essentially a linear mapping is used to minimise the mean square error between the actual data and the soft output of the conventional detector. As it takes the background noise into account, the MMSE detector generally provides a higher performance gain than the decorrelating detector.

Non-linear multiuser detectors attempt to cancel interference by estimating the contribution of interference presented by each mobile and cancelling it from the overall composite signal so that other mobiles can be detected more accurately. These detectors require one or more stages of interference cancellation and the performance gain at each subsequent stage is usually less than the previous stage. Two commonly cited non-linear multiuser detection techniques are successive interference cancellation (SIC) and parallel interference cancellation (PIC) [10, 85].

The major advantage of non-linear multiuser detection techniques is the flexibility to trade off complexity with performance; for example it is possible to cancel a given number of mobiles' signals (usually those with the strongest power) from the overall composite signal so that performance is improved. This flexibility has made non-linear multiuser detector techniques popular in both academia and industry, where several prototypes have been developed [14–18]. Due to the excellent complexity/performance trade-off of non-linear multiuser detectors, this thesis focuses on the performance gains attainable with the implementation of SIC and PIC in indoor/outdoor DS-CDMA systems. The subsequent Sections 6.3 and 6.4 give an overview of SIC and PIC respectively, including models to estimate their performance.

6.3 Successive interference cancellation

The purpose of this section is to give an overview of SIC and identify the key criteria influencing its performance. The material presented in this section forms the basis for

evaluating SIC performance in indoor/outdoor DS-CDMA systems in Chapter 7 of this thesis. Section 6.3.1 presents a model of a simple SIC receiver and derives a simple closed-form solution for evaluating the performance of SIC in terms of signal to interference ratio (SIR). As the performance of SIC is heavily dependent on the disparities in the received signal power for the various mobiles, Section 6.3.2 discusses the impact of uplink power control on SIC performance.

6.3.1 Successive interference cancellation model

As its name indicates, an SIC receiver attempts to cancel interference by sequentially cancelling received mobile signals. At each stage of the detector, a signal from an individual mobile is estimated, regenerated and then subtracted from the overall (composite) signal, so that mobiles at subsequent stages are presented with reduced MAI.

To be able to perform interference cancellation, knowledge of various parameters is required. These parameters include the spreading codes of the mobiles and amplitude/phase information of the mobiles' received signals at the base station [9,10]. The amplitude and phase of the received signals are unknown and therefore need to be estimated. This estimation may be performed using the outputs of the conventional detector (e.g. correlator) or using separate channel estimates [10]. SIC may use either soft estimates or hard estimates (i.e. bit decisions) at the output of the correlator to regenerate the mobile signals for cancellation. The benefit of the approach using soft estimates is that it is easier to implement and the cancellation process can withstand inaccurate amplitude estimates. The approach using hard estimates (i.e. the actual bit decisions) cancels interference more accurately than that using soft estimates if accurate estimates of the bits are made for the regeneration of mobile signals [91].

Performance of a simple SIC receiver

An example of a simple coherent SIC receiver is presented in [93,94] and a block diagram demonstrating its functionality is shown in Figure 6.2. As this receiver is coherent, the phase of each received mobile signal can be tracked accurately. The amplitudes of the received mobile signals are estimated using the correlator outputs. The front end of the receiver is a conventional correlator bank. After the composite received signal *r(t)* is passed through the correlator bank, the various mobiles are ranked in order of strongest to weakest received power using the magnitudes of the correlator outputs for the mobiles. The mobile with the highest received power (i.e. that with the maximum correlation value) is selected first for decoding, regenerating and cancelling. This process is repeated for each mobile sequentially (in order of decreasing correlator values) until a given number of signals are cancelled or all mobiles have been decoded.

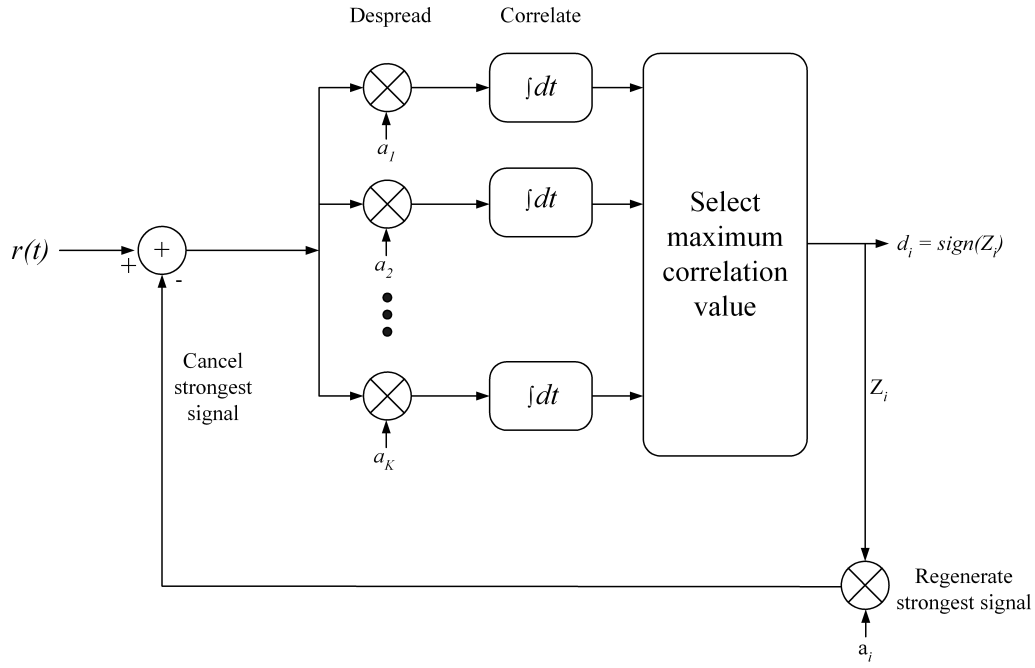

Figure 6.2: A simple SIC receiver [93, 94]

In summary, the procedure for detecting the various mobiles using SIC is as follows:

1. Determine the strongest mobile.
2. Decode the strongest mobile.
3. Estimate the amplitude and phase of the strongest mobile from the output of the correlator.
4. Regenerate the strongest mobile's signal using its spreading code and the estimate of its amplitude and phase.
5. Cancel the strongest mobile by subtracting its regenerated signal from the overall (composite) received signal.
6. Perform Steps 1 to 5 for the next strongest mobile.
7. Repeat Steps 1 to 6 until all users are decoded or a permissible number of mobiles are cancelled.

The signal received by the SIC receiver shown in Figure 6.2 is given by [93, 94]

$$r(t) = \sum_{k=1}^{K} A_k \cdot a_k(t - \tau_k) \cdot b_k(t - \tau_k) \cdot cos(\omega_c t + \phi_k) + n(t), \tag{6.3}$$

where K is the number of active mobiles, A_k is the amplitude of the kth mobile, $a_k(t-\tau_k)$ is the spreading code of the kth mobile, $b_k(t-\tau_k)$ is the data sequence of the kth mobile,

ω_c is the carrier frequency, τ_k is the time delay of the kth mobile and ϕ_k is the phase delay of the kth mobile. The term $n(t)$ in (6.3) represents the noise due to receiver imperfections and inter-cell interference, modelled as additive white Gaussian noise (AWGN).

At the receiver, the amplitudes of the received signals for the various mobiles are unknown. However, this information is required for two reasons: firstly, for maximum performance gain, the sequential cancellation process should be performed in order of decreasing signal strength. Secondly, the signals for each of the mobiles must be regenerated using their individual amplitudes so that they can be cancelled from the composite received signal during the interference cancellation process.

In Figure 6.2, it is shown that the received composite signal is despread and correlated with the spreading codes of each of the mobiles (performed by the bank of correlators). The strongest mobile is assumed to be the one with the maximum correlator output, Z_i. After j cancellations, the decision variable for the $(j+1)^{\text{th}}$ mobile is given by [93, 94]

$$Z_{j+1} = \frac{1}{2} A_{j+1} b_{j+1} + C_{j+1}, \tag{6.4}$$

where

$$C_{j+1} = \sum_{k=j+2}^{K} A_k I_{k,j+1}(\tau_{k,j+1}, \phi_{k,j+1}) + (n_{j+1}^I + n_{j+1}^Q) - \sum_{i=1}^{j} C_i I_{i,i+1}(\tau_{i,i+1}, \phi_{i,i+1}). \tag{6.5}$$

In (6.5), the first term represents the interference caused by uncancelled mobiles $j+2$ to K, the second term represents the uncancellable noise caused by receiver imperfections and mobiles in other cells, while the third term is the residual interference due to imperfect cancellations of the previous j strongest mobiles.

Assuming that the system is interference limited and the noise due to receiver imperfections is insignificant, further analysis of the decision variables in [93, 94] yields the following simple equation for the signal-to-interference ratio of the signal representing the $(j+1)^{\text{th}}$ mobile

$$\text{SIR}_{j+1} = \frac{P_{j+1}}{\frac{2\alpha}{3N}\left(\sum_{k=j+2}^{K} P_k + \sum_{i=1}^{j} \eta_i + P_{oc}\right)}, \tag{6.6}$$

where

$$\eta_{j+1} = \frac{2\alpha}{3N}\left(\sum_{k=j+2}^{K} P_k + \sum_{i=1}^{j} \eta_i + P_{oc}\right). \tag{6.7}$$

In (6.6), α is the voice-activity factor, P_{j+1} is the received power of the $(j+1)^{\text{th}}$ mobile's signal and $\sum_{k=j+2}^{K} P_k$ is a summation of the uncancelled (weaker) signals received from

mobiles (j+2) to K. The term $\sum_{i=1}^{j} \eta_i$ is the residual interference which results from the detections of the previous j (stronger) mobiles, while P_{oc} is the inter-cell interference which cannot be cancelled.

Generalised model for SIC performance

The residual interference in (6.7) is based on the assumption that the phase of the mobile signals can be tracked accurately, which is not possible in reality. A generalised solution for the SIR is presented in [95, 96], whereby a fractional residual interference cancellation error is introduced

$$\mathrm{SIR}_{j+1} = \frac{P_{j+1}}{\frac{2\alpha}{3N}\left(\sum_{k=j+2}^{K} P_k + \sum_{i=1}^{j} \varepsilon_i P_i + P_{oc}\right)}, \tag{6.8}$$

where ε_i is the fractional residual interference cancellation error for the ith mobile, which represents the fraction of the ith mobile's power not cancelled. Equation (6.8) is generalised in that it accounts for a variety of cancellation errors that SIC receivers might have depending on the accuracy with which they are able to estimate the phase and amplitude of the received mobile signals. Due to its generalised nature, the SIC model represented by (6.8) is used in this thesis. The BER (assuming the implementation of SIC) can be estimated by using the SIR obtained from (6.8) and the complementary Gauss probability integral introduced in Section 3.2.1.

Modelling the fractional residual interference cancellation error

Residual interference is generated during the interference cancellation process for two major reasons:

- inaccuracies in the amplitude and phase estimates of the received mobile signals, also known as the estimation error.
- errors in the decoded bit sequences for the mobiles.

Assuming that the system operates at low BERs, the residual interference will primarily be caused by estimation error. It is shown in [97] that the estimation error may be modelled by a zero-mean Gaussian distribution with standard deviation σ_ϵ. Therefore it is assumed that the fractional residual interference cancellation error for each mobile, ε_i, is also modelled by a zero-mean Gaussian distribution with same standard deviation as that of the estimation error, σ_ϵ [97].

6.3.2 Implications of power control on SIC performance

Optimal power control distribution

Conventional DS-CDMA systems use uplink power control in an attempt to ensure that mobiles adjust their transmit powers so that their signals are received at the base station with equal power levels [45]. As a result, the near-far effect is combatted as mobile signals are received with approximately the same SIR, thereby ensuring fairness of performance for mobiles across the system.

However, the concept of SIC is based on the premise that there will be disparities in the received powers of mobile signals at the base station. If SIC is implemented in conjunction with existing power control algorithms that attempt to equalise the received powers of mobile signals, this would lead to a fairness problem; in this situation despite the similar received power levels of the mobiles, the mobile detected first would be presented with the most interference, while the mobile detected last would be presented with the least interference [96,98,99]. As a result, mobiles detected earlier would have worse performance in comparison to those detected subsequently.

Consider a DS-CDMA system with K mobiles in a cell of interest. Assuming that there are SIC receivers at the base stations, the SIRs for the mobiles 1, 2, ... K, are given by [96]

$$SIR_1 = \sqrt{\frac{P_1}{\frac{2\alpha}{3N}\left(\sum_{k=2}^{K} P_k + P_{oc}\right)}}, \tag{6.9}$$

$$SIR_2 = \sqrt{\frac{P_2}{\frac{2\alpha}{3N}\left(\sum_{k=3}^{K} P_k + \varepsilon_1 P_1 + P_{oc}\right)}}, \ldots \tag{6.10}$$

$$SIR_K = \sqrt{\frac{P_K}{\frac{2\alpha}{3N}\left(\sum_{k=1}^{K-1} \varepsilon_k P_k + P_{oc}\right)}}. \tag{6.11}$$

To ensure fair performance for all mobiles across the system, it is desirable for the SIRs for the mobiles to be the same, i.e. $SIR_1 = SIR_2 ... = SIR_K$. This may be achieved by using an optimal power control distribution that allocates power to the mobiles so that their SIRs are the same. One of the key considerations in solving this set of equations is that the fractional residual interference cancellation error, ε_k, for each mobile, k, is unknown.

For simplicity in deriving the power control distribution it may be assumed that $\varepsilon_k = 0$ for all mobiles (i.e. perfect cancellation). However, it is shown in [10, 95, 96, 100, 101] that if the power control distribution is derived based on this assumption and the actual fractional residual cancellation error is greater than 20%, the performance of the SIC

receiver becomes *worse* than if a conventional receiver (without interference cancellation) is used. Therefore, an optimal power control distribution accounting for ε_k is derived in [10, 95, 96, 100, 101] and the following result is obtained

$$P_k = P_{k-1} - \frac{(1-\varepsilon_{k-1})\,P_{k-1}^2}{V_{k-1} + P_{oc}}, \tag{6.12}$$

where V_{k-1} is the total remaining multiple access interference (MAI) for mobile k plus its own power, and is given by

$$V_k = \sum_{i=1}^{K} P_i - \sum_{i=1}^{k-1} (1-\varepsilon_i)\,P_i. \tag{6.13}$$

It is shown in [10, 95, 96, 100, 101] that while the fractional residual interference cancellation error, ε_k for each of the mobiles is unknown, a guess at or estimate of its value, $\hat{\varepsilon}$, can be made to derive the power control distribution. Analysis of the performance yielded by the power control distribution in [10, 95, 96, 100, 101] shows that

- the system performance is less sensitive to ε_k being overestimated than underestimated.
- it is best to choose $\hat{\varepsilon}$ conservatively as appreciable performance gains will still be realised over the conventional receiver.

Another consideration in deriving the power control distribution using (6.12) is that the inter-cell interference, P_{oc}, is unknown and is in fact directly dependent on the power control distribution itself. In this thesis, an estimate of the inter-cell interference is made ($\widehat{P}_{oc}$) so that the power control distribution can be derived.

Optimal power allocation for reduction of inter-cell interference

For an interference cancellation scheme to be effective, it is important to minimise the uncancellable interference. It is not possible to cancel inter-cell interference due to the practical difficulty in coordinating base stations during the decoding process. However, the transmit power allocated to the mobiles influences the relative levels of intra- and inter-cell (uncancellable) interference at the system level.

To explain this further, consider two adjacent cells of a hypothetical 'uniform' macrocellular system shown in Figure 6.3. Each of the two cells, A and B, serve three mobiles that are labelled $M_x^{(y)}$, where x is an identifier for the mobile while y is the cell to which the mobile belongs. Assuming that $P_x^{(y)}$ represents the transmit power from the mobile $M_x^{(y)}$, then with conventional power control and assuming free space propagation, $P_3^{(A)} > P_2^{(A)} > P_1^{(A)}$ while $P_3^{(B)} > P_2^{(B)} > P_1^{(B)}$. In essence, the mobiles at the cell

edge transmit at power levels that are higher than those close to the base station. The mobile presenting the highest inter-cell interference to Cell A is $M_3^{(B)}$, while that presenting the highest inter-cell interference to Cell A is $M_3^{(B)}$. This is because $M_3^{(B)}$ and $M_3^{(A)}$ have the closest proximity to the respective neighbouring cell as well the highest transmit power allocation of any of the mobiles within their respective cells.

If SIC receivers are used at the base stations, the above transmit power allocation is undesirable because the level of inter-cell interference is likely to be high; as it is only possible to cancel *intra-cell* interference with multiuser detection, it is desirable to *maximise* intra-cell interference and *minimise* inter-cell interference. An alternative approach for power control might be to allocate the uplink transmit power such that $P_3^{(A)} < P_2^{(A)} < P_1^{(A)}$ while $P_3^{(B)} < P_2^{(B)} < P_1^{(B)}$, i.e. mobiles close to the base station are assigned higher power levels (and decoded earlier) than those far away from the base station [99,100,102]. This would ensure that less interference is presented to other cells and therefore using SIC it is possible to cancel a greater proportion of the overall interference.

In the literature, an F-factor [73] is often used to quantify the ratio between the intra-cell interference and the total (intra-cell and inter-cell) interference as follows

$$F = \frac{P_{ic}}{P_{ic} + P_{oc}},$$

where P_{ic} is the total intra-cell interference power and P_{oc} is the total inter-cell interference power. In a system that operates with interference cancellation receivers at the base station end, it is highly desirable to maximise the F-factor so that the greatest proportion of overall interference can be cancelled.

6.4 Parallel interference cancellation

While an SIC receiver detects mobiles and cancels their interference sequentially, a parallel interference cancellation (PIC) receiver attempts to simultaneously remove from each mobile's detected signal the interference presented by all other mobiles within the same cell. This requires the PIC receiver to detect, estimate and regenerate all the mobile signals in *parallel* and then perform the required cancellations. Similar to SIC, it is not possible to cancel all interference due to amplitude and/or phase estimation errors. However, multiple cancellation stages may be used to yield improved estimates of the received mobiles' signals for further (more accurate) cancellation.

An example of a PIC receiver is presented in [94] and a block diagram of this receiver is shown in Figure 6.4. This receiver uses a conventional detector (bank of correlators) at the front end followed by two stages of cancellation. At each stage improved estimates of the received signal are made using the correlator outputs, ${Z_i}^{(s)}$, from the previous stage,

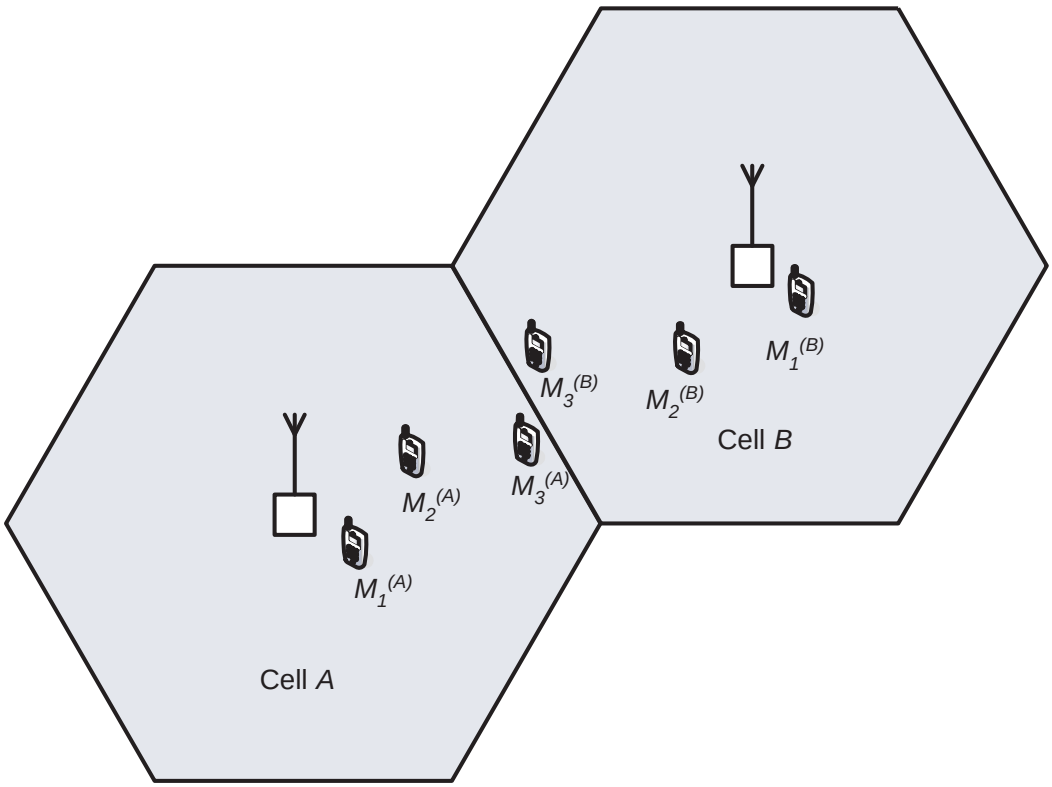

Figure 6.3: Macrocellular system with three mobiles in each of two cells.

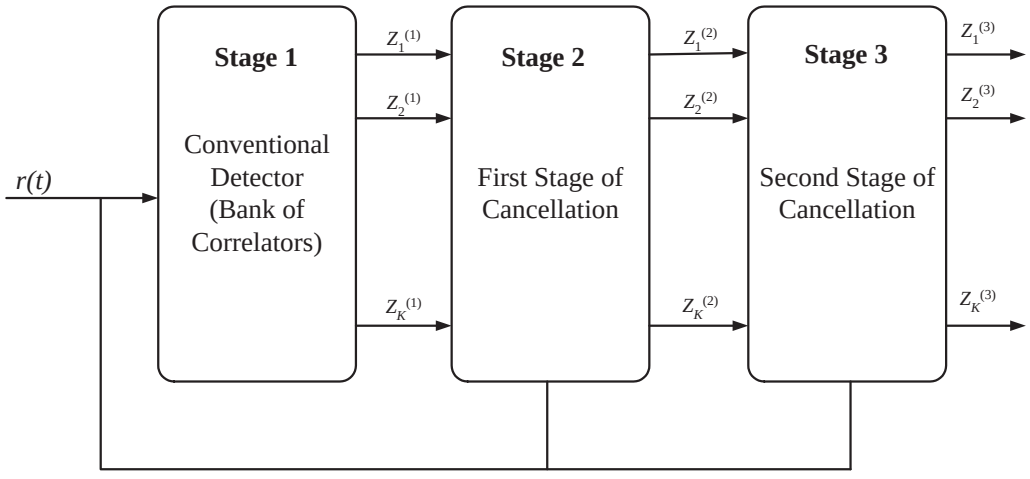

Figure 6.4: A parallel interference cancellation scheme that uses two cancellation stages [94].

where i represents the unique identifier of the decoded mobile while s represents the stage of the receiver ($s = 1$ represents the conventional detector stage).

The conventional detector correlates the received signal with the spreading sequences of each of the mobiles to obtain the correlator outputs $Z_i{}^{(1)}$. These correlator outputs are used in the first stage of cancellation (i.e. Stage 2 of the PIC receiver) to estimate and regenerate the signals for all the mobiles. For each mobile, the regenerated signals of all *other* mobiles are subtracted from the original received signal *r(t)*. The resulting signal is correlated with the mobile's spreading code to yield more accurate correlator outputs [94]. While only two cancellation stages are shown in Figure 6.4, this process may be continued for an arbitrary number of cancellation stages.

Although there have been many PIC receivers theorised to date (using both hard decision estimates and soft decision estimates, i.e. correlator outputs), the analysis of PIC is difficult due to the complexity of the correlator outputs. For this reason most researchers have relied on bit-level computer simulations to estimate the performance of PIC. One exception to this is a closed-form solution of the SIR of a PIC receiver for an arbitrary number of stages presented in [103, 104], given by

$$SIR_k^{(s)} = \left[\frac{1}{2\frac{E_b}{N_o}} \left(\frac{1 - \left(\frac{K-1}{3N}\right)^s}{1 - \left(\frac{K-1}{3N}\right)} \right) + \frac{2\alpha}{(3N)^s} \left(\frac{(K-1)^s - (-1)^s}{K} \left(\frac{\sum_{k=1}^{K} P_j}{P_k} \right) + (-1)^s \right) \right]^{-1/2}. \tag{6.14}$$

In (6.14), $SIR_k^{(s)}$ is the SIR for mobile k at stage s of the cancellation process, N_o is the one-sided power spectral density of background Gaussian noise (may be used to model both receiver thermal noise and inter-cell interference), α is the voice activity factor, N is the processing gain, K is the number of mobiles in the cell of interest, and P_k is the received power of the kth mobile.

In deriving (6.14), it is assumed that it is possible for the phase of the received mobile signals to be tracked accurately, but the power of each mobile signal is estimated from the correlator outputs [103, 104]. In practice, however, it is not possible to track the phase with complete accuracy and the correlator outputs are biased in their estimation of the powers of the mobile signals.

For this reason, a generalised estimation of the SIR for a PIC receiver is used in this thesis [15, 105]

$$SIR_k^{(s)} = \sqrt{\frac{P_k}{\frac{2\alpha}{3N}\left(\sum_{i=1, i\neq k}^{K} \varepsilon_i^{(s)} P_i + P_{oc}\right)}}, \tag{6.15}$$

where $\varepsilon_i^{(s)}$ is the fractional residual interference cancellation error for mobile i at stage s of the PIC receiver. For the first stage ($s = 1$) of the PIC receiver (i.e. the conventional

detector stage), $\varepsilon_i^{(1)} = 1$ because no interference is cancelled. Similar to the SIC performance estimation described in Section 6.3, the fractional residual interference cancellation error is assumed to be a zero-mean Gaussian distributed random variable with a standard deviation σ_ε for stages $s \geq 2$. Equation (6.15) accounts for the variations in fractional residual interference cancellation error that are likely to be observed for a variety of PIC receivers.

The performance of the PIC receiver suffers at the first stage of cancellation as the estimates of the weaker mobiles' signals are likely to be inaccurate due to dominating interference from other (stronger) mobiles [14]. The resulting poor cancellations of the weaker mobiles' signals serve to degrade the estimate of the stronger mobiles in the second stage of cancellation. Consequently, when the stronger mobiles are cancelled from a weak mobile's signal in the second stage of cancellation, it is also likely to be inaccurate. This process continues from stage to stage with a slight improvement in estimates at each stage.

6.5 SIC and PIC performance evaluation – a literature review

A unique contribution of this thesis is that it presents a performance evaluation of SIC and PIC in actual propagation environments for which measured mean path loss data has been obtained (discussed in subsequent Chapters 7 and 8).

The majority of previous studies on SIC and PIC have focused on

- theoretical estimation of system performance at the link level with non-specific propagation models (i.e. single cell systems with background noise modelled using a Gaussian distribution) [14, 93, 98, 100, 102–104, 106–112];
- implementing multiuser detection algorithms in digital signal processors [14–18]; and
- optimising power control algorithms for multiuser detection implementation [96, 99].

To the author's knowledge previous research has not investigated and compared the performance of SIC and PIC in indoor or mixed indoor/outdoor environments. This is a fundamentally important issue as system performance is heavily interrelated with the deployment strategy in mixed indoor/outdoor environments.

The seminal research on SIC (outlined in Section 6.3) developed closed-form expressions for the BER based on soft estimates assuming fairly accurate amplitude and phase estimates. Since then, several researchers have attempted to investigate other issues related to SIC, such as the optimisation of power control algorithms and the implementational complexity of SIC receivers. However, the vast majority of the studies investigating

SIC performance at the system level (i.e. for multiple cells) have been performed for systems operating in *outdoor* environments. An exception to this is in [113] where Hwang et al. estimated an upper bound for the performance of an indoor optical wireless PPM-CDMA system with SIC. However, this research does not investigate the implications of SIC on the optimal deployment of base stations, nor does it consider the influence of outdoor interference on indoor systems operating with SIC.

PIC was first proposed by Varanasi et al. [114]. This scheme uses hard estimates that can potentially degrade performance during the initial stages of detection. For this reason, Divsalar [108] proposed an approach to partially cancel interference at the earlier stages using soft estimates, and cancel a greater proportion of interference at later stages where improved estimates are obtained. As stated in Section 6.4, closed-form expressions for the performance of these PIC receivers are not obtainable due to the complexity of analysing the correlator outputs. This makes it difficult to accurately assess the performance of PIC in realistic system level scenarios.

The majority of studies investigating PIC have focused on link level performance (i.e. single cells). To the author's knowledge, there has not been any previous research investigating PIC performance in indoor or mixed indoor/outdoor environments. However, there are a limited number of studies documenting system level performance analyses in outdoor environments. For example, in [15] a PIC prototype was developed and its system level performance was assessed in outdoor environments by both simulation and practical measurements in a real network. The results of this study showed that the PIC receiver supports a 40% increase in uplink network capacity for walking mobile users in a typical urban outdoor radio environment.

While there has been much debate as to whether SIC or PIC provides the best complexity/performance trade-off, it is generally agreed that SIC has the higher performance gain in near-far channels and in cases where there are large disparities between the received signal powers of the mobiles [94]. However, PIC yields higher performance gains in the familiar equal power control case [94]. One of the key issues with any interference cancellation technique is the latency due to the cancellation process. A complication of SIC is that the latency for the detection of each individual mobile increases with the number of stages of cancellation. However, in PIC the latency for all the mobiles at each stage of cancellation is the same as they are all detected in parallel [10].

The complexity of PIC is proportional to PK, where P is the number of cancellation stages and K is the number of mobiles decoded. For SIC, the complexity is K if full cancellation (i.e. of all mobile signals) is performed. In this context, one of the major benefits of SIC is that a chosen number of mobile signals can be cancelled to reduce the complexity. With PIC, this is not desirable as all mobile signals must be cancelled to ensure fairness of performance [10].

6.6 Summary

This chapter has given an overview of the field of multiuser detection for DS-CDMA systems and its application in various propagation environments. While multiuser detection has been researched for the last twenty years, there has been little or no take-up in industry due to its implementational complexity and the lack of knowledge surrounding the performance gains attainable in realistic systems. This thesis aims to address the latter issue.

Two non-linear multiuser detection techniques, namely successive interference cancellation (SIC) and parallel interference cancellation (PIC), have been identified for future investigation in indoor/outdoor DS-CDMA systems.

SIC cancels uplink interference by ranking mobiles in order of decreasing received signal strength and detecting and cancelling them sequentially. A closed-form solution for the SIR with the implementation of SIC was presented. This solution accounts for the fractional residual interference cancellation error that is caused by inaccurate phase and amplitude estimates, which results in imperfect cancellation. It was shown that SIC relies on disparities in the received powers of the mobile signals, and therefore conventional (equal) power control is no longer optimal. An optimal power control technique for SIC (that attempts to equalise the SIR for the various mobile signals) was presented. It is desirable to maximise the ratio of intra-cell interference to total interference (quantified using the F-factor) as it is only possible to cancel intra-cell interference using multiuser detection. By intelligently assigning transmit power to the mobiles during the power control process, the F-factor can be maximised and therefore inter-cell interference can be kept to a minimum.

PIC cancels uplink interference for mobiles by estimating *all* mobiles' signals, regenerating them, and cancelling them upon detecting each individual mobile. Fortunately, PIC implementation has been shown to be optimal with conventional power control. Accurate closed-form solutions for estimating the SIR with PIC implementation are rare due to the complexity of analysing the correlator outputs. Therefore, a simple closed-form solution that generically accounts for errors in amplitude and phase estimates was presented and is used subsequently in this thesis.

The subsequent Chapters 7 and 8 present the impact of SIC and PIC on the performance of indoor/outdoor DS-CDMA systems and compare their relative performances.

Chapter 7

Successive interference cancellation in indoor/outdoor DS-CDMA systems

7.1 Introduction

Chapter 6 introduced multiuser detection as a class of digital signal processing techniques that are likely to be implemented in future DS-CDMA systems. Two techniques were identified for future investigation: successive interference cancellation (SIC) and parallel interference cancellation (PIC). Simple closed-form expressions for estimating the performance of DS-CDMA systems with the implementation of SIC and PIC were presented.

The purpose of this chapter is to investigate the implementation of SIC in indoor/outdoor DS-CDMA systems. Of particular importance to this investigation is the acquisition of the performance gains attainable with SIC and the implications for the optimal deployment of base stations. As discussed in Chapters 5 and 6, the sources of interference (i.e. their location and strength) and the uplink power control algorithms used are likely to have a significant influence on the efficacy of SIC to improve system performance.

Chapter 5 outlined a performance evaluation for a *conventional* indoor/outdoor DS-CDMA system (without multiuser detection). The performance evaluation in Chapter 5 was conducted for *both* the downlink and the uplink. This chapter uses the theory presented in Chapter 6 to integrate SIC into the system performance estimation testbed discussed in Chapter 5. As it is likely that multiuser detection will only be implemented on the uplink of commercial DS-CDMA systems, this chapter evaluates the performance with SIC receivers for *only* the uplink.

The scenarios presented in this chapter are the same as those considered in Chapter 5 to give a reliable basis for the comparison between SIC and conventional receivers. Section 7.2 discusses the integration of SIC into the system performance testbed outlined in Chapter 5. Section 7.3 investigates the performance for the various scenarios assuming conventional (equal) power control. The implications of several uplink power control al-

gorithms on SIC performance is investigated in Section 7.4. Finally, a summary of the major findings in this chapter is presented in Section 7.5.

7.2 System performance estimation with SIC

This section describes a modification to the uplink system performance estimation algorithm (outlined in Section 5.2.3.2) to include the implementation of SIC at the base stations (Section 7.2.1). The efficacy of SIC to improve uplink system performance is potentially influenced by the uplink power control algorithm used, as discussed in Section 6.3.2. Section 7.2.2 presents three uplink power control algorithms investigated in this chapter and their implementation in the uplink system performance testbed.

7.2.1 Modified uplink system performance estimation algorithm

The modified uplink system performance estimation algorithm is shown in Figure 7.1. As described in Section 5.2.3.2, this algorithm uses a Monte Carlo analysis to randomly place mobiles on floors of interest and calculates the mean uplink outage probability after several thousand iterations (sufficient for accuracy to four decimal places).

The steps in the algorithm are the same as those in Section 5.2.3.2 (for conventional DS-CDMA systems), except for Step (vi) in which the SIC cancellation process is performed and the SIRs for the various mobiles are calculated.

In Steps (i) to (iv), the mobiles are randomly placed on the floors of interest and the mean received powers of the mobile signals at the desired base station are calculated. It should be noted that in calculating the mean received powers of the mobile signals in Step (iv), one of three power control algorithms may be used. Details of these power control algorithms are presented in Section 7.2.2.

In Step (v), Rayleigh fading is applied to the signal from each mobile, m, to the desired base station, b_{des}, using an exponential distribution. In particular, the *instantaneous* received signal strengths, $P_{r_{b_{des}}}(m)$ (in units of dBm), are modelled as

$$P_{r_{b_{des}}}(m) = 10 \log_{10}(X), \tag{7.1}$$

where the exponential random variable X has the probability density function

$$p_X(x) = \frac{1}{\mu} \exp\left(\frac{-x}{\mu}\right). \tag{7.2}$$

In (7.2), μ is the mean received signal power at the desired base station b_{des} from the mobile m in linear units, i.e. $\mu = 10^{\frac{\overline{P_{r_{b_{des}}}}(m)}{10}}$.

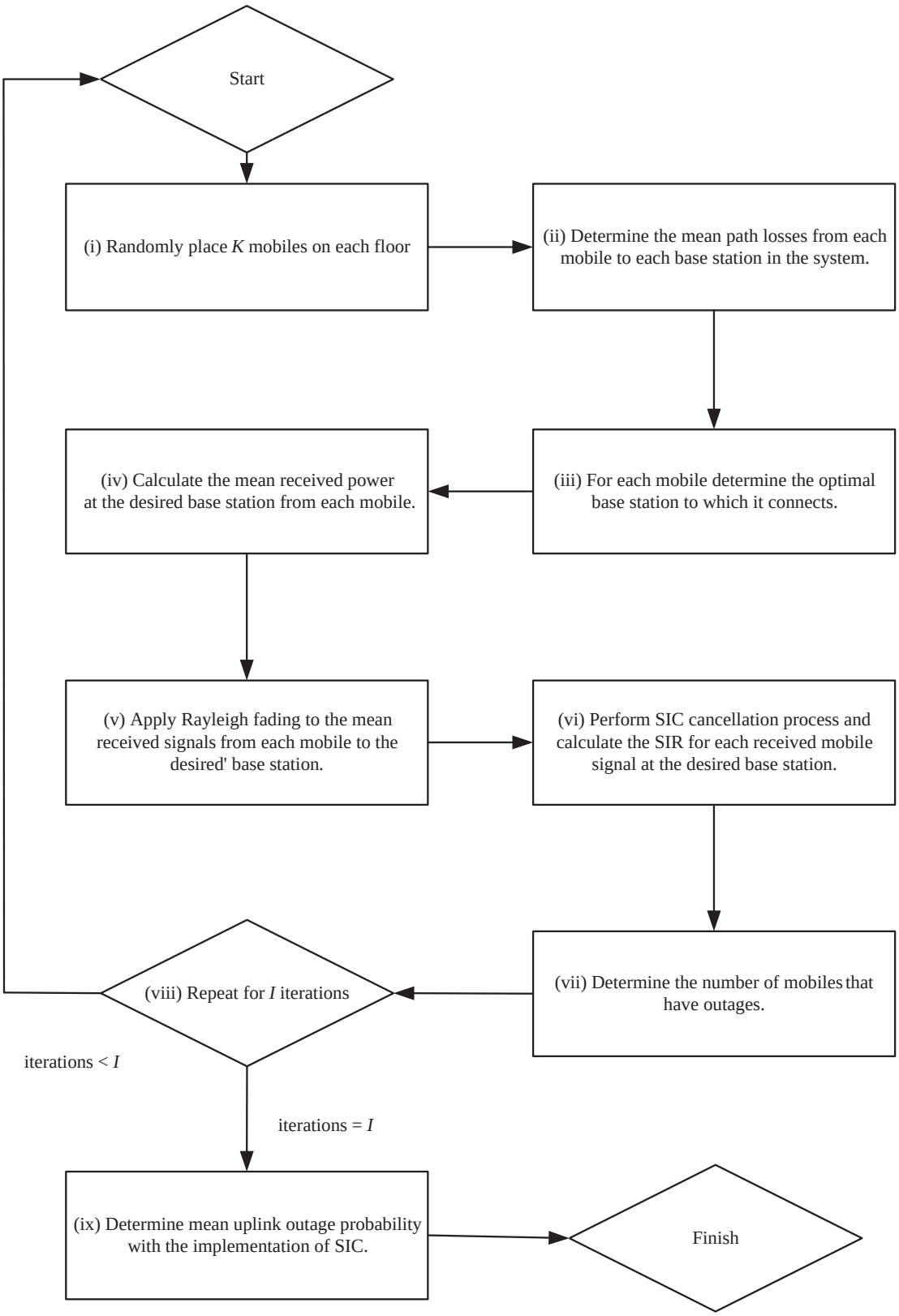

Figure 7.1: Uplink system performance estimation algorithm assuming the implementation of SIC receivers at the base stations.

In Step (vi), SIC is performed and the SIR for each mobile is calculated. The received signals of the mobiles connected to the desired base station, b_{des}, are ranked from the highest to the lowest instantaneous received power. Assuming that a total of K mobiles are connected to the desired base station and that the received signals are ranked such that $P_{r_{b_{des}}}(1) > P_{r_{b_{des}}}(2) > ... > P_{r_{b_{des}}}(K)$, the SIR for the mobile $m = j + 1$ following the cancellation process is

$$SIR_{j+1} = \sqrt{\frac{10^{\frac{P_{r_{b_{des}}}(j+1)}{10}}}{\frac{2\alpha}{3N}\left(\sum_{m=j+2}^{K} 10^{\frac{P_{r_{b_{des}}}(m)}{10}} + \sum_{m=1}^{j} \varepsilon_m \cdot 10^{\frac{P_{r_{b_{des}}}(m)}{10}} + \sum_{m=K+1}^{L} 10^{\frac{P_{r_{b_{des}}}(m)}{10}}\right)}}. \tag{7.3}$$

In (7.3), the numerator, $10^{\frac{P_{r_{b_{des}}}(j+1)}{10}}$, represents the power of the desired signal from mobile $m = j + 1$. The first term in the denominator, $\sum_{m=j+2}^{K} 10^{\frac{P_{r_{b_{des}}}(m)}{10}}$, is the summation of the powers of the uncancelled interfering mobile signals, $m = j + 2$ to $m = K$, which are also connected to the desired base station b_{des}. The second term in the denominator, $\sum_{m=1}^{j} \varepsilon_m \cdot 10^{\frac{P_{r_{b_{des}}}(m)}{10}}$, is a summation of the residual interference from the previous j cancelled mobiles. The parameters ε_m represent the fractional residual interference cancellation errors for the mobile cancellations and are modelled using zero-mean Gaussian random variables with a predefined standard deviation σ_ε (as outlined in Chapter 6). The last term in the denominator, $\sum_{m=K+1}^{L} 10^{\frac{P_{r_{b_{des}}}(m)}{10}}$, represents the inter-cell interference (which is uncancellable) caused by the mobiles represented by the unique identifiers $m = K + 1$ to $m = L$.

In Step (vii), the number of mobiles that have outages on the uplink is calculated by determining whether the instantaneous SIR for each mobile is below a certain threshold at which the BER is greater than 0.02.

In Step (viii), the above process (from Steps (i) to (vii)) is repeated for a given number of iterations (I) such that the resulting mean uplink outage probability is accurate to four decimal places.

Finally in Step (ix), the mean uplink outage probability is calculated by dividing the total number of mobiles having outages by the total number of connections made to the desired base station in all iterations.

7.2.2 Power control algorithms

The performance of SIC is potentially influenced by the uplink power control algorithm used. Three power control algorithms have been implemented in the uplink system performance testbed:

- Conventional power control;
- No power control (fixed mobile transmit power); and
- Optimal power control.

These power control algorithms are used to calculate the mean received powers of the mobile signals in Step (iv) of the uplink system performance estimation algorithm shown in Figure 7.1.

Conventional power control

Conventional power control is identical to that implemented in the system performance estimation algorithm for conventional DS-CDMA systems in Chapter 5. With conventional power control, the mobiles adjust their transmit powers so that their signals are received with the same mean received strengths at the base station to which they are connected.

In Step (iv) of Figure 7.1, the mean received power from each mobile at the desired base station, b_{des}, is calculated using

$$\overline{P_{r_{b_{des}}}}(m) = P_{des} + PL_{b_{con}}(m) - PL_{b_{des}}(m), \tag{7.4}$$

where P_{des} is the desired mean received power for the mobile at the base station to which it is connected, $PL_{b_{con}}(m)$ is the mean path loss between the unique mobile m (located at the three-dimensional coordinates (x, y, z)) and the base station to which the mobile is connected (b_{con}). In (7.4), $PL_{b_{des}}(m)$ is the mean path loss between the unique mobile location m and the desired base station, b_{des}, for which the performance is being quantified.

No power control (fixed mobile transmit power)

This case considers the absence of power control and therefore assumes that the mobiles have a fixed transmit power.

In Step (iv) of Figure 7.1, the mean received power from each mobile at the desired base station, b_{des}, is calculated using

$$\overline{P_{r_{b_{des}}}}(m) = P_t - PL_{b_{des}}(m), \tag{7.5}$$

where P_t is the fixed transmit power from the mobile and $PL_{b_{des}}(m)$ is the mean path loss between the unique mobile location m and the desired base station, b_{des}, for which the performance is being quantified.

Optimal power control

The optimal power control algorithm for SIC, presented in Section 6.3.2, attempts to equalise the mean SIRs for the mobiles' signals received at the base station. Additionally, transmit powers are 'intelligently' allocated to the mobiles so that levels of inter-cell interference are minimised. In essence, mobiles close to the base station (that have a low mean path loss) are allocated lower transmit powers than mobiles further away from the base station (that have a high mean path loss).

Similar to conventional power control, it is assumed that the *mean* received powers of the mobiles' signals at the base station can be controlled by adjusting the transmit powers of the mobiles. However, there are variations in the *instantaneous* received powers of the mobiles' signals at the base stations due to short-term fading. The optimal power control distribution for mobiles connected to a particular base station, b_{con}, is calculated using [10, 95, 96, 100, 101]

$$10^{\frac{\overline{P_{r_{b_{con}}}}(m)}{10}} = 10^{\frac{\overline{P_{r_{b_{con}}}}(m-1)}{10}} - \frac{(1-\varepsilon_{m-1}) \cdot \left(10^{\frac{\overline{P_{r_{b_{con}}}}(m-1)}{10}}\right)^2}{V_{m-1} + \widehat{P_{oc}}}, \tag{7.6}$$

where V_m is the total remaining multiple-access interference (MAI) for mobile m plus its own power

$$V_m = \sum_{i=1}^{M} 10^{\frac{\overline{P_{r_{b_{con}}}}(i)}{10}} - \sum_{i=1}^{m-1} (1-\varepsilon_i) \cdot 10^{\frac{\overline{P_{r_{b_{con}}}}(i)}{10}}. \tag{7.7}$$

In (7.6) and (7.7), the fractional residual interference cancellation error, ε_m, and the inter-cell interference, $\widehat{P_{oc}}$, are unknown and have to be estimated. The parameter M represents the total number of mobiles connected to the base station b_{con}. Equation (7.6) cannot be solved analytically and therefore an iterative process is used to determine the optimal mean received powers for the mobiles, $\overline{P_{r_{b_{con}}}}(m)$. The algorithm used for this iterative process is presented in [10, 95, 96, 100, 101] and is shown in Figure 7.2. A variable $P_T = \sum_{m=1}^{M} \overline{P_{r_{b_{con}}}}(m)$ is introduced to represent the total mean received power allocation for all mobiles within a cell of interest. The mean received power allocations for the mobiles are calculated to an arbitrary accuracy, given by a chosen step size Δ of 0.1 mW.

After the optimal power control distribution has been computed and the powers have been 'intelligently' allocated to the mobiles (to minimise inter-cell interference), the transmit power for each mobile, m, is then calculated using

$$P_t(m) = \overline{P_{r_{b_{con}}}}(m) + PL_{b_{con}}(m), \tag{7.8}$$

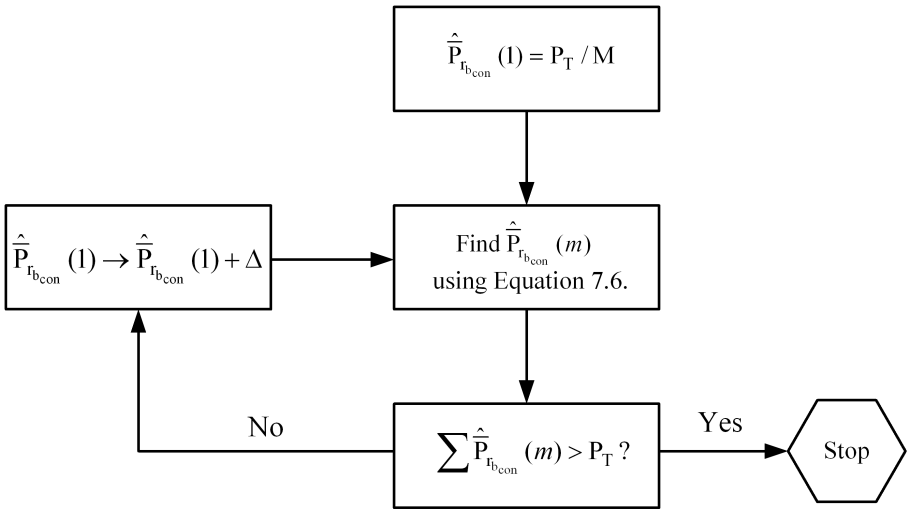

Figure 7.2: Algorithm for computing the optimal power control distribution [10,95,96,100,101].

where $PL_{b_{con}}(m)$ is the mean path loss between the unique mobile m and the base station to which the mobile is connected (b_{con}).

Finally, the mean received powers of all the mobile signals at the desired base station are calculated using

$$\overline{P_{r_{b_{des}}}}(m) = P_t(m) - PL_{b_{des}}(m), \tag{7.9}$$

where $PL_{b_{des}}(m)$ is the mean path loss between the desired base station, b_{des}, and the mobile m.

7.3 SIC performance estimation results with conventional uplink power control

This section presents a comprehensive set of performance results for the deployment configurations in the three propagation campaigns assuming SIC receivers at the base stations. It is assumed throughout this section that *conventional* uplink power control is implemented in the system (as was done for the DS-CDMA systems operating without multiuser detection in Chapter 5). With conventional uplink power control, the mobiles connected to a particular base station adjust their signal transmit powers so that they are received at the base station with the same *mean* received power. However, variations in the actual, instantaneous received mobile signal strengths occur due to short-term fading. SIC exploits these variations by ranking the signals in decreasing order of signal strength and cancelling them sequentially.

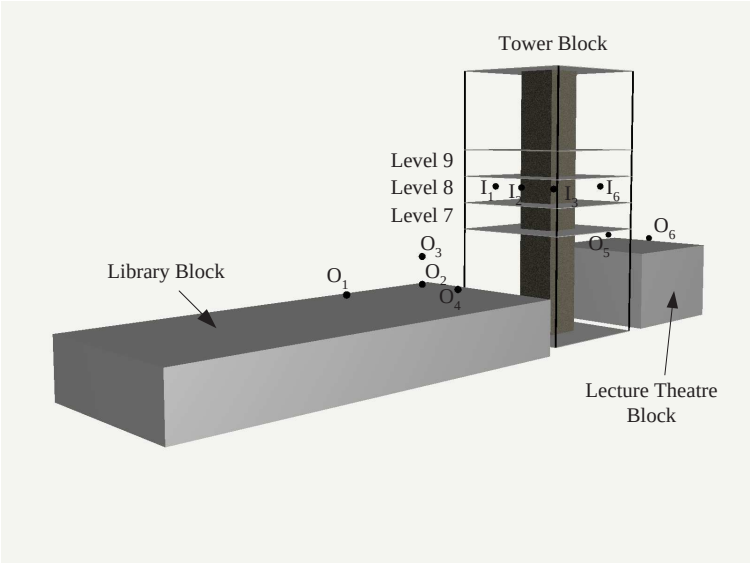

Figure 7.3: Transmitter locations in PM A. N.B. Transmitters I_4 and I_5 are obscured from view by the central steel-reinforced concrete core in the Tower Block.

7.3.1 Single floor indoor system coexisting with outdoor system (PM A)

A three-dimensional diagram showing the transmitter locations in PM A is in Figure 7.3. The following sections present the uplink performance estimates for the *indoor-only* scenario (Section 7.3.1.1) and the *interfering indoor/outdoor* scenario (Section 7.3.1.2) assuming SIC receivers at the base stations.

7.3.1.1 Indoor-only scenario

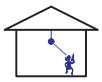

Simple configurations deploying two base stations on a single floor in the Tower Block of the School of Engineering are shown in Table 7.1. Configurations Ad.x have the base stations **ad**jacently located within 5 metres of each other. In Configurations Di.x, the base stations are **di**agonally opposite each other, while in Configurations Op.x the base stations are located on **op**posite sides of the building. Finally Configurations Si.x have the base stations on the same **si**de of the building but with a longer separation distance than those in Configurations Ad.x. For simplicity, the central steel-reinforced concrete core is not shown in the diagrams in Table 7.1, but is a key factor that influences system performance.

Assuming that there are 20 mobiles in the system, Figure 7.4 is a graph of the mean uplink outage probabilities for the various deployment configurations in Table 7.1 assuming various standard deviations of the fractional residual interference cancellation error

Configuration	Ad.1	Ad.2	Ad.3	Di.1	Di.2
Layout					
Configuration	**Op.1**	**Op.2**	**Op.3**	**Si.1**	**Si.2**
Layout					

Table 7.1: Indoor base station deployment configurations in PM A.

(σ_ε). To demonstrate the performance gains attainable with SIC, the graph also shows the mean of the mean uplink outage probabilities for all the deployment configurations assuming *conventional receivers* (i.e. without SIC) at the base stations.

It is evident from Figure 7.4 that the disparities in uplink outage probabilities between the various configurations operating with SIC are much greater than those observed if conventional receivers are used at the base station (presented in Chapter 5). If there is perfect interference cancellation (i.e. $\sigma_\varepsilon = 0$), the uplink outage probability reduces by as much as thirty times (in Configuration Op.3) compared to that obtained with conventional receivers. With the implementation of SIC receivers at the base stations, the optimal deployment configurations are Op.2 and Op.3. In Chapter 5, it was shown that these configurations are also optimal for the case where conventional receivers are implemented.

7.3.1.2 Interfering indoor/outdoor scenario

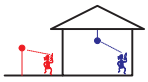

In this section, it is assumed that outdoor interference is presented to an indoor system operating with a single base station that has an SIC receiver. The deployment configurations considered are shown in Table 7.2. In Configurations SSI.1 to SSI.3 the indoor base station is at the **s**ame **s**ide of the building from where the outdoor **i**nterference emanates. In Configurations OSI.1 to OSI.3, the indoor base station is at the **o**pposite **s**ide of the building from where the outdoor **i**nterference emanates.

Figure 7.5 is a graph showing the mean uplink outage probabilities for indoor mobiles in the configurations in Table 7.2. This figure also shows the mean of the mean uplink outage probabilities for the various configurations assuming conventional receivers at the

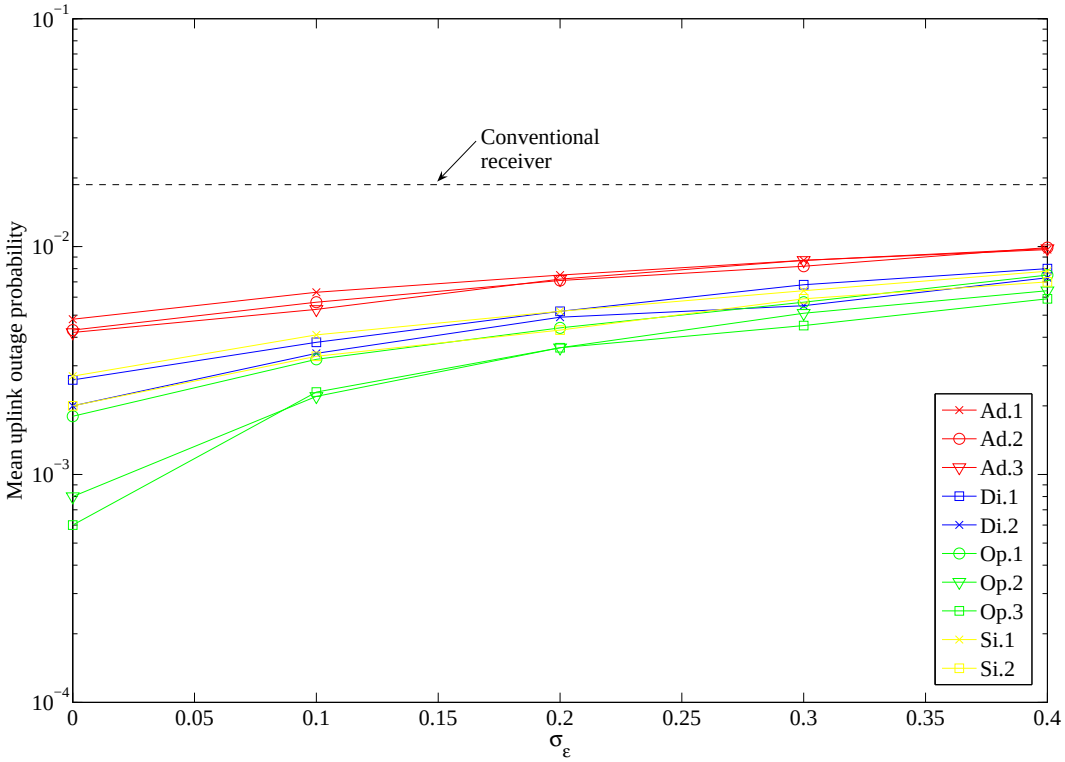

Figure 7.4: Graph of the mean uplink outage probability versus the standard deviation of the fractional residual interference cancellation error (σ_ε) for various indoor deployment configurations in PM A assuming SIC receivers at the base stations.

Configuration	SSI.1	SSI.2	SSI.3
Layout	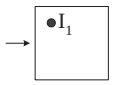	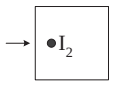	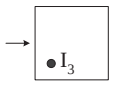
Configuration	OSI.1	OSI.2	OSI.3
Layout	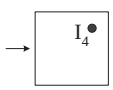	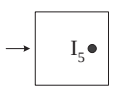	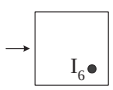

Table 7.2: Interfering indoor/outdoor deployment configurations for which the uplink system performance is investigated in PM A. N.B. Arrows indicate the origin of uplink interference from outdoors.

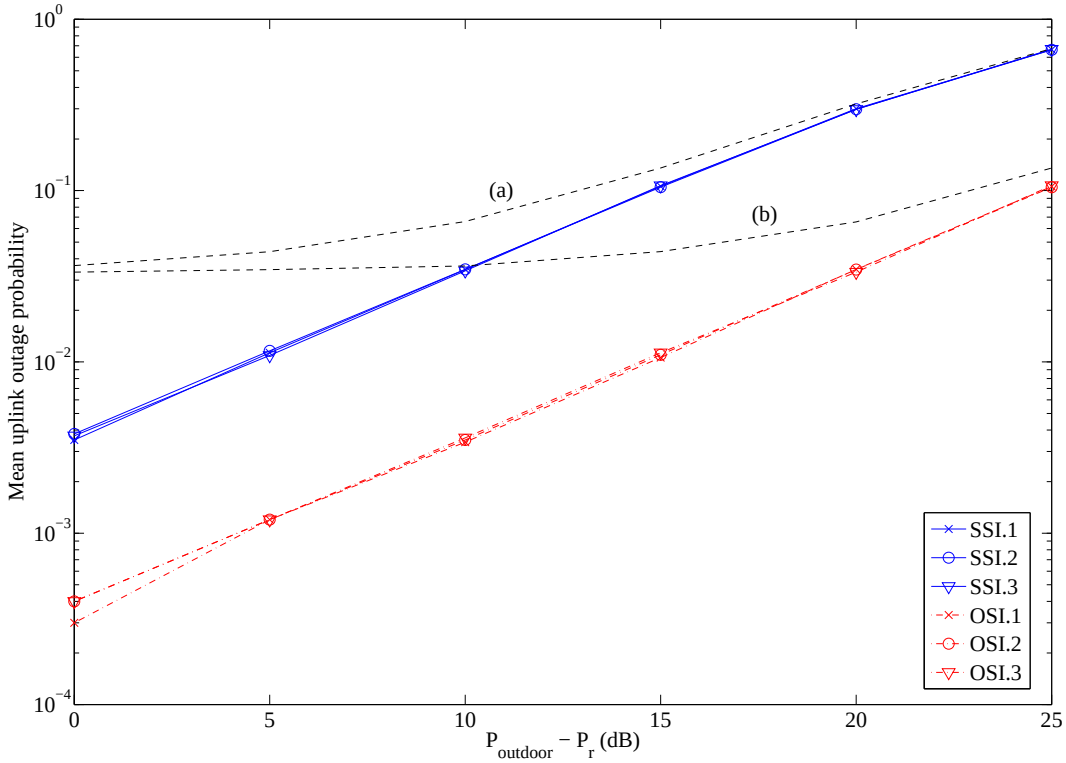

Figure 7.5: Mean uplink outage probability for mobiles on Level 8 for various interfering indoor/outdoor configurations (shown in Table 5.4) assuming SIC receivers, 20 mobiles per base station and the outdoor interference level shown. The parameter $P_{outdoor}$ is the mean power of each of the outdoor interfering mobile signals measured indoors at one side of the building while P_r is the power controlled mean received power of the indoor mobiles (at the indoor base station). N.B. The line labelled (a) represents the mean of the mean uplink outage probabilities assuming the use of conventional receivers and the indoor base station on the *same* side of the building from where the outdoor interference emanates. The line labelled (b) represents the mean of the mean uplink outage probabilities assuming the use of conventional receivers and the indoor base station on the *opposite* side of the building from where the outdoor interference emanates.

base station (detailed in Chapter 5) for two cases: (a) the indoor base station on the same side of the building from where the outdoor interference emanates and (b) the indoor base station on the opposite side of the building from where the outdoor interference emanates. It is assumed that there are 20 mobiles served by each base station and the SIC receiver at the indoor base station is able to cancel interference perfectly (i.e. $\sigma_\varepsilon = 0$).

It is evident from Figure 7.5 that more appreciable improvements in uplink system performance are attained for the SSI.x and OSI.x configurations if the outdoor interference level is lower. As the level of outdoor interference increases, the mean uplink outage probabilities for both the SSI.x and OSI.x configurations (assuming SIC receivers) converge towards those obtained with conventional receivers. This occurs because the outdoor interference becomes increasingly dominant as its strength increases, thereby diminishing

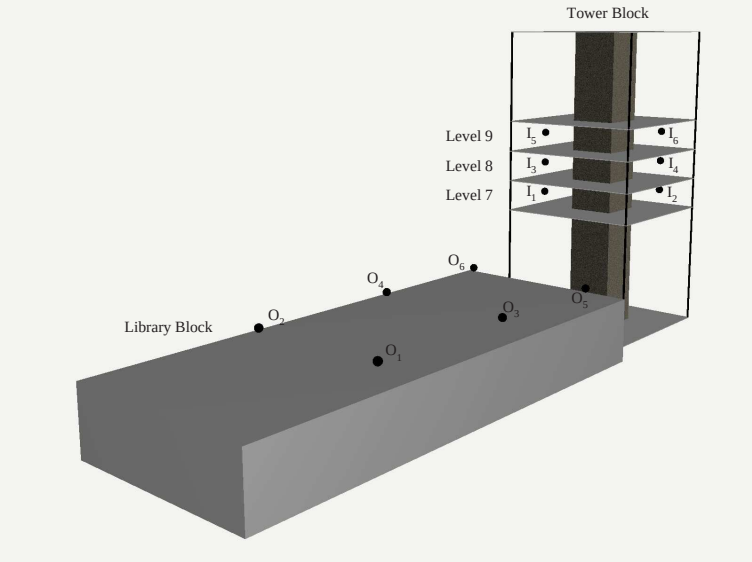

Figure 7.6: Transmitter locations in PM B.

any performance gain provided by the SIC receiver (which can only cancel interference from indoor mobiles).

7.3.2 Multi-floor indoor system coexisting with outdoor system (PM B)

This section investigates the deployment and performance of base stations in a three-dimensional configuration inside a building coexisting with an outdoor system. Propagation measurement results from PM B are used and it is assumed that SIC receivers operate at the base stations. A three-dimensional drawing of the base station locations in PM B is shown in Figure 7.6.

This section begins by presenting uplink system performance estimation results (assuming SIC receivers) for three-dimensional configurations of indoor base stations *without* the influence of outdoor interference (*indoor-only* scenario) in Section 7.3.2.1. Following this, the influence of outdoor interference on indoor system performance is investigated (*interfering indoor/outdoor* scenario) in Section 7.3.2.2.

7.3.2.1 Indoor-only scenario

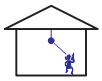

Possible base station deployment configurations deploying base stations and mobiles on three levels of the Tower Block are shown in Table 7.3.

In Configurations *Aligned 1* and *Aligned 2*, all the base stations are vertically aligned with each other while in Configurations *Offset 1* and *Offset 2* the base stations are

Config.	Aligned 1	Aligned 2	Offset 1	Offset 2
Base Station Layout	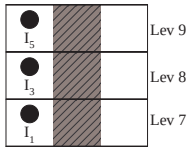	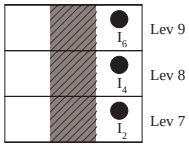	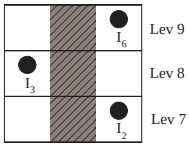	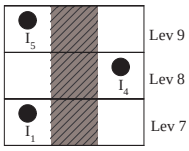
Config.	Aligned/Offset 1	Aligned/Offset 2	Aligned/Offset 3	Aligned/Offset 4
Base Station Layout	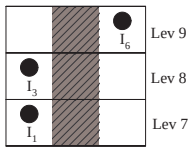	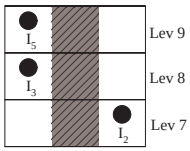	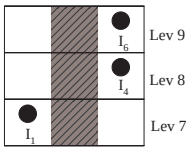	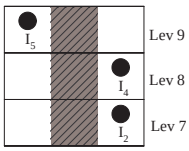

Table 7.3: Front view of indoor base station deployment configurations in PM B (Indoor-only scenario).

vertically offset from each other. In Configurations *Aligned/Offset 1* to *Aligned/Offset 4*, one base station is aligned with the base station on Level 8 while the other is vertically offset from the base station on Level 8.

Figure 7.7 is a graph showing the mean uplink outage probabilities for the various deployment configurations in Table 7.3 assuming 20 mobiles on each of the three floors and various standard deviations of the fractional residual interference cancellation error (σ_ε).

It is evident from Figure 7.7 that similar to the observations in PM A, the differences in the mean uplink outage probabilities for the various deployment configurations are much greater than those observed for conventional DS-CDMA systems (Chapter 5). This is because of the increased dominance of inter-cell interference (which varies for the different deployment configurations) due to the SIC process. An improvement in mean uplink outage probability by as much as 15 times over the conventional receiver is possible (in Configurations *Aligned 1* and *Aligned 2*). The optimal deployment configurations are *Aligned 1* and *Aligned 2*, which is the same as those observed for conventional DS-CDMA systems in Chapter 5.

7.3.2.2 Interfering indoor/outdoor scenario

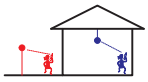

In this scenario, the system performance on the uplink is estimated assuming that outdoor interference emanates from one side of the Tower Block. Table 7.4 shows the

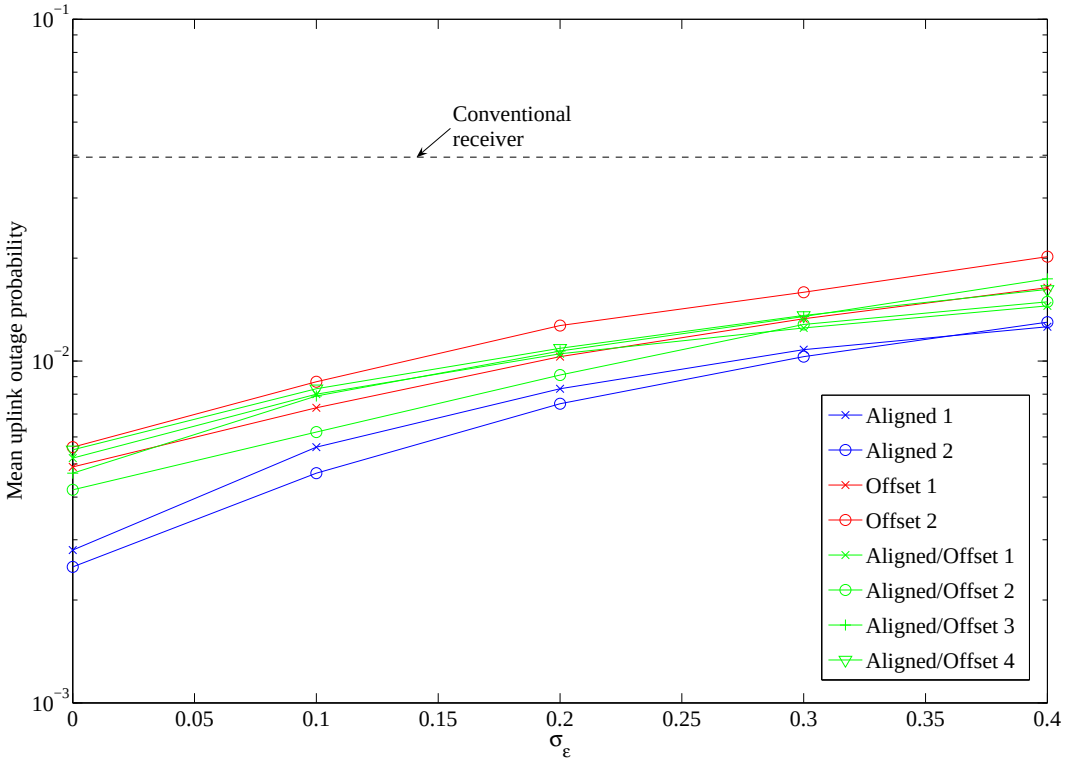

Figure 7.7: Graph of the mean uplink outage probability versus the standard deviation of the fractional residual interference cancellation error (σ_ε) for the various indoor deployment configurations in PM B shown in Table 7.3. N.B. This graph assumes SIC receivers at the base stations.

deployment configurations considered. Figure 7.8 shows the mean uplink outage probabilities for the configurations in Table 7.4 assuming SIC receivers at the base stations. Also shown on this figure is the mean of the mean uplink outage probabilities for the various configurations assuming conventional receivers at the base station (detailed in Chapter 5) for: (a) the indoor base station on Level 8 on the same side of the building from where the outdoor interference emanates and (b) the indoor base station on Level 8 on the opposite side of the building from where the outdoor interference emanates. It is assumed that there are 20 mobiles outdoors and on each floor of the building indoors. Additionally, it is assumed that the SIC receivers at the indoor base stations can cancel interference perfectly (i.e. $\sigma_\varepsilon = 0$).

The behaviour observed in Figure 7.8 is similar to that observed for the deployment configurations considered in PM A (Section 5.4.1.2). For increased outdoor interference, the mean uplink outage probabilities for the configurations with SIC converges to the mean uplink outage probabilities attained with conventional receivers. For lower levels of outdoor interference (e.g. $P_{outdoor} - P_r = 0$ dB), there are greater differences in the mean uplink outage probabilities for the various configurations. This occurs due to dominance of the indoor inter-cell interference in the various configurations when the outdoor interference is low. Because there are significant differences in the indoor inter-cell interference

Config.	Aligned 1 + OutdoorInt	Aligned 2 + OutdoorInt	Offset 1 + OutdoorInt	Offset 2 + OutdoorInt
Base Station Layout	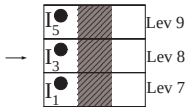	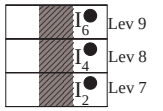	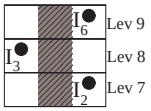	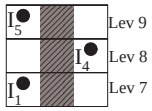
Config.	Aligned/Offset 1 + OutdoorInt	Aligned/Offset 2 + OutdoorInt	Aligned/Offset 3 + OutdoorInt	Aligned/Offset 4 + OutdoorInt
Base Station Layout	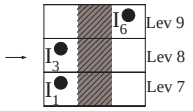	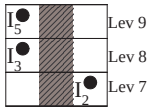	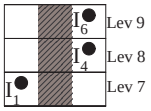	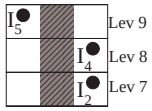

Table 7.4: Front view of interfering indoor/outdoor base station configurations considered in the investigation of uplink system performance in PM B. N.B. Arrows indicate the origin of uplink interference from outdoors.

for the various configurations, these differences manifest themselves as variations in the mean uplink outage probabilities.

7.3.3 Coexisting single floor indoor systems in adjacent buildings (PM C)

This section investigates the deployment and performance of two indoor DS-CDMA systems operating with SIC receivers in two buildings located adjacent to each other (using propagation measurement results from PM C). Figure 7.9 is a plan of the locations of the transmitters deployed in PM C.

This section presents the SIC uplink performance results for the *indoor-only* scenario (Section 7.3.3.1) followed by the *adjacent interfering* scenario (Section 7.3.3.2).

7.3.3.1 Indoor-only scenario

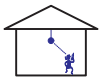

In this scenario, the deployment and performance of simple configurations deploying two base stations are considered for each of the Science and Functions buildings in PM C, assuming that there is no external interference presented to each system.

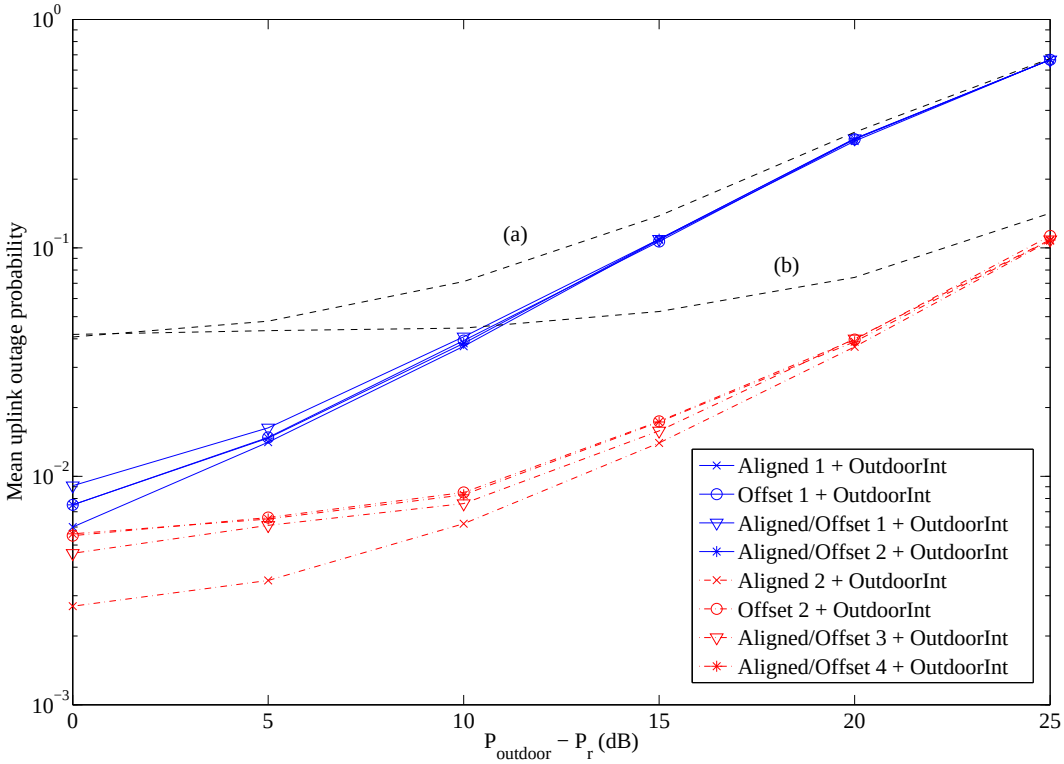

Figure 7.8: Mean uplink outage probability for mobiles on Level 8 for various interfering indoor/outdoor configurations (shown in Table 7.4) assuming SIC receivers, 20 mobiles per base station and the outdoor interference level shown. The parameter $P_{outdoor}$ is the mean power of each of the outdoor interfering mobile signals measured indoors at one side of the building while P_r is the power controlled mean received power of the indoor mobiles (at the indoor base station). N. B. The line labelled (a) represents the mean of the mean uplink outage probabilities assuming the use of conventional receivers and the indoor base station on Level 8 on the *same* side of the building from where the outdoor interference emanates. The line labelled (b) represents the mean of the mean uplink outage probabilities assuming the use of conventional receivers and the indoor base station on Level 8 on the *opposite* side of the building from where the outdoor interference emanates.

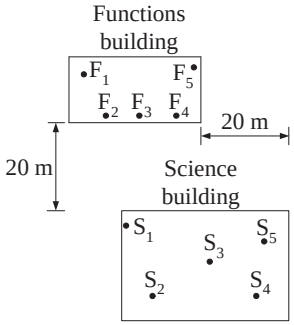

Figure 7.9: Relative locations of transmitters deployed in the Science and Functions buildings in PM C.

Configuration	S_1S_4	S_2S_5	S_2S_3
Layout	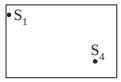	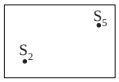	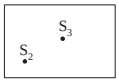
Configuration	S_3S_4	S_1S_2	S_4S_5
Layout	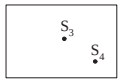	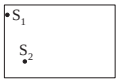	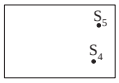

Table 7.5: Simple indoor configurations deploying two base stations in the Science building (PM C).

Science building

Table 7.5 shows a selection of base station configurations for a system deployed on a single floor of the Science building. Configurations S_1S_4 and S_2S_5 have base stations that are diagonally opposite to each other. Configurations S_2S_3 and S_3S_4 have a single base station on the centre of the floor and a base station at one corner of the floor. In Configurations S_1S_2 and S_4S_5, the base stations are located on the left and right hand side of the building respectively. The mobiles are randomly located at positions at which measurements were made on the same floor as the base stations.

Figure 7.10 is a graph showing the mean uplink outage probabilities for the deployment configurations in Table 7.5 assuming various standard deviations of the fractional residual interference cancellation error (σ_ε). The observations made are largely similar to those made for PM A and PM B in Sections 7.3.1.1 and 7.3.2.1. Firstly, the variations in uplink outage probabilities between the various configurations are much greater with SIC than with conventional receivers (investigated in Chapter 5). Secondly, the mean uplink outage probability decreases by as much as 10 times relative to that attained with conventional receivers. However, there is no particular relationship between the deployment strategy used and the mean uplink outage probability attained.

Functions building

A sample of configurations deploying two base stations in the Functions Building are shown in Table 7.6. These configurations are similar to those investigated for the Science building. Configurations F_1F_4 and F_2F_5 have base stations that are diagonally opposite to each other. Configurations F_2F_3 and F_3F_4 have base stations located on the bottom side

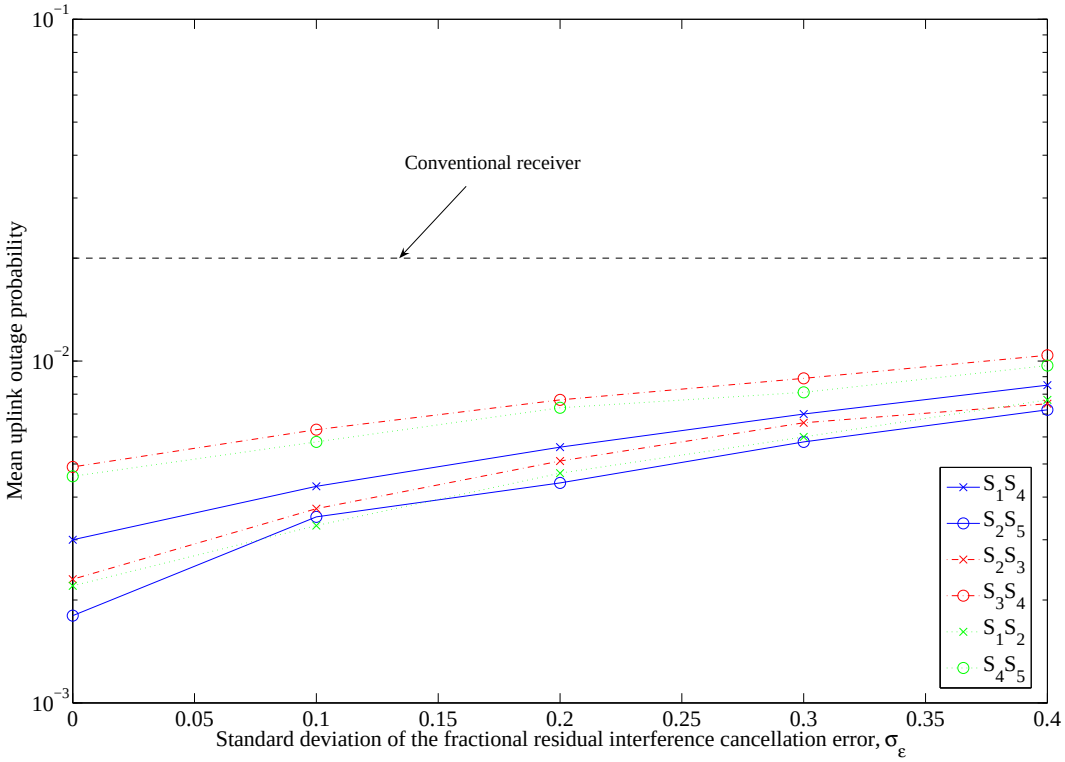

Figure 7.10: Graph of the mean uplink outage probability versus the standard deviation of the fractional residual interference cancellation error (σ_ε) for various indoor deployment configurations operating with SIC receivers in the Science building in PM C.

of the building. In Configurations F_1F_2 and F_4F_5, the base stations are located on the left and right hand side of the building respectively. The mobiles are randomly located at positions at which measurements were made on the same floor as the base stations.

Figure 7.11 shows the mean uplink outage probabilities for the deployment configurations shown in Table 7.6 assuming various standard deviations of the fractional residual interference cancellation error (σ_ε). With SIC, the uplink outage probabilities are reduced by as much as 10 times over the conventional receiver, similar to performance gains observed for the configurations in the Science building. There is however no relationship observed between the deployment configuration used and the uplink system performance attained.

7.3.3.2 Interfering adjacent scenario

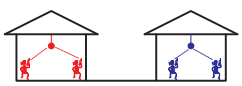

In this scenario, it is assumed that an indoor DS-CDMA system operating in the Functions building mutually interferes with another indoor DS-CDMA system operating in the Science building. Both systems have SIC receivers operating at the base stations. In such a scenario it is desirable for wireless operators to 'balance' the performance of the two

Configuration	F_1F_4	F_2F_5	F_2F_3
Layout	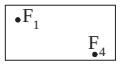	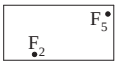	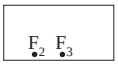
Configuration	F_3F_4	F_1F_2	F_4F_5
Layout	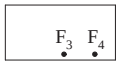	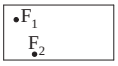	

Table 7.6: Simple indoor configurations deploying two base stations in the Functions building (PM C).

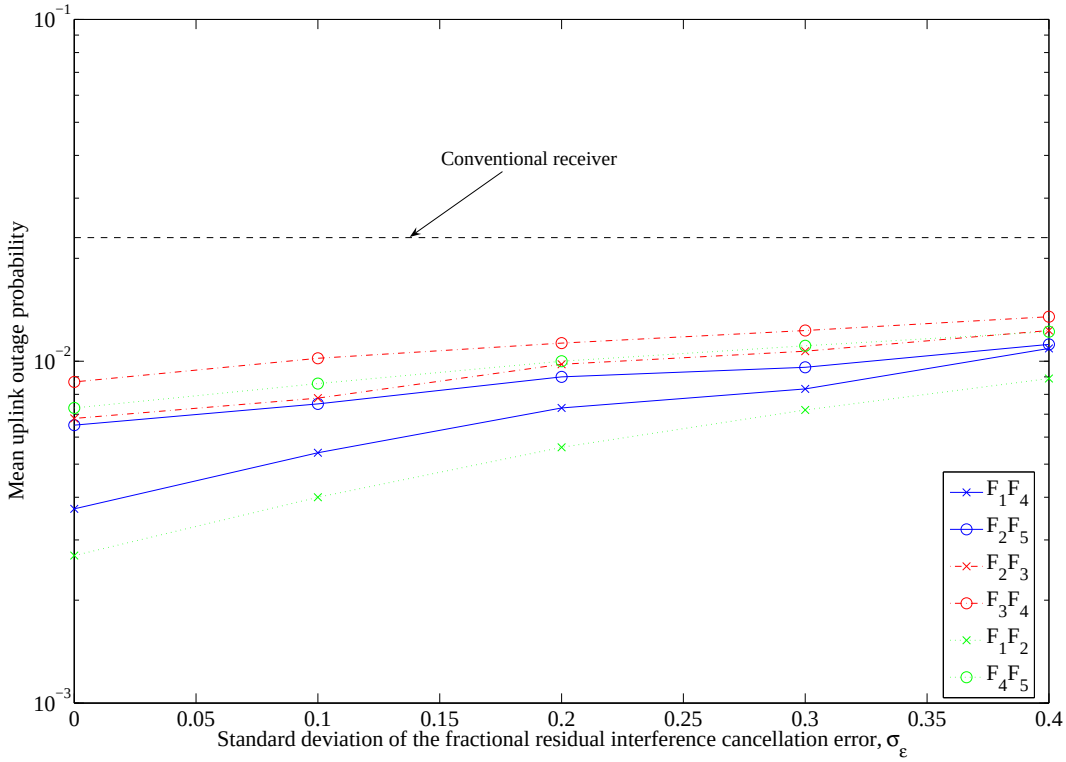

Figure 7.11: Graph of the mean uplink outage probability versus the standard deviation of the fractional residual interference cancellation error (σ_ε) for various indoor deployment configurations operating with SIC receivers in the Functions building in PM C.

Configuration	F_1S_1	F_3S_1	F_5S_5
Layout	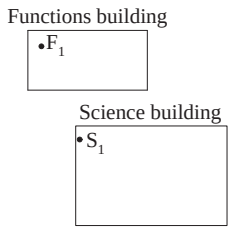	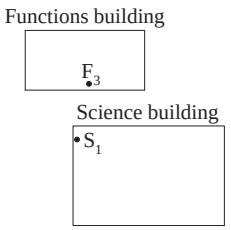	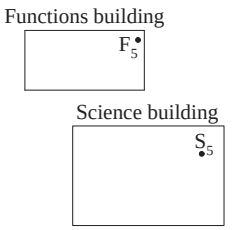
Configuration	F_1S_4	F_3S_2	F_3S_3
Layout	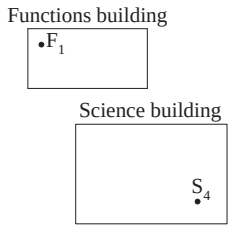	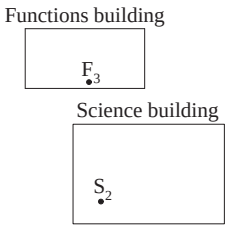	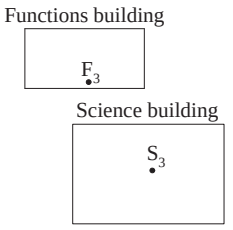

Table 7.7: Base station deployment configurations investigating interfering adjacent systems in PM C.

indoor DS-CDMA systems so that neither system has a significantly worse performance than the other.

Six simple configurations that deploy one base station in the Functions building and one base station in the Science building are shown in Table 7.7. This section begins with an in-depth discussion of the uplink system performance estimates for mobiles in the Science building (with the use of SIC) . It is shown that the performance of the system operating in the Science building is heavily dependent on the interference emanating from the Functions building. The issue of performance 'balancing' between the systems operating in the Science building and Functions building is then investigated by comparing uplink outage probability estimates for both systems at a fixed interference level. Throughout this section it is assumed that there are 20 mobiles randomly located in each of the Science and Functions buildings. Additionally, it is assumed that perfect interference cancellation is achieved (i.e. $\sigma_\varepsilon = 0$).

Uplink system performance in Science building assuming SIC receivers

Figure 7.12 is a graph showing the mean uplink outage probabilities for mobiles in the Science building, assuming various levels of uplink interference from mobiles in the Functions building. It is evident that significant differences (as much as three orders-of-magnitude)

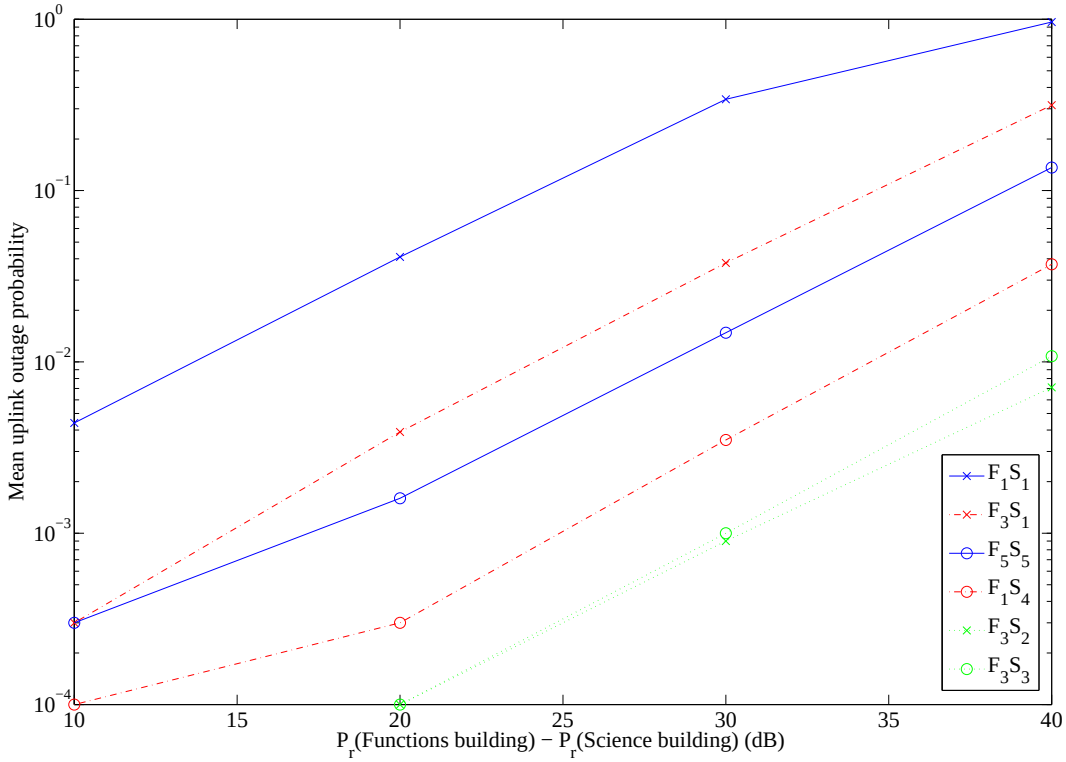

Figure 7.12: Mean uplink outage probabilities for mobiles in the Science building for the adjacent interfering base station configurations shown in Table 7.7 (assuming the implementation of SIC with perfect cancellation). N.B. P_r(Functions building) is the power controlled mean received power for mobiles in the Functions building while P_r(Science building) is the power controlled mean received power for mobiles in the Science building.

in mean uplink outage probabilities are observed for the various configurations. The optimal deployment configurations are F_3S_2 and F_3S_3, which is the same as for the case where conventional receivers are used (investigated in Chapter 5). It should be noted that in F_3S_2 and F_3S_3, no outages are observed if P_r(Functions building) – P_r(Science building) < 20 dB.

Figure 7.12 does not show the uplink outage probabilities for the various configurations with the implementation of conventional receivers. However, similar to the findings in PM A and PM B, the uplink performances of the configurations (assuming SIC receivers) converge towards those attained with conventional receivers for increased levels of interference emanating from the Functions building.

Uplink system performance balancing between Functions and Science buildings

In practice wireless operators will need to 'balance' the performance of both systems so that one system does not have a significant advantage over the other. A 'snapshot' of the mean uplink outage probabilities for the mobiles in both the Functions and Science

buildings at a given level of interference is shown in Table 7.8 assuming 20 mobiles in each building. In obtaining the mean uplink outage probabilities for the mobiles in the Science building it is assumed that the power controlled mean received power (at the base station) for mobiles in the Functions building is 30 dB greater than that for mobiles in the Science building. Similarly, in obtaining the mean uplink outage probabilities for mobiles in the Functions building, it is assumed that the power controlled mean received power for mobiles in the Science building is 30 dB greater than that for mobiles in the Functions building.

Table 7.8 shows the mean uplink outage probabilities for mobiles in the buildings for both conventional receivers and SIC receivers. It is evident that while significant performance gains are achieved with SIC receivers in the Science building, little or no performance gains are achieved with SIC receivers in the Functions building. This is due to the higher *transmit* powers of the mobiles in the Science building than the Functions building. While the *relative* mean received powers at the base stations in both buildings are the same, the larger area of the Science building and the presence of internal partitions cause the mobiles in the Science building to transmit with a higher power than those in the Functions building. Therefore, the interference presented from the Science building to the Functions building is actually greater than that presented from the Functions building to the Science building.

Considering the performance for mobiles in the Science building, it is evident that Configuration F_1S_1 has very little improvement in the mean uplink outage probabilities with the use of SIC receivers, while the other configurations have far more significant improvements (reducing the mean uplink outage probabilities by as much as 34 times in Configuration F_3S_3). The lack of performance gain for mobiles in the Science building in F_1S_1 is largely due to the dominance of the uncancellable interference emanating from the Functions building. This, in turn, is caused by the relative locations of the base stations in the Functions and Science building; in Configuration F_1S_1, the transmitter in the Functions building (F_1) is located at the side of the Functions building furthest from the Science building. Therefore mobiles in the Functions building that are closest to the Science building have high transmit powers, thereby presenting a high level of interference to the system in the Science building.

7.4 Implications of uplink power control algorithms

Section 7.3 considered the influence of SIC on the uplink system performance of a variety of system deployment configurations. It was assumed that conventional uplink power control was implemented in the system – i.e. mobiles adjust their transmit powers so that their signals are received with the same mean received powers at the base station to which they

Config.	F_1S_1	F_3S_1	F_5S_5	F_1S_4	F_3S_2	F_3S_3
Layout	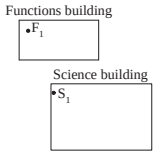	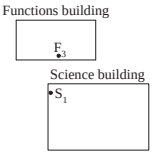	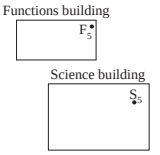	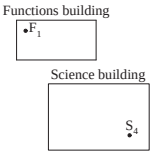	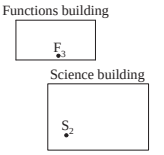	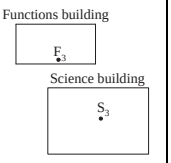
Functions building						
Uplink outage prob. (*Conv.*)	0.126	0.762	0.122	0.508	0.985	0.905
Uplink outage prob. (*SIC*)	0.097	0.756	0.092	0.492	0.985	0.902
Science building						
Uplink outage prob. (*Conv.*)	0.361	0.070	0.047	0.037	0.033	0.034
Uplink outage prob. (*SIC*)	0.341	0.038	0.014	0.004	0.001	0.001

Table 7.8: Comparison of mean uplink outage probabilities for interfering adjacent indoor DS-CDMA systems assuming conventional receivers and SIC receivers (perfect cancellation).

Config.	Aligned	Offset
Base Station Layout	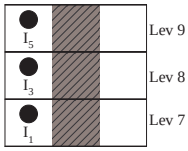	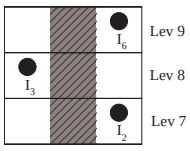

Table 7.9: Front view of two indoor base station deployment configurations in PM B (Indoor-only scenario).

are connected. However, in Sections 6.3.2 and 7.2.2, it was shown that conventional uplink power control is likely to be suboptimal for implementation with SIC. For this reason an optimal power control algorithm (derived in [10, 95, 96, 100, 101]) was implemented in the uplink system performance testbed, as was outlined in Section 7.2.2.

The purpose of this section is to demonstrate the implications of three uplink power control algorithms (introduced in Section 7.2.2) on the efficacy of SIC to yield performance gains. This investigation is performed for simple *indoor-only* deployment configurations from the propagation measurement campaign PM B.

7.4.1 Indoor-only scenario – PM B

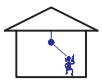

This section evaluates the influence of uplink power control algorithms on the efficacy of SIC to improve the performance of two simple *indoor* deployment configurations in PM B. The configurations studied are the *Aligned* and *Offset* configurations shown in Table 7.9.

Figure 7.13 is a graph of the mean uplink outage probabilities for the *Aligned* and *Offset* deployment configurations shown in Table 7.9. This graph shows the mean uplink outage probabilities for a variety of receivers and power control algorithms. For the cases in which an SIC receiver is implemented at the base stations, it is assumed that perfect cancellation (i.e. $\sigma_\varepsilon = 0$) is achieved. The three uplink power control algorithms considered are conventional power control (PC), no PC and optimal PC (details of which are outlined in Section 7.2.2). For the optimal PC algorithm it is assumed that the estimate of the inter-cell interference ($\widehat{P_{oc}}$), necessary for deriving the power control distribution, is made such that optimal system performance is achieved. This involves running the uplink system performance estimation algorithm for a variety of estimates (i.e. predictions) of inter-cell interference and determining the optimal uplink system performance attained.

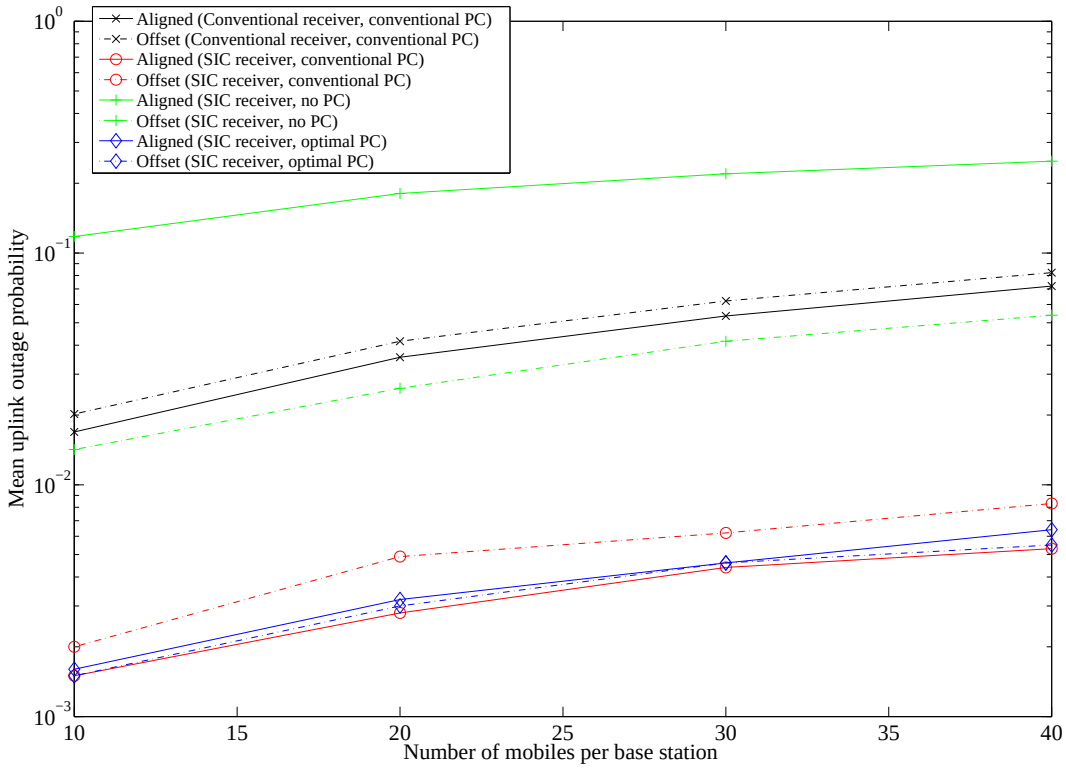

Figure 7.13: Mean uplink outage probabilities for various power control algorithms and receivers at the base stations for the deployment configurations shown in Table 7.9 (PM B). N.B. The SIC receivers are assumed to have perfect cancellation (i.e. $\sigma_\varepsilon = 0$).

As perfect cancellation is assumed, the estimate of the fractional residual interference cancellation error is assumed to be $\widehat{\varepsilon} = 0$.

It is evident from Figure 7.13 that mid-range performance levels are achieved if conventional receivers are used at the base station together with conventional PC. If SIC is implemented with no PC, the performance of the *Aligned* configuration is degraded to the extent that it performs the worst of any of the configurations, while the *Offset* configuration actually has marginally better performance than if conventional receivers are used.

Figure 7.13 shows that there is no significant benefit to be gained if the optimal PC algorithm is used instead of the conventional PC algorithm. However, the uplink system performance appears to be less sensitive to the deployment strategy if the optimal PC algorithm is used (i.e. both the deployment strategies have very similar performance levels). Further analysis of the optimal PC algorithm shows that the mean received power allocations for the strongest and weakest mobiles typically differ by approximately 11 dB. Short-term fading causes variations in signal strength by as much as 30 to 40 dB, and is therefore likely to have a more dominant impact on system performance than the relatively small adjustments made to the mean received power by the optimal PC algorithm. Additionally, as it is necessary to make fixed estimates of the inter-cell interference to

obtain the optimal PC distribution, this causes inherent inaccuracies in the optimal PC distribution obtained. These inaccuracies occur because there are instantaneous variations in the levels of inter-cell interference (caused by fading), whereas the estimates of inter-cell interference need to be fixed in order to obtain the optimal PC distribution.

Although the optimal PC algorithm 'intelligently' allocates transmit powers to mobiles so that levels of inter-cell interference are minimised, only marginal improvements in the F-factors are obtained if conventional PC is used. For example, in the *Aligned* configuration the F-factor is 0.92 with conventional PC and 0.95 with optimal PC. This marginal increase in the F-factor does not cause any significant improvements in uplink system performance.

It is evident that with the implementation of SIC, the optimal power control algorithm provides similar performance to the conventional power control algorithm. If no power control is implemented (i.e. fixed mobile transmit powers), there are significant differences between the uplink outage probabilities attained and those attained with the conventional power control algorithm. For example, the *Offset* configuration actually outperforms the *Aligned* configuration if no power control is used, whereas the *Aligned* configuration outperforms the *Offset* configuration if conventional power control is used.

It should be noted that the implementation of spatial diversity at the base stations is likely to reduce the variations in received signal strength significantly (eliminating small-scale fading to a great extent). In such a situation, the adjustments made by the optimal PC algorithm will have a more dominant influence on the optimal deployment strategy. Note that for the BER threshold considered in this thesis, there are no outages in any of the deployment configurations (with conventional or SIC receivers) if small-scale fading is removed completely.

7.5 Summary

This chapter has investigated the implications of SIC on the deployment and performance of indoor/outdoor DS-CDMA systems using a variety of deployment configurations from three propagation measurement campaigns outlined in Chapter 4. The uplink system performance algorithm outlined in Chapter 5 was modified to include the implementation of SIC receivers at the base stations. Additionally, due to the potential influence of power control on the efficacy of SIC to improve uplink system performance, three different power control algorithms were implemented in the uplink system performance estimation testbed: conventional power control, no power control and optimal power control.

The uplink system performance estimates have shown that the implementation of SIC receivers at the base stations have the potential to reduce uplink outage probabilities by orders-of-magnitude (as much as thirty times). Assuming the implementation of con-

ventional power control, it has been shown that the optimal deployment configurations with the implementation of SIC receivers are similar to those with the implementation of conventional receivers. However, there are increased differences between the uplink outage probabilities of the various configurations with the implementation of SIC receivers. This is caused by the dominance of inter-cell interference (after interference cancellation), which varies significantly among the different deployment configurations.

For the case of indoor DS-CDMA systems presented with outdoor interference, it has been shown that with increased outdoor interference the uplink outage probabilities with SIC receivers converge to those attained with conventional receivers. This is due to the increased dominance of the uncancellable outdoor interference as its strength increases.

In interfering DS-CDMA systems located in adjacent buildings, the improvements in uplink outage probabilities due to the implementation of SIC receivers are highly dependent on both the relative locations of the base stations and the levels of interference presented from one building to the other. The uplink interference level presented from one building to the other is strongly related to the transmit powers of the mobiles, which are influenced by the distance to the base station – if there is a greater floor area, it is likely that mobiles will need to transmit at a higher power and therefore a higher uplink interference is presented to an adjacent building.

An investigation was conducted to determine the influence of power control algorithms on the efficacy of SIC to improve the uplink performance of two simple three-dimensional indoor system configurations. This investigation revealed that the optimal power control algorithm (developed in [10, 95, 96, 100, 101]) yields a similar uplink performance to the conventional power control algorithm.

Chapter 8

Parallel interference cancellation in indoor/outdoor DS-CDMA systems

8.1 Introduction

Chapter 7 investigated the implementation of successive interference cancellation (SIC) to improve the performance of indoor/outdoor DS-CDMA systems. It was assumed that intra-cell interference on the uplink is cancelled at the base station in decreasing order of the received signal strengths of the mobiles. It was shown that SIC has significant implications on the design of indoor/outdoor DS-CDMA systems and that its ability to improve uplink system performance is interrelated with the uplink power control algorithm, the deployment strategy and levels of interference.

This chapter investigates the impact of cancelling the uplink interference presented by the mobiles in *parallel* – also known as parallel interference cancellation (PIC). In Chapter 6 a simple technique for evaluating uplink system performance assuming PIC receivers was presented. This technique has been implemented in the system performance estimation testbed, outlined in Section 8.2. The uplink system performance results for various indoor/outdoor DS-CDMA system deployment scenarios with PIC are presented in Section 8.3. To provide a basis for comparison with conventional and SIC receivers, the scenarios considered are the same as those in Chapters 5 and 7. A comparison between PIC and SIC is presented in Section 8.4. Finally, Section 8.5 summarises this chapter.

8.2 System performance estimation with PIC

This section describes a modification to the uplink system performance estimation algorithm outlined in Section 5.2.3.2 so that uplink outage probabilities can be estimated assuming the implementation of PIC at the base stations. The modified uplink system

performance estimation algorithm is shown in Figure 8.1. As described in Section 5.2.3.2, this algorithm uses a Monte Carlo analysis to randomly place mobiles on floors of interest and calculates the mean uplink outage probability after several thousand iterations (sufficient for accuracy to four decimal places).

The steps in the algorithm are the same as those in Section 5.2.3.2 (for conventional DS-CDMA systems), except for Step (vi) in which the PIC cancellation process is performed and the SIRs for the various mobiles are calculated.

In Steps (i) to (iv), the mobiles are randomly placed on the floors of interest and the mean received powers of the mobile signals at the desired base station are calculated. It should be noted that in Step (iv) conventional power control is used, as this has been shown to be optimal for PIC implementation [94].

In Step (v), Rayleigh fading is applied to the signal from each mobile, m, to the desired base station, b_{des}, using an exponential distribution. In particular, the *instantaneous* received signal strengths, $P_{r_{b_{des}}}(m)$ (in units of dBm), are modelled as

$$P_{r_{b_{des}}}(m) = 10\log_{10}(X), \tag{8.1}$$

where the exponential random variable X has the probability density function

$$p_X(x) = \frac{1}{\mu}\exp\left(\frac{-x}{\mu}\right). \tag{8.2}$$

In (8.2), μ is the mean received signal power at the desired base station b_{des} from the mobile m in linear units, i.e. $\mu = 10^{\frac{\overline{P_{r_{b_{des}}}}(m)}{10}}$.

In Step (vi), the PIC cancellation process is performed and the SIR for each mobile is calculated. The SIR for the kth mobile at the sth stage of the PIC receiver is

$$SIR_k^{(s)} = \sqrt{\frac{10^{\frac{P_{r_{b_{des}}}(k)}{10}}}{\frac{2\alpha}{3N}\left(\sum_{m=1,m\neq k}^{K}\varepsilon_m^{(s)}10^{\frac{P_{r_{b_{des}}}(m)}{10}} + \sum_{m=K+1}^{L}\varepsilon_m^{(s)}10^{\frac{P_{r_{b_{des}}}(m)}{10}}\right)}}, \tag{8.3}$$

where the numerator, $10^{\frac{P_{r_{b_{des}}}(k)}{10}}$, represents the power of the desired signal from mobile k. The term $\sum_{m=1,m\neq k}^{K}\varepsilon_m^{(s)}10^{\frac{P_{r_{b_{des}}}(m)}{10}}$ is the summation of the residual interference from the cancellations of the other $K-1$ mobiles connected to the desired base station b_{des}. The summation of the inter-cell interference from mobiles $m = K+1$ to $m = L$ is given by the term $\sum_{m=K+1}^{L}\varepsilon_m^{(s)}10^{\frac{P_{r_{b_{des}}}(m)}{10}}$. The parameters $\varepsilon_m^{(s)}$ represent the fractional residual interference errors for the cancellations of each mobile i at the sth stage of the PIC receiver. At the conventional receiver stage ($s = 1$), $\varepsilon_m^{(1)} = 1$ as no interference is cancelled. For subsequent stages ($s \geq 2$), the fractional residual interference cancellation errors $\varepsilon_m^{(s)}$

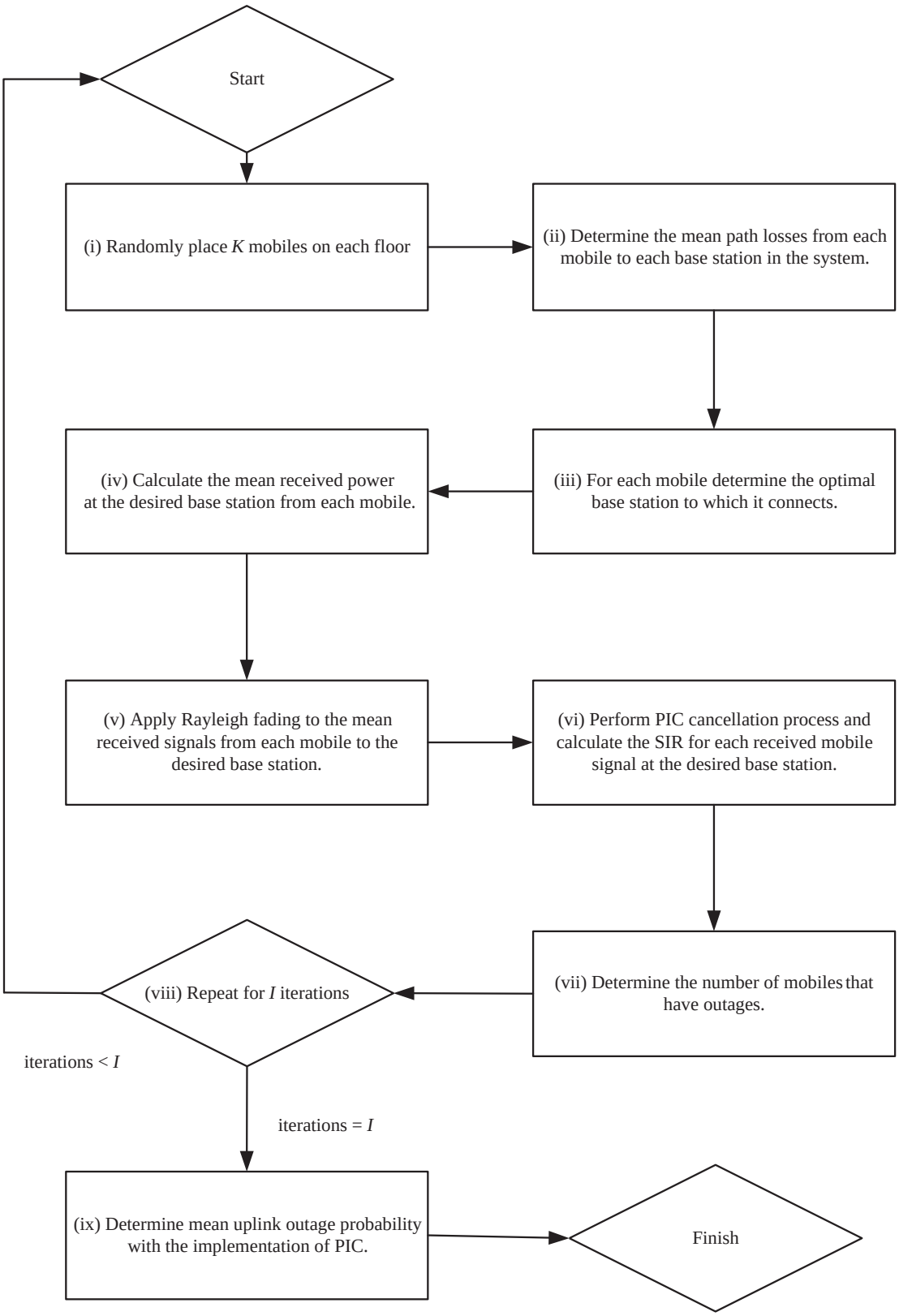

Figure 8.1: Uplink system performance estimation algorithm assuming the implementation of PIC receivers at base stations.

are modelled using zero-mean Gaussian random variables with a predefined standard deviation σ_ε (as discussed in Section 6.4).

In Step (vii), the number of mobiles that have outages on the uplink is calculated by determining whether the instantaneous SIR for each mobile is below a certain threshold at which the BER is 0.02.

In Step (viii), the above process (from Steps (i) to (vii)) is repeated for a sufficient number of iterations (I) such that the resulting mean uplink outage probability is accurate to four decimal places.

Finally in Step (ix), the mean uplink outage probability is calculated by dividing the total number of mobiles having outages by the total number of connections made to the desired base station in all iterations.

8.3 PIC performance estimation results

This section presents a comprehensive set of performance results for the deployment configurations in the three propagation campaigns assuming PIC receivers at the base stations. It is assumed throughout this section that *conventional* uplink power control is implemented in the system (as was done for the DS-CDMA systems operating without multiuser detection in Chapter 5). With conventional uplink power control, the mobiles connected to a particular base station adjust their signal transmit powers so that they are received at the base station with the same *mean* received power. However, variations in the actual, instantaneous received mobile signal strengths occur due to short-term fading.

8.3.1 Single floor indoor system coexisting with outdoor system (PM A)

A three-dimensional diagram showing the transmitter locations in PM A is in Figure 8.2. The following sections present the uplink performance estimates for the *indoor-only* scenario (Section 8.3.1.1) and the *interfering indoor/outdoor* scenario (Section 8.3.1.2) assuming PIC receivers at the base stations.

8.3.1.1 Indoor-only scenario

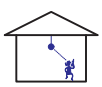

Simple configurations deploying two base stations on a single floor in the Tower Block of the School of Engineering are shown in Table 8.1. Configurations Ad.x have the base stations **ad**jacently located within five metres of each other. In Configurations Di.x, the base stations are **di**agonally opposite each other, while in Configurations Op.x the base

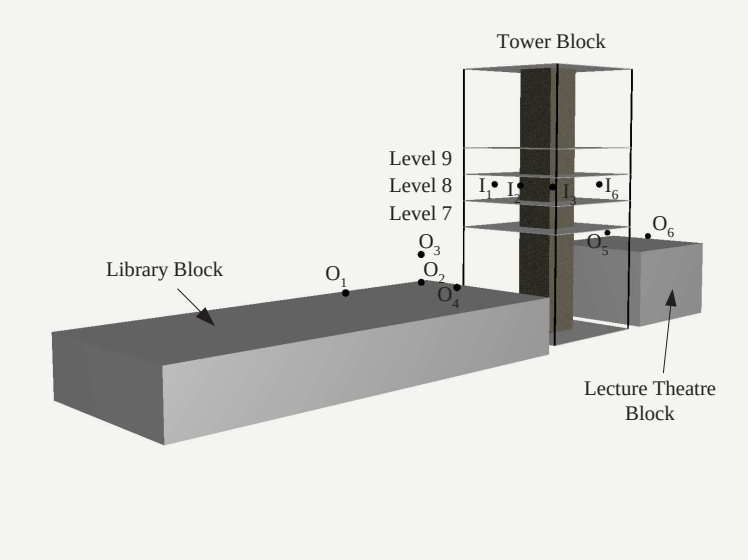

Figure 8.2: Transmitter locations in PM A. N.B. Transmitters I_4 and I_5 are obscured from view by the central steel-reinforced concrete core in the Tower Block.

stations are located at **op**posite sides of the building. Finally Configurations Si.x have the base stations on the same **si**de of the building but with a longer separation distance than those in Configurations Ad.x. For simplicity, the central steel-reinforced concrete core is not shown in the diagrams in Table 8.1, but is a key factor that influences system performance.

To demonstrate the influence of the number of PIC receiver stages on uplink system performance, Figure 8.3 is a graph of the mean uplink outage probabilities at various stages of the PIC receiver assuming Configuration Ad.1. For simplicity, it is assumed that the standard deviation of the fractional residual interference cancellation error for each mobile at each stage of the PIC receiver is $\sigma_\varepsilon = 0.22$. Also shown on the graph are the uplink outage probabilities if perfect PIC is performed (i.e. $\sigma_\varepsilon = 0$), which represents the best attainable uplink performance with PIC (as *intra-cell* interference is completely cancelled).

In Figure 8.3, the uplink outage probabilities at Stage 1 are the same as those obtained at the output of the conventional receiver (i.e. no interference cancellation). It is evident that the uplink performance improves with a greater number of stages of the PIC receiver, but the incremental performance gain at each stage reduces. For example, assuming 20 mobiles on the floor in Configuration Op.3, the uplink outage probabilities decrease by a magnitude of five times from Stage 1 to Stage 2, whereas a decrease by a magnitude of 2.5 times is observed from Stage 2 to Stage 3. By Stage 3 of the PIC receiver, the majority of the maximum attainable uplink performance gain is achieved.

Assuming that perfect PIC is performed (i.e. $\sigma_\varepsilon = 0$), Figure 8.4 is a graph showing the mean uplink outage probabilities for the various deployment configurations in

Configuration	Ad.1	Ad.2	Ad.3	Di.1	Di.2
Layout					
Configuration	**Op.1**	**Op.2**	**Op.3**	**Si.1**	**Si.2**
Layout					

Table 8.1: Indoor base station deployment configurations in PM A.

Table 8.1. The graph also shows the mean of the mean uplink outage probabilities for all the deployment configurations assuming *conventional receivers* (i.e. without PIC) at the base stations. The findings are similar to those observed with the implementation of SIC in Chapter 7. The disparities in uplink outage probabilities between the various configurations operating with PIC are much greater than those observed if conventional receivers are used at the base station (presented in Chapter 5). The uplink performance gain with perfect PIC is strongly dependent on the deployment configuration. The lowest performance gain is achieved in the adjacent configurations Ad.x, while the highest performance gains are achieved in Configurations Op.2 and Op.3.

8.3.1.2 Interfering indoor/outdoor scenario

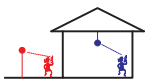

In this section, it is assumed that outdoor interference is presented to an indoor system operating with a single base station that has an SIC receiver. The deployment configurations considered are shown in Table 8.2. In Configurations SSI.1 to SSI.3 the indoor base station is on the **s**ame **s**ide of the building from where the outdoor **i**nterference emanates. In Configurations OSI.1 to OSI.3, the indoor base station is on the **o**pposite **s**ide of the building from where the outdoor **i**nterference emanates.

A graph of the mean uplink outage probabilities for the indoor mobiles in the configurations in Table 8.2 is shown in Figure 8.5. This figure also shows the mean of the mean uplink outage probabilities for the various configurations assuming conventional receivers at the base station for two cases: (a) the indoor base station on the same side of the building from where the outdoor interference emanates and (b) the indoor base station on the opposite side of the building from where the outdoor interference emanates. It is

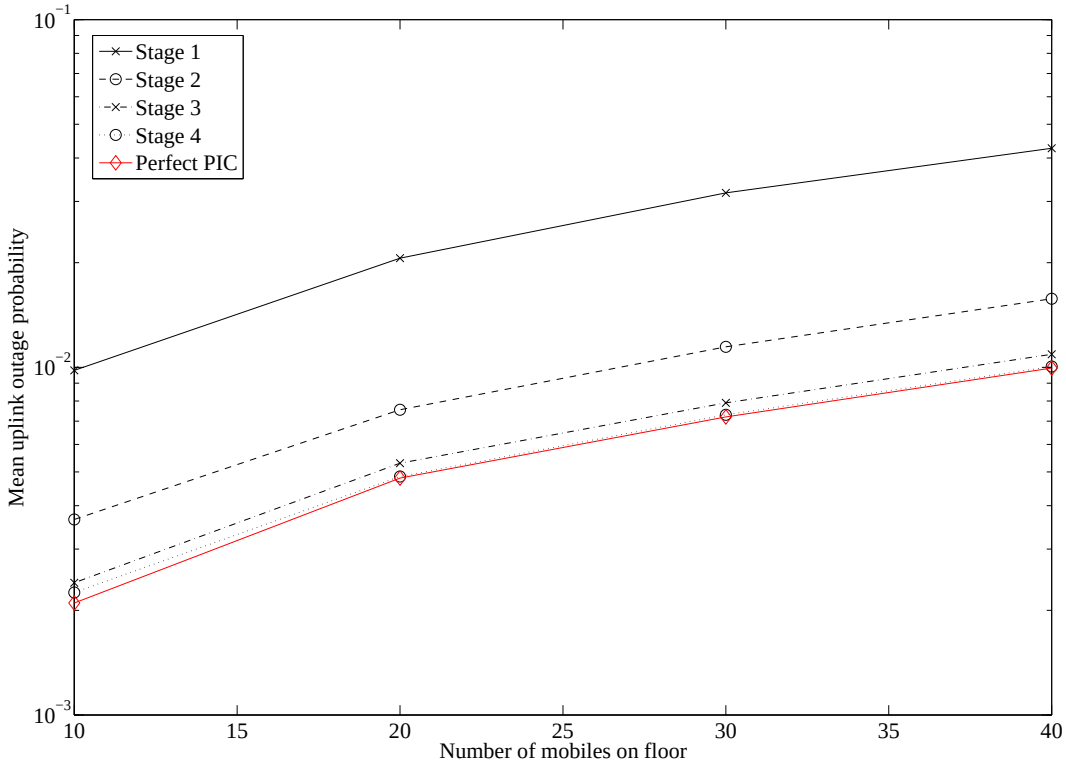

Figure 8.3: Graph of the mean uplink outage probability versus the number of mobiles at various stages of the PIC receiver assuming Configuration Ad.1 in PM A (Table 8.1). N.B. It is assumed that $\sigma_\varepsilon = 0.22$.

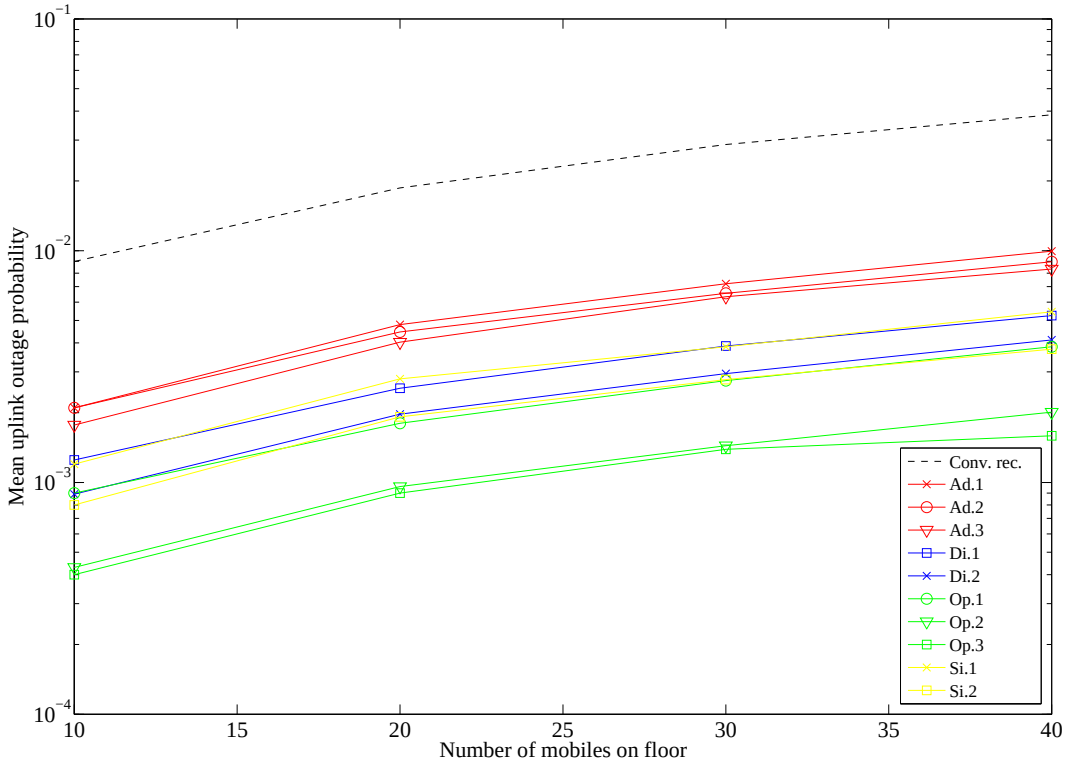

Figure 8.4: Graph of the mean uplink outage probability versus the number of mobiles for the indoor configurations in PM A (Table 8.1). N.B. It is assumed that PIC receivers with perfect cancellation are implemented at the base stations (i.e. $\sigma_\varepsilon = 0$).

Configuration	SSI.1	SSI.2	SSI.3
Layout			
Configuration	**OSI.1**	**OSI.2**	**OSI.3**
Layout			

Table 8.2: Interfering indoor/outdoor deployment configurations for which the uplink system performance is investigated in PM A. N.B. Arrows indicate the origin of uplink interference from outdoors.

assumed that there are 20 mobiles served by each base station and the PIC receiver at the indoor base station is able to completely cancel intra-cell interference (i.e. $\sigma_\varepsilon = 0$).

The trends observed for the configurations assuming PIC receivers in Figure 8.5 are identical to the those observed assuming SIC receivers in Chapter 7. Firstly, the uplink outage probabilities are approximately an order-of-magnitude lower if the indoor base station is located on the opposite side of the building from where the outdoor interference emanates than if it is located on the same side of the building from where the outdoor interference emanates. With increased outdoor interference, the uplink performance gains attainable with PIC are reduced to the extent that the uplink performance with PIC converges to that obtained with the conventional receiver. This occurs because the outdoor interference is uncancellable and therefore has a more dominant influence on system performance if it is stronger.

8.3.2 Multi-floor indoor system coexisting with outdoor system (PM B)

This section investigates the deployment and performance of base stations in a three-dimensional configuration inside a building coexisting with an outdoor system. Propagation measurement results from PM B are used and it is assumed that PIC receivers are implemented at the base stations. A three-dimensional drawing of the base station locations in PM B is shown in Figure 8.6.

This section begins by presenting uplink system performance estimation results (with SIC) for three-dimensional configurations of indoor base stations *without* the influence of outdoor interference (*indoor-only* scenario) in Section 8.3.2.1. Following this, the in-

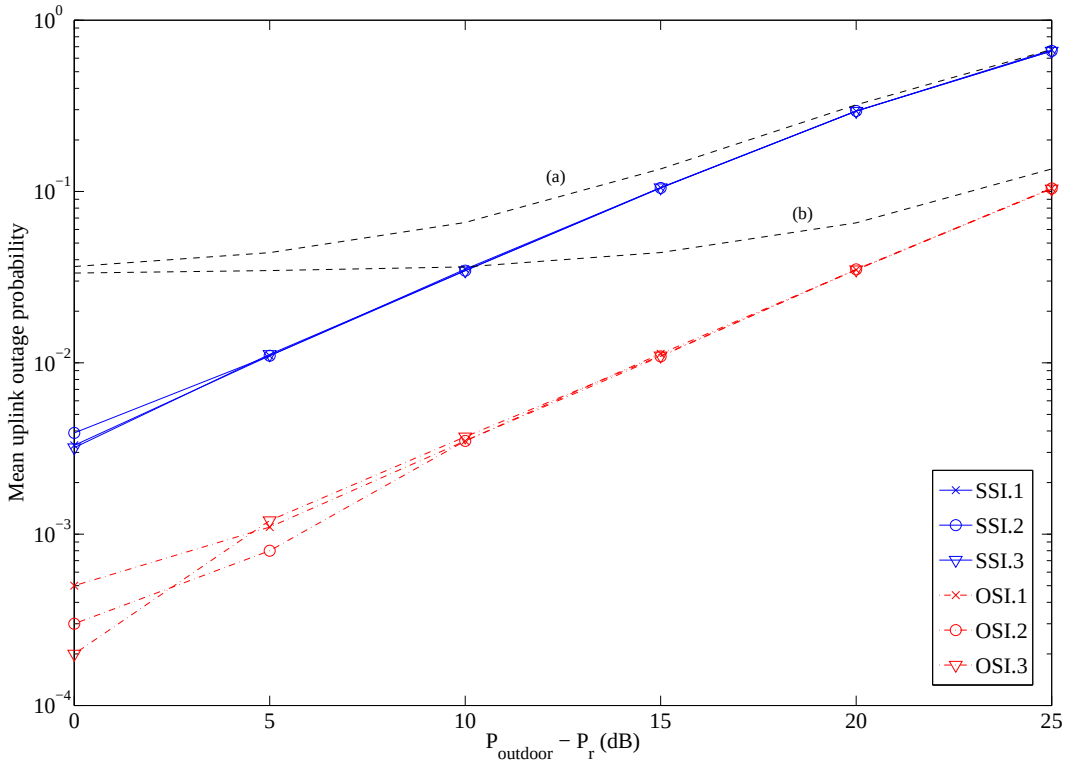

Figure 8.5: Mean uplink outage probability for mobiles on Level 8 for various interfering indoor/outdoor configurations (shown in Table 8.2) assuming PIC receivers, 20 mobiles per base station and the outdoor interference level shown. The parameter $P_{outdoor}$ is the mean power of each of the outdoor interfering mobile signals measured at one side of the building while P_r is the power controlled mean received power of the indoor mobiles (at the indoor base station). N.B. The line labelled (a) represents the mean of the mean uplink outage probabilities assuming the use of conventional receivers and the indoor base station on the *same* side of the building from where the outdoor interference emanates. The line labelled (b) represents the mean of the mean uplink outage probabilities assuming the use of conventional receivers and the indoor base station on the *opposite* side of the building from where the outdoor interference emanates.

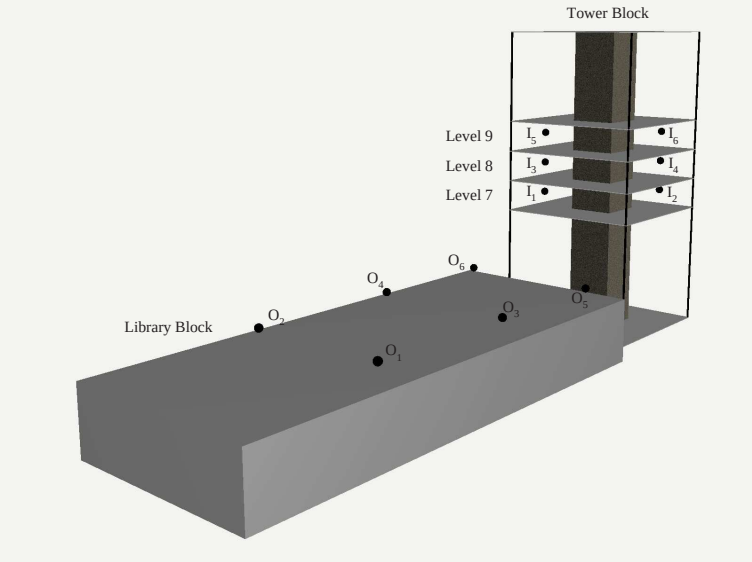

Figure 8.6: Transmitter locations in PM B.

fluence of outdoor interference on indoor system performance is investigated (*interfering indoor/outdoor* scenario) in Section 8.3.2.2.

8.3.2.1 Indoor-only scenario

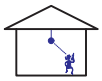

Possible base station deployment configurations deploying base stations and mobiles on three levels of the Tower Block are shown in Table 8.3.

In Configurations *Aligned 1* and *Aligned 2*, all the base stations are vertically aligned with each other while in Configurations *Offset 1* and *Offset 2* the base stations are vertically offset from each other. In Configurations *Aligned/Offset 1* to *Aligned/Offset 4*, one base station is aligned with the base station on Level 8 while the other is vertically offset from the base station on Level 8.

Figure 8.7 is a graph showing the mean uplink outage probabilities at various stages of the PIC receiver for mobiles on Level 8 of the Tower Block in Configuration *Aligned 1*. It is assumed that the standard deviation of the fractional residual interference cancellation error is $\sigma_\varepsilon = 0.22$. Also shown on this graph are the uplink outage probabilities assuming perfect PIC (i.e. $\sigma_\varepsilon = 0$), which represents the best attainable uplink system performance with PIC (as all *intra-cell* interference is cancelled). It is evident from Figure 8.7 that similar to the observations in PM A, the maximum performance gain is achieved from Stage 1 to Stage 2 of the PIC receiver. At each subsequent stage of the PIC receiver, the incremental performance gain is less than the previous stage of the PIC receiver.

Figure 8.8 compares the uplink outage probabilities for the various deployment configurations in Table 8.3 assuming perfect PIC receivers at the base stations (i.e. $\sigma_\varepsilon =$

Config.	Aligned 1	Aligned 2	Offset 1	Offset 2
Base Station Layout	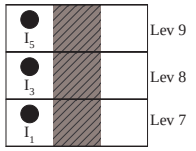	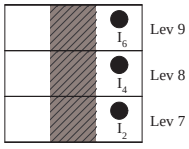	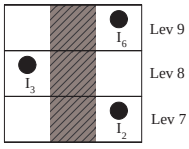	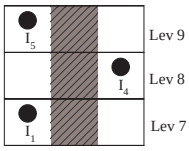
Config.	Aligned/Offset 1	Aligned/Offset 2	Aligned/Offset 3	Aligned/Offset 4
Base Station Layout	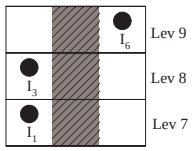	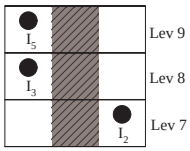	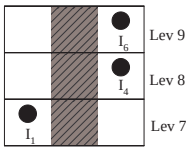	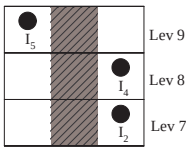

Table 8.3: Front view of indoor base station deployment configurations in PM B (Indoor-only scenario).

0). Clearly the aligned deployment configurations yield the optimal uplink performance with PIC receivers, while the aligned/offset configurations and offset deployment configurations yield similar uplink performances.

8.3.2.2 Interfering indoor/outdoor scenario

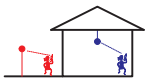

In this scenario, the system performance on the uplink is estimated for the various configurations shown in Table 8.4 assuming that outdoor interference emanates from one side of the Tower Block. Figure 8.9 shows the mean uplink outage probabilities for the configurations in Table 8.4 assuming PIC receivers at the base stations. Also shown on this figure is the mean of the mean uplink outage probabilities for the various configurations assuming conventional receivers at the base station (detailed in Chapter 5) for: (a) the indoor base station on Level 8 on the same side of the building from where the outdoor interference emanates and (b) the indoor base station on Level 8 on the opposite side of the building from where the outdoor interference emanates. It is assumed that there are 20 mobiles outdoors and on each floor of the building indoors. Additionally, it is assumed that the PIC receivers at the indoor base stations cancel intra-cell interference perfectly (i.e. $\sigma_\varepsilon = 0$).

The uplink outage probabilities attained assuming PIC receivers in Figure 8.9 are similar to those attained assuming SIC receivers in Chapter 7. Clearly, for lower levels of

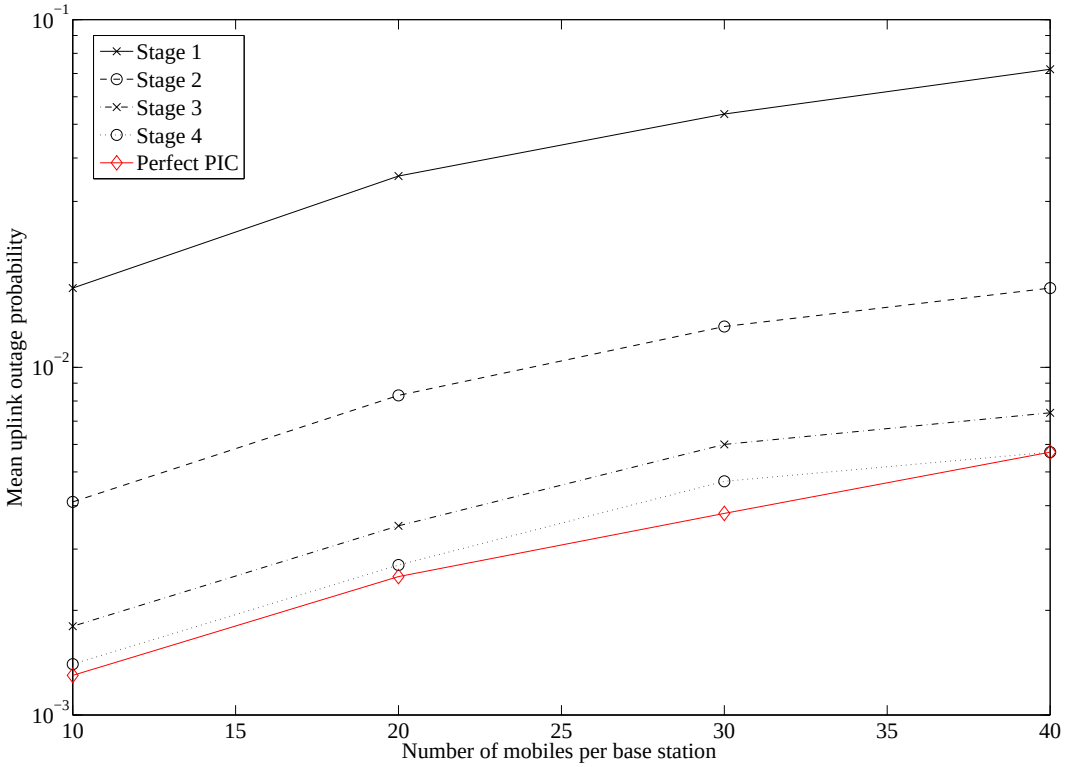

Figure 8.7: Graph of the mean uplink outage probability versus the number of mobiles at various stages of the PIC receiver assuming indoor Configuration *Aligned 1* in PM B (Table 8.3). N.B. It is assumed that $\sigma_\varepsilon = 0.22$.

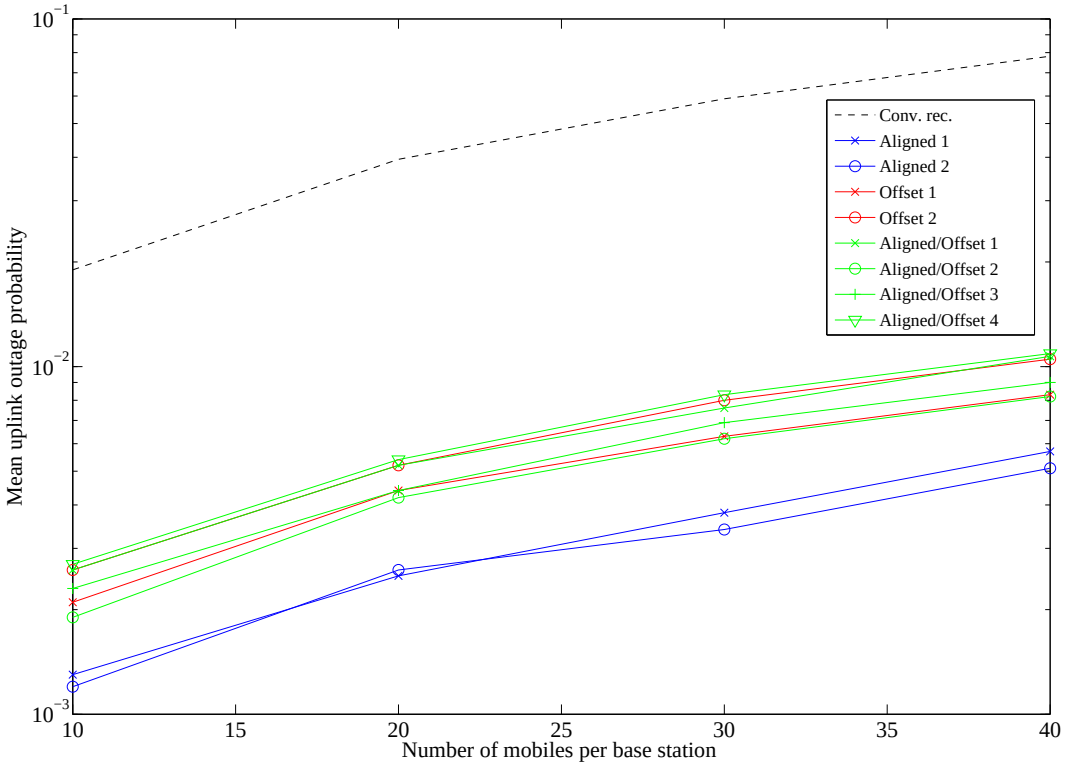

Figure 8.8: Graph of the mean uplink outage probability versus the number of mobiles for the indoor configurations in PM A (Table 8.3). N.B. It is assumed that PIC receivers with perfect cancellation are implemented at the base stations (i.e. $\sigma_\varepsilon = 0$).

Config.	Aligned 1 + OutdoorInt	Aligned 2 + OutdoorInt	Offset 1 + OutdoorInt	Offset 2 + OutdoorInt
Base Station Layout	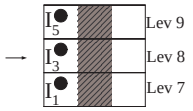	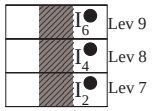	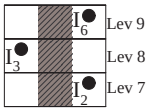	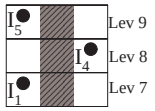
Config.	Aligned/Offset 1 + OutdoorInt	Aligned/Offset 2 + OutdoorInt	Aligned/Offset 3 + OutdoorInt	Aligned/Offset 4 + OutdoorInt
Base Station Layout	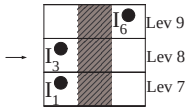	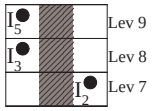	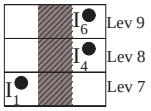	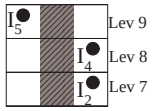

Table 8.4: Front view of interfering indoor/outdoor base station configurations considered in the investigation of uplink system performance in PM B. N.B. Arrows indicate the origin of uplink interference from outdoors.

outdoor interference, there are greater differences in the uplink performances of the various configurations. With increased outdoor interference, the uplink performance converges to that obtained assuming conventional receivers at the base stations. For higher levels of interference, better uplink system performance is achieved if the indoor base station on the desired floor is further away from the side of the building from where the outdoor interference emanates.

8.3.3 Coexisting single floor indoor systems in adjacent buildings (PM C)

This section investigates the deployment and performance of two interfering indoor DS-CDMA systems operating with PIC receivers in two buildings located adjacent to each other (using propagation measurement results from PM C). Figure 8.10 is a plan of the locations of the transmitters deployed in PM C.

This section presents the uplink system performance results assuming PIC receivers at the base stations for the *indoor-only* scenario (Section 8.3.3.1) followed by the *adjacent interfering* scenario (Section 8.3.3.2).

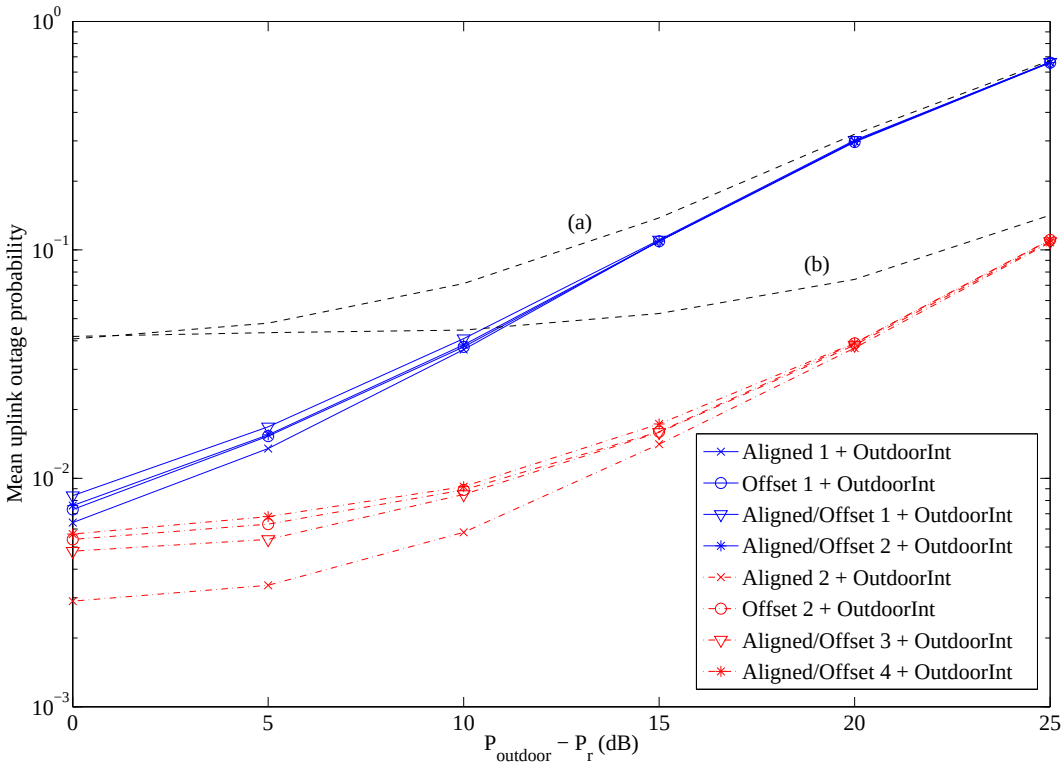

Figure 8.9: Mean uplink outage probability for mobiles on Level 8 for various interfering indoor/outdoor configurations (shown in Table 8.4) assuming PIC receivers, 20 mobiles per base station and the outdoor interference level shown. The parameter $P_{outdoor}$ is the mean power of each of the outdoor interfering mobile signals measured at one side of the building while P_r is the power controlled mean received power of the indoor mobiles (at the indoor base station). N.B. The line labelled (a) represents the mean of the mean uplink outage probabilities assuming the use of conventional receivers and the indoor base station on Level 8 on the *same* side of the building from where the outdoor interference emanates. The line labelled (b) represents the mean of the mean uplink outage probabilities assuming the use of conventional receivers and the indoor base station on Level 8 on the *opposite* side of the building from where the outdoor interference emanates.

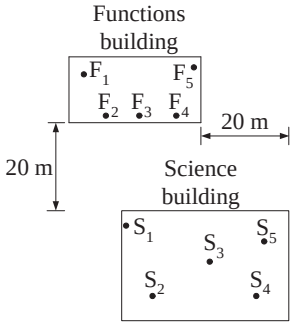

Figure 8.10: Relative locations of transmitters deployed in the Science and Functions buildings in PM C.

Configuration	S_1S_4	S_2S_5	S_2S_3
Layout	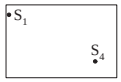	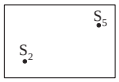	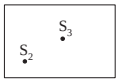
Configuration	S_3S_4	S_1S_2	S_4S_5
Layout	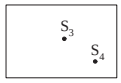	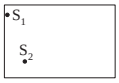	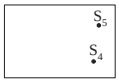

Table 8.5: Simple indoor configurations deploying two base stations in the Science building (PM C).

8.3.3.1 Indoor-only scenario

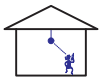

In this scenario, the deployment and performance of simple configurations deploying two base stations are considered for each of the Science and Functions buildings in PM C, assuming that there is no external interference presented to the system.

Science building

Table 8.5 shows a selection of base station configurations for a system deployed on a single floor of the Science building. Configurations S_1S_4 and S_2S_5 have base stations that are diagonally opposite to each other. Configurations S_2S_3 and S_3S_4 have a single base station on the centre of the floor and a base station at one corner of the floor. In Configurations S_1S_2 and S_4S_5, the base stations are located near the left and right hand side of the building respectively. The mobiles are randomly located at positions at which measurements were made on the same floor as the base stations.

A graph of the mean uplink outage probabilities for Configuration S_1S_4 (shown in Table 8.5) at various stages of the PIC receiver is shown in Figure 8.11. It is assumed that the standard deviation of the fractional residual interference cancellation error at each stage of the PIC receiver is $\sigma_\varepsilon = 0.22$. The observations made are very similar to those made for PM A and PM B in Sections 8.3.1.1 and 8.3.2.1. The majority of the uplink performance gains are achieved at the first two cancellation stages (i.e. Stages 2 and 3) of the PIC receiver. A graph of the mean uplink outage probabilities for the various configurations in Table 8.5 is shown in Figure 8.12. This graph assumes perfect PIC receivers (i.e. $\sigma_\varepsilon = 0$). Although there are differences in the mean uplink outage

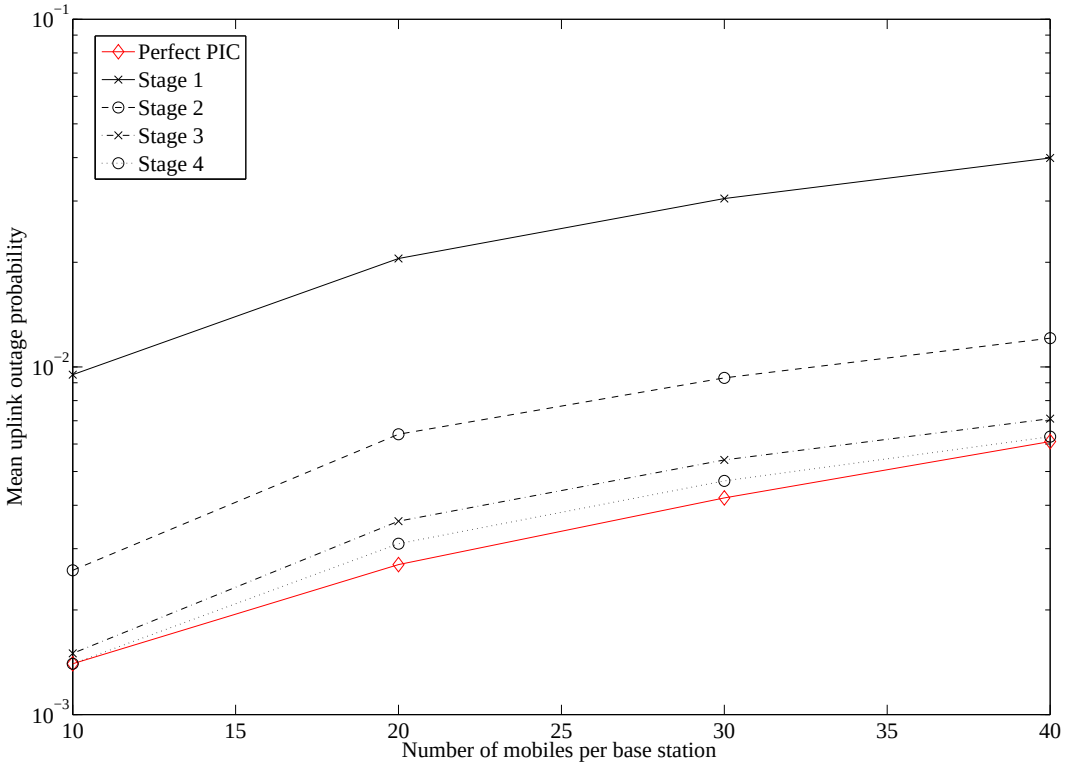

Figure 8.11: Graph of the mean uplink outage probability versus the number of mobiles at various stages of the PIC receiver assuming Configuration S_1S_4 operating in the Science building in PM C. N.B. it is assumed that $\sigma_\varepsilon = 0.22$.

probabilities yielded by the various configurations, there is no particular relationship between the deployment strategy used and the mean uplink outage probability attained using PIC receivers.

Functions building

A sample of configurations deploying two base stations in the Functions Building is shown in Table 8.6. These configurations are similar to those investigated for the Science building. Configurations F_1F_4 and F_2F_5 have base stations that are diagonally opposite to each other. Configurations F_2F_3 and F_3F_4 have base stations located at the lower side of the building. In Configurations F_1F_2 and F_4F_5, the base stations are located on the left and right hand side of the building respectively. The mobiles are randomly located at positions at which measurements were made on the same floor as the base stations.

Figure 8.13 shows the mean uplink outage probabilities for Configuration F_1F_4 at various stages of the PIC receiver, assuming that the standard deviation of the fractional residual interference cancellation error at each stage is $\sigma_\varepsilon = 0.22$. Also shown on this graph are the uplink outage probabilities assuming perfect PIC receivers (i.e. $\sigma_\varepsilon = 0$). Clearly the majority of the uplink performance gain is attained at Stage 2 and Stage 3 of

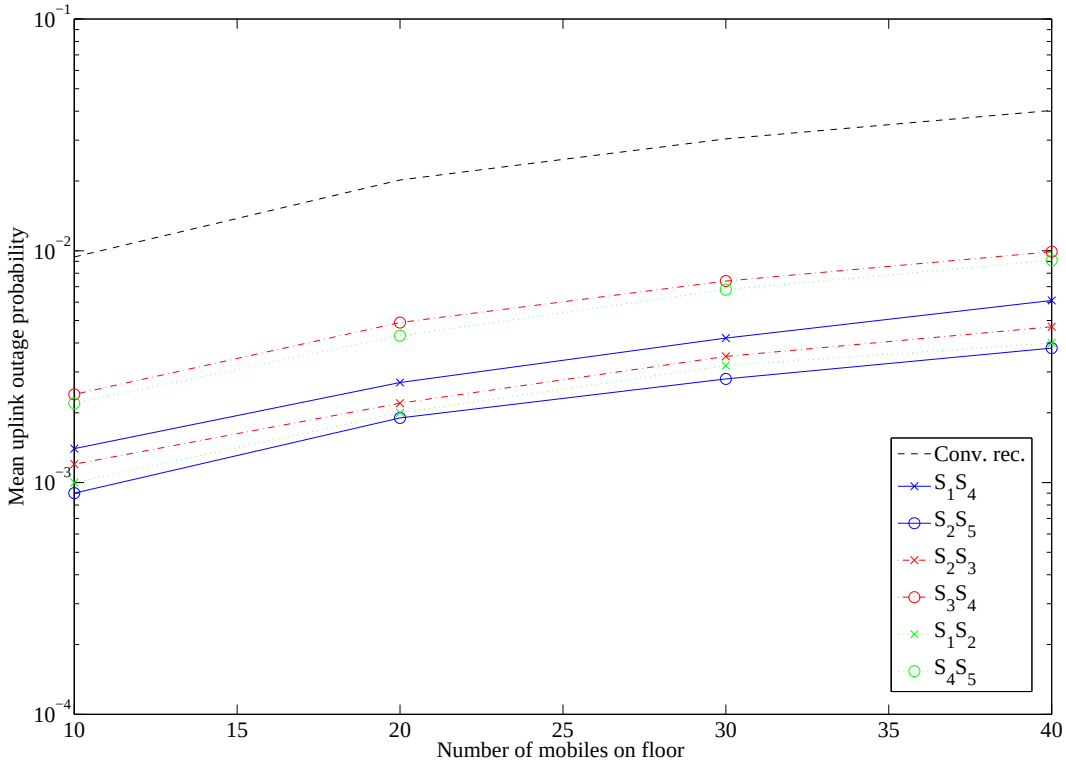

Figure 8.12: Graph of the mean uplink outage probability versus the number of mobiles for the configurations in the Science building in PM C (Table 8.5). N.B. It is assumed that PIC receivers with perfect cancellation are implemented at the base stations (i.e. $\sigma_\varepsilon = 0$).

Configuration	F_1F_4	F_2F_5	F_2F_3
Layout	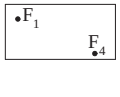	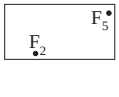	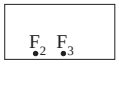
Configuration	F_3F_4	F_1F_2	F_4F_5
Layout	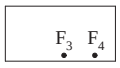	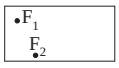	

Table 8.6: Simple indoor configurations deploying two base stations in the Functions building (PM C).

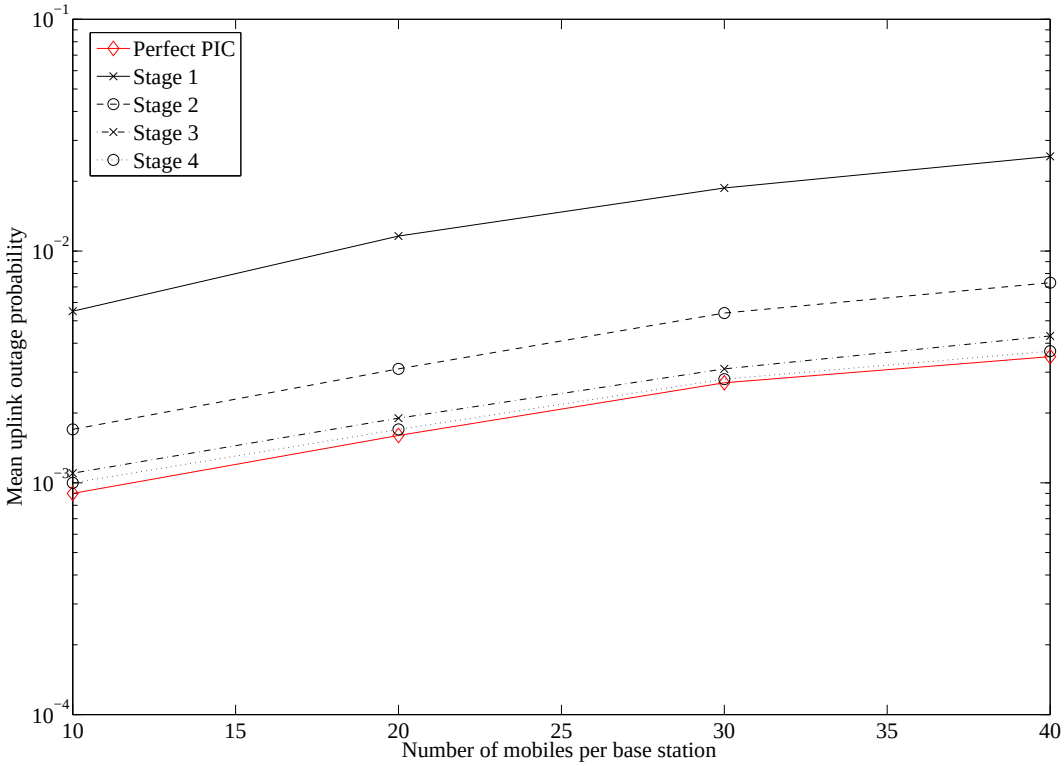

Figure 8.13: Graph of the mean uplink outage probability versus the number of mobiles at various stages of the PIC receiver assuming Configuration F_1F_4 operating in the Functions building in PM C. N.B. It is assumed that $\sigma_\varepsilon = 0.22$.

the PIC receiver. Very little additional performance gain is achieved beyond Stage 3 of the PIC receiver.

Assuming perfect PIC receivers (i.e. $\sigma_\varepsilon = 0$), the uplink outage probabilities for the various configurations in Table 8.6 are shown in Figure 8.14. Also shown on this graph is the mean of the mean uplink outage probabilities for the configurations assuming conventional receivers at the base stations. Clearly there are variations in the performance gains attained for the various configurations, but there is no particular relationship observed between the deployment configuration and the uplink system performance attained.

8.3.3.2 Interfering adjacent scenario

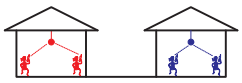

In this scenario, it is assumed that an indoor DS-CDMA system operating in the Functions building mutually interferes with another indoor DS-CDMA system operating in the Science building. Both systems have PIC receivers operating at the base stations. In such a scenario it is desirable for wireless operators to 'balance' the performance of the two indoor DS-CDMA systems so that neither system has a significantly worse performance than the other.

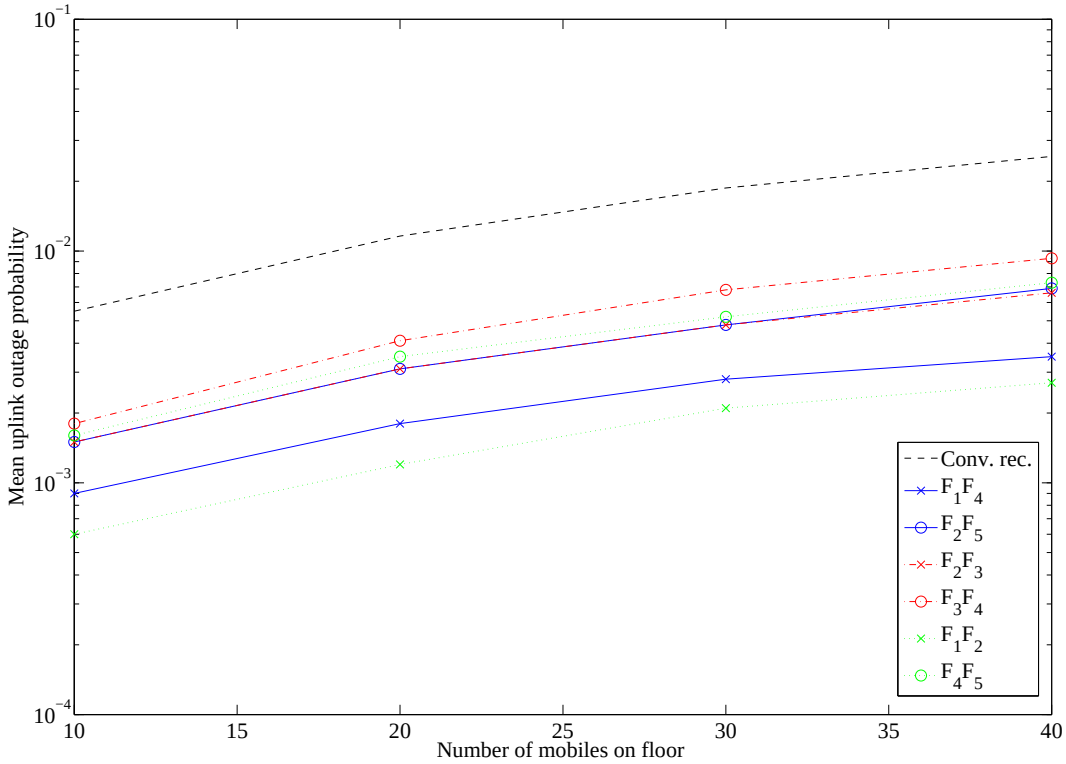

Figure 8.14: Graph of the mean uplink outage probability versus the number of mobiles for the configurations in the Functions building in PM C (Table 8.6). N.B. It is assumed that PIC receivers with perfect cancellation are implemented at the base stations (i.e. $\sigma_\varepsilon = 0$).

Six simple configurations that deploy one base station in the Functions building and one base station in the Science building are shown in Table 8.7. This section begins with an in-depth discussion of the uplink system performance estimates for mobiles in the Science building assuming PIC receivers at the base stations. The issue of performance 'balancing' between the systems operating in the Science building and Functions building is then investigated by comparing uplink outage probability estimates for both systems at a fixed interference level. Throughout this section it is assumed that there are 20 mobiles randomly located in each of the Science and Functions building. Additionally, it is assumed that perfect interference cancellation is achieved and for this reason intra-cell interference is completely cancelled (i.e. $\sigma_\varepsilon = 0$).

Uplink system performance in Science building assuming PIC receivers

Assuming various levels of uplink interference from mobiles in the Functions building and perfect PIC receivers at the base stations, a graph of the mean uplink outage probabilities for mobiles in the Science building is shown in Figure 8.15. Similar to the results for SIC (in Chapter 7), it is evident that significant differences (as much as three orders of magnitude) in mean uplink outage probabilities are observed for the various configurations. It should be noted that in Configuration F_1S_4 no outages are observed if P_r(Functions

Configuration	F_1S_1	F_3S_1	F_5S_5
Layout	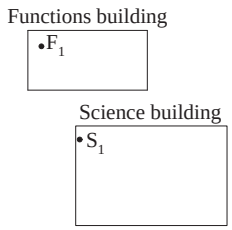	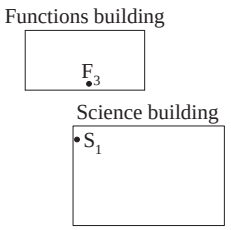	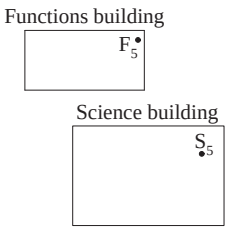
Configuration	F_1S_4	F_3S_2	F_3S_3
Layout	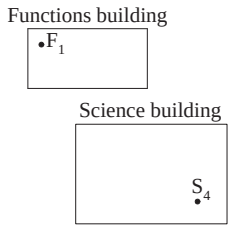	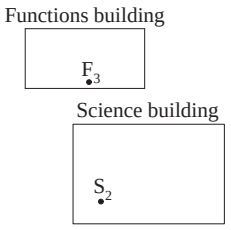	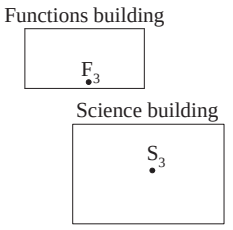

Table 8.7: Base station deployment configurations investigating interfering adjacent systems in PM C.

building) – P_r(Science building) < 20 dB, while in Configuration F_3S_2, no outages are observed if P_r(Functions building) – P_r(Science building) < 30 dB. The optimal deployment configurations are F_3S_2 and F_3S_3, which is the same as for the case where conventional receivers or SIC receivers are used (investigated in Chapters 5 and 7).

Uplink system performance balancing between Functions and Science buildings

A 'snapshot' of the mean uplink outage probabilities for the mobiles in both the Functions and Science buildings at a given level of interference is shown in Table 8.8 assuming 20 mobiles in each building. In obtaining the mean uplink outage probabilities for the mobiles in the Science building it is assumed that the power controlled mean received power (at the base station) for mobiles in the Functions building is 30 dB greater than that for mobiles in the Science building. Similarly, in obtaining the mean uplink outage probabilities for mobiles in the Functions building, it is assumed that the power controlled mean received power for mobiles in the Science building is 30 dB greater than that for mobiles in the Functions building.

Table 8.8 shows the mean uplink outage probabilities for mobiles in the buildings for both conventional receivers and PIC receivers. The trends observed assuming PIC

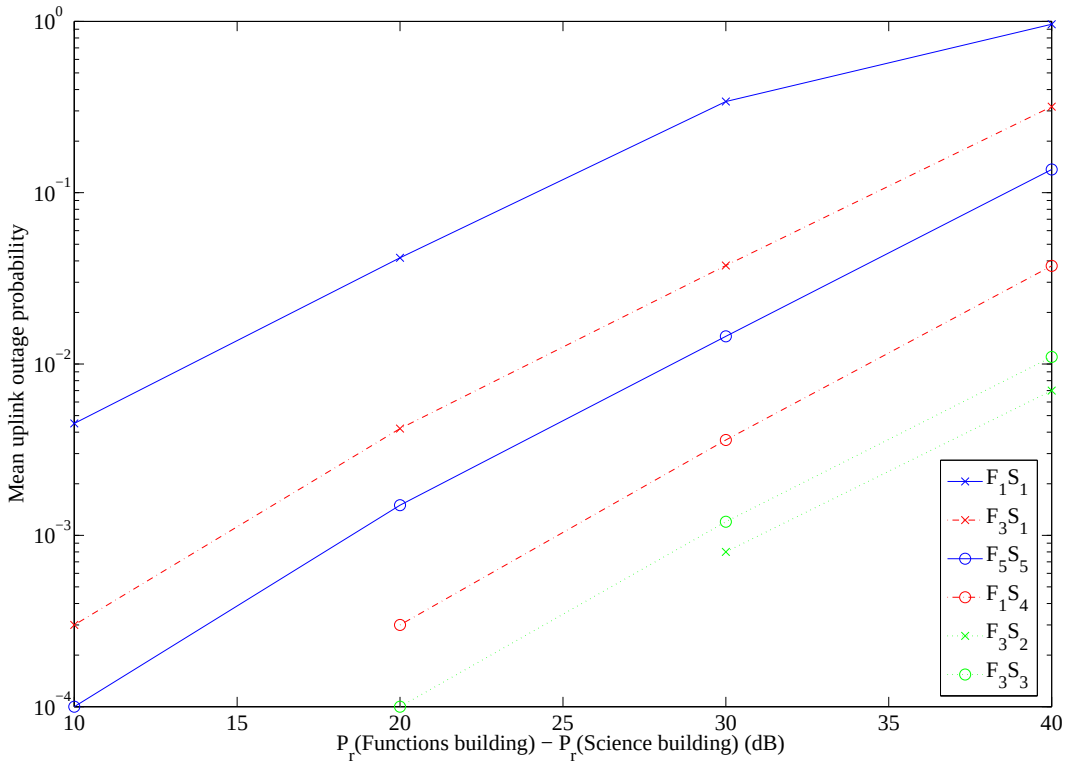

Figure 8.15: Mean uplink outage probabilities for mobiles in the Science building for the adjacent interfering base station configurations shown in Table 8.7 (assuming the implementation of PIC with perfect cancellation). N.B. P_r(Functions building) is the power controlled mean received power for mobiles in the Functions building while P_r(Science building) is the power controlled mean received power for mobiles in the Science building.

Config.	F_1S_1	F_3S_1	F_5S_5	F_1S_4	F_3S_2	F_3S_3
Layout	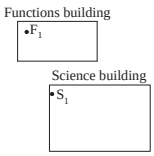	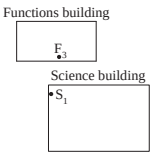	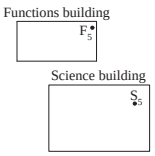	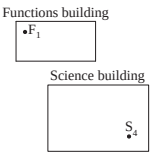	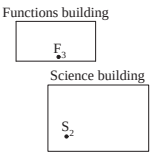	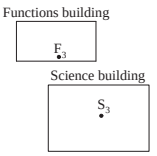
Functions building						
Uplink outage prob. (*Conv.*)	0.126	0.762	0.122	0.508	0.985	0.905
Uplink outage prob. (*PIC*)	0.095	0.751	0.089	0.492	0.985	0.902
Science building						
Uplink outage prob. (*Conv.*)	0.361	0.070	0.047	0.037	0.033	0.034
Uplink outage prob. (*PIC*)	0.341	0.038	0.014	0.004	0.001	0.001

Table 8.8: Comparison of mean uplink outage probabilities for interfering adjacent indoor DS-CDMA systems assuming conventional receivers and PIC receivers (perfect cancellation).

receivers at the base stations are similar to those for SIC receivers in Chapter 7. Although significant performance gains are generally achieved using PIC receivers in the Science building, little or no performance gains are achieved using PIC receivers in the Functions building. This is due to the higher transmit powers of mobiles in the Science building than those in the Functions building, caused by the greater floor area of the Science building. This, in turn, causes a higher level of interference from the Science building to the Functions building than vice versa.

8.4 A comparison between PIC and SIC

Section 8.3 investigated the uplink system performance for various configurations assuming PIC receivers at the base stations. In the investigation it was shown that the highest

uplink performance gain is attained after the first stage of cancellation in the PIC receiver and at subsequent stages incrementally less uplink performance gain is achieved. Additionally, assuming perfect interference cancellation, the differences in the uplink outage probabilities between the various deployment configurations assuming PIC receivers at the base stations were observed to be similar to those observed assuming SIC receivers (investigated in Chapter 7).

The purpose of this section is to compare the uplink outage probabilities achieved with PIC and SIC receivers using three-dimensional indoor deployment configurations from PM B as an example. Table 8.9 compares the uplink outage probabilities yielded by eight deployment configurations using either conventional receivers, PIC receivers or SIC receivers at the base stations. In obtaining these outage probabilities, it is assumed that perfect cancellation is achieved by both the PIC and SIC receivers (i.e. $\sigma_\varepsilon = 0$). The uplink outage probabilities for PIC and SIC receivers in Table 8.9 are identical to each other. This shows that cancelling *all* intra-cell interference signals (in PIC) does not provide any benefit over ranking the signals in decreasing order of signal strength and cancelling them sequentially (in SIC). Both PIC and SIC reduce the uplink outage probabilities by up to an order-of-magnitude (e.g. in Configuration *Aligned 1*).

Assuming that the standard deviation of the fractional residual interference cancellation error is $\sigma_\varepsilon = 0.2$ for both the SIC receiver and at each stage of the PIC receiver, Figure 8.16 is a graph showing the mean uplink outage probabilities for the SIC receiver and at each stage of the PIC receiver. At Stage 1 of the PIC receiver, the uplink outage probabilities attained are the same as those for the conventional receiver because no interference is cancelled. The uplink outage probabilities at Stage 2 of the PIC receiver are almost identical to those obtained for the SIC receiver. However, at subsequent stages of the PIC receiver, additional uplink performance gains are attained and the outage probabilities approach those attained with perfect PIC (in which all intra-cell interference is cancelled).

8.5 Summary

This chapter has investigated the implications of PIC on the deployment and performance of indoor/outdoor DS-CDMA systems using a simple PIC model outlined in Chapter 6. The mean uplink outage probabilities at various stages of a PIC receiver were estimated for the various deployment configurations by modifying the uplink system performance algorithm (developed in Chapter 5) to include PIC.

Assuming a fixed standard deviation of fractional residual interference cancellation error (σ_ε) for each mobile at each stage of the PIC receiver, it has been shown that the majority of the potential uplink performance gain is achieved at the first stage of cancel-

Config.	Aligned 1	Aligned 2	Offset 1	Offset 2
Base Station Layout	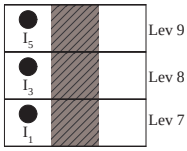	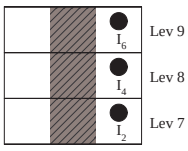	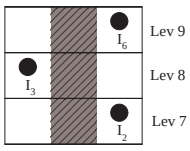	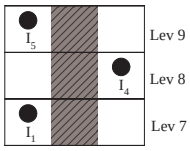
Uplink outage prob. (*Conv.*)	0.035	0.036	0.041	0.052
Uplink outage prob. (*PIC*)	0.003	0.003	0.004	0.005
Uplink outage prob. (*SIC*)	0.003	0.003	0.004	0.005

Config.	Aligned/Offset 1	Aligned/Offset 2	Aligned/Offset 3	Aligned/Offset 4
Base Station Layout	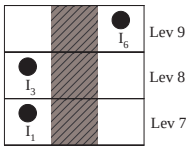	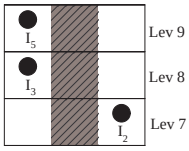	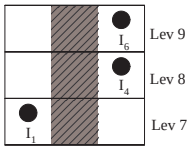	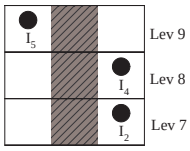
Uplink outage prob. (*Conv.*)	0.035	0.037	0.041	0.039
Uplink outage prob. (*PIC*)	0.005	0.004	0.004	0.005
Uplink outage prob. (*SIC*)	0.005	0.004	0.004	0.005

Table 8.9: A comparison of the uplink outage probabilities assuming various receivers (Conventional, PIC and SIC) for indoor base station deployment configurations in PM B (Indoor-only scenario). N.B. It is assumed that there are 20 mobiles per floor and that PIC and SIC achieve perfect cancellation.

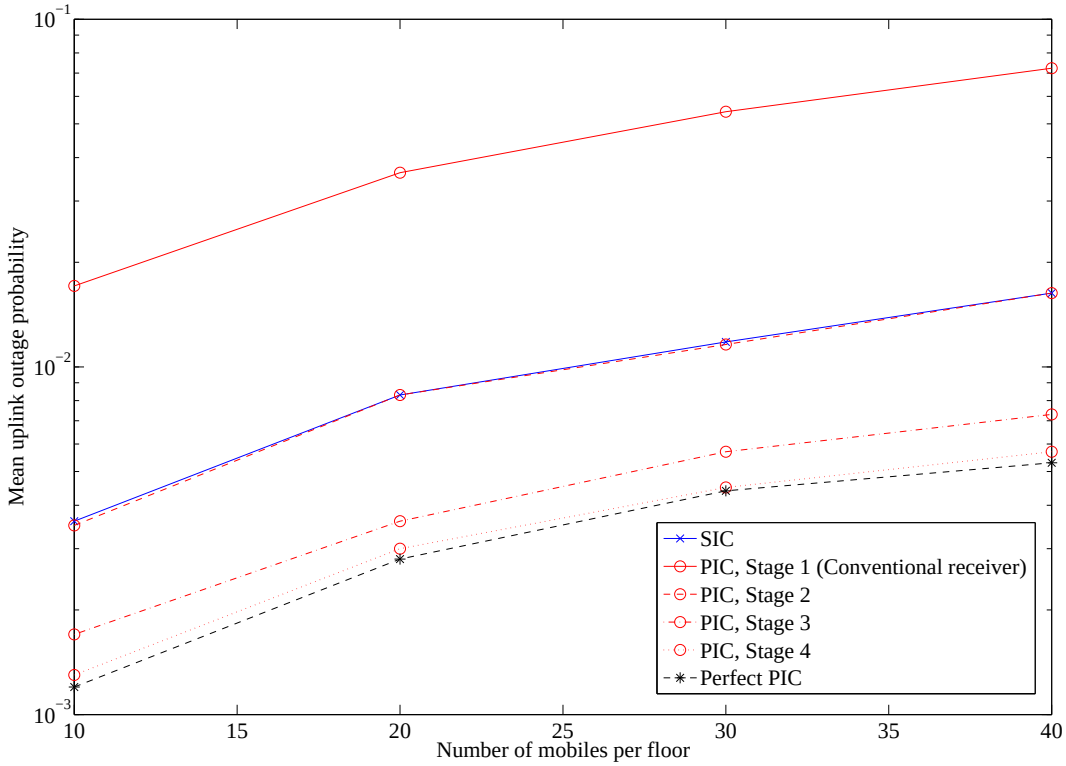

Figure 8.16: Mean uplink outage probability versus the number of mobiles assuming indoor Configuration *Aligned 1* in PM B (shown in Table 8.9) and either PIC or SIC receivers at the base stations. N.B. It is assumed that $\sigma_\varepsilon = 0.2$ for both the PIC and SIC receivers.

lation. The incremental uplink performance gain at each subsequent stage of cancellation reduces.

The differences in the mean uplink outage probabilities for the various configurations in each of the propagation measurement campaigns with PIC receivers were shown to be very similar to those observed with SIC receivers (investigated in Chapter 7). Assuming perfect cancellation (i.e. $\sigma_\varepsilon = 0$), the uplink outage probabilities improve by up to 30 times with PIC receivers in comparison to those attained with conventional receivers.

The similar uplink outage probabilities for PIC and SIC receivers shows that there is no additional benefit in cancelling *all* intra-cell interfering signals as compared to ranking mobiles in decreasing order of received signal strength and cancelling them sequentially.

Chapter 9

Implications for system planning and deployment

9.1 Introduction

This thesis has investigated the deployment and performance of indoor/outdoor DS-CDMA systems assuming both conventional receivers and multiuser detection receivers at the base stations. The two multiuser detection techniques chosen for investigation after a literature survey were successive interference cancellation (SIC) and parallel interference cancellation (PIC).

Using a scenario-based approach, it has been shown quantitatively in Chapters 5, 7 and 8 that several factors influence the downlink and uplink performance of indoor/outdoor DS-CDMA systems. These factors include the propagation environment, deployment strategy, type of receivers used at the base stations and the strength and sources of interference.

The purpose of this chapter is to present guidelines for planning and deploying indoor/outdoor DS-CDMA systems. These guidelines summarise the most important factors that wireless operators will need to account for when designing DS-CDMA systems in indoor/outdoor environments.

Section 9.2 presents the guidelines for conventional indoor/outdoor DS-CDMA systems while Section 9.3 discusses the influence of multiuser detection (SIC and PIC) on the deployment of indoor/outdoor DS-CDMA systems. Recommendations for future work are presented in Section 9.4 and a summary of this chapter is presented in Section 9.5.

9.2 Conventional indoor/outdoor DS-CDMA systems

The performance of a conventional indoor/outdoor DS-CDMA system (operating without multiuser detection) is strongly related to the relative locations of the base stations and mobiles. In particular, the identification of the sources and strength of interference gives significant insight into the likely downlink and uplink performance. Additionally, the correlation between desired and interfering signals has significant implications on system performance. This thesis has shown that by choosing base station locations carefully, the phenomenon of signal correlation can be exploited so as to yield optimal performance. A particular contribution of this thesis is that it quantifies the correlation between indoor and outdoor base stations and relates the correlation to the system performances attained for several deployment strategies.

Indoor-only scenario

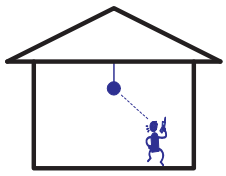

Assuming base stations and mobiles are located *indoor-only*, this thesis has investigated configurations of two base stations on a single floor as well as multi-floor configurations with one base station on each floor. In general, the disparities in performance for the various indoor deployment configurations on the downlink were observed to be much greater than those on the uplink.

For the configurations on a single floor, this thesis has shown that positioning two base stations close together yields significantly worse performance than positioning the base stations at opposite sides of the building. For multi-floor configurations, it was shown that the deployment of base stations in a *vertically aligned* configuration yields improved performance (on both the downlink and the uplink) than a *vertically offset* configuration. The downlink outage probability of the vertically aligned configuration is as much as 10 times (i.e. an order-of-magnitude) better than that of the vertically offset configuration. This confirms the findings reported in [25, 26].

Interfering indoor/outdoor scenario

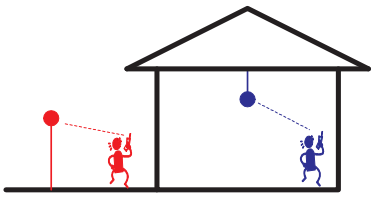

For the case where base stations and mobiles are located both indoors and outdoors, this thesis has investigated the influence of outdoor interference on indoor DS-CDMA system performance assuming both single floor configurations (deploying a single base station indoors) as well as multi-floor configurations (deploying a single base station on each floor indoors).

It has been shown in this thesis that for the deployment configurations evaluated, the downlink and uplink have 'conflicting' optimal deployment strategy requirements. For example, consider the deployment of a single indoor base station with interference emanating from one side of a building. For the downlink, the outage probabilities were observed to be lower if the indoor base station was on the *same* side of the building from where the outdoor interference emanates than if it was on the *opposite* side of the building from where the outdoor interference emanates. However, on the uplink, the outage probabilities were lower if the base station was on the *opposite* side of the building from where the outdoor interference emanates. Therefore, in such a case wireless operators will need to find an effective compromise between the downlink and uplink performance.

For multi-floor indoor deployment configurations, the strength of the interference emanating from outdoors has a strong influence on the optimal deployment strategy. On the downlink it has been observed that the *offset* deployment configurations are more robust to outdoor interference than the *aligned* deployment configurations. For the uplink, the performance of the offset deployment configuration is largely dependent on the location of the individual base stations, e.g. if the indoor base station is close to the side of the building from where the outdoor interference emanates, it is likely that the mobiles it serves will experience poorer performance than if the indoor base station is further away from the side of the building from where the outdoor interference emanates.

Adjacent interfering scenario

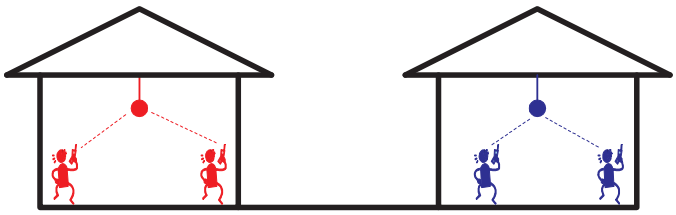

This thesis has investigated the influence of mutually interfering indoor DS-CDMA systems operating in adjacent buildings. Simple deployment configurations that use one base station in each system were assumed. It was shown that positioning the base stations in the buildings so that they are as far away from each other as possible balanced the performance achieved on the downlink and uplink in both systems. For most other configurations (e.g. if the base station in one building is at the side nearest to the other building), poor performance is yielded on either the downlink or uplink of each of the systems. The disparities in performance for the various configurations in each system is highly dependent on the levels of interference emanating from the other system.

9.3 Indoor/outdoor DS-CDMA systems with multiuser detection

This thesis has investigated the implications of two non-linear multiuser detection techniques, namely SIC and PIC, on the deployment and performance of indoor/outdoor DS-CDMA systems. It has been shown that both SIC and PIC can improve uplink outage probabilities by orders-of-magnitude in certain deployment configurations. The extent of the uplink system performance improvement is dependent on a number of different factors including the strength and sources of interference, the accuracy of SIC and PIC receivers in estimating and cancelling interference and the power control algorithm used (in the case of SIC). This section presents guidelines for deploying indoor/outdoor DS-CDMA systems operating with SIC and PIC receivers in Sections 9.3.1 and 9.3.2 respectively.

9.3.1 Successive interference cancellation (SIC)

Deployment and performance assuming conventional uplink power control

For the various deployment scenarios (*indoor-only*, *interfering indoor/outdoor* and *interfering adjacent*) investigated in this thesis, the implementation of SIC receivers has the potential to yield significant performance improvements on the uplink. Assuming that conventional uplink power control is implemented to equalise the mean received powers of the mobiles' signals, the optimal deployment configurations for the various scenarios with

perfect SIC receivers were generally observed to be the same as those with conventional receivers.

For the case of the *indoor-only* deployment scenarios, increased differences in the uplink outage probabilities for the various deployment configurations with SIC receivers were observed due to the dominance of inter-cell interference (that varies significantly among the different deployment configurations) after interference cancellation.

If outdoor interference is presented to a single floor indoor DS-CDMA system (*interfering indoor/outdoor* scenario), the maximum uplink performance gain with SIC is achieved if the indoor base station is positioned as far away from the source of outdoor interference as possible. However, the downlink system performance results (assuming conventional receivers at the base stations) show that optimal downlink performance is achieved if the indoor base station is close to the source of the outdoor interference. Hence, there are 'conflicting' deployment requirements for the downlink and the uplink and for this reason wireless operators will need to find an effective compromise between downlink and uplink performance.

For the case of two interfering indoor DS-CDMA systems located adjacent to each other, it has been shown that positioning base stations as far away from each other as possible yields the optimal performance with SIC receivers. However, the extent of the uplink performance enhancement due to SIC is strongly dependent on the relative levels of interference from one building to the other.

Implications of uplink power control

Using simple three-dimensional indoor configurations, the implications of uplink power control on system deployment were investigated for three algorithms, namely, (i) conventional power control (that equalises the mean received *powers* of the mobile signals); (ii) optimal power control (that equalises the mean received *SIRs* of the mobile signals); and (iii) no power control (that assumes mobiles have fixed signal transmit powers).

Very similar uplink outage probabilities were achieved in the indoor deployment configurations for conventional power control and optimal power control. The lack of uplink performance gain occurs because the system performance is dominated by short-term fading which causes instantaneous variations of as much as 30 to 40 dB in the power controlled mobile signals (regardless of the specific power control algorithm used). Any adjustments to the mean received power levels due to optimal power control are relatively small compared to the variations caused by short-term fading.

If no power control is implemented, the optimal deployment strategies are different from the conventional power control and optimal power control cases. In particular, an offset multi-floor configuration outperforms the aligned multi-floor configuration (whereas the reverse is true for conventional power control).

9.3.2 Parallel interference cancellation (PIC)

Assuming perfect interference cancellation and conventional uplink power control, the uplink outage probabilities with PIC receivers were similar to those with SIC receivers in the various deployment configurations studied. Additionally, in the *indoor-only* deployment scenarios investigated, the disparities in uplink outage probabilities between the various deployment configurations with PIC receivers were much greater than those observed with conventional receivers.

Assuming a fixed fractional residual interference cancellation error of $\sigma_\varepsilon = 0.22$ at each stage of the PIC receiver, it was shown that the majority of the uplink performance gain is attained in the first stage of cancellation. At each subsequent stage of cancellation the uplink performance gain is incrementally less. The majority of the maximum attainable uplink performance gain is attained in the first two to three stages of cancellation in all the deployment scenarios investigated.

9.4 Recommendations for future work

This thesis has presented an investigation into the performance of indoor/outdoor DS-CDMA systems assuming both conventional receivers and multiuser detection receivers at the base stations. The guidelines derived from the investigation are likely to be useful for wireless operators in the deployment of future wireless systems. However, the research in this thesis can be extended in the future to investigate several important issues that wireless operators will encounter. The recommendations for future work are now discussed.

Additional deployment scenarios and frequencies

This thesis has been based on three propagation measurement campaigns that were conducted in two different mixed indoor/outdoor environments. Although the mixed indoor/outdoor environments were significantly different in terms of both layout and architecture, in reality there are a plethora of possible building types that wireless operators will need to consider. A useful extension to the research in this thesis would be to conduct the system performance analyses for a wider range of mixed indoor/outdoor environments.

A limited number of indoor deployment configurations using either two base stations on a single floor or base stations on multiple floors of a building were considered in this thesis. For the interfering indoor/outdoor configurations considered, it was assumed that indoor mobiles could only connect to indoor base stations, while outdoor mobiles could only connect to outdoor base stations. This study was useful as it enabled an evaluation of the strength of outdoor interference on indoor system performance. However, in practice there

are many possible system settings and configurations. For example, an indoor/outdoor DS-CDMA system could allow for mobiles to connect to the *best* base station regardless of where the base station is located. Additionally in a multi-floor indoor configuration, frequency sectorisation could be used such that only base stations on alternate floors share the same frequency band. This might have implications on the deployment configuration that yields optimal performance both in the absence and presence of outdoor interference.

In the interfering indoor/outdoor DS-CDMA systems considered in this thesis, only the downlink and uplink performance attained for *indoor* mobiles have been evaluated. A future contribution would be to evaluate the performance for *outdoor* mobiles as well, and determine how to balance the system performance for both outdoor and indoor mobiles.

Refinement and validation of propagation models

In this thesis, the system performance analyses used measured propagation data which was collected in three propagation measurement campaigns. This approach was adopted due to the limited accuracy and applicability of existing indoor-to-indoor and outdoor-to-indoor propagation models in the literature. However, the development of accurate propagation models (that have been validated by measured propagation data) is extremely important as the models can then be used by system designers to estimate system performance, thus removing the need to conduct time-consuming and costly propagation measurement campaigns. A useful future contribution would be to validate and refine commonly-used existing propagation models (e.g. the Seidel model) using the measured propagation data collected in this thesis. Additionally, it would be useful to study the sensitivity of the predicted system performance (i.e. the predicted mean outage probabilities) to errors in the parameters used in the propagation models.

Improved solutions for estimating SIC and PIC performance

Two multiuser detection techniques have been investigated in this thesis, namely SIC and PIC. Due to the inherent complexity of analysing multiuser detection techniques, there are very few closed-form solutions for determining the SIR which incorporate SIC and PIC. As the purpose of this thesis was to determine the key factors influencing system deployment and performance at the *system* level, only simple closed-form solutions were used to calculate the SIR assuming SIC and PIC receivers in the uplink system performance testbed.

In the PIC performance estimation, it was assumed that the standard deviation of the fractional residual interference cancellation error was the same at each stage of the PIC receiver. However, in practice it is likely that the standard deviation of the fractional residual interference cancellation error will decrease at each stage of the PIC receiver

due to improved estimates of the various mobiles' signals [14]. It was not possible to account for this in the PIC performance estimation due to a lack of knowledge about the extent to which the mobile signal estimates improve at each stage of the PIC receiver. Such information could be obtained by running bitwise (link level) simulations or by taking measurements using actual PIC receivers. The typical values for fractional residual interference cancellation error could then be used in the system performance analyses of this thesis to determine the relationship between system deployment/performance and PIC.

Influence of different antenna types and macrodiversity

Omni-directional antennas were used in the propagation measurement campaigns conducted for this thesis. With the availability of improved antennas and multiple-input-multiple-output (MIMO) systems, further performance enhancements are possible. For example, directional antennas are designed to radiate energy in a particular direction with a much narrower beamwidth than omni-directional antennas. A future contribution would be to study the joint implications of different antenna types and multiuser detection on the performance of indoor/outdoor DS-CDMA systems.

With the use of macrodiversity, it is possible for widely separated base stations to share information about mobiles [115]. Therefore, inter-cell interference can be transformed into useful information during the multiuser detection process. In addition to removing intra-cell interference from other mobiles within the cell of interest, interference caused by mobiles from other cells (i.e. inter-cell interference) can also be removed. An evaluation of the joint use of macrodiversity and multiuser detection in indoor/outdoor DS-CDMA systems would be a useful contribution.

Influence of spatial diversity on SIC performance and deployment

In this thesis, the joint influence of SIC and an optimal power control algorithm (developed in [96]) on indoor/outdoor system performance and deployment was investigated. It was found that the relatively fine adjustments to mean received power made by the optimal power control algorithm have a negligible impact on system performance and deployment. This is because there are much greater variations in the instantaneous received signal power caused by small-scale fading, which has a more dominant impact on system performance. Micro-diversity can be used to reduce the small-scale fading and thus also lower the variation in instantaneous received signal powers. In the future, it would be useful to examine the impact of spatial diversity on indoor/outdoor DS-CDMA system performance and deployment assuming SIC receivers at the base stations operating with the optimal power control algorithm. It would also be worthwhile to examine the extent

to which the small-scale fading must be removed in order for the optimal power control algorithm to have an influence on the optimal system deployment strategy (if any).

Mobility and traffic modelling

The system performance analysis in this thesis has used a semi-static approach in which mobiles are placed at random locations on the floor(s) of interest in each iteration. However, in practice users will not strictly be at random locations because they are more likely to be in certain areas of the building. Additionally, users are likely to have certain patterns of movement (e.g. walking from one office to another through a corridor). The addition of relevant user mobility profiles to the system performance analysis would be a useful contribution for a more accurate evaluation of system performance.

The DS-CDMA model in this thesis has assumed a simple circuit-switched system that is used for voice connections between mobiles. With the advent of data intensive services (i.e. packet switched data), the traffic presented to the system is likely to be significantly different from that encountered in conventional voice-based systems. Further investigation into the impact of likely traffic distributions on system performance (with and without multiuser detection) in indoor/outdoor DS-CDMA systems would be an important extension to this research.

Improved modulation and coding techniques

This thesis has considered a voice-based DS-CDMA system with a high spreading factor and BPSK modulation. In enhanced 3rd generation systems that use HSDPA and HSUPA [19], low spreading factors with higher order modulation schemes (e.g. QPSK and 16QAM) are used in combination with error coding and a variety of code rates (adjusted depending on the quality of the channel). Further investigation is required to evaluate the joint implementation of these modelling/coding techniques and multiuser detection in indoor/outdoor DS-CDMA systems.

9.5 Summary

This chapter has presented guidelines on deploying indoor/outdoor DS-CDMA systems assuming a variety of deployment scenarios and either conventional receivers or multiuser detection receivers at the base stations. These guidelines have been derived from the downlink and uplink system performance estimation results presented in Chapters 5, 7 and 8. This chapter has also presented recommendations for future extensions to the research in this thesis.

Regardless of the type of receiver used at the base station, the key factors that wireless operators will need to account for when deploying indoor/outdoor DS-CDMA systems are the building architectural features, base station locations and the source and strength of interference. For the case of multiuser detection receivers (SIC and PIC), the fractional residual interference cancellation error and the number of receiver stages (for PIC receivers) give significant insight into the potential uplink system performance improvements.

The recommendations for future work presented in this chapter include investigating additional deployment scenarios and indoor/outdoor propagation environments. A useful contribution would also be to investigate the implications of directional antennas, MIMO systems and macrodiversity on system deployment and performance with the implementation of multiuser detection receivers at the base stations. This thesis has used a semi-static analysis technique and assumed fixed voice-based traffic. The introduction of mobility profiles and traffic modelling to the system performance analysis would be an important contribution.

Chapter 10

Conclusions

The tremendous growth of wireless communications has transformed society and created new opportunities for people around the world. There has been increasing necessity to implement high performing, high capacity wireless communication systems for indoor environments. Additionally, the provision of seamless wireless communications for mobile users *anywhere* (both indoors and outdoors) is viewed by wireless operators as an important business opportunity. In the future it is likely that one or more technologies (e.g. Wi-Fi and 3rd generation systems) will be used to provide seamless indoor/outdoor coverage. Regardless of the exact technologies used, the deployment of high performing indoor wireless communication systems and the influence of interference between indoors and outdoors are likely to be important issues for wireless operators.

This thesis has investigated the deployment and performance of indoor/outdoor wireless communication systems for a variety of likely deployment scenarios. The spread spectrum multiple access technique assumed was DS-CDMA due to its popularity in commercial implementations. This thesis also investigated the influence of multiuser detection (in particular SIC and PIC) on the deployment and performance of indoor/outdoor DS-CDMA systems.

In this thesis, three propagation measurement campaigns were conducted to obtain measured mean path loss data in mixed indoor/outdoor environments. While several propagation models have been developed to predict mean path loss behaviour for both indoor-to-indoor and outdoor-to-indoor propagation, a literature review revealed that most of these models do not have sufficient accuracy for the purposes of this thesis.

A system performance testbed using a Monte Carlo analysis was developed to estimate the performance of conventional DS-CDMA systems (without multiuser detection), which was then extended to include two multiuser detection techniques (SIC and PIC) at later stages of this thesis. In the system performance testbed, both the downlink and uplink performance are estimated using a mean outage probability that represents the likelihood that a mobile within the system will have an outage.

The three propagation measurement campaigns represent three general cases which wireless operators are likely to encounter:

1. Single floor indoor DS-CDMA system coexisting with an outdoor DS-CDMA system.
2. Multiple floor indoor DS-CDMA system coexisting with an outdoor DS-CDMA system.
3. Two adjacent indoor DS-CDMA systems coexisting with each other.

For each of these cases, one or more deployment scenarios were investigated. These deployment scenarios included an *indoor-only* scenario, *interfering indoor/outdoor* scenario and *adjacent interfering* scenario. In the *indoor-only* deployment scenario, it was assumed that base stations and mobiles are located indoors only and no interference emanates from outdoors. In the *interfering indoor/outdoor* deployment scenario, an indoor and outdoor system operate separately but share the same bandwidth and therefore interfere with each other. The *adjacent interfering* deployment scenario considers the performance of two adjacently-located indoor DS-CDMA systems that interfere with each other.

The performance of a conventional indoor/outdoor DS-CDMA system is dependent on several factors including the base station deployment strategy and the sources and strength of interference. The signal correlation between desired and interfering signals has been shown to have a significant influence on system performance. Levels of signal correlation are directly related to the base station deployment strategy. Therefore, the careful selection of base station locations is important to optimise the performance of indoor/outdoor DS-CDMA systems.

For the case of indoor-only DS-CDMA systems, this thesis has investigated the provision of coverage to a single floor (using two base stations) as well as multiple floors (using a single base station on each floor). The downlink outage probabilities for the various deployment configurations investigated had greater differences than the uplink outage probabilities. For the case of single floor coverage, the positioning of base stations close together yields worse downlink and uplink performance than if the base stations are located at opposite sides of the building. For multiple floor coverage, the positioning of base stations in an aligned configuration yields improved performance in comparison to an offset configuration.

In interfering indoor/outdoor DS-CDMA systems, the strength and location of outdoor interference has a significant influence on the performance of the indoor system and therefore the optimal indoor base station deployment strategy. However, it was shown that the downlink and uplink often have 'conflicting' deployment requirements. Therefore, the base station deployment strategy chosen to ensure optimal indoor performance might require operators to prioritise the downlink over the uplink or vice versa.

For the case of two interfering single floor indoor DS-CDMA systems that are located in adjacent buildings, the relative interference from one building to the other significantly influences downlink and uplink system performance. The positioning of base stations so that they are as far away from each other as possible was shown to 'balance' downlink and uplink system performance in both buildings.

This thesis has also investigated the performance of indoor/outdoor DS-CDMA systems assuming both successive interference cancellation (SIC) and parallel interference cancellation (PIC) receivers at the base stations. In general, the uplink performance gains attainable with both SIC and PIC are related to levels of interference in the system, the accuracy with which interference cancellation is performed and the power control algorithm used (in the case of SIC).

For the deployment configurations investigated in this thesis, both the SIC and PIC receivers were observed to reduce the uplink outage probabilities by as much as thirty times relative to those obtained with conventional receivers (assuming perfect interference cancellation and conventional power control). Furthermore, it was also evident that both SIC and PIC yield similar uplink outage probabilities. This shows that cancelling all intra-cell interfering signals in parallel (PIC) provides no additional benefit compared to ranking and cancelling the signals sequentially (SIC).

In all the scenarios investigated in this thesis (*indoor-only*, *interfering indoor/outdoor* and *adjacent interfering*), the optimal deployment strategies assuming either SIC or PIC receivers at the base stations were the same as those assuming conventional receivers. However, greater differences in the uplink outage probabilities for the *indoor-only* deployment configurations were observed for SIC and PIC receivers than conventional receivers. This occurs due to the dominance of *inter-cell* interference (which varies among the different indoor deployment configurations) after interference cancellation has been performed.

For the case of *interfering indoor/outdoor* configurations, the efficacy of both SIC and PIC receivers is dependent on the level of uncancellable outdoor interference. For increased interference emanating from outdoors, lower uplink performance gains are attainable for indoor mobiles.

In addition to the investigation of the influence of SIC and PIC receivers on the optimal deployment strategies for various scenarios, issues specific to each of the receivers were also investigated.

Firstly, the influence of the uplink power control algorithm on the efficacy of SIC to improve uplink system performance was evaluated for multi-floor indoor deployment configurations. It was shown that an optimal uplink power control algorithm (that attempts to equalise the mean received SIRs for the various mobiles) yields similar performance to the conventional power control algorithm. This occurs due to the dominance of short-term fading and inherent inaccuracies in obtaining the mobile received power distributions

using the optimal uplink power control algorithm. However, it should be noted that if spatial diversity is implemented, this is likely to reduce signal variation due to short-term fading and the optimal power control will have a greater influence on system performance. If no uplink power control was implemented, it was shown that the optimal deployment strategies were different from those obtained if conventional uplink power control was implemented.

Secondly, for the PIC receivers it was shown that the first stage of cancellation provides the maximum uplink performance gain, and that each additional stage of cancellation provides incrementally less performance gain. In general, the majority of the maximum uplink performance gain is attained after two or three stages of cancellations.

In summary, this thesis has made the following contributions. Firstly, the performance of indoor/outdoor DS-CDMA systems has been investigated using a variety of likely scenarios that wireless operators will encounter. Guidelines for optimal system deployment have been developed using the performance results. Secondly, this thesis has evaluated the implications of two multiuser detection receivers (SIC and PIC) on the deployment of indoor/outdoor DS-CDMA systems. Regardless of the type of receivers used at the base stations, it has been shown that a number of 'key' factors should be accounted for by wireless operators during the design process, including the base station locations and the sources and strength of interference.

Appendix A

Propagation measurement equipment

A.1 Introduction

The purpose of this appendix is to describe the measurement equipment used in the propagation measurement campaigns conducted for this thesis (outlined in Chapter 4). The overall setup of the measurement system is discussed in Section A.2, while the transmitter and receiver equipment are detailed in Sections A.3 and A.4 respectively.

A.2 Overall setup of propagation measurement system

A block diagram of the propagation measurement system is shown in Figure A.1. The transmitter equipment consists of narrowband transmitters connected to discone antennas, while the receiver equipment includes a dipole antenna with a Rohde & Schwarz ESVN40 test receiver and laptop computer (for data acquisition).

In the propagation measurement campaigns, the narrowband transmitters were programmed to transmit CW (sinusoidal) signals at frequencies ranging from 1880 to 1885.5 MHz (with a frequency separation of 0.5 MHz between the transmit frequencies). At the receiving end, the dipole antenna was rotated in a 1 metre radius circular path. The ESVN40 test receiver and software on a laptop computer were used to take approximately 2000 samples of the instantaneous received power during the rotation of the dipole antenna. These samples were then averaged to obtain the local area *mean* received power. The mean path loss between the transmitter and receiver was then calculated based on the mean received power and the known transmit power (taking into account relevant cable losses).

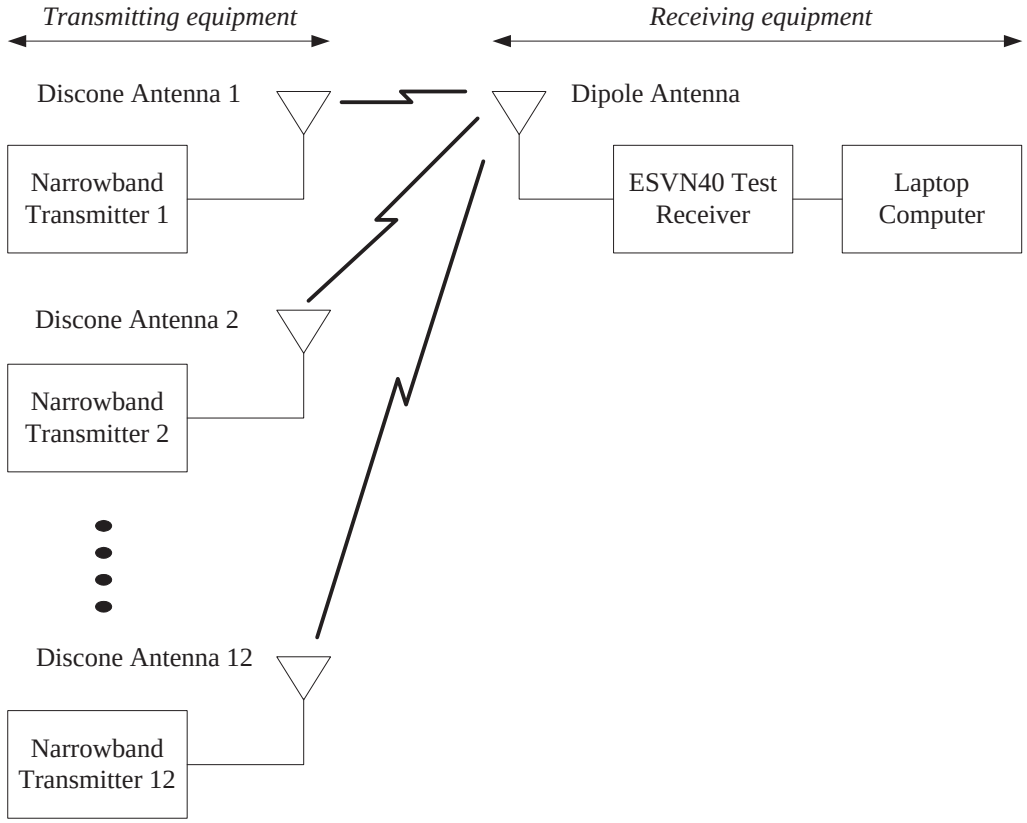

Figure A.1: Overall setup of the propagation measurement system.

A.3 Transmitter equipment

A.3.1 Narrowband transmitter equipment

The twelve narrowband transmitters (shown in Figure A.1) were custom-built in the Radio Systems Group of The University of Auckland [26]. The transmitters are capable of transmitting continuous wave (CW) signals with a very narrow bandwidth.

A block diagram of the narrowband transmitter implementation is shown in Figure A.2. The transmitters use a voltage controlled oscillator (VCO) that is capable of generating signals over the range of 1370 to 2000 MHz. The frequency synthesiser is provided with a reference 10 MHz signal from a crystal oscillator and a sample of the VCO output is fed back to the synthesiser via a passive loop filter. The frequency of the output signal from the frequency synthesiser is the difference between that of the crystal reference oscillator output signal and the VCO output signal. The current pulses are then filtered, amplified and applied to the VCO control port to reduce phase error and achieve phase lock. The output power following amplification is approximately 18 dBm.

A view inside one of the narrowband transmitter boxes is shown in Figure A.3. The power supplied to the transmitter box uses either an AC 12V plug pack or a DC battery. At the lower left is a box containing the VCO and frequency synthesiser. The frequency

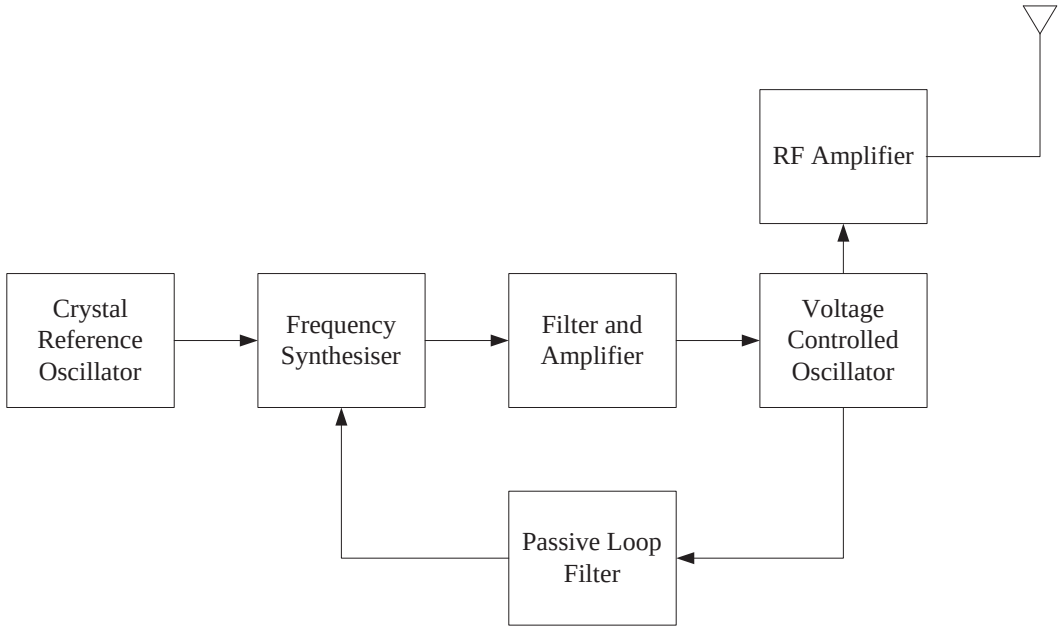

Figure A.2: Block diagram of the narrowband transmitter implementation.

synthesiser is programmed to transmit at a desired frequency using a laptop computer via a parallel port interface. On the lower right is an amplifier that is fed with the output of the VCO. The output of the amplifier is fed to the connector on the outside of the box (on the panel on the lower right of the transmitter).

A.3.2 Discone antennas

A photograph of one of the discone antennas is shown in Figure A.4. The discone antennas were designed and optimised to operate at frequencies in the region of 1800 MHz. The design was performed using the guidelines in [116].

A.4 Receiver equipment

As shown in Figure A.1, a dipole antenna is used for the reception of the transmitted signal. This dipole antenna is connected to a Rohde & Schwarz ESVN40 test receiver and a laptop computer which contains software for data acquisition from the test receiver.

A photograph of the test receiver is shown in Figure A.5. It is capable of measuring and demodulating both amplitude-modulated and frequency-modulated signals as well as narrowband and broadband interference. Further information regarding the test receiver specifications and capabilities can be found in [117].

The software for acquiring received signal strength data from the test receiver was designed in the Radio Systems Group at The University of Auckland. Further information regarding this software and its capabilities can be found in [8].

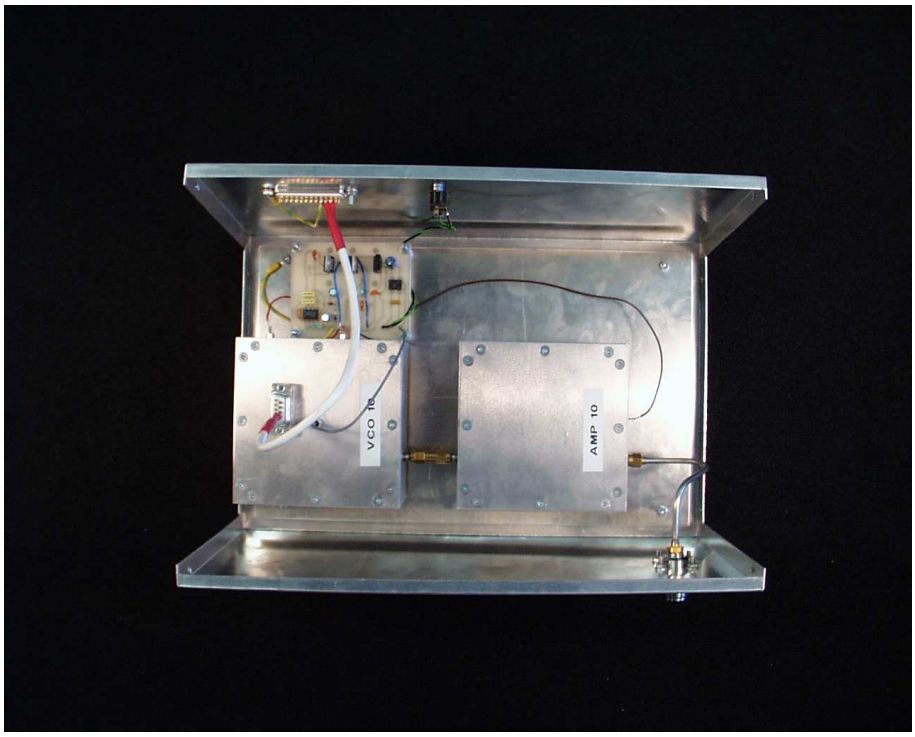

Figure A.3: View inside the box of the custom-built narrowband transmitter.

Figure A.4: A view of a discone antenna.

Figure A.5: Front view of the Rohde & Schwarz ESVN40 test receiver.

Appendix B

Signal correlation results

B.1 Introduction

The phenomenon of signal correlation has the potential to significantly influence system performance, as explained in Chapters 3 and 4. This appendix presents the full set of correlation results for the three propagation measurement campaigns described in Chapter 4. In Chapter 4, only a selection of the correlation coefficients were used to demonstrate typical behaviour.

B.2 Propagation Measurement Campaign A (PM A)

In PM A, which was conducted in the School of Engineering at The University of Auckland, transmitters were deployed inside the Tower Block as well as outdoors on the roofs of the adjacent Library Block and Lecture Theatre Block, as shown in Figure B.1. Measurements of the mean path loss were taken inside the Tower Block on the same floor as that on which the indoor transmitters were deployed.

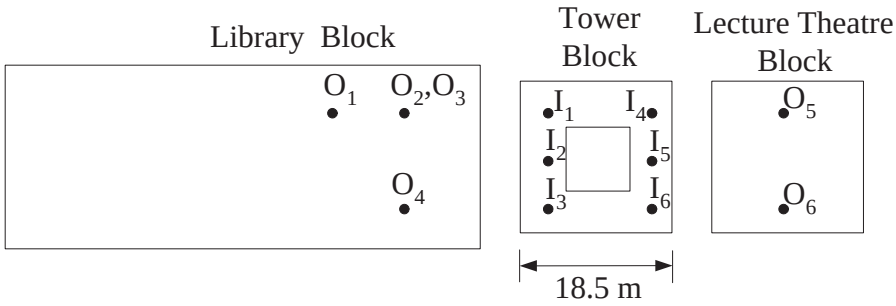

Figure B.1: Locations of transmitters deployed in PM A.

Correlations between signals from indoor transmitters

The correlation coefficients between signals from indoor transmitters in PM A are shown in Table B.1. The coefficients are positive for pairs of transmitters located on the same side of the building (e.g. for I_1I_2, $\rho = 0.80$), while they are negative for pairs of transmitters located on opposite sides of the building (e.g. for I_2I_4, $\rho = -0.42$).

ρ	I_1	I_2	I_3	I_4	I_5	I_6
I_1	1	0.80	0.35	0.06	-0.46	-0.66
I_2	0.80	1	0.71	-0.42	-0.75	-0.51
I_3	0.35	0.71	1	-0.51	-0.51	0.02
I_4	0.06	-0.42	-0.51	1	0.77	0.18
I_5	-0.46	-0.75	-0.51	0.77	1	0.66
I_6	-0.66	-0.51	0.02	0.18	0.66	1

Table B.1: Correlation coefficients between signals from indoor transmitters in PM A.

Correlations between signals from outdoor transmitters

The correlation coefficients between signals from outdoor transmitters in PM A are shown in Table B.2. The coefficients are strongly positive for pairs of transmitters located on the roof of the same building (e.g. for O_1O_2, $\rho = 0.91$). The coefficients are moderately to strongly negative if the transmitters are located on roofs of different buildings (e.g. for O_1O_5, $\rho = -0.60$).

ρ	O_1	O_2	O_3	O_4	O_5	O_6
O_1	1	0.91	0.90	0.95	-0.60	-0.69
O_2	0.91	1	0.99	0.81	-0.62	-0.74
O_3	0.90	0.99	1	0.80	-0.63	-0.75
O_4	0.95	0.81	0.80	1	-0.44	-0.59
O_5	-0.60	-0.62	-0.63	-0.44	1	0.90
O_6	-0.69	-0.74	-0.75	-0.59	0.90	1

Table B.2: Correlation coefficients between signals from outdoor transmitters in PM A.

Correlations between signals from indoor and outdoor transmitters

The correlation coefficients between signals from indoor and outdoor transmitters in PM A are shown in Table B.3. If the indoor transmitter is on the side of the building nearest to where the outdoor interference emanates from, a positive correlation is observed (e.g. for

I_1O_2, $\rho = 0.48$). However, if the indoor transmitter is on the side of the building opposite to where the outdoor interference emanates from, a negative correlation is observed (e.g. for I_4O_1, $\rho = -0.63$).

ρ	I_1	I_2	I_3	I_4	I_5	I_6
O_1	0.41	0.61	0.40	-0.63	-0.83	-0.56
O_2	0.48	0.66	0.39	-0.61	-0.88	-0.66
O_3	0.49	0.67	0.42	-0.62	-0.87	-0.64
O_4	0.31	0.49	0.28	-0.57	-0.73	-0.51
O_5	-0.39	-0.77	-0.72	0.59	0.68	0.22
O_6	-0.55	-0.84	-0.66	0.53	0.74	0.40

Table B.3: Correlation coefficients between signals from indoor and outdoor transmitters in PM A.

B.3 Propagation Measurement Campaign B (PM B)

In PM B, which was conducted in the School of Engineering at The University of Auckland, transmitters were deployed in a three-dimensional configuration inside the Tower Block as well as outdoors on the roof of the adjacent Library Block, as shown in Figure B.2. Measurements of the mean path loss were taken on the middle level (Level 8) of the Tower Block.

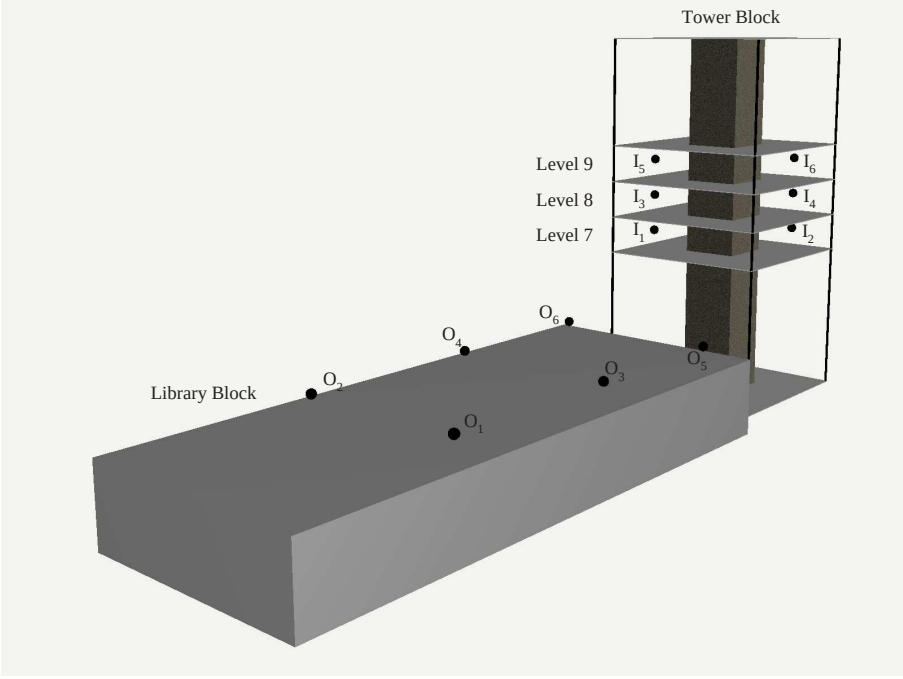

Figure B.2: Transmitter locations in PM B.

Correlations between signals from indoor transmitters

The correlation coefficients between signals from indoor transmitters in PM B are shown in Table B.4. The coefficients are strongly positive for pairs of transmitters that are vertically aligned with each other (e.g. for I_1I_3, $\rho = 0.95$), while they are negative for pairs of transmitters that are vertically offset from each other (e.g. for I_1I_4, $\rho = -0.44$).

ρ	I_1	I_2	I_3	I_4	I_5	I_6
I_1	1	-0.41	0.95	-0.44	0.97	-0.49
I_2	-0.41	1	-0.46	0.93	-0.37	0.95
I_3	0.95	-0.46	1	-0.49	0.96	-0.55
I_4	-0.44	0.93	-0.49	1	-0.41	0.93
I_5	0.97	-0.37	0.96	-0.41	1	-0.48
I_6	-0.49	0.95	-0.55	0.93	-0.48	1

Table B.4: Correlation coefficients between signals from indoor transmitters in PM B.

Correlations between signals from outdoor transmitters

The correlation coefficients between signals from outdoor transmitters in PM B are shown in Table B.4. The coefficients are strongly positive for all pairs of outdoor transmitters located on the roof of the Library Block.

ρ	O_1	O_2	O_3	O_4	O_5	O_6
O_1	1	0.96	0.97	0.96	0.95	0.84
O_2	0.96	1	0.95	0.96	0.90	0.87
O_3	0.97	0.95	1	0.97	0.96	0.86
O_4	0.96	0.96	0.97	1	0.92	0.90
O_5	0.95	0.90	0.96	0.92	1	0.78
O_6	0.84	0.87	0.86	0.90	0.78	1

Table B.5: Correlation coefficients between signals from outdoor transmitters in PM B.

Correlations between signals from indoor and outdoor transmitters

The correlation coefficients between signals from indoor and outdoor transmitters in PM B are shown in Table B.6. If the indoor transmitter is on the side of the building from where the outdoor interference emanates, a positive correlation is observed (e.g. for I_1O_1, $\rho = 0.38$). However, if the indoor transmitter is on the side of the building opposite to where the outdoor interference emanates from, a negative correlation is observed (e.g. for I_2O_1, $\rho = -0.34$).

ρ	I_1	I_2	I_3	I_4	I_5	I_6
O_1	0.38	-0.34	0.34	-0.33	0.43	-0.50
O_2	0.43	-0.34	0.38	-0.34	0.48	-0.49
O_3	0.37	-0.36	0.33	-0.35	0.41	-0.52
O_4	0.45	-0.41	0.41	-0.43	0.50	-0.57
O_5	0.29	-0.38	0.24	-0.39	0.32	-0.53
O_6	0.54	-0.52	0.49	-0.51	0.53	-0.62

Table B.6: Correlation coefficients between signals from indoor and outdoor transmitters in PM B.

B.4 Propagation Measurement Campaign C (PM C)

PM C was conducted in the Functions and Science buildings at The University of Auckland. In this propagation measurement campaign, transmitters were deployed on Level 2 of the Functions and Science buildings, as shown in Figure B.2. The mean path loss was obtained at various locations across Level 2 of both the Functions and Science buildings. The sections below present the correlation coefficients for measurements taken in the Functions and Science buildings in turn.

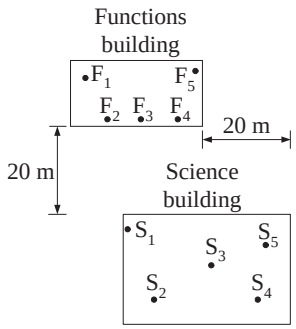

Figure B.3: Locations of transmitters deployed in PM C.

B.4.1 Functions building measurements

Correlations between signals from transmitters in the Functions building

The correlation coefficients between the signals from the transmitters deployed in the Functions building are shown in Table B.7. It is evident that if the transmitters are close to each other a positive correlation is obtained (e.g. for F_1F_2, $\rho = 0.48$), while a negative correlation is obtained if the transmitters are at opposite sides of the building or further away from each other (e.g. for F_1F_4, $\rho = -0.57$).

ρ	F_1	F_2	F_3	F_4	F_5
F_1	1	0.48	-0.29	-0.57	-0.69
F_2	0.48	1	0.20	-0.26	-0.14
F_3	-0.29	0.20	1	0.52	0.20
F_4	-0.57	-0.26	0.52	1	0.48
F_5	-0.69	-0.14	0.20	0.48	1

Table B.7: Correlation coefficients between signals from transmitters in the Functions building in PM B (Measurements taken in the Functions building).

Correlations between signals from transmitters in the Science building

The correlation coefficients between the signals from the transmitters deployed in the Science building are shown in Table B.8. A moderate to strong positive correlation is usually obtained for the measurements taken in the Functions building.

ρ	S_1	S_2	S_3	S_4	S_5
S_1	1	0.83	0.52	0.53	0.47
S_2	0.83	1	0.57	0.43	0.45
S_3	0.52	0.57	1	0.81	0.81
S_4	0.53	0.43	0.81	1	0.87
S_5	0.47	0.45	0.81	0.87	1

Table B.8: Correlation coefficients between signals from transmitters in Science building in PM B (Measurements taken in the Functions building).

Correlations between signals from transmitters in Functions and Science buildings

The correlation coefficients between the signals from the transmitters deployed in the Functions and Science buildings are shown in Table B.9. A positive correlation is observed between the signals if the transmitter in the Functions building is close to the side nearer to the Science building (e.g. for F_3S_1, $\rho = 0.66$). However, a negative or poor correlation is observed if the transmitter in the Functions building is close to the side further from the Functions building (e.g. for F_1S_3, $\rho = -0.45$).

B.4.2 Science building measurements

Correlations between signals from transmitters in Science building

The correlation coefficients between the signals from the transmitters deployed in the Science building are shown in Table B.10. Similar to the trends observed in the mea-

ρ	F_1	F_2	F_3	F_4	F_5
S_1	-0.10	0.21	0.66	0.56	0.07
S_2	-0.33	0.09	0.80	0.64	0.14
S_3	-0.45	-0.12	0.64	0.72	0.41
S_4	-0.31	0.06	0.55	0.69	0.46
S_5	-0.46	-0.13	0.55	0.74	0.48

Table B.9: Correlation coefficients between signals from transmitters in Functions and Science buildings in PM B (Measurements taken in the Functions building).

surements for the Functions building, it is evident that if the transmitters are close to each other a positive correlation is obtained (e.g. for S_1S_2, $\rho = 0.37$), while a negative correlation is obtained if the transmitters are on opposite sides of the building or further away from each other (e.g. for S_1S_4, $\rho = -0.79$).

ρ	S_1	S_2	S_3	S_4	S_5
S_1	1	0.37	-0.26	-0.79	-0.29
S_2	0.37	1	0.02	-0.23	-0.69
S_3	-0.26	0.02	1	0.54	0.38
S_4	-0.79	-0.23	0.54	1	0.43
S_5	-0.29	-0.69	0.38	0.43	1

Table B.10: Correlation coefficients between signals from transmitters in Science building in PM B (Measurements taken in the Science building).

Correlations between signals from transmitters in Functions building

The correlation coefficients between the signals from the transmitters deployed in the Functions building are shown in Table B.11. A strong positive correlation is usually obtained for measurements taken in the Science building.

ρ	F_1	F_2	F_3	F_4	F_5
F_1	1	0.93	0.92	0.89	0.92
F_2	0.93	1	0.95	0.92	0.91
F_3	0.92	0.95	1	0.95	0.86
F_4	0.89	0.92	0.95	1	0.90
F_5	0.92	0.91	0.86	0.90	1

Table B.11: Correlation coefficients between signals from transmitters in the Functions building in PM B (Measurements taken in the Science building).

Correlations between signals from transmitters in Functions and Science buildings

The correlation coefficients between the signals from the transmitters deployed in the Functions and Science buildings are shown in Table B.9. A positive correlation is observed between the signals if the transmitter in the Science building is close to the side nearer to the Functions building (e.g. for F_1S_1, $\rho = 0.54$). However, a negative correlation is observed if the transmitter in the Science building is close to the side further from the Functions building (e.g. for F_5S_2, $\rho = -0.55$).

ρ	S_1	S_2	S_3	S_4	S_5
F_1	0.54	-0.36	-0.22	-0.42	0.28
F_2	0.62	-0.37	-0.29	-0.54	0.24
F_3	0.69	-0.26	-0.26	-0.56	0.15
F_4	0.55	-0.41	-0.15	-0.43	0.31
F_5	0.40	-0.55	-0.26	-0.33	0.43

Table B.12: Correlation coefficients between signals from transmitters in Science building and Functions building in PM B (Measurements taken in the Science building).

Appendix C

System performance gain in terms of capacity of serviceable mobiles

C.1 Introduction

In this thesis, the performance estimates of the various deployment configurations are expressed in terms of a mean outage probability. Comparisons between the deployment configurations are made in terms of a difference (in magnitude) between the observed mean outage probabilities. As an alternative, it is often useful to compare the deployment configurations in terms of the capacity of serviceable mobiles. This information can be inferred from the majority of the graphs in this thesis. In this appendix, the simple procedure for doing this is described using examples from PM A and PM B, discussed in Sections C.2 and C.3 respectively.

C.2 Indoor-only scenario in PM A

The deployment configurations investigated in the indoor-only scenario in PM A (discussed in Chapter 5) are reproduced in Table C.1, while a graph showing the mean downlink outage probabilities for these configurations is reproduced in Figure C.1. If the maximum allowable mean downlink outage probability is defined to be 0.003 (shown by the dashed orange line in Figure C.1), then the system capacity for each deployment configuration can be easily inferred by reading the number of mobiles served at this value (i.e. 0.003). The system capacity for the deployment configurations in Table C.1 is shown in Table C.2.

Configuration	Ad.1	Ad.2	Ad.3	Di.1	Di.2
Layout					
Configuration	**Op.1**	**Op.2**	**Op.3**	**Si.1**	**Si.2**
Layout					

Table C.1: Indoor base station deployment configurations in PM A.

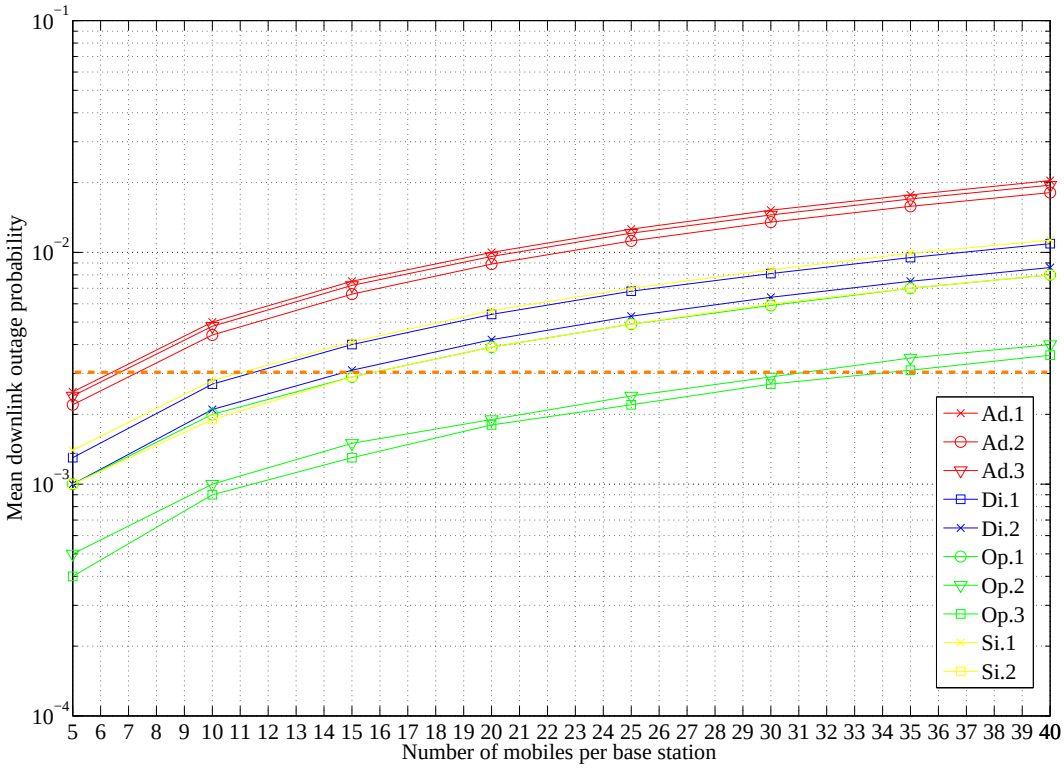

Figure C.1: Mean downlink outage probability for mobiles on Level 8 of the Tower Block for the configurations shown in Table C.1 (PM A). The dashed orange line shows the chosen mean downlink outage probability threshold of 0.003.

Deployment configuration	Downlink system capacity (Maximum number of mobiles per base station)
Ad.1	6
Ad.2	7
Ad.3	6
Di.1	11
Di.2	15
Op.1	15
Op.2	31
Op.3	34
Si.1	11
Si.2	15

Table C.2: Downlink system capacity for deployment configurations considered in the indoor-only scenario in PM A assuming a mean downlink outage probability threshold of 0.003.

C.3 Indoor-only scenario in PM B

The deployment configurations investigated in the indoor-only scenario in PM B (discussed in Chapter 5) are reproduced in Table C.3, while a graph showing the downlink outage probabilities for these configurations is reproduced in Figure C.2. If the maximum allowable mean downlink outage probability is defined to be 0.004 (shown by the dashed orange line in Figure C.2), then the system capacity for each deployment configuration can be easily inferred by reading the number of mobiles served at this value (i.e. 0.004). The system capacity for the deployment configurations in Table C.3 is shown in Table C.4.

Config.	Aligned 1	Aligned 2	Offset 1	Offset 2
Base Station Layout	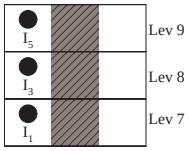	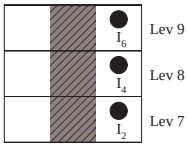	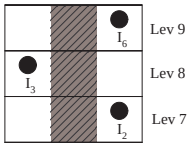	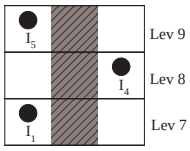

Config.	Aligned/Offset 1	Aligned/Offset 2	Aligned/Offset 3	Aligned/Offset 4
Base Station Layout	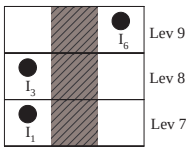	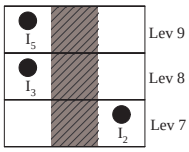	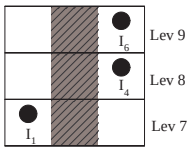	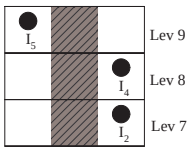

Table C.3: Front view of indoor base station deployment configurations in PM B (Indoor-only scenario).

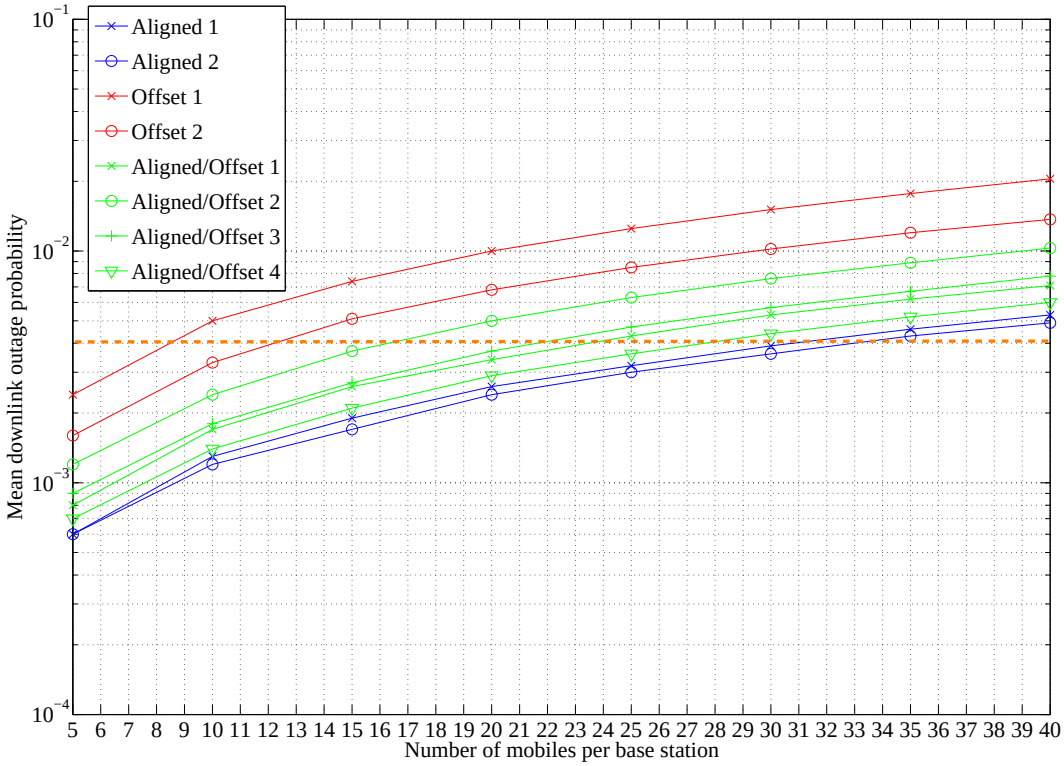

Figure C.2: Mean downlink outage probability for mobiles on Level 8 of the Tower Block for the configurations shown in Table C.3 (PM B). The dashed orange line shows the chosen mean downlink outage probability threshold of 0.004.

Deployment configuration	Downlink system capacity (Maximum number of mobiles per base station)
Aligned 1	31
Aligned 2	33
Aligned/Offset 1	24
Aligned/Offset 2	16
Aligned/Offset 3	22
Aligned/Offset 4	28
Offset 1	8
Offset 2	12

Table C.4: Downlink system capacity for deployment configurations considered in the indoor-only scenario in PM B assuming a mean downlink outage probability threshold of 0.004.

References

[1] "Worldwide Mobile Market Forecasts: 2006-2011," Portio Research, 2006.

[2] T. S. Rappaport, *Wireless Communications Principles and Practice.* Upper Saddle, River, NJ, USA: Prentice Hall, 1996.

[3] "World Telecommunication/ICT Development Report 2006: Measuring ICT for Social and Economic Development," ITU, 2006.

[4] M. Warschauer, *Technology and Social Inclusion: Rethinking the Digital Divide.* Cambridge, MA, USA: MIT Press, 2003.

[5] L. Servon, *Bridging the Digital Divide: Technology, Community and Public Policy.* Malden, MA, USA: Blackwell, 2002.

[6] G. Cayla, *WiMax: An Efficient Tool to Bridge the Digital Divide.* WiMax Forum whitepaper, 2005.

[7] S. Scheinert. (2006) Wireless Net DesignLine – In-building cellular: Why it is a Wi-Fi alternative. [Online]. Available: http://www.wirelessnetdesignline.com/howto/wlan/192701513.

[8] A. Wong, "Antenna selection and deployment strategies for indoor wireless communication systems," Ph.D. dissertation, The University of Auckland, 2006.

[9] S. Verdu, *Multiuser Detection.* Cambridge, UK: Cambridge University Press, 1998.

[10] J. G. Andrews, "Interference cancellation for cellular systems: a contemporary overview," *IEEE Wireless Commun. Mag.*, vol. 12, no. 2, pp. 19–29, Apr. 2005.

[11] A. Duel-Hallen, J. Holtzman, and Z. Zvonar, "Multiuser detection for CDMA systems," *IEEE Personal Commun. Mag.*, vol. 2, no. 2, pp. 46–58, Apr. 1995.

[12] L. Hanzo, *Single- and Multi-Carrier DS-CDMA: Multi-user Detection, Space-Time Spreading, Synchronisation, Networking, and Standards.* New York, USA: John Wiley & Sons Ltd., 2003.

[13] S. Moshavi, "Multi-user detection for DS-CDMA communications," *IEEE Commun. Mag.*, vol. 34, no. 10, pp. 124–136, Oct. 1996.

[14] R. M. Buehrer, "The application of multiuser detection to cellular CDMA," Ph.D. dissertation, Virginia Polytechnic Institute and State University, 1996.

[15] B. Hagerman, F. Gunnarsson, H. Murai, and J. Karlsson, "WCDMA uplink parallel interference cancellation - system simulations and prototype field trials," *EURASIP J. Applied Signal Processing*, vol. 11, pp. 1725–1735, Nov. 2005.

[16] M. Sawahashi, K. Higuchi, H. Andoh, and F. Adachi, "Experiments on pilot symbol-assisted coherent multistage interference canceller for DS-CDMA mobile radio," *IEEE J. Sel. Areas Commun.*, vol. 20, no. 2, pp. 433–449, Feb. 2002.

[17] K. I. Pedersen, T. E. Kolding, I. Seskar, and J. M. Holtzman, "Practical implementation of successive interference cancellation in DS/CDMA systems," in *Proc. IEEE Int. Conf. Universal Personal Commun.*, Cambridge, MA, USA, Sept. 29 – Oct. 2, 1996, pp. 321–325.

[18] G. Xu, "VLSI implementation of the multistage detector for next generation wide-band CDMA receivers," *J. VLSI Signal Processing*, vol. 30, pp. 21–33, 2002.

[19] H. Holma and A. Toskala, *HSDPA/HSUPA for UMTS: High Speed Radio Access for Mobile Communications.* Chichester, UK: John Wiley & Sons Ltd., 2006.

[20] A. Aragon and S. R. Saunders, "Measurement-based optimisation of in-building coverage for UMTS," in *Proc. 3rd Int. Conf. 3G Mobile Communication Technologies*, London, UK, May 8–10, 2002, pp. 167–172.

[21] T. Fruhwirth and P. Brisset, "Placing base stations in wireless indoor communication networks," *IEEE Intell. Syst. Appl.*, vol. 15, no. 1, pp. 49–53, 2000.

[22] L. Gatzoulis, A. Aragon, G. Povey, and S. R. Saunders, "Performance analysis of in-building FDD deployment using measured data," in *Proc. 4th Int. Conf. 3G Mobile Communication Technologies*, London, UK, June 25–27, 2003, pp. 167–172.

[23] K. J. Grandell, "Indoor antennas for WCDMA systems," in *Proc. 11th Int. Conf. Antennas Propag.*, vol. 1, Manchester, UK, Apr. 17–20, 2001, pp. 208–211.

[24] K. Hiltunen, B. Olin, and M. Lundevall, "Using dedicated in-building systems to improve HSDPA indoor coverage and capacity," in *Proc. 61st IEEE Veh. Technol. Conf. Spring*, vol. 4, Stockholm, Sweden, May 30 – June 1 2005, pp. 2379–2383.

[25] K. S. Butterworth, K. W. Sowerby, and A. G. Williamson, "Base station placement for in-building mobile communication systems to yield high capacity and efficiency," *IEEE Trans. Commun.*, vol. 48, no. 4, pp. 658–669, 2000.

[26] K. Butterworth, "Performance, planning and deployment of DS-CDMA in-building wireless communication systems," Ph.D. dissertation, The University of Auckland, 2000.

[27] D. Molkdar, "Review on radio propagation into and within buildings," *IEE Proc. Microwaves, Antennas and Propagation*, vol. 138, no. 1, pp. 61–73, 1991.

[28] R. Owen, P. Jones, S. Dehgan, and D. Lister, "Uplink WCDMA capacity and range as a function of inter-to-intra cell interference: theory and practice," in *Proc. 51st IEEE Veh. Technol. Conf. Spring*, vol. 1, Tokyo, Japan, May 15–18, 2000, pp. 298–302.

[29] A. Sathyendran, "A statistical approach to the analysis of DS/CDMA cellular radio systems," Ph.D. dissertation, The University of Auckland, 1997.

[30] L. B. Milstein, T. S. Rappaport, and R. Barghouti, "Performance evaluation for cellular CDMA," *IEEE J. Sel. Areas Commun.*, vol. 10, no. 4, pp. 680–689, May 1992.

[31] A. V. Pais, K. W. Sowerby, and M. J. Neve, "The influence of multiple outdoor interference on in-building DS-CDMA wireless system performance," in *Proc. 58th IEEE Veh. Technol. Conf. Fall*, vol. 2, Orlando, Florida, USA, Oct. 6–9, 2003, pp. 967–971.

[32] ——, "Outdoor-to-indoor signal correlation and its influence on indoor system performance at 2 GHz," *IEE Electron. Letters*, vol. 39, no. 2, pp. 236–238, 2003.

[33] ——, "Indoor DS-CDMA system deployment and performance with successive interference cancellation," *IEE Electron. Letters*, vol. 40, no. 19, pp. 1200–1201, 2004.

[34] ——, "Implications of power control and successive interference cancellation on indoor DS-CDMA system deployment and performance," *IEEE Commun. Letters*, vol. 9. no. 3, pp. 204–206, 2005.

[35] ——, "The performance of indoor DS-CDMA systems with multistage parallel interference cancellation," in *Proc. 61st IEEE Veh. Technol. Conf. Spring*, vol. 3, Stockholm, Sweden, May 30 – June 1 2005, pp. 1735–1739.

[36] D. Parsons, *The Mobile Radio Propagation Channel*. Chichester, UK: John Wiley & Sons Ltd., 2000.

[37] D. Lee, "Environmental modification for indoor wireless communications systems," Ph.D. dissertation, The University of Auckland, 2006.

[38] H. Suzuki, "A statistical model for urban radio propagation," *IEEE Trans. Commun.*, vol. 23, no. 7, pp. 673–680, 1977.

[39] D. M. J. Devasirvatham, "Time delay spread measurements of wideband radio signals within a building," *IEE Electron. Letters*, vol. 20, no. 23, pp. 950–951, 1984.

[40] D. Devasirvatham, "A comparison of time delay spread and signal level measurements within two dissimilar office buildings," *IEEE Trans. Antennas Propag.*, vol. 35, no. 3, pp. 319–324, Mar. 1987.

[41] A. A. M. Saleh and R. A. Valenzuela, "A statistical model for indoor multipath propagation," *IEEE J. Sel. Areas Commun.*, vol. 5, no. 2, pp. 128–137, Feb. 1987.

[42] R. J. C. Bultitude, "A comparison of indoor radio propagation characteristics at 910 MHz and 1.75 GHz," *IEEE J. Sel. Areas Commun.*, vol. 7, no. 1, pp. 20–30, Jan. 1989.

[43] D. M. J. Devasirvatham, "Time delay spread and signal measurements at 850 MHz and 1.7 GHz inside a metropolitan office building," *IEE Electron. Letters*, vol. 25, no. 3, pp. 194–196, 1989.

[44] H. Hashemi, "The indoor radio propagation channel," *Proc. IEEE*, vol. 81, no. 7, pp. 943–968, 1993.

[45] H. Holma and A. Toskala, *WCDMA for UMTS*. New York, USA: John Wiley & Sons Ltd., 2000.

[46] S. E. Alexander, "Radio propagation within buildings at 900 MHz," *IEE Electron. Letters*, vol. 18, no. 21, pp. 913–914, 1982.

[47] A. J. Motley and J. M. P. Keenan, "Personal communication radio coverage in buildings at 900 MHz and 1700 MHz," *IEE Electron. Letters*, vol. 24, no. 12, pp. 763–764, 1988.

[48] T. S. Rappaport, "900 MHz multipath propagation measurements for U.S. digital cellular radiotelephone," *IEEE Trans. Veh. Technol.*, vol. 39, no. 2, pp. 132–139, 1990.

[49] A. Motley and J. Keenan, "Radio coverage in buildings," *British Telecom Technical J.*, vol. 8, no. 1, pp. 19–24, 1990.

[50] W. Honcharenko, H. L. Bertoni, J. Dailing, J. Qian, and H. D. Yee, "Mechanisms governing UHF propagation on single floors in modern office buildings," *IEEE Trans. Veh. Technol.*, vol. 41, no. 4, pp. 496–504, 1992.

[51] J. Horikishi, K. Tanaka, and T. Morinaga, "1.2 GHz band wave propagation measurements in concrete buildings for indoor radio communications," *IEEE Trans. Veh. Technol.*, vol. 35, no. 4, pp. 146–152, 1986.

[52] K. Pahlavan, G. Ganesh, and T. Hotaling, "Multipath propagation measurements on manufacturing floors at 910 MHz," *IEE Electron. Letters*, vol. 25, no. 3, pp. 225–227, 1989.

[53] D. A. Hawbaker and T. S. Rappaport, "Indoor wideband radiowave propagation at 1.3 GHz and 4.0 GHz," *IEE Electron. Letters*, vol. 26, no. 21, pp. 1800–1802, 1990.

[54] A. M. D. Turkmani and A. F. D. Toledo, "Radio transmission at 1800 MHz, into and within, multistory buildings," *IEE Proc. I Communications, Speech and Vision*, vol. 138, no. 6, pp. 577–584, 1991.

[55] S. Y. Seidel and T. S. Rappaport, "914 MHz path loss prediction models for indoor wireless communications in multifloored buildings," *IEEE Trans. Antennas Propag.*, vol. 40, no. 2, pp. 207–217, 1992.

[56] J. B. Andersen, T. S. Rappaport, and S. Yoshida, "Propagation measurements and models for wireless communications channels," *IEEE Commun. Mag.*, vol. 33, no. 1, pp. 42–49, Jan. 1995.

[57] A. F. D. Toledo, A. M. D. Turkmani, and J. D. Parsons, "Estimating coverage of radio transmission into and within buildings at 900, 800, and 2300 MHz," *IEEE Personal Commun. Mag.*, vol. 5, no. 2, pp. 40–47, Apr. 1998.

[58] M. Hata, "Empirical formulae for propagation loss in land mobile radio services," *IEEE Trans. Veh. Technol.*, vol. VT-29, pp. 317–325, 1980.

[59] D. Cox, R. Murray, and A. Norris, "800 MHz attenuation measured in and around suburban houses," *AT&T Bell Laboratories Technical J.*, vol. 673, no. 6, pp. 921–954, 1984.

[60] T. S. Rappaport, "Wireless personal communications: trends and challenges," *IEEE Antennas Propag. Mag.*, vol. 33, no. 5, pp. 19–29, Oct. 1991.

[61] J. F. Lafortune and M. Lecours, "Measurement and modelling of propagation losses in a building at 900 MHz," *IEEE Trans. Veh. Technol.*, vol. 39, no. 2, pp. 101–108, 1990.

[62] J. M. Keenan and A. J. Motley, "Radio coverage in buildings," *BT Technology J.*, vol. 8, no. 1, pp. 19–24, 1990.

[63] S. Seidel, T. S. Rappaport, J. Feuerstein, and K. L. Blackard, "The impact of surrounding buildings on propagation for wireless in-building personal communications system design," in *Proc. 42nd IEEE Veh. Technol. Conf.*, vol. 2, Denver, Colorado, USA, May 10–13, 1992, pp. 814–818.

[64] A. M. D. Turkmani, J. D. Parsons, and D. G. Lewis, "Radio propagation into buildings at 441, 900, and 1400 MHz," in *Proc. 4th Int. Conf. Land Mobile Radio*, Warwick, England, Dec. 1987, pp. 129–138.

[65] A. M. D. Turkmani and A. F. D. Toledo, "Propagation into and within buildings at 900, 1800, and 2300 MHz," in *Proc. 42nd IEEE Veh. Technol. Conf.*, vol. 2, Denver, Colorado, USA, May 10–13, 1992, pp. 633–636.

[66] E. H. Walker, "Penetration of radio signals into buildings in cellular radio environments," *Bell Systems Technical J.*, vol. 62, no. 9, pp. 2719–2735, 1983.

[67] J. M. Durante, "Building penetration loss at 900 MHz," in *Proc. 24th IEEE Veh. Technol. Conf.*, vol. 24, Cleveland, Ohio, USA, Dec. 3–5, 1973, pp. 81–87.

[68] J. Horikishi, K. Tanaka, and T. Morinaga, "1.2 GHz band wave propagation measurements in concrete buildings for indoor radio communications," *IEEE Trans. Veh. Technol.*, vol. VT-35, no. 4, pp. 146–152, 1986.

[69] P. Kreuzgruber, P. Unterberger, and R. Gahleitner, "A ray splitting model for indoor radio propagation associated with complex geometrics," in *Proc. 43rd IEEE Veh. Technol. Conf.*, Secaucus, New Jersey, USA, May 18–20, 1993, pp. 227–230.

[70] J. W. McKown and R. L. Hamilton, "Ray tracing as a design tool for radio networks," *IEEE Netw.*, vol. 5, no. 6, pp. 27–30, Nov. 1991.

[71] S. Y. Seidel and T. S. Rappaport, "A ray tracing technique to predict path loss and delay spread inside buildings," in *Proc. IEEE Global Telecommunications Conf.*, vol. 2, Orlando, Florida, USA, Dec. 6–9, 1992, pp. 649–653.

[72] C. Smith and C. Gervelis, *Wireless Network Performance Handbook.* New York, USA: McGraw-Hill, 2003.

[73] H. Holma, "A study of UMTS terrestrial radio access performance," Ph.D. dissertation, Helsinki University of Technology, 2003.

[74] M. B. Pursley, "Performance evaluation for phase-coded spread-spectrum multiple-access communication - Part I: System analysis," *IEEE Trans. Commun.*, vol. COM-25, no.8, pp. 795–799, 1977.

[75] A. Goldsmith, *Wireless Communications*. Cambridge, UK: Cambridge University Press, 2005.

[76] R. K. Morrow and K. S. Lehnert, "Bit-to-bit error dependence in slotted DS/SSMA packet systems with random signature sequences," *IEEE Trans. Commun.*, vol. 37, no. 10, pp. 1052–1061, 1989.

[77] R. E. Schuh, R. Andersson, A. Stranne, M. Sommer, and P. Karlsson, "Interference analysis for dedicated indoor WCDMA systems," in *Proc. 58th IEEE Veh. Technol. Conf. Fall*, vol. 2, Orlando, Florida, USA, Oct. 6–9, 2003, pp. 992–994.

[78] H. Andersson, R. S. Karlsson, P. Larsson, and P. Wilkstrom, "Improving system performance in a WCDMA FDD network using indoor pico base station," in *Proc. 56th IEEE Veh. Technol. Conf. Fall*, vol. 1, Vancouver, British Columbia, Canada, Sept. 24–28, 2002, pp. 467–471.

[79] H. Bertoni, *Radio Propagation for Modern Wireless Systems*. Upper Saddle River, NJ, USA: Prentice Hall, 2000.

[80] R. Vaughan and J. B. Andersen, *Channels, Propagation and Antennas for Mobile Communications*. London, UK: IEE, 2003.

[81] C. Johnson, P. Moris, and D. Fraley, "Indoor WCDMA solutions cochannel with the macrocellular layer," in *Proc. 5th Int. Conf. 3G Mobile Communication Technologies*, London, UK, Oct. 18–20, 2004, pp. 470–474.

[82] E. Perahia and D. C. Cox, "Shadow fading correlation between uplink and downlink," in *Proc. 53rd IEEE Veh. Technol. Conf. Spring*, vol. 1, Rhodes, Greece, May 6–9, 2001, pp. 308–312.

[83] E. Perahia, D. C. Cox, and S. Ho, "Shadow fading cross correlation between base stations," in *Proc. 53rd IEEE Veh. Technol. Conf. Spring*, vol. 1, Rhodes, Greece, May 6–9, 2001, pp. 313–317.

[84] R. D. Stevens and I. J. Dilworth, "Mobile radio shadowing loss variability and co-channel signal correlation at 452 MHz," *IEE Electron. Letters*, vol. 32, no. 1, pp. 16–17, 1996.

[85] A. Papasakellariou, "Overview of interference cancellation for CDMA wireless systems," in *Proc. Int. Conf. Information Technology: Coding and Computing*, Las Vegas, Nevada, USA, Mar. 27–29, 2000, pp. 86–91.

[86] S. Parkvall, E. Englund, M. Lundevall, and J. Torsner, "Evolving 3G mobile systems: broadband and broadcast services in WCDMA," *IEEE Commun. Mag.*, vol. 44, no. 2, pp. 30–36, Feb. 2006.

[87] J. Voigt, J. Deissner, J. Hubner, D. Hunold, and S. Mobius, "Optimising HSDPA performance in the UMTS network planning process," in *Proc. 61st IEEE Veh. Technol. Conf. Spring*, vol. 4, Stockholm, Sweden, May 30 – June 1, 2005, pp. 2384–2388.

[88] S. Verdu, "Minimum probability of error for asynchronous Gaussian multiple access channels," *IEEE Trans. Inf. Theory*, vol. IT-32, no. 1, pp. 85–96, Jan. 1986.

[89] K. S. Schneider, "Optimum detection of code division multiplexed signals," *IEEE Trans. Aerosp. Electron. Syst.*, vol. AES-15, pp. 181–185, Jan. 1979.

[90] R. Kohno, M. Hatori, and H. Imai, "Cancellation techniques of co-channel interference in asynchronous spread spectrum multiple access systems," *Electronics and Communication in Japan*, vol. 66-A, no. 5, pp. 20–29, May 1983.

[91] S. Moshavi, E. G. Kanterakis, and D. L. Schilling, "Multistage linear receivers for DS-CDMA systems," *Int. J. Wireless Information Networks*, vol. 3, no. 1, pp. 1–17, Jan. 1996.

[92] Z. Xie, R. T. Short, and C. K. Rushforth, "A family of suboptimum detectors for coherent multiuser communications," *IEEE J. Sel. Areas Commun.*, vol. 8, no. 4, pp. 683–690, May 1990.

[93] P. Patel and J. Holtzman, "Analysis of a simple successive interference cancellation scheme in a DS/CDMA system," *IEEE J. Sel. Areas Commun.*, vol. 12, no. 5, pp. 796–807, June 1994.

[94] ——, "Performance comparison of a DS/CDMA system using successive interference cancellation (IC) scheme and a parallel IC scheme under fading," in *Proc. IEEE Int. Conf. Commun.*, vol. 1, New Orleans, Louisiana, USA, May 1–5, 1994, pp. 510–514.

[95] J. G. Andrews, "Successive interference cancellation for uplink CDMA," Ph.D. dissertation, Stanford University, 2002.

[96] J. G. Andrews and T. H. Y. Meng, "Optimum power control for successive interference cancellation with imperfect channel estimation," *IEEE Trans. Wireless Commun.*, vol. 2, no. 2, pp. 375–383, 2005.

[97] A. Hasan and J. G. Andrews, "Cancellation error statistics in a power-controlled CDMA system using successive interference cancellation," in *8th IEEE Int. Symp. Spread Spectrum Techniques and Applications*, Sydney, Australia, Aug. 30 – Sept. 2, 2004, pp. 419–423.

[98] P. Hatrack and J. M. Holtzman, "Reduction of other-cell interference with integrated interference cancellation/power control," in *Proc. 47th IEEE Veh. Technol. Conf.*, vol. 3, Phoenix, Arizona, USA, May 4–7, 1997, pp. 1842–1846.

[99] D. Warrier and U. Madhow, "On the capacity of cellular CDMA with successive decoding and controlled power disparities," in *Proc. 48th IEEE Veh. Technol. Conf.*, vol. 3, Ottawa, Ontario, Canada, May 18–21, 1998, pp. 1873–1877.

[100] J. G. Andrews and T. H. Y. Meng, "Transmit power and other-cell interference reduction via successive interference cancellation with imperfect channel estimation," in *Proc. IEEE Int. Conf. Commun.*, vol. 6, Helsinki, Finland, June 11–14, 2001, pp. 1940–1944.

[101] ——, "Performance of multicarrier CDMA with successive interference cancellation in a multipath fading channel," *IEEE Trans. Commun.*, vol. 52, no. 5, pp. 811–822, 2004.

[102] H. Nie and P. T. Mathiopoulos, "Reverse link inter-cell analysis for cellular CDMA systems with controlled power disparities," in *Proc. 10th Int. Conf. Telecommunications*, vol. 1, Papeete, Tahiti, Feb. 23 – Mar. 1, 2003, pp. 788–792.

[103] A. Kaul and B. D. Woerner, "Analytic limits on performance of adaptive multistage interference cancellation for CDMA," *IEE Electron. Letters*, vol. 30, no. 25, pp. 2093–2095, 1994.

[104] ——, "An analysis of adaptive multistage interference cancellation for CDMA," in *Proc. 45th IEEE Veh. Technol. Conf.*, vol. 1, Chicago, Illinois, USA, July 25–28, 1995, pp. 82–85.

[105] F. Gunnarsson and B. Hagerman, "System aspects of WCDMA uplink parallel interference cancellation," in *Proc. 61st IEEE Veh. Technol. Conf. Spring*, vol. 3, Stockholm, Sweden, May 30 – June 1, 2005, pp. 1935–1939.

[106] A. Agrawal, J. Andrews, J. Cioffi, and T. Meng, "Power control for successive interference cancellation with imperfect cancellation," in *Proc. IEEE Int. Conf. Commun.*, vol. 1, New York, USA, Apr. 28 – May 2, 2002, pp. 356–360.

[107] P. R. Patel and J. M. Holtzman, "Analysis of a DS/CDMA successive interference cancellation scheme using correlations," in *Proc. IEEE Global Telecommunications Conf.*, vol. 1, Houston, Texas, USA, Nov. 29 – Dec. 2, 1993, pp. 76–80.

[108] D. Divsalar, M. K. Simon, and D. Raphaeli, "Improved parallel interference cancellation for CDMA," *IEEE Trans. Commun.*, vol. 26, no. 2, pp. 258–268, 1998.

[109] P. Frenger, P. Orten, and T. Ottosson, "Bit error rate calculation for nonlinear interference cancellation," *IEE Electron. Letters*, vol. 35, no. 18, pp. 1572–1573, 1999.

[110] ——, "Code-spread CDMA with interference cancellation," *IEEE J. Sel. Areas Commun.*, vol. 17, no. 12, pp. 2090–2095, Dec. 1999.

[111] H. Nie and P. T. Mathiopoulos, "Reverse link capacity for cellular CDMA systems employing successive interference cancellation," in *Proc. Int. Conf. Commun. Tech.*, vol. 2, Beijing, China, Apr. 9–11, 2003, pp. 770–773.

[112] K. Puttegowda, G. Verma, S. Bali, and R. M. Buehrer, "On the effect of cancellation order in successive interference cancellation for CDMA systems," in *Proc. 58th IEEE Veh. Technol. Conf. Fall*, vol. 2, Orlando, Florida, USA, Oct. 6–9, 2003, pp. 1035–1039.

[113] S. Hwang, C. Park, and J. H. Lee, "Performance of an indoor optical wireless PPM-CDMA system with interference cancellation schemes," in *Proc. IEEE Int. Symp. Personal, Indoor and Mobile Radio Commun.*, vol. 3, Helsinki, Finland, Sept. 1–4, 1997, pp. 974–978.

[114] M. K. Varanasi and B. Aazhang, "Multistage detection in asynchronous code division multiple access channels," *IEEE Trans. Commun.*, vol. 8, no. 4, pp. 509–519, 1990.

[115] L. Welburn, "Macrodiversity and multiuser detection: High performance tools in a DS-CDMA system," Ph.D. dissertation, Simon Fraser University, 2001.

[116] T. S. Rappaport, "Simple-to-build wide-band antennas," *RF Design*, pp. 37–41, Apr. 1988.

[117] *Rohde & Schwarz ESVN40 receiver manual.*